10.0 STEAM AND POWER CONVERSION SYSTEM

TABLE OF CONTENTS

TABLE OF CONTENTS

Page

TABLE OF CONTENTS

LIST OF TABLES

LIST OF FIGURES

10.0 - STEAM AND POWER CONVERSION SYSTEM

10.1 SUMMARY DESCRIPTION

The steam and power conversion system is designed to accept steam from the nuclear steam supply system (NSSS) and convert its thermal energy into electrical energy. It consists of the turbine-generator, main steam supply system, main condenser, turbine bypass system, condensate and feedwater system, steam generator blowdown system, main condenser evacuation system, turbine gland sealing system, and circulating water system. The steam and power conversion system has a capability of 2831 MWt / 953.3 MWe. A flow diagram is provided for the main steam supply system in drawings D-175033, sheet 1, D-175033, sheet 2, D-170114, sheet 1, D-170114, sheet 2, D-205033, sheet 1, D-205033, sheet 2, and D-200007. A summary of major equipment is provided in table 10.1-1. Heat balances are shown in figures 10.1-1 and 10.1-2 for both normal and maximum volumetric flow rates, respectively.

The turbine is a Westinghouse (modified by Siemens) 1800 rpm, tandem compound, 4-flow exhaust with 45.5-in. last-stage blades. It is equipped with an automatic stop and emergency trip system which will trip the stop and control valves to a closed position in the event of turbine overspeed, low bearing oil pressure, low vacuum, or thrust bearing failure. (See section 10.2.)

The main steam supply system includes the associated piping and valves required to conduct the steam through the steam and power conversion system. Steam generated in the three steam generators will be conducted through the containment wall in three lines. Isolation valves and spring-loaded safety valves will be located outside of containment in each of the three steam lines, with the safety valves being located upstream of the isolation valves. Beyond the isolation valves, the three main steam lines join in a header, and downstream of the header, the flow splits into two separate lines which both lead to the turbine. At the turbine, flow from each of these two main steam supply lines will feed the turbine. Steam to the auxiliary feedwater pump turbine will be taken in separate lines from two of the three main steam lines. Steam will be supplied to the steam reheaters, the gland steam sealing system, the auxiliary steam system, the steam generator feedwater pump turbine, and other components and systems. (See section 10.3.)

The main condenser serves as a heat sink for the main turbine exhaust, feed pump turbine exhaust, turbine bypass steam, and other flows. It also provides for deaeration and storage for the condensate. Each low-pressure turbine casing is connected by the use of a single-convolution, stainless steel expansion joint to its condenser. (See subsection 10.4.1.)

The turbine bypass system provides a route for throttle steam to bypass the turbine and enter the condenser directly. This route is provided for the case of large turbine load reduction which could cause an undesired magnitude of nuclear system transients. The bypass system is capable of allowing a 50-percent load decrease in the turbine load without reactor trip. (See subsection 10.4.4.)

The condensate and feedwater system is a closed cycle which serves to conduct condensed steam from the main condenser to the steam generators located inside the containment.

Deaeration of the condensate is performed in the hot well of the main condenser. The condensate is then pumped through five stages of low-pressure feedwater heaters, followed by one stage of high-pressure feedwater headers, before entering the steam generators. (See subsection 10.4.7.)

The steam generator blowdown system is designed to maintain the water chemistry in the secondary coolant system at an optimum purity level. Blowdown liquid is taken off at the steam generator stage and processed with the use of ion exchange resins to remove impurities which may have been added through leaks in the steam and power conversion system. This system also removes radioactive contaminants which may enter the secondary side of the steam generator through defects in the steam generator tubing. After the contaminants have been removed for offsite disposal, the purified blowdown liquid is recycled to the main condenser.

The main condenser evacuation system, by the use of hogging ejectors during startup and steam jet air ejectors during normal running, creates a vacuum on the main condenser to ensure proper flow of the condensing steam. (See subsection 10.4.2.)

The turbine gland sealing system acts to seal the turbine shaft from leakage of air into the turbine interior or leakage of steam out of the turbine into the turbine building. (See subsection 10.4.3.)

The circulating water system is designed to remove the waste heat from the thermal cycle. It will also remove the heat released into the condenser by the steam dump system during plant startup, cooldown, or during steam dump operation following a large load reduction. (See subsection 10.4.5.)

Portions of the main steam supply system and the condensate and feedwater system are safety related. There is an extremely small amount of radioactivity in the steam and power conversion system during normal operation; therefore, no radiation shieldings (besides piping and housing) are required for this system. The portion of the steam and power conversion system which is located outside containment is continuously accessible under normal operating conditions.

TABLE 10.1-1 (SHEET 1 OF 2)

MAJOR STEAM AND POWER CONVERSION EQUIPMENT
SUMMARY DESCRIPTION

Number of Units	2
Reactor core (net MWt, each unit)	2,831
Reactor coolant pump heat input (MWt, each unit)	10
Total NSSS power (MWt, each unit)	2,841
NSSS total steam flow (lb/h, at maximum calculated, each unit)	12.56E+06
Steam generator design pressure (psia)	1,100.0
Steam generator design temperature (°F)	600.0
NSSS steam outlet moisture (%)	0.10
NSSS inlet feedwater temperature (°F, at maximum calculated) (T)	446.0

Turbine-Generator Ratings[1,3,4]

Unit	1	2
Turbine		
Throttle steam pressure (psia)	748.0	742.0
Throttle steam temperature (°F)	510.5	509.6
Throttle steam moisture (%)	0.3	0.3
Throttle steam flow (lb/h)	12,038,301	12,045,299
Exhaust pressure (in. Hg abs)	3.0	3.0
Generator		
Nameplate output (kW)	954,400	952,800
Power factor (pf)	0.85 (note 2)	0.85 (note 2)

TABLE 10.1-1 (SHEET 2 OF 2)

Generator rating (kVA)	1,045,000.0	1,045,000.0
Voltage	22,000.0	22,000.0
H_2 pressure (psig)	75.0	75.0

Notes:

(1) Ratings unchanged for power uprate. Uprate was evaluated based on the representative conditions reflected in figures 10.1-1 and 10.1-2.

(2) The Units operate near a power factor of 1.0.

(3) Nameplate output (kW, each unit) changed as a result of LP turbine replacement. Other ratings including throttle steam pressure, throttle steam temperature, throttle steam moisture, throttle steam flow, and exhaust pressure were not changed as a result of the LP turbine replacement but were revised by Siemens with the vendor manual transmittal for the LP turbine replacement.

(4) Turbine ratings updated as a result of the replacement of the HP turbines at Measurement Uncertainty Recapture (MUR) uprate conditions.

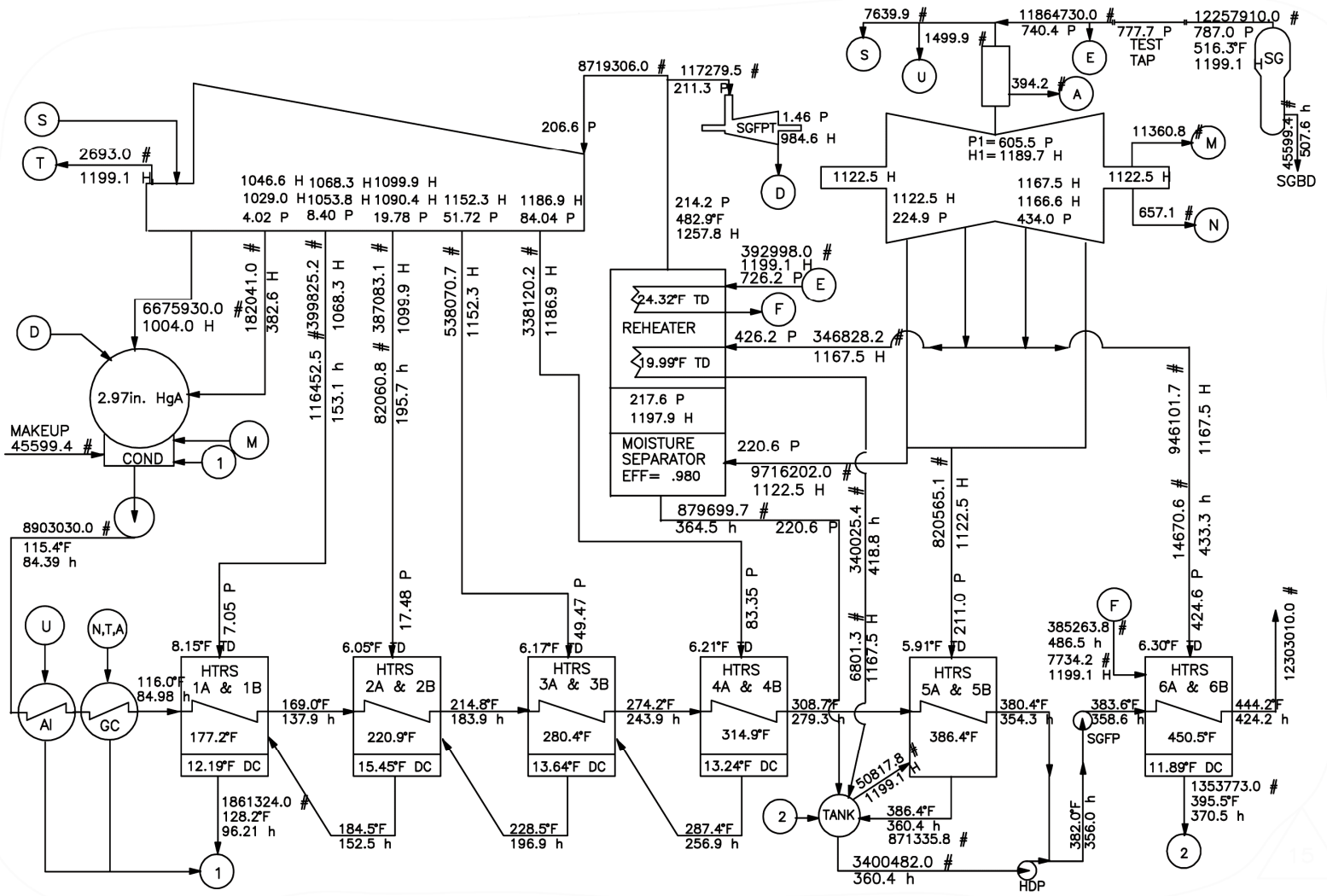

Note: Flow conditions downstream of the LP turbine and HP turbine to the condenser have changed as a result of the LP turbine and HP turbine replacement.

REV 30 10/21

SOUTHERN COMPANY *Energy to Serve Your World®*	**JOSEPH M. FARLEY NUCLEAR PLANT UNIT 1 AND UNIT 2**	HEAT BALANCE – NORMAL FIGURE 10.1-1

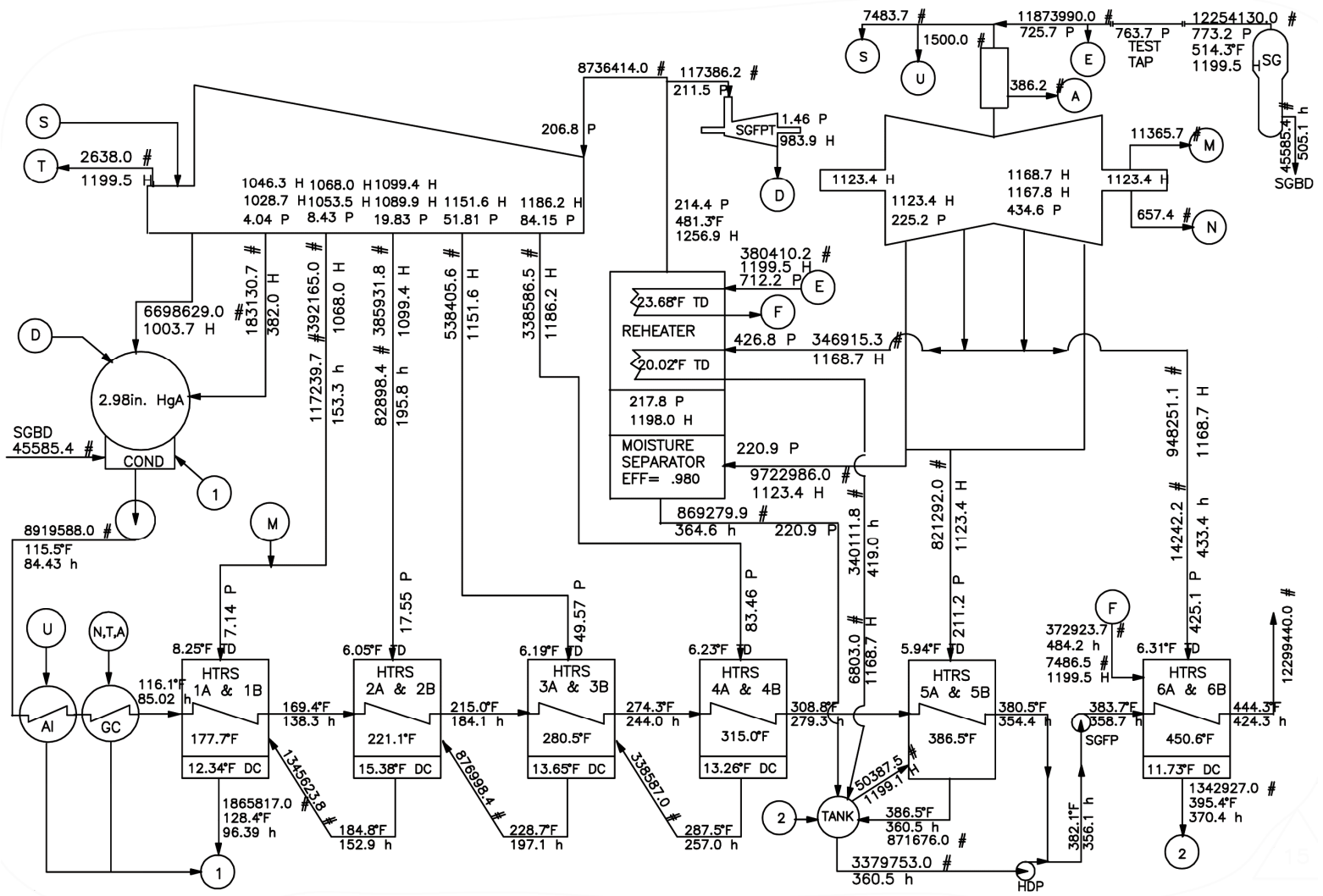

Note: Flow conditions downstream of the LP turbine and HP turbine to the condenser have changed as a result of the LP turbine and HP turbine replacement.

REV 30 10/21

SOUTHERN COMPANY
Energy to Serve Your World®

JOSEPH M. FARLEY
NUCLEAR PLANT
UNIT 1 AND UNIT 2

HEAT BALANCE – MAXIMUM

FIGURE 10.1-2

10.2 TURBINE-GENERATOR

10.2.1 DESIGN BASES

The turbine-generator is designed to convert the thermal energy of the steam generated by the nuclear steam supply system (NSSS) into electrical energy. As stated in section 10.1, it is a Westinghouse (modified by Siemens) 1800 rpm, tandem compound, 4-flow exhaust with 45.5-in. last-stage blades. The turbine was designed at maximum flow to accept up to 11,701,421 lb/h of throttled steam at a pressure of 750 psia, a temperature of 510.8°F, and 0.4-percent moisture for a maximum output of 895,534 kW by the generator. Modifications for power uprate conditions (representative data presented in figures 10.1-1 and 10.1-2) have increased expected output to approximately 910 MWE (gross). The LP turbine replacements increased expected output to approximately 933.4 MWE (gross). Implementation of the Unit 1 and Unit 2 measurement uncertainty recapture (MUR) power uprate and HP turbine replacement increased expected output to approximately 954.4 MWe with maximum throttled steam flow of 12,038,301 lb/hr for Unit 1 and 952.8 MWe with maximum throttled steam flow of 12,045,299 lb/hr for Unit 2. It is intended for a base-loaded operation with capabilities for load following when required.

The turbine-generator is designed to accommodate a 100-percent step-load reduction with the use of the turbine bypass system.

This capability is limited by the reactor coolant system (RCS) which is designed to accommodate a step change of 10 percent of full power step and a 5-percent per minute ramp up to and including but not exceeding 100 percent of full power without reactor trip. The reactor coolant system can accept a complete loss of load from full power with reactor trip. In addition, the steam dump system makes it possible to accept a 50-percent load rejection from full power without reactor trip.

The turbine is considered a machine and Westinghouse and Siemens have developed their own internal proprietary standards and specifications which are continuously updated in comparison to ASME codes and standards. The generator is designed to ANSI C50 standards.

10.2.2 DESCRIPTION

Saturated steam is supplied to the turbine throttle from the steam generators through four stop valves and four control valves. The steam flows through a two-flow, high-pressure turbine and then through four combination moisture separators reheaters in parallel to two double-flow, low-pressure turbines which exhaust to the main condenser. There are two stages of feedwater reheating off the high-pressure turbine and four stages of feedwater reheating off the low-pressure turbines; the steam supplied to these stages of feedwater reheating is provided by the extraction steam system. This extraction steam system is designed to supply steam from various stages of the high-pressure and low-pressure turbines to the moisture separators, high-pressure heaters, low-pressure heaters, auxiliary steam system, and condensate recovery system. The extraction steam provisions are shown in drawings C-170072, C-170073, C-170074, C-170075, C-170076, D-170076, D-170077, and D-200009.

The turbine-generator system and auxiliaries are capable of accepting a greater instantaneous or rate-of-load change than can be supplied by the reactor coolant system. Therefore, load transients which may occur are dictated by the reactor coolant system rather than the turbine generator.

The ac generator is a direct-coupled, 60-cycle, 3-phase, 22,000-V unit rated at 1,045,000 kVA at 0.85 power factor (the units operate near a power factor of 1.0); it has a short-circuit ratio of 0.58. The generator shaft seals are oil sealed to prevent hydrogen leakage. The generator has its own shaft-driven excitation equipment.

The turbine lubricating oil system supplies oil for lubricating the bearings. A bypass stream of turbine lubricating oil will flow continuously through an oil conditioner to remove water and other impurities.

The turbine is equipped with an automatic stop and emergency trip system which will trip the stop and control valves to a closed position in the event of turbine overspeed, low bearing oil pressure, low vacuum, or thrust bearing failure. An electric solenoid trip is provided for remote manual trips and for various automatic trips. The occurrence of a turbine trip from any of the above when operating at approximately 50-percent power or greater will cause a reactor trip signal to be supplied to the reactor protection system thus tripping the reactor.

High-pressure steam enters the turbine through four turbine throttle valves and four governor valves. Two turbine throttle and two governor valves form a single assembly. The steam exhausts from the high-pressure cylinder, flows through the reheaters, and reenters the turbine through the four reheat stop valves and the four reheat intercept valves.

The turbine-generator system is equipped with a digital electrohydraulic (DEH) control system to control steam flow through the turbine. The DEH control system performs two main functions--control of turbine speed and control of turbine load.

The spring-loaded valves are positioned by hydraulic actuators which receive their motive fluid from a high-pressure fluid supply system.

The digital controller positions the throttle and governor valves by means of electrohydraulic servo loops. In the event of a partial loop drop, the interceptor valves are closed by energizing a solenoid valve on the appropriate valve actuators.

The digital controller receives three feedbacks from the turbine--speed, generator megawatt output, and first-stage pressure, which is proportional to turbine load.

The operator controls the turbine and receives his information from the human machine interface (HMI) installed on the operator workstation (OWS) in the main control room (MCR).

The Ovation DEH turbine controller contains a redundant OA/OPC (operator auto/overspeed protection controller) drop to perform all base DEH functions. If the primary OA/OPC distributed processing unit (DPU) fails, the backup OA/OPC DPU will automatically take over for reliability. If both primary and backup OA/OPC drops should fail, the turbine will be tripped. This ensures that the turbine overspeed protection features of the DEH control system are continuously available during automatic or manual turbine operation.

The high-pressure fluid supply system is of the constant pressure type and is completely separate from the lubricating oil system. A dual pump system is used with one pump serving as a complete backup. The backup pump starts automatically from low header oil pressure.

The high-pressure fluid trip headers connected to each valve actuator assembly are controlled by a diaphragm-operated emergency trip valve and solenoid valves.

The mechanical overspeed trip arrangement is also retained. When the trip valve is opened, either by overspeed or other emergency conditions, the pressure in the two headers is released initiating quick closing of all steam valve actuators. A solenoid valve actuated by a pressure switch on the autostop oil trip header serves as an electrical backup for the interface valve. This redundant solenoid valve arrangement controls the trip header for all steam valves.

The servoposition loop previously described is optimized to obtain a steady-state position accuracy of less than 0.005 in., a transient response of approximately 10 Hz at 90-degree phase lag, and a valve closing time for dump conditions of 0.1 to 0.15 s. This performance assures adequate overspeed protection and stable operation for the changes in steam forces or fluid supply pressure.

Turbine overspeed is prevented by the rapid cutoff of steam admission to the turbine. Main steam and reheat steam admission are both controlled by series alignments of stop and control valves which are held open against strong spring pressure by high-pressure hydraulic fluid. Overspeed control is by trip valve release of the hydraulic fluid pressure. Redundant shaft-speed sensors and trip valving systems assure a highly reliable prevention of turbine overspeed.

The digital electrohydraulic control system contains a turbine shaft-speed transducer and is the basic control system for turbine overspeed. At 103 percent of rated shaft speed, this system releases the actuating hydraulic fluid pressure to move the main steam control and reheat intercept valves toward the closed position in an attempt to maintain shaft speed at less than 103 percent of rated speed.

Backup control is supplied by an overspeed trip valve and mechanical overspeed mechanism which consists of a spring-loaded eccentric weight mounted in the end of the turbine shaft. At 111 percent of rated shaft speed, centrifugal force moves the weight outward to mechanically actuate the overspeed trip valve which dumps autostop oil pressure, and in turn releases the actuating hydraulic fluid pressure to close the main steam stop and control valves and the reheat steam stop and intercept valves. The supply steam pressure acts to hold the stop valves closed.

Upon loss of the actuating hydraulic fluid pressure, an air pilot valve closes the extraction nonreturn valves to all feedwater heaters.

The secondary backup overspeed control is provided by the electrohydraulic control system if the turbine speed exceeds approximately 111.5 percent of rated speed. At this point, the solenoid trip is energized to dump the autostop oil, which in turn dumps the actuating hydraulic fluid pressure, to ensure closing of the main steam stop and control valves and the reheat steam stop and intercept valves.

Alabama Power Company (APC) has developed a comprehensive program for maintenance calibration and testing of the turbine overspeed protection system with the overall objective of maintaining the high reliability of this system. The program, which is entitled "Turbine Overspeed Reliability Assurance Program," is based on recommendations by Westinghouse regarding valve maintenance and on operating experience at FNP.

The maintenance program includes provisions for inspections and maintenance of the throttle, governor, reheat stop and intercept valves.

The calibration program includes provisions for the calibration of the turbine overspeed protection system. Calibration is performed during each refueling outage or following major maintenance on the turbine generator or the overspeed protection system.

The testing program includes provisions for turbine valve and turbine overspeed protection system testing. Testing is performed during each turbine startup, unless tested within the previous 7 days, including startup after each refueling outage. This program also includes a test of all the turbine throttle and governor valves on an approximate 6-month interval and all reheat stop and intercept valves on an approximate interval of 18 months. The turbine overspeed trip system functional test is performed each refueling outage or when major maintenance is performed on the turbine. This test involves manually controlling turbine speed up to the trip set points to observe actual turbine overspeed trips.

SNC will monitor the reliability information of the turbine valves as results are obtained from the Westinghouse Nuclear Plant fleet experience and the FNP valve experience.

This comprehensive program is the subject of ongoing review and evaluation. The schedules and/or scope of the maintenance, calibration, and testing programs are subject to revision as appropriate, based on operating experience or changes to the manufacturer's recommendations. This program and any subsequent changes will be reviewed and approved as specified in existing plant administrative procedures. The program will be performed in accordance with procedures, maintenance work orders, and/or outage work schedules as appropriate. All deviations from the program and deficiencies identified through the specified maintenance, calibration, or testing activities will be evaluated by SNC to determine appropriate action to be taken such as correcting the deviation or deficiency, performing compensatory action, or removing the turbine from service.

10.2.3 TURBINE MISSILES

Nondestructive examination (NDE) of low pressure (LP) turbine rotor discs is performed to confirm that, if cracks exist, they do not pose an unacceptable risk for continued operation. Assessment of the NDE data is performed to determine the next required inspection interval. This assessment may be based on approved deterministic or probabilistic methods (References 3, 4, and 5).

The Siemens methodology presented in TP-04124 (reference 6) justifies the external missile generation probability in extending the disc inspections of the Siemens 13.9 m^2 retrofit design of LP rotors for up to 100,000 operating hours with quarterly test frequency for the main turbine stop and control valves as outlined in FSAR subsection 10.2.2. The results of this methodology demonstrate the turbine missile probability, P1, to be well below the NRC's acceptance criteria of 1E-05 per turbine year at a quarterly control valve surveillance interval provided that no crack is detected in the disc. Siemens further extended the recommended maximum valve surveillance interval to 6 months in Service Bulletin SB3-13-0009-ST-EN-01 (reference 7).

10.2.4 EVALUATION

The turbine generator and related steam-handling equipment is a concept of proven design that is capable of handling the plant load requirements. During normal operation, this system is designed to have an extremely small level of radioactivity.

Assuming steam generator tube leakage, the small amount of radioactivity which may enter the turbine generator is monitored in the steam jet air ejector discharge. Radioactivity which may be present in the secondary coolant loop is also monitored in the steam generator blowdown system and the steam generator sample system. Because of the low activity levels, sufficient shielding is provided by the piping, turbine casing, and other components. There is continuous access to the turbine area. (Refer to section 11.4 for monitoring and shielding information.)

REFERENCES

1. Regulatory Guide 1.115, Revision 1, dated July 1977, titled “Protection Against Low-Trajectory Turbine Missiles.”

2. Letter from Charles E. Rossi of NRC to James A. Martin of Westinghouse dated February 2, 1987, transmitting approval of various topical reports related to calculating probability of turbine missiles.

3. Letter from H.C. Bissell of Westinghouse to Don Mansfield of Southern Nuclear dated May 25, 1994, titled “Turbine Valve Testing Frequency.”

4. Letter from S. A. Varga of NRC to F. L. Clayton of APC dated August 24, 1981, titled “Turbine Disc Cracking.”

5. Letter from F. L. Clayton of APC to S. A. Varga of NRC dated September 21, 1981, titled “Turbine Disc Inspection Intervals.”

6. Siemens-Westinghouse Topical Report TP-04124 dated June 7, 2004, titled “Missile Probability Analysis for the Siemens 13.9M^2 Retrofit Design of Low-Pressure Turbine by Siemens AG.”

7. Siemens Service Bulletin SB3-13-0009-ST-EN-01 dated April 16, 2013, titled “Nuclear Steam Turbine Inlet Valve Testing Frequency.”

10.3 MAIN STEAM SUPPLY SYSTEM

The main steam supply system (MSSS) carries the steam generated in the three steam generators through the containment to the following components and systems:

A. Turbine-generator.

B. Moisture separator reheaters.

C. Steam jet air ejector system.

D. Turbine shaft gland seals.

E. Steam generator feedwater pump turbines.

F. Turbine-driven auxiliary feedwater pump.

G. Turbine bypass system.

Drawings D-175033, sheet 1, D-175033, sheet 2, D-170114, sheet 1, D-170114, sheet 2, D-205033, sheet 1, D-205033, sheet 2, and D-200007 show the schematic arrangement of the MSSS piping. The main steam piping up to and including the isolation valves in the main steam lines to the turbine-generator and the main steam piping to the auxiliary feedwater pump turbine have safety-related functions.

10.3.1 DESIGN BASES

10.3.1.1 Functional Requirements

The MSSS conducts the generated steam from the outlet of the steam generators to the various system components. The steam is used for various operational auxiliary services such as shaft steam seals, turbine drives for main and auxiliary feedwater pumps, and steam jet air ejectors, as well as for its principal purpose of supplying the main turbine and reheaters. This system also provides steam to other systems associated with steam generator pressure relief heat removal from the nuclear steam supply system (NSSS), such as the steam generator safety valves, relief valves, and steam dump valves.

The performance requirements for the MSSS are as follows:

A. Optimum pressure drop between steam generators and turbine valves.

B. Similar steam conditions between each turbine stop valve and between each steam generator must be maintained. The maximum pressure variance between one steam generator and any other is 50 psi. To ensure even steam pressure at all loads, the main steam piping is interconnected downstream of the isolation valves and also prior to the turbine stop valves.

C. Adequate piping flexibility is provided to limit forces and moments at the anchor points and upon all plant components to acceptable levels. Stress levels within the piping itself are within the limits specified in the applicable piping codes.

D. Adequate draining provisions for startup and for operation with saturated steam are provided. All low points and closed-end lines are drained to preclude any water accumulation.

10.3.1.2 Safety Requirements

The safety aspects of the main steam system are concentrated on the portions of main steam lines from the steam generators, out through the containment, and up to and including the main steam line isolation valves.

The safety requirements for the MSSS are as follows:

A. The steam lines and the shell side of the steam generator are basically considered as an extension of the containment boundary and, as such, must not be damaged as a consequence of reactor coolant system (RCS) damage. The steam generator shell and steam lines within the containment are therefore protected against a reactor coolant system missile. The reverse is also true in that a steam line break will not cause damage to the reactor coolant system.

B. The measured steam flowrate has a functional requirement. Functionally, the flowrate signal is used by the three-element feedwater controller and as a load index signal for the plant's variable speed main feedwater pumps. It is also used in the development of a steam flow-feed flow mismatch alarm.

   The flowrate is determined by measuring the dynamic pressure losses between the steam generator and a downstream point in the steam line before the containment.

C. The portion of the MSSS up to and including the main steam isolation valves is necessary for the safe shutdown of the plant and is Safety Class 2A and Category I Seismic.

D. Uncontrolled steam release as a result of a steam line failure is limited to the contents of one steam generator in order to keep the related effect upon the reactor core within prescribed bounds.

E. The failure of any main steam line or malfunction of a valve installed therein will not:

   1. Render inoperable any engineered safety feature (ESF).

   2. Result in the containment pressure exceeding the design value or impairing its integrity.

Other safety-related design provisions include:

A. The steam generator safety valves.

B. The steam generator relief valves.

C. The steam supply to the turbine-driven auxiliary feedwater pump. The steam supply to this turbine has a safety classification because of the safety-related functions of the auxiliary feedwater system. The turbine steam supply lines are connected to two steam generator steam lines upstream of the steam line protective valving to provide both redundancy and dependability of supply. Isolation valves in each line maintain the separation of the main steam lines by preventing any interconnecting backflow.

D. Each steam generator includes an internal restriction which acts to limit the maximum flow and the resulting thrust forces created by a main steam line break.

10.3.1.3 Design Data

A.	Number of steam generators 3	
B.	Total flow (lb/h)	12.26 E+06
C.	Design pressure (psig)	1085
D.	Design temperature (□F)	600
E.	Percent moisture (original design value; replacement steam generators outlet moisture is 0.10% or less)	0.25
F.	Number of safety valves	15
G.	Number of relief valves	3

10.3.1.4 Design Codes

The piping and components from the steam generators up to and including main steam line isolation valves are designed to meet Seismic Category I requirements and are in accordance with the ASME Code, Section III, Class 2. The remainder of the piping downstream of the main steam isolation valves is designed to meet Seismic Category II requirements and is in accordance with ANSI B31.1.0.

10.3.2 DESCRIPTION

10.3.2.1 General Description

Saturated steam generated in the three steam generators flows out through the containment wall in three 32-in. main steam lines to a common header.

A flow restrictor integral with the steam generator is provided in each of the three main steam lines inside the containment to limit steam blowdown in the event of a main steam line break. A description of these flow restrictors is presented in subsection 5.5.4, Main Steam Line Flow Restrictors.

The main steam line from each steam generator is provided with five spring-loaded safety valves and one power-operated relief valve. These are located between the containment penetration and the corresponding main steam line isolation valve. The power-operated relief valves are set to open before the first spring-loaded safety valve opens. The power-operated relief valves and the spring-loaded safety valves discharge to the atmosphere.

Two quick-acting, pneumatic-cylinder-operated isolation valves are installed in each main steam line outside the containment and downstream of the safety valves. A full description of these valves is included in subsection 5.5.5, Main Steam Line Isolation System, and in subsection 10.3.9, Main Steam Isolation Valves.

Connections for supplying main steam to the auxiliary feedwater pump turbine are provided on the main steam lines from steam generators B and C. These connections are outside the containment and before the isolation valves. This piping is described in section 6.5, Auxiliary Feedwater System.

The three main steam lines combine into a common header downstream of the isolation valves. Two 36-in. lines conduct the steam from this header, which is located in the auxiliary building, to the turbine building. Both of these lines branch into two 24-in. lines which conduct the steam to the high-pressure turbine. Upstream of the point where the 36-in. lines branch into 24-in. lines, there is a 24-in. crosstie between the 36-in. lines. Lines branch off this crosstie pipe to conduct steam to the following systems:

A. Turbine steam bypass system.

B. Moisture separator reheaters second-stage reheat.

C. Feedwater pump turbines.

D. Turbine gland sealing system.

E. Steam jet air ejectors.

F. Auxiliary steam supply system.

10.3.2.2 Components

10.3.2.2.1 Isolation Valves

See subsections 5.5.5 and 10.3.9 for a detailed description.

10.3.2.2.2 Flow Restrictor

See subsection 5.5.4 for a detailed description.

10.3.2.2.3 Safety Valves

Five spring-loaded safety valves are installed on each main steam line upstream of the main steam isolation valves and outside the containment. These valves are Safety Class 2A and Category I Seismic.

The range of pressure settings of the safety valves on each line is in equal increments from 1075 psig to 1129 psig. The maximum actual capacity of a single valve fully open at 1085 psig is 890,000 lb/h.

10.3.2.2.4 Relief Valves

Installed on each main steam line upstream of the main steam isolation valves and downstream of the safety valve is one atmospheric relief valve. The valves are pneumatically actuated and sized to pass 405,500 lb/h of steam at 1025 psig. They are capable of going from fully closed to fully open within 35 seconds or less. The valves are also capable of being modulated over the pressure range of 1085 psig to 100 psig. Valve control is automatic by steam line pressure with remote manual control of the setpoint. A local manual operator is provided for valve operation in the event of complete loss of automatic control. An emergency source of control air is provided to enable remote manual operation.

10.3.3 EVALUATION

Following a sudden load rejection of up to 50 percent, the MSSS prevents a reactor trip by bypassing the steam directly to the condenser as described in subsection 10.4.4. Following a turbine trip or load rejection above 50 percent or when the turbine bypass system is not available, the MSSS effects a safe reactor trip by removing excessive heat from the reactor coolant through the exhausting of secondary steam through atmospheric power-operated relief valves and the spring-loaded safety valves. The power-operated relief valves and the spring-loaded safety valves also protect the steam generator and the main steam piping from overpressure.

In the unlikely event of a main steam line rupture, the isolation valves in the main steam lines provide steam line isolation, as described in subsection 5.5.5. The valving safety requirements are established to cover the following situations:

A. Break in the Steam Line From One Steam Generator Inside Containment

The steam generator associated with the damaged line will discharge completely into the containment. Without reverse flow protection, the other steam generators would act to feed steam through the interconnecting header to reverse flow through the damaged line and into the containment, resulting in a significant pressure rise in the containment. To prevent discharge of more than one steam generator, the main steam isolation valves are capable of closing within 7 s against a steam flow in the forward direction with a differential pressure across the valve of 775 psig.

Two redundant main steam isolation valves are installed in each main steam line and are designed to stop flow in the forward direction. Both isolation valves are Safety Class 2A and Category I Seismic.

B. Break in the Steam Header Downstream of the Isolation Valve

The time requirement established in A above is the limiting case and is satisfactory for requirements resulting from this situation.

C. Steam Generator Tube Rupture

This requirement is not limiting. A fast-acting valve is not required nor is valve redundancy. The isolation valve serves to limit the total amount of primary coolant leakage during the shutdown period by isolating the damaged steam generator after primary coolant pressure is reduced below steam generator shell-side design pressure.

Automatic operation of the isolation valves is initiated by a steam break or high-high containment pressure signal. Provision is also made for remote manual operation from the control room.

The steam generated in the three steam generators is normally not radioactive; however, in the event of primary to secondary leakage due to a steam generator tube leak, it is possible for the main steam to become radioactively contaminated. A full discussion of the radiological aspects of primary to secondary leakage, including anticipated releases to the environment as a result of the opening of the power-operated relief valves and the safety valves, is contained in chapter 11.

10.3.4 INSPECTION AND TESTING REQUIREMENTS

The MSSS safety valves located in the main steam piping at the outlet from each steam generator were individually tested during initial startup by checking the actual pop and closing pressures of the valve as indicated by pressure gauges mounted in the steam piping as compared to the required design opening and closing pressures specified for the safety valves.

The opening and closing of the atmospheric power relief valves were likewise checked during initial startup by comparing design opening and closing pressures with the actual values as measured by a pressure gauge mounted in the steam line.

The atmospheric relief valves and their associated manual isolation valves are tested in accordance with the Technical Specifications.

The main steam line isolation valves were checked for closing time prior to startup and after each shutdown. A complete discussion of tests and inspections provided for the main steam line isolation valves is given in subsection 5.5.5.

The various alarm and trip pressure setpoints used to isolate the steam generator feedwater pumps to prevent overpressurization were checked by comparing design setpoints versus actual measured trip settings.

Before placing the systems into service, all foreign material and loose oxides were removed from the piping. During cleaning, entry of any fluid into the steam generator was prevented.

The MSSS piping was hydrostatically tested in accordance with the applicable codes.

Power conversion system thermal expansion and vibration measurement tests were conducted as outlined in subsection 14.1.3.

As required by the Technical Specifications, the three main steam lines from the rigid anchor points of the containment penetrations downstream to and including the main steam header shall be inspected in accordance with the Main Steamline Inspection Program.

10.3.5 WATER CHEMISTRY

The primary objective of secondary system water chemistry control is to minimize corrosion of the steam generator internals.

Secondary objectives include:

A. Avoiding or minimizing turbine deposits due to carryover from the steam generator.

B. Reducing corrosion in the feedwater cycle ahead of the steam generator.

C. Elimination of sludge from its point of concentration, the steam generator.

D. Preventing scale deposits on the steam generator heat transfer surfaces and in the turbine.

E. Minimizing feedwater oxygen content prior to entry into steam generator.

F. Controlling condenser air ejector radioactive iodine effluent releases.

These objectives are met by exercising careful chemistry control over the systems, including comprehensive sampling and analysis (inline and laboratory), chemical injection at selected points, continuous system blowdown from the steam generator, and effective protection of the steam generator and feedwater train internals during periods of inactivity.

The method of secondary water chemistry control used is monoethanolamine/hydrazine, morpholine/hydrazine, morpholine/hydrazine/boric acid, or monoethanolamine/hydrazine/ boric acid. Morpholine and monoethanolamine have proven in both laboratory and field experience to be beneficial for reducing erosion-corrosion of secondary side components and subsequent corrosion product transfer to steam generators. Polyacrylic acid (PAA) may be added to disperse iron in the secondary system and steam generators so it is removed via steam generator blowdown and does not remain in the steam generators. Hydrazine is added to scavenge dissolved oxygen to within appropriate limits. The decomposition of hydrazine produces ammonia in sufficient quantity such that the intentional addition of ammonia for pH control is not required. Boric acid is injected as needed into the secondary system to inhibit stress corrosion cracking of steam generator tubes.

Controlling system pH to achieve proper alkaline conditions reduces general corrosion and decreases the release of soluble corrosion products from metal surfaces. Ensuring the absence of free caustic eliminates the possibility of caustic stress corrosion. Ammonium chloride may be added to the secondary system, when necessary, for molar ratio control to change crevice pH.

Reducing dissolved oxygen to the lowest possible levels also contributes to diminished rates of general corrosion. Oxygen in the system is removed from the condenser by the steam jet air ejectors and is further reduced by scavenging with hydrazine introduced at the condensate pump discharge.

Excluding other impurities from the steam generator reduces scale formation on heat transfer surfaces and prevents corrosion caused by concentration of the reactant products of these impurities. Addition of impurities to the steam generator is limited by the careful control of feedwater purity. Of prime importance in this regard is an aggressive program of condenser maintenance to ensure its leak-tight integrity. The concentration effect of the impurities in the steam generator is minimized through continuous blowdown.

A steam generator iodine partition factor of 100 and alkali metal partition factor of 1000 have been used in the evaluation of environmental consequences of postulated accidents (steam generator tube rupture, control rod ejection, main steam line break, and locked rotor, see section 15.4). These partition factors are in conformance with RG 1.183.

10.3.6 INSTRUMENTATION APPLICATIONS

The steam flow restrictors installed in the steam generators are also used for steam flow measurements during normal operation. Two flow transmitters and two pressure transmitters are installed in the main steam line from each steam generator. The steam flow and pressure signals are fed into reactor protection and feedwater control system circuits to control the feedwater flow to each steam generator, to close the isolation valves in case of rupture in main steam lines, and to open the power-operated relief valves in case of overpressure.

10.3.7 MAIN STEAM SAFETY VALVES

Overpressure protection for the three steam generators is provided by the main steam safety valves. The design basis for the main steam safety valves is that they must have sufficient capacity so that main steam pressure does not exceed 110% of the steam generator shell-side design pressure. Based on this requirement, the valves are sized to relieve 105% of the original maximum calculated steam flow at an accumulation pressure not exceeding 110% of the steam generator shell design pressure.

Design parameters for the main steam safety valves are given in table 10.3-1.

Due to the large mass flowrate, each steam generator is protected by a number of valves. The maximum actual capacity of a single valve fully open at 1085 psi gauge does not exceed 890,000 lb/h. This provision serves to limit steam release if any one valve inadvertently sticks open.

The main steam safety valves are located on the main steam lines outside the containment and upstream of the main steam isolation valves. Each of the three main steam lines is equipped with five safety valves. To prevent chattering during operation of the safety valves, each of the five valves on a steam line is set at a different set pressure. The first valve set pressure is 1075 psig, which corresponds to the steam generator shell design pressure minus the pressure loss from the steam generator to the valve. Each of the remaining valves is set at a higher pressure such that all valves are open and at full relief without exceeding 110 percent of the steam generator shell design pressure.

The design of the main steam header where the safety valves are located is described in subsection 3.9.2.

Umbrella-type vent stacks route steam discharge from the safety valves to the atmosphere through penetrations in the auxiliary building roof. These vent stacks have been analyzed for seismic loadings in addition to the normal operating loads.

Prior to shipment, all safety valves were hydrostatically tested in the manufacturer's facilities in accordance with the applicable code. No leakage was observed. In addition, each valve was given a setpoint test and a seal-leakage test. The popping point tolerance did not exceed plus or minus 1 percent of the setpoint pressure. During normal plant operation, the valves are accessible for inspection.

10.3.8 MAIN STEAM ATMOSPHERIC POWER RELIEF VALVES

The steam generator atmospheric relief valves provide the capability for the removal of reactor decay heat during periods when the main heat sinks are not available. Such periods are when the turbine-generator or condenser is not in service, when the plant is being started up or following shutdown, during physics testing, in the event of turbine trip as a result of the loss of condenser vacuum, or when there is a loss of offsite electrical power. Design parameters for the atmospheric power relief valves are given in table 10.3-2.

A single power relief valve is provided on each main steam line upstream of the main steam isolation valves outside of the containment and exhausts to the atmosphere. The valves are of the modulating type and are under the automatic control from a steam line pressure controller with provisions for adjustment of the pressure setpoint from the control room. Additionally, a control scheme similar to that available from the control room is provided at the hot shutdown feedwater panel. Thus, control of the valve is provided in the event of control room evacuation. Each valve is provided with a manual operator so that the valves can be opened or closed locally, even in the event of a loss of all power sources (electric and air).

In the event of a high-energy line break which prohibits operator access to the manual handwheel located on each power-operated relief valve and the simultaneous loss of offsite power and valve air supply, an alternate air supply is located in the el 100-ft area in room 189 as shown in figure 1.2-4 for Unit 1 and in room 2189 for Unit 2 directly beneath the EL 127-ft main steam and feedwater valve room. This area is isolated from the main steam and feedwater valve room and would be accessible following any main steam or feedwater line break that makes the atmospheric dump valves inaccessible for manual control. The alternate air supply consists of two redundant, seismic, self-contained, nonlubricated cylinder type air compressors rated at 38.5 ft^3/min at 100 psig.

The alternate Seismic Category I air supply connections are as shown in drawing D-175035, sheet 2. The three-way solenoid valves (SV3371 AA, BA, CA) between each valve positioner output and the valve actuator selects positioner or alternate air supply control of the atmospheric steam dump valves. When the solenoid valve is energized, the atmospheric steam dump valve is controlled by the valve positioner. When the solenoid valve is deenergized, the atmospheric steam dump valve is controlled by the alternate air supply. The solenoid valve is energized automatically only when there is a signal to the valve positioner to open the atmospheric steam dump valve. Hand switches, one for each steam dump valve, are provided to maintain solenoid valves (SV3371 AA, BA, CA) deenergized when alternate air control is required. The hand switches also control solenoid valves (SV3371 AB, BB, CB). Solenoid valves (SV3371 AB, BB, CB), located with the alternate air supply outside the main steam room, provide for alternate air supply control of the atmospheric steam dump valves. A manual means is available to provide for alternate air supply operation of the atmospheric steam dump valves without electrical power to the solenoid valves (SV3371 AA, BA, CA, AB, BB, CB).

Each valve fails closed on loss of electrical or air supply. They are capable of modulating over the pressure range of 100 to 1085 psig with a stroke time of 35 seconds or less. Each valve is sized to pass a total of approximately 405,500 lb/h of steam (10 percent of plant maximum calculated steam flow) at the no-load pressure of 1025 psig. Additionally, the maximum actual

capacity of any single valve at an inlet steam pressure corresponding to the steam generator shell design pressure (1085 psig) shall not exceed 890,000 lb/h steam. This provision serves to limit the steam release if any one valve inadvertently sticks open.

Discharge from the power-operated relief valves is piped to the atmosphere through penetrations in the auxiliary building roof. The discharge piping was analyzed for seismic and dynamic loads in addition to the normal operating conditions.

During emergency conditions, the main steam atmosphere power relief valves provide a means to control non-faulted steam generator pressures, and, or cool down the plant. During normal plant conditions these relief valves also give the plant flexibility of operation and the capability for a controlled cooldown. Isolation valves are provided upstream of each valve to allow maintenance. During a period when all other valves are out of service, the steam generator safety valves provide the necessary relieving capability.

Prior to shipment, each valve was hydrostatically tested in the manufacturer's facilities in accordance with the applicable code. Leakage was 40 cm^3/h in the valves that were tested. During plant operation, the valves are accessible for inspection. The operability of the alternate air supply system may be demonstrated during refueling shutdowns by using the alternate air supply to cycle open and closed each of the power-operated relief valves.

10.3.9 MAIN STEAM ISOLATION VALVES

The main steam isolation valves consist of two swing-disc check valves in each of the three main steam lines. These valves are located outside of the containment downstream of the main steam safety valves.

The main steam line isolation valves and their bypass valves are designed to stop forward flow and to isolate the steam generators and the main steam lines on signal initiated by engineered safety features actuation system under any of the following conditions:

A. High steam line flow (2/3) in coincidence with low-low T_{avg} (2/3) or low steam line pressure (2/3 break in main steam line).

B. High-high (2/3) pressure in the containment.

C. Manually from the control room.

The main steam isolation valves and bypass valves are designed in accordance with the requirements of the ASME Code for Pumps and Valves for Nuclear Power draft, November 1968 edition including March 1970 addenda, for Class II valves. These valves are classified as Safety Class 2A. The valves are of fail closed design and are designed to meet Seismic Category I requirements. Main steam isolation valve material specifications are listed in table 10.3-4.

Valve design conditions and steam line break flow values are given in table 10.3-3.

The swing-disc trip valves are designed to withstand a single event closing following a postulated rupture of a main steam line. Table 10.3-3 gives the maximum calculated flowrates obtainable at the valve in the event of a steam line break. Case A is based on assumed dry saturated steam flow and case B is based on assumed maximum moisture content. It was conservatively assumed that the steam generator outlet pressure at the time of the break was 1020 psia.

The main steam isolation valve line break design flow conditions were calculated using the Moody critical flow model for FL/D = 0[(1).] Assumptions used include:

A. Isentropic flow from reservoir (steam generator) to valve level.

B. Choked flow occurs in the flow restrictor prior to initiation of valve movement.

C. System pressure is equal to no-load pressure at initiation of transient, and reservoir pressure remains constant at this pressure (1020 psia) throughout the transient.

D. Main steam line restrictor throat diameters are 14 in.

This flow is seen by the steam line isolation valve after the expansion wave generated by the break travels from the valve to the flow restrictor and back. This time is simply t = 2L/c, where L is the length (one way) and c is the sonic velocity. The most conservative time was found to be 0.68 s. A 1.0-s time delay has therefore been introduced before valve actuation to ensure that the time will be > 0.68 s.

The swing-disc trip valve, figure 10.3-1, is a 32-in., 600-lb, swing check valve with bolted bonnet and welding ends. An air-actuated cylinder operator is mounted where the disc shaft penetrates the valve body. This piston operator uses instrument air pressure to hold the valve disc in the open position against the force of a spring. Removal of instrument air pressure from the piston allows the spring to close the valve.

In the normal open position, the disc is held well out of the steam flow by the air operator. An air test cylinder is provided on the trip valve. A manual isolation valve in the normally closed position is provided at the test cylinder. This test cylinder can be remote manually actuated from the control room to stroke the trip valve disc through a small arc to ensure that the disc is not stuck in the open position. This motion is limited to a region within the bonnet of the valve and will not lower the disc into the steam flow. Position switches in the control room indicate the test position of the valve.

The instrument air supply and exhaust schematic drawing for the isolation valves is shown in figure 10.3-2.

Plant instrument air at 80-100 psig pressure is supplied to the actuator cylinder. Each of the redundant isolation valves has its own means of closing and venting the air supply to relieve the cylinder pressure and close the valve.

Each isolation valve is provided with a normally open, three-way solenoid valve which, when deenergized, provides instrument air to the actuator cylinder. As the solenoid valves are normally deenergized, loss of dc power will not cause the valves to close. An air reservoir is also provided for each isolation valve, to allow it to remain open upon loss of instrument air. Each solenoid valve receives a separate signal from the engineered safety features actuation system and has a separate 125-volt dc power supply. When the solenoid valve is energized, it vents the air reservoir and actuator cylinder to the atmosphere and closes the main steam isolation valves.

A 3-in. bypass line is provided around each pair of trip valves for warming the steam line and for equalizing pressure across the trip valves prior to opening. Each bypass line contains two air-operated, fail closed, redundant bypass valves. Each of the redundant bypass valves has its own means of closing and venting the air supply to relieve cylinder pressure and close the valve. Each redundant bypass valve receives a separate signal from the engineered safety features actuation signal.

REFERENCES

1. Moody, F. S., "Transactions of the ASME," Journal of Heat Transfer, p 134, figure 3, February 1965.

TABLE 10.3-1

MAIN STEAM SAFETY AND RELIEF VALVES DESIGN DATA

Main Steam Safety Valves

Quantity	15 (5 per steam generator)
Design pressure (psig)	1085
Design temperature (°F)	600
Capacity	Each bank of 5 valves relieves 4,328,230 lb/h from 1 steam generator (105% of maximum steam flow)
Set pressure (psig)	1075 (for first valve)
Full relieving pressure (psig)	1173 (including tolerance and accumulation)
Limiting flow (per valve) (lb/h)	890,000 at 1085 psig
Applicable code	ASME Section III, Class 2

Main Steam Atmospheric Relief Valve

Quantity	3 (1 per steam generator)
Design pressure (psig)	1085
Design temperature (°F)	600
Capacity (lb/h)	405,500 at 1025 psig 610,000 at 1085 psig
Setpoint (psig)	1025 (adjustable from control room)
Limiting flow (lb/h)	890,000 at 1085 psig
Applicable code	ASME Section III, Class 2

TABLE 10.3-2

ATMOSPHERIC POWER RELIEF VALVES

Valve Design Data

Design pressure (psig)	1085
Design temperature (°F)	600
Nuclear Class	ASME Section III, Class 2
Seismic	Class I
Design flow (lb/h)	405,500 at 1025 psig 610,000 at 1085 psig
Limiting flow (lb/h)	890,000 at 1085 psig

TABLE 10.3-3

MAIN STEAM ISOLATION VALVES FUNCTIONAL REQUIREMENTS

Valves	
Quantity	6
Design pressure (psig)	1085
Design temperature (°F)	600
Operator (trip valve)	Air piston
Full-Load Steam Conditions(1)	
Flow (per valve) (lb/h)	3.875×10^6
Pressure (psig)	775
Temperature (°F)	517
Steam Line Break Design Flow Conditions	
Case A (dry saturated steam flow through valve) (lb/s)	2300
Case B (4% quality steam flow through valve) (lb/s)	7800

(1) MSIVs have been evaluated for steam flows up to 4.152×10^6 lb/h for MUR power uprate.

TABLE 10.3-4

MAIN STEAM ISOLATION VALVES MATERIALS

Component	**Materials**
Body	A-216 WCB
Disc arm	A-216 WCB
Disc	SA-182 Gr. 304F
Cover	A-515 Gr. 70
Shaft	A-564 Gr. 630
Locking plate studs	A-193 Gr. B7
Locking plate nuts	A-194 Gr. 2H
Load key	A-182 Gr. F6a CL2

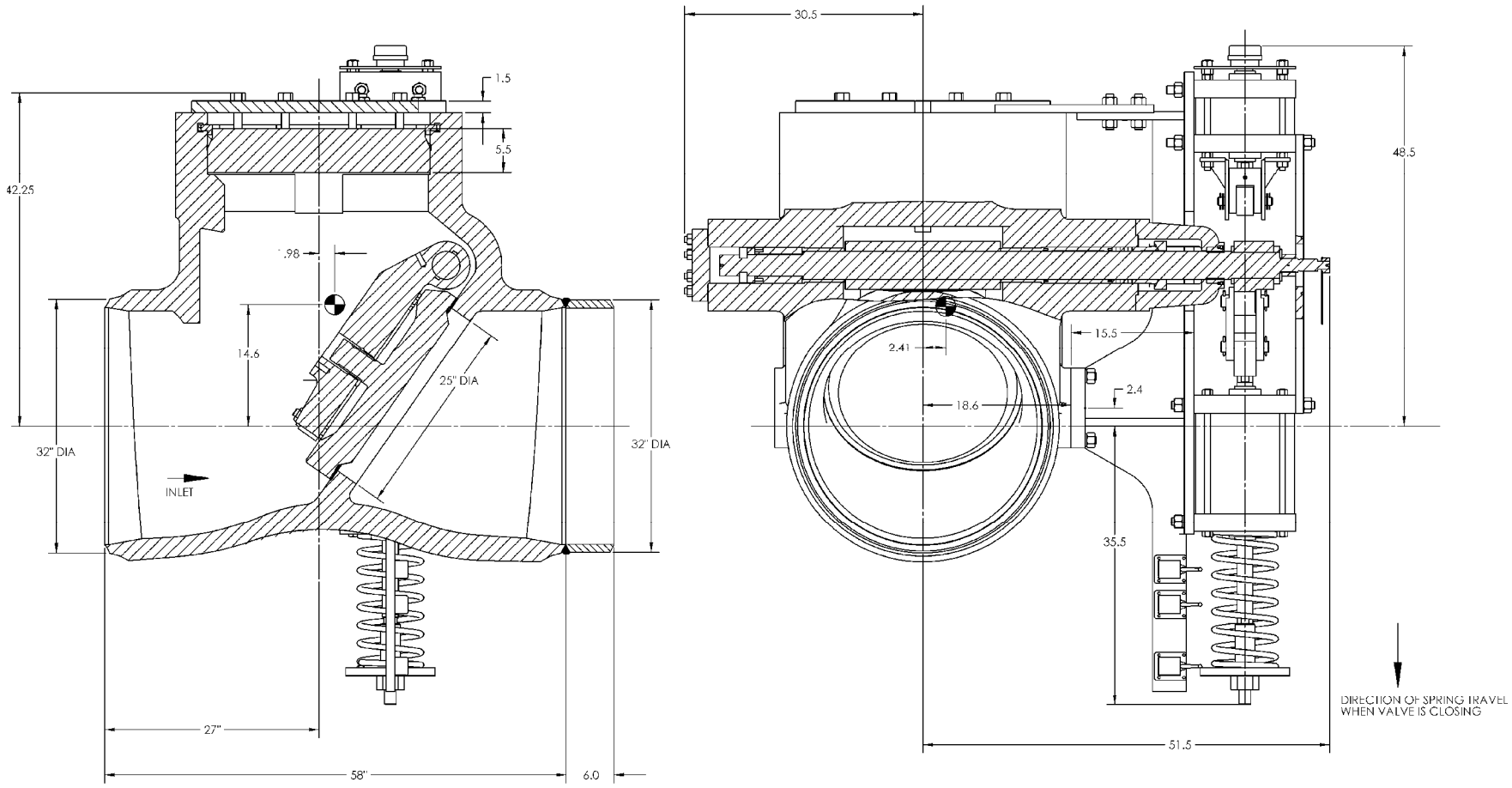

REV 23 5/11

SOUTHERN COMPANY
Energy to Serve Your World®

JOSEPH M. FARLEY
NUCLEAR PLANT
UNIT 1 AND UNIT 2

MAIN STEAM SWING-DISC
TRIP VALVE

FIGURE 10.3-1

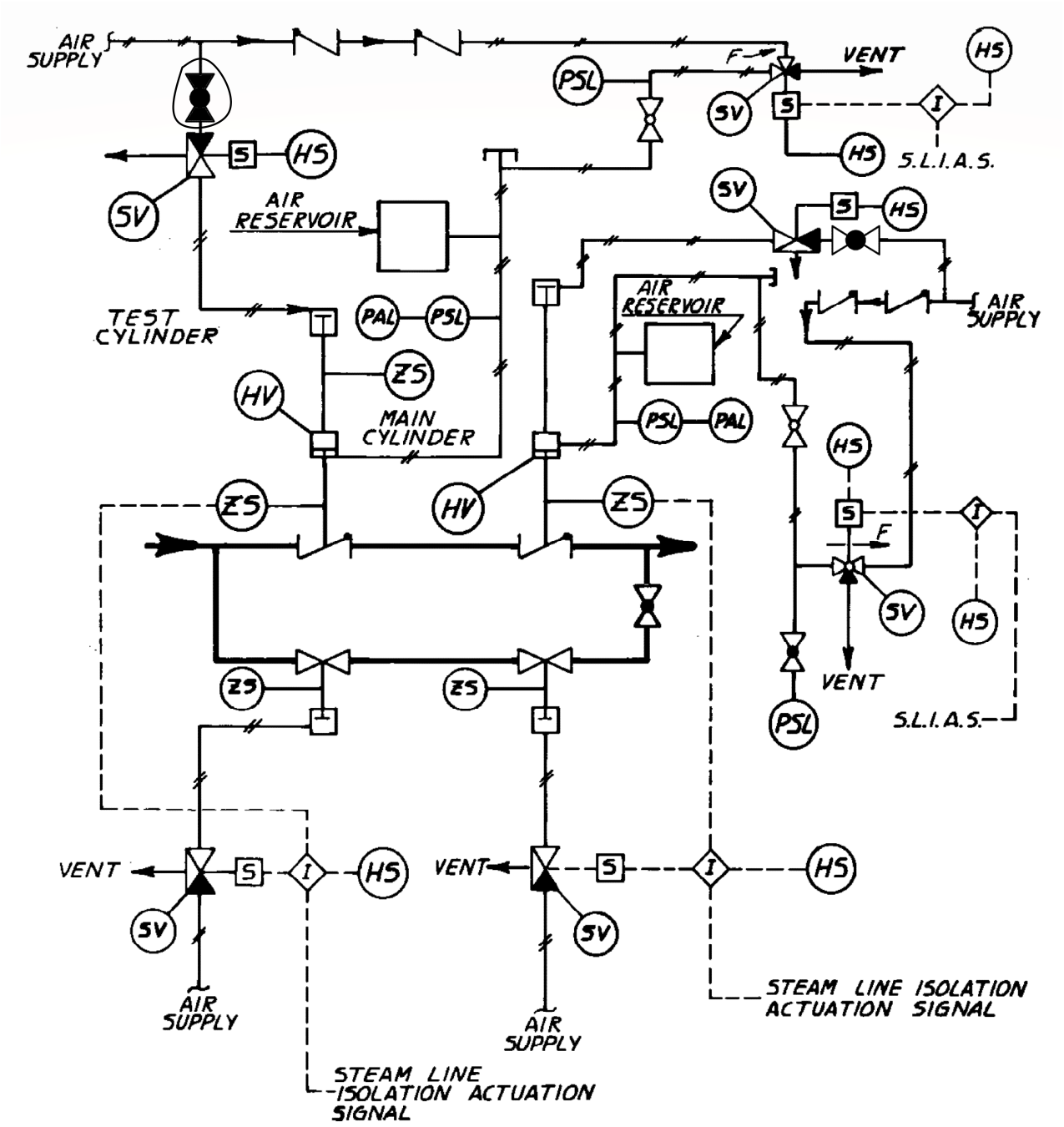

LEGEND

HS	HAND SWITCH
PAL	LOW PRESSURE ALARM
PSL	LOW PRESSURE SWITCH
S	SOLENOID
SV	SOLENOID VALVE
ZS	POSITION SWITCH

REV 30 10/21

SOUTHERN COMPANY
Energy to Serve Your World®

JOSEPH M. FARLEY NUCLEAR PLANT UNIT 1 AND UNIT 2

MAIN STEAM ISOLATION VALVES

FIGURE 10.3-2

10.4 OTHER FEATURES OF THE STEAM AND POWER CONVERSION SYSTEM

This section provides information on the principal design features and subsystems of the steam and power conversion system.

10.4.1 MAIN CONDENSER

10.4.1.1 Design Bases

The main condenser is designed to function as the steam cycle heat sink and collection point for the following flows:

A. Main turbine exhaust.

B. Feedwater heater drains and vents.

C. Steam generator feedwater pump turbine exhaust.

D. Turbine steam bypass system flow.

E. Condensate and steam generator feedwater pump recirculation flow.

F. Condensate and feedwater system makeup flow.

G. Steam jet air ejector intercondenser and aftercondenser drains.

H. Gland steam condenser drain.

I. Miscellaneous equipment drains and vents.

The function of the main condenser is to provide a heat sink for the main turbine exhaust, feed pump turbine exhaust, turbine steam bypass, and other flows. It also deaerates and provides storage capacity for secondary system condensate.

10.4.1.2 System Description

The condenser is a two-shell, radial-flow, single-pass unit which is connected to the exhaust opening of each low-pressure turbine casing by single-convolution, stainless steel expansion joints. Each condenser shell is supported from the turbine building base slab by four concrete pads, and there are pressure-equalizing lines between the shells. These lines ensure that the maximum differential temperature between turbine exhausts will not exceed 30°F.

The condenser has two (one each shell) 3600 ft^3 hot wells which provide sufficient water storage capacity to accommodate system surges and condensate makeup during moderate transients without relying upon reserve condensate storage.
Each circulating water inlet and outlet line to the condenser is provided with a motor-operated shutoff valve.

The condenser has approximately 52,164 tubes giving it an effective surface area of approximately 680,000 ft^2.

During normal operation, the condenser uses 690,000 gal/min of cooling water to remove 67.9 x 10^8 Btu/h of energy from the main turbine exhaust, feed pump turbines exhaust, heater drains, and various other sources.

The noncondensable gasses are concentrated in the air cooling section of the condenser shells, from which they are removed by the steam jet hogging ejectors during startup and by the steam jet air ejectors during normal operation (see subsection 10.4.2). The condenser is designed to have no air leakage and will limit the free oxygen content in the condensate to a maximum of 0.0005 cc/liter at the hot well.

In addition to serving the usual function of a condenser, each shell is capable of accepting 2,432,840 lb/h of turbine bypass steam at an enthalpy of 1192.2 Btu/lb and a pressure of 250 psia without exceeding an exhaust hood temperature of 175°F and a back pressure of 6 in. Hg abs.

10.4.1.3 Safety Evaluation

The main condenser is normally used to remove residual heat from the reactor coolant system (RCS) during the initial cooling period after plant shutdown when the main steam is bypassed to the condenser by the turbine steam bypass system. The condenser is also used to condense the main steam bypassed to the condenser in the event of sudden load rejection by the turbine-generator or a turbine trip.

In the event of load rejection above 50 percent (including 100-percent load rejection due to turbine trip), the condenser will condense 40 percent of full-load main steam flow bypassed to it by the turbine bypass system, and the power-operated relief valves and spring-loaded safety valves will discharge remaining main steam flow to atmosphere to effect safe reactor shutdown and to protect the main steam supply system from overpressure.

If the main condenser is not available during normal plant shutdown, sudden load rejection, or turbine-generator trip, the power-operated relief valves and the spring-loaded safety valves can discharge full main steam flow to the atmosphere and effect a safe reactor shutdown. Nonavailability of the main condenser considered here includes failure of circulating water pumps to supply cooling water, failure of condenser evacuation system to remove noncondensable gases, excessive leakage of air through turbine gland packings due to failure of the gland seal system, or failure of the condenser due to any other reason.

Leakage of condensate from the condenser is not considered possible during operation since the condenser is at a vacuum and any leakage will be into the condenser. A tube leak occurring during operation will not cause a sudden decrease of condenser performance.

During normal operation and shutdown, the main condenser will have no radioactive contaminants inventory. Radioactive contaminants can only be obtained through primary to secondary system leakage due to a steam generator tube leak. A full discussion of the radiological aspects of primary to secondary leakage, including anticipated operating concentrations of radioactivity contaminants, is included in chapter 11. No hydrogen buildup in the main condenser is anticipated.

10.4.1.4 Tests and Inspections

The condenser is basically a welded structure. Air leaks, if any, will probably be found at valve stems or flanged joints. To test for leaks, the condenser will be filled with water prior to startup. Any tubes that develop leaks will be plugged at each end until an opportune time arises for their replacement. Condenser water boxes were hydrostatically tested in accordance with applicable codes.

10.4.1.5 Instrumentation Applications

The main condenser hot wells are equipped with level control devices for automatic control of system water makeup and reject as described in subsection 9.2.6.

The condenser and the steam system auxiliaries are centrally controlled and operation of the system is practically automatic. However, the condenser pressure and temperature will be monitored to see that they remain normal. Local and remote indicating devices are also provided for monitoring water levels in the condenser shells.

There is negligible influence of condenser functions on the reactor coolant system operation, and there is negligible potential for hydrogen buildup in the condenser.

10.4.2 MAIN CONDENSER EVACUATION SYSTEM

10.4.2.1 Design Bases

The main condenser evacuation system is designed to establish the initial condenser vacuum and to maintain it during operation by removing all noncondensable gasses from the condenser. The air ejectors are designed to meet Heat Exchange Institute standards.

10.4.2.2 System Description

The main condenser evacuation system is shown in drawings D-170064 (Unit 1) and D-200003 (Unit 2). The following components are included:

A. Steam Jet Hogging Ejectors

Two steam jet hogging ejectors are used to establish condenser vacuum during startup. Each hogging ejector requires 8,060 lb/h of driving steam at a pressure of 100 psig. The auxiliary steam system supplies this required steam up to approximately 215 psig and pressure-regulating valves reduce the pressure to 100 psig. The discharge from the hogging ejectors is vented directly to the atmosphere.

B. Steam Jet Air Ejectors

For maintaining condenser vacuum, two (one standby) twin-element, two-stage, 100-percent capacity steam jet air ejector systems are used. Each system is capable of removing 40 ft^3/min of saturated air at 71.5°F with 1-in. HgA back pressure.

Each system requires 2640 lb/h driving steam at 100 psig. During normal operation, this steam is extracted from the main steam supply header. An alternate steam source coming from the auxiliary steam system can be used to drive the air ejectors when the main steam is not available.

The steam gas mixture discharge from the ejector elements enters the intercondenser/aftercondenser where 700,000 lb/h of condensate condenses the steam.

The noncondensable gases are normally exhausted to the atmosphere while the condensed steam is drained to the condenser. Noncondensable gases can be exhausted through a charcoal filter system in the event of primary to secondary leakage

10.4.2.3 Safety Evaluation

The main condenser evacuation system can be used during reactor cooldown following a turbine-generator or reactor trip when the main steam is bypassed to the condenser. The air ejectors can be operated with the low-pressure steam generated in the steam generators during reactor cooldown. However, in the event that the main condenser evacuation system is not operable, it is possible that the bypassed steam is not condensed after accumulation of noncondensable gases and inleaking air in the condenser. This is considered a main condenser failure; safe shutdown of the reactor in such an event is discussed in subsection 10.4.1.

The noncondensable gases and vapor mixture discharged to atmosphere from the main condenser evacuation system is not normally radioactive. However, in the event of primary to secondary system leakage due to a steam generator tube leak, it is possible for mixture discharged to become radioactively contaminated. A full discussion of radiological aspects of a primary to secondary leakage and limiting conditions for operation is included in chapter 11.

10.4.2.4 Tests and Inspections

The system was tested in accordance with written procedures during the initial testing and operation program.

Operation of air ejectors is simple and dependable, requiring minimum maintenance at the designed steam conditions. Redundancy allows inspection on one ejector while the other is in service.

10.4.2.5 Instrumentation Applications

The steam jet air ejectors and hogging ejectors are controlled by operator manual selection. Local indicating devices such as pressure, temperature, and flow indicators are provided as required for monitoring the system operation. There are no control functions of the system which could influence operation of the reactor coolant system.

10.4.3 TURBINE GLAND SEALING SYSTEM

10.4.3.1 Design Bases

The gland steam seal system controls the gland steam pressure to maintain adequate sealing of both the main turbine and the steam generator feed pump turbine under all conditions of plant operation. The system is Safety Class Nonnuclear Safety (NNS) and Category II Seismic.

10.4.3.2 System Description

The annulus space where the turbine shaft penetrates the casings is sealed by steam supplied to labyrinth packings. Where the packing seals against vacuum, the sealing steam leaks outward to a vent annulus that is maintained at a slight vacuum. The vent annulus also receives air leakage from the outside. The air-steam mixture is conducted to the gland condenser. Where the packing seals against positive pressure, the sealing steam connection acts as a leak off.

The steam supplied to seals is automatically regulated at approximately 1 to 5 psig using auxiliary steam at low loads. At higher loads, when leak off from pressure packings is more than that required by vacuum packings, the excess is discharged to the gland condenser. The gland condenser returns seal leak off to the condenser as condensate. Noncondensable gasses are discharged to the atmosphere by the gland exhauster.

The gland steam seal system for each Unit can receive steam directly from its corresponding main steam system or via the auxiliary steam system.

10.4.3.3 Safety Evaluation

The system can be used during reactor cooldown following a turbine-generator or reactor trip when the main steam is bypassed to the condenser. The turbine gland seals can be supplied with the low-pressure steam generated in the steam generators during reactor cooldown. However, in the event that the turbine gland sealing system is not operable, it is possible that the bypassed steam is not condensed due to accumulation of inleaking air in the main condenser. This is considered as a main condenser failure, and safe shutdown of the reactor in such an event is discussed in subsection 10.4.1.

The condensable gases and vapor mixture discharged to the atmosphere by the steam packing exhauster fan are not normally radioactive. However, in the event of primary to secondary system leakage due to a steam generator tube leak, it is possible for the mixture discharged to be radioactively contaminated. A full discussion of the radiological aspects of primary to secondary system leakage, including anticipated releases from the turbine gland sealing system and limiting conditions for operation, is included in chapter 11.

10.4.3.4 Tests and Inspections

The system will be tested in accordance with written procedures during the initial testing and operation program. Because the gland sealing system is in constant use during plant operation, the availability and performance of all components is evident to plant operators.

10.4.3.5 Instrumentation Applications

A pressure controller is provided to maintain the gland seal steam pressure. In case of high pressure, the pressure controller signal opens the steam packing unloading valves and excess steam is bypassed to the main condenser. During startup or in case of low gland seal steam pressure, the controller signal opens a pressure-reducing valve to supply steam from the main steam line or the auxiliary steam system.

Local and remote indicating and alarm devices are provided, as required, for monitoring the system.

10.4.4 TURBINE BYPASS SYSTEM

The turbine bypass system, shown in drawings D-175033, sheet 1, D-175033, sheet 2, D-170114, sheet 1, D-170114, sheet 2, D-205033, sheet 1, D-205033, sheet 2, and D-200007, bypasses main steam directly to the main condenser during the transient conditions of a sudden

load rejection by the turbine-generator or a turbine trip and during plant startup and shutdown. The system is not an engineered safety features (ESF) system.

10.4.4.1 Design Bases

The turbine bypass system is designed with a capacity to bypass up to 40 percent of the full-load main steam flow directly to the main condenser. The system thus provides an artificial load on the reactor coolant system during the transient conditions of a sudden load rejection by the turbine-generator or a turbine trip.

The capacity of the turbine bypass system, combined with the 10-percent step-load change characteristics of the reactor, provides the capability of accepting a sudden load rejection of up to 50 percent without reactor trip or operation of the spring-loaded safety valves or power-operated relief valves.

In the event of a load rejection above 50 percent, the reactor will trip and the turbine bypass system will bypass up to 40 percent of full-load main steam flow to the main condenser. Operation of the power-operated relief and the spring-loaded safety valves will prevent system pressure from exceeding design pressure of the main steam supply system.

The system is also used to bypass steam to the main condenser during plant startup and to remove residual heat from the reactor core during the initial cooling period after plant shutdown by bypassing the steam to the main condenser.

The turbine bypass system piping is designed to Seismic Class II requirements and in accordance with ANSI B31.1.0. The design pressure rating is the same as for the main steam supply system as described in section 10.3.

The turbine bypass system is Safety Class NNS.

10.4.4.2 System Description

The turbine bypass system is shown in drawings D-175033, sheet 1, D-175033, sheet 2, D-170114, sheet 1, D-170114, sheet 2, D-205033, sheet 1, D-205033, sheet 2, and D-200007. The turbine bypass piping branches off from the main steam crosstie piping with a 26-in. header which breaks down into eight 12-in. lines with a condenser dump valve located in each. Downstream of the dump valves, the eight 12-in. lines combine into four 18-in. lines before entering the condenser.

During modulating service, the eight dump valves open two at a time in sequence, with equal flow always going to each condenser shell. This allows fine control of flow and an even heat distribution throughout the condenser. On a large step-load reduction or plant trip, the valves will all open within 3 s after receiving a trip open signal. The condenser dump valves will fail closed automatically with instrument air failure, loss of condenser vacuum, or loss of circulating water pumps.

The steam dump valves reduce the main steam line pressure to a maximum of 250 psia before the steam enters the condenser. These valves are capable of going from full closed to full open within 3 s after receiving a trip open signal, and of going from full open to full closed within 5 s after deenergization of their solenoid valves. The valves can also be positioned automatically to pass required flows during modulating service resulting from a gradual steam supply load change. The valves will fail closed on loss of instrument air.

The maximum capacity of each of the eight dump valves is 890,000 lb/h with an inlet pressure of 1100 psia.

10.4.4.3 Safety Evaluation

The steam bypassed to the main condenser is not normally radioactive. However, in the event of primary to secondary leakage due to a steam generator tube leak, it is possible for the bypassed steam to become radioactively contaminated. A full discussion of the radiological aspects of primary to secondary leakage is contained in chapter 11.

The turbine bypass system protects the reactor by maintaining an artificial load on the reactor coolant system during a turbine trip or a sudden load rejection. In the event the bypass system is not operable because of failure of the main condenser or system malfunction, the spring-loaded safety valves and the power-operated relief valves on the main steam lines will discharge the required amount of steam to the atmosphere to effect a safe reactor shutdown and prevent system pressure from exceeding design pressure of the main steam supply system.

The dump system is not essential to the safe operation of the plant. However, it is required to give the plant flexibility of operation and a controlled cooldown.

10.4.4.4 Tests and Inspections

Before placing the system in service, the dump valves will be tested to confirm opening and closing times, and all foreign material and loose oxides will be removed from the piping.

As the valves are subjected to modulating control, maintenance is quite possible, and isolation valves are provided for each control valve.

10.4.4.5 Instrumentation Applications

The dump system during normal operating transients for which the plant is designed is automatically regulated by the reactor coolant temperature control system to maintain the programmed coolant temperature.

Reactor coolant temperature is controlled by a programmed load temperature relationship. Turbine impulse chamber pressure establishes the programmed load temperature.

During a load variation, there will be a deviation between the reactor and turbine outputs. Turbine steam flow and impulse chamber pressure will change with load. Steam generator steam flow and, therefore, pressure will also change. This will result in a change in heat transfer due to the change in steam pressure from the reactor coolant to the steam generator water. There will be a corresponding change in reactor coolant temperature resulting from the transient. Reactor coolant actual temperature will deviate from the programmed temperature derived from the turbine impulse chamber. The magnitude and rate of change of the deviation will depend on the transient.

A signal derived from turbine impulse chamber pressure establishes a rate of load change and unblocks the dump control, provided there is no other block signal (such as loss of condenser vacuum) present.

Reference T_{avg}, derived from impulse chamber pressure, and T_{avg} actual signals are used to activate the control rods and steam dump system. These signals select the number and mode of operation of the dump valves.

On large step-load reductions or plant trip, the valves open rapidly in 3 s. During the 3-s period, while the turbine valves are closing and dump valves are closed, there is a pressure rise in the nuclear steam supply system (NSSS). In the initial part of a large step-load transient, all dump valves are fully open. Then the valves are modulated closed at a design load change in the reactor of 5 percent per minute. The valves are fully closed when the reactor power matches the turbine power.

Steam system header pressure is used when the plant is at no load. The control signal is derived from a point in the steam piping between the steam generator valves and turbine valves.

10.4.5 CIRCULATING WATER SYSTEM

10.4.5.1 Design Bases

The objective of the circulating water system is to provide the main condenser with the continuous water supply required to remove the heat load rejected to the main condenser.

All pumps in the circulating water system are designed and constructed in accordance with the standards of the Hydraulic Institute. The piping of the system is designed in accordance with ANSI B31.1.

The cooling towers are designed and constructed in accordance with all applicable regulations and codes.

All components of the circulating water system are designed to meet Category II Seismic requirements.

10.4.5.2 System Description

This system, shown in drawings D-170119, sheet 9, D-170119, sheet 10, D-200013, sheet 6 and D-200013, sheet 7, circulates water from the cooling tower basins, through the main condenser, and back through the cooling towers. The systems are basically identical for Units 1 and 2.

There are two circulating water pumps, each rated at 327,200 gal/min and 70 ft TDH, which are housed in a separate structure between the turbine building and cooling towers. Fixed screens located at the pump intake structure prevent possible debris from entering the pumps. The circulating water system is treated as necessary to control organic fouling.

The circulating water system is constructed of open concrete flumes, reinforced concrete pipe, large diameter steel pipe, rubber expansion joints, and butterfly valves.

System makeup water is supplied by utilizing the service water discharge flow from the turbine building, auxiliary building, containment, and diesel heat exchangers as shown in drawings D-170119, sheet 2 and D-200013, sheet 8.

Motor-operated butterfly valves which can be operated locally are provided at the discharge of the circulating water pumps and at the inlets and outlets of the condenser.

10.4.5.3 Safety Evaluation

The circulating water system is normally used to supply cooling water to the main condenser to remove residual heat from the reactor coolant system during the initial cooling period of plant shutdown when the main steam is bypassed to the condenser. However, if the circulating water system fails to supply cooling water due to either failure of circulating water pumps, cooling tower, or circulating water piping, the bypassed main steam cannot be condensed in the main condenser. This is considered a condenser failure and safe shutdown of the reactor in such an event is discussed in subsection 10.4.1.

Passage of condensate from the condenser to the circulating water system through a condenser tube leak is not considered possible during operation since the circulating water system will be at a greater pressure than the condenser and any leakage will be into the condenser.

In the event of a rupture of the circulating water piping or condenser water boxes which would cause flooding in the turbine building, the system provides no automatic means of shutting off the circulating water pumps. If the total volume of the circulating water system (including the water in the cooling tower basin, circulating water pump wet pit, the canals leading from the cooling towers to the pump wet pit, the risers at the cooling towers, and the water in transit in the cooling towers), plus a 10-min supply of the 20,000 gal/min makeup from the service water system normally added to the circulating water system to replace the cooling tower losses, were discharged into the turbine building, the water level would reach el 149 ft 0 in. in Units 1 and 2 approximately 6 ft below grade. There are no passageways, pipe chases, cableways, or other flow paths below this elevation leading to other spaces containing essential systems and

components. Since there are no essential electrical trains or safety-related equipment located within the turbine building, a circulating water system failure of this nature and extreme magnitude would not damage any systems necessary for safe shutdown of the plant.

There would be no damage to other plant structures in the unlikely event of collapse of the cooling towers.

10.4.5.4 Tests and Inspections

System components will be tested and inspected during preoperational activities to ensure proper operational integrity.

10.4.5.5 Instrumentation Application

The circulating water pumps are arranged for manual startup and shutdown using a control switch located in the control room.

The circulating water pump and discharge valve motor controls are provided with an interlock to assure that the pump motor will start with the discharge valve in the closed position. As the pump motor is started, the discharge valve motor operator will be energized by a relay in the pump motor control circuit. After a time delay, the pump motor will be automatically tripped if the discharge valve fails to open. Adjacent pumps and associated discharge valves will not be interlocked; however, when a pump is shut down, the discharge valve will automatically close and remain closed unless manually opened by operator action.

Indicating lights are provided in the circulating water pit to indicate open and closed positions of the circulating water pump discharge motor-operated butterfly valves.

Pressure indicators are provided at the inlet of each condenser shell. Local and remote indicators are provided for circulating water temperature at the inlet and outlet to each condenser shell.

10.4.5.6 Chemical Treatments

Chemicals are added as necessary to the circulating water system to control corrosion, deposition, and biofouling and to improve the cooling tower efficiency.

Addition rates and blowdown rates are controlled to ensure that the chemicals discharged to the river via the cooling tower blowdown meet the criteria of the National Pollutant Discharge Elimination System (NPDES) permit, as issued by the State of Alabama. Treatment chemicals may be added by the following methods:

A. Direct addition to the circulating water.

B. Direct application to cooling towers.

C. Addition to the service water system (circulating water makeup).

The blowdown rate may be varied or periodically terminated provided the solids content of the circulating water is maintained within acceptable limits.

The blowdown flow is diluted with plant cooling water discharge which is in excess of that required for makeup to the circulating water system (approximately 10,900 gal/min).

A circulating water sample is analyzed periodically to determine the chemistry of the circulating water. Adjustments to the chemical feed are based on sample analysis to maintain the residuals within acceptable limits.

10.4.6 CONDENSATE AND FEEDWATER RECIRCULATION AND CLEANUP SYSTEM

10.4.6.1 Design Bases

The objective of the condensate/feedwater recirculation and cleanup system is to provide recirculation and cleanup capability for the condensate/feedwater system prior to startup of the plant following an extended plant shutdown.

The components of the system located in the auxiliary building are constructed to meet Seismic Category I requirements and the components of the system located outside auxiliary building and inside the turbine building are constructed to meet Seismic Category II requirements.

The piping of the system is designed in accordance with ANSI B31.1.0. The piping and miscellaneous components are designed for 9,750 gal/min. The design flow of one condensate pump is 9,680 gal/min at 1,120 ft.

10.4.6.2 System Description

The condensate and feedwater recirculation and cleanup system is shown on drawings D-200011, sheet 1; D-200011, sheet 2; D-200011, sheet 3; and D-205073.

The system for Unit 2 consists of 14-in. piping which ties into the existing feedwater flow control valve bypass lines and recirculates condensate flow to condensers A and B. This system is no longer applicable to Unit 1.

One condensate pump is used to pump condensate from the hotwell of the condensers through the condensate/feedwater system and back to the condensers via the recirculation line.

10.4.6.3 Safety Evaluation

This system is operated only during modes 5 and 6 of plant operation. The isolation valves to the steam generator feed regulators and steam generator feed regulators bypass loop are closed during operation of this system. The closure of these valves diverts the condensate flow from the feedwater piping through the recirculation line and to the condensers. Since the isolation valves are closed during modes 1 through 4 of plant operation, these modes are not affected by the existence of the recirculation/cleanup system. Because the system operates only during modes 5 and 6, the system is not essential to the safe operation of the plant, and the basic function of the existing condensate/feedwater system is not affected.

The structural integrity of the system is such that it is compatible with and does not compromise the structural integrity of the existing condensate/feedwater system. That is, the system is designed to Seismic Class I for the portion of the system located in the auxiliary building and down-graded to Seismic Class II for the portion of the system located in the turbine building since no Seismic Class I system would be compromised due to the structural failure of the system.

The design of this system incorporates the appropriate criteria such that it is consistent with the plant safety analysis.

10.4.7 CONDENSATE AND FEEDWATER SYSTEMS

10.4.7.1 Design Bases

The condensate and feedwater systems return the condensed steam from the turbine condenser and drain from the regenerative feed heating cycle to the steam generators while maintaining the water inventories throughout the cycle.

These systems automatically maintain the steam generator water level during steady-state and transient operation.

The steady-state flow varies with Unit load as calculated by the turbine heat balances. During steam generator blowdown, the feed flow will be in excess of the heat balance flow by the rate of blowdown. When steam is extracted from the nuclear steam supply system ahead of the turbine cycle for other processes, the condensate and feed systems will recover this process flow and return it to the steam generators.

The pressurized water nuclear steam supply system steam pressure varies with load. The pressure in the steam generators drop with increased thermal output. This characteristic, combined with the lower feed system frictional resistance at lower flow, results in a small increase in total pumping head required from full load to no load. There is sufficient margin allowed above the system required head/flow for feed control, pump wear, design and testing, and system fouling to ensure adequate flow to the steam generators during steady-state and transient operation.

Uniform feedwater temperature to all steam generators is ensured under all operating conditions. A continuous steady feed flow will be maintained at all loads.

Sufficient feedwater storage capacity is maintained within the condensate feed systems to accommodate the mass transfer of fluid due to the expansion and contraction arising from the thermal and pressure effects on steam generator fluid inventory and condensate feed systems during load changes. This will also compensate for loss of fluid from the system during load changes or plant cooldown by atmospheric steam dump.

The feed system from the steam generators, back to and including the first stop and nonreturn valve outside the containment, is Safety Class 2A and Category I Seismic system. This portion of the feed system is an integral part of the auxiliary feed system described in section 6.5. The remainder of the condensate and feedwater systems is Safety Class NNS.

Provision is made for inservice inspection of all piping and components that are Safety Class 2A.

10.4.7.2 System Description

The condensate and feedwater system is shown in drawings D-170117, sheet 1, D-170117, sheet 2, D-170117, sheet 3, D-170117, sheet 4, D-175073, D-200011, sheet 1, D-200011, sheet 2, D-200011, sheet 3, and D-205073.

The system is composed of two low-pressure turbines; one twin- shell condenser; three 50-percent condensate pumps; two 50-percent variable-speed, turbine-driven feed pumps; two 50- percent heater drains pumps; two strings of feedwater heaters; two 100-percent steam jet air ejectors; and one turbine gland steam condenser.

The condensate pumps take their suction from the condenser hot well and pump through the air ejector condensers, gland steam condenser, and five stages of low-pressure feed heating to the feed pump suction.

The feed pump discharges through one stage of high-pressure feed heating into a common header. Each of the three steam generators is supplied through a single line taken from the common header.

An ultrasonic feedwater flow measurement system is installed in each of the three feedwater lines just upstream of the existing feedwater flow venturis. The system is comprised of three metering sections for the feedwater lines (each metering section includes two electronic transmitters, two pressure transmitters, 16 acoustic transducers, RTDs [resistance temperature detectors], and a pressure port), and the system includes two Processing Units, and instrument cables for each transducer in the system. The ultrasonic flow measurement system provides high accuracy mass flow, feedwater temperature and feedwater pressure signals to the plant computer system via a digital communication link. These signals are utilized as inputs to the secondary power calorimetric calculation performed by the plant computer.

The individual steam generators are supplied with feed regulators and flow elements. A bypass loop containing a feedwater bypass control valve is installed in parallel with the main feed regulator for each steam generator.

To allow plant maintenance, bypasses are provided around feed heaters. The bypass around the final feed heater joins the common steam generator feed header to ensure adequate mixing and equal temperature feed to the individual steam generators.

As the plant is designed for condenser dump only and 50-percent load rejection without reactor trip, no fluid loss to the atmosphere is considered while the main feed system is operating. The feed pump turbines exhaust into the main condenser. On loss of the condenser vacuum or main feed system, the plant will trip; maintaining steam generator inventory is no longer a requirement for the main feed system. Under these circumstances, the auxiliary feed system takes over. Sufficient water is stored in the condenser hot well to make up system fluid inventories on a 50-percent load rejection. The makeup pipe between the condenser and condensate tank is sized to provide flow to make up fluid inventory during a ramp load change of 5 percent per minute.
Uniform feed temperature to all steam generators is assured by the length and routing of the common feed header after the high-pressure heater bypass.

10.4.7.3 Safety Evaluation

All pieces of major equipment in the condensate and feedwater systems are bypassed so that their individual failure will not affect the basic functions of the systems. If multiple pump failures or loss of ac power results in loss of feedwater flow, the reactor will trip and the auxiliary feedwater system will provide feedwater to remove the residual heat.

Major breaks in the condensate and feedwater systems would cause flow and pressure losses great enough to trip the reactor. Upon reactor trip, the feedwater control valves and the feedwater bypass control valves will automatically close and the auxiliary feedwater system described in section 6.5 will supply the feedwater necessary to insure a safe reactor shutdown.

During normal operation, condensate and feedwater contain no radioactive contaminants. However, in the event of primary to secondary system leakage due to a steam generator tube leak, it is possible for the condensate and feedwater to become radioactively contaminated. A full discussion of the radiological aspects of primary to secondary leakage, including anticipated operating concentrations of radioactive contaminants, means of detection of radioactive contamination, anticipated releases to the environment, and limiting conditions for operation, is included in section 11.3.

Samples of the condensate and feedwater are taken from condenser hot wells, condensate pump discharge, feedwater line to the steam generators, and steam generator blowdown lines; they are analyzed as described in subsection 9.3.2, Process Sampling System, to control the quality of the condensate and feedwater. Samples from the steam generator blowdown lines are analyzed to detect radioactivity.

As a result of water hammer associated with feedwater flow instabilities at operating pressurized water reactors (PWRs), efforts have been initiated to identify the causes of water hammer and to determine its effect on the Farley feedwater system. As a result of the early efforts in this program, the Farley feedwater piping was modified to minimize the length of the horizontal run of piping attached to the steam generator feedwater nozzle. Figure 10.4-1 shows the piping modification.[a] The dotted line shows the original layout, which consisted of approximately 9 to 13 ft of horizontal piping between the steam generator nozzle and the 90-degree elbow. The current layout, shown as the solid line, utilizes a 45-degree elbow immediately adjacent to the 16-in. x 14-in. reducer which connects directly to the steam generator nozzle.[b]

Indications based on our efforts to date are that these modifications have reduced the energy which would be associated with a postulated water hammer by a factor of about 2-1/2 to 4, on a relative basis. Likewise, the peak pressure which would be associated with a postulated water hammer is estimated to have been reduced by approximately 20 percent , again on a relative basis.

10.4.7.4 Tests and Inspections

The feedwater stop valves, control valves, and bypass control valves are tested in accordance with the Technical Specifications and the Inservice Testing Program.

All foreign material and loose oxides will be removed from the piping prior to plant operation.

All of the components of the system will be continually monitored during operation to ensure satisfactory operation.

10.4.7.5 Instrumentation Applications

The steady-state steam generator water level is controlled by the feedwater control valves. In steady-state, the feedwater control valves (one for each steam generator) adjust the individual water levels and compensate for different pressure drops through the steam generators, feedwater, and steam pipes resulting from different piping layouts. Steam generator water level control at low-power levels is achieved by a feedwater control valve installed in a parallel loop around the main feedwater control valve for each steam generator.

---

a. For all Units except 2B.

b. Figure 10.4-2 shows the piping modification for steam generator 2B feedwater line. This unit's feedwater line utilizes a 45-degree elbow down and a 90-degree bend to the horizontal immediately adjacent to the 16-in. x 14-in. reducer. This results in a horizontal run of about 12 ft of pipe whose top is 6.5 in. below the bottom of the horizontal section connected to the steam generator nozzle.

Since the feed pump speed is variable, the steady-state throttling in the feedwater control valve shares its duty to maintain level with the ability of the speed control system to increase the pump speed and head above the initial steady-state values.

The feedwater control valves and the feed pump speed control are considered as two complementary parts of the feed flow control system, whose purpose is to maintain the level in all steam generators within limits required for safe and continued plant operation.

A large-load reduction is the governing transient in the design of the feed control system. The closing of the turbine governing valve results in a pressure increase and a level decrease in the steam generators. To limit this level decrease, the feed flow should be increased. The increased pressure results in a decreasing flowrate from the feed pumps as long as the valves position and the pump speed remain unchanged.

To minimize the duty of the valve, the control system increases the speed of the pump so that the pump discharge pressure increases at least as much as the pressure in the steam generator. To achieve this, the pressure difference between feed header (after the last heater) and steam header is used as a control variable and is compared with a setpoint in order to generate a pump speed signal.

The feed pump speed control system consists of the following three interrelated parts:

A. The setpoint calculators which sum the three steam flows and contain the basic scaling adjustments.

B. The differential pressure controller (board mounted) which compares the steam header pressure, feedwater header pressure, and the calculated setpoint to determine the speed signal required.

C. The feed pump manual/auto stations (board mounted, one per pump) which provide the operator with the flexibility of choosing various operating modes.

Instrumentation, including pressure indicators, flow indicators, and temperature indicators, are provided in the control room to monitor the system.

10.4.8 STEAM GENERATOR BLOWDOWN PROCESSING SYSTEM

As part of the comprehensive steam-side chemistry control program employed in this plant, the steam generator blowdown processing system functions to eliminate harmful concentrations of chemical deposits from accumulating in the steam generators.

The effluents from the secondary side of the steam generators are normally dispersed to the environment following dilution with cooling tower blowdown water.

In the event the secondary side becomes contaminated with primary-side coolant, the blowdown processing system conditions the water such that it can be reused on the secondary side, and collects the radioactive contaminants and other solids for offsite disposal.

The use of multiple forms of instrumentation to detect primary/secondary leakage and the use of the steam generator blowdown processing system are provided to assure that the public health and safety is not compromised.

10.4.8.1 Design Bases

Secondary-side water chemistry control specifications require a minimum of 5 gal/min blowdown from each steam generator to achieve optimum effectiveness from the steam generator chemistry control program.

The steam generator blowdown processing system is designed to accommodate blowdown under a wide range of conditions.

Under conditions of steam generator tube leakage and/or condenser leakage, a continuous blowdown rate of 12.5 gal/min maximum per generator may be required to maintain proper chemistry control in the generator. The design basis of the processing portion of the blowdown processing system is 50 gal/min total. This permits 12.5 gal/min continuous blowdown for each generator plus some additional capacity as margin.

To facilitate the removal of any accumulated solids from the tube sheet when no tube leaks exist, the system is designed to accommodate, through the bypass portion of the system, an intermittent blowdown rate of 50 gal/min per generator or 150 gal/min total. If solids removal is required coincident with steam generator tube leakage, the processing system can accommodate only one steam generator blowing down at the maximum rate.

Processed system effluent will ordinarily be released to the environment. The system is also designed to permit recycling of processed steam generator blowdown to the main condenser. The average discharge concentration will not exceed 2×10^{-8} $\mu Ci/cm^3$.

Sampling of blowdown fluid for radioactive elements will be based on the criteria presented in subsection 11.4.3. Sampling of blowdown fluid for secondary-side chemistry control purposes will be performed on a once-per-day basis.

The blowdown processing equipment is located in the auxiliary building. The ventilation system for this building is designed to provide temperatures not exceeding 110°F during the summer, which is well below the temperature limitations for this equipment.

The system is not essential to nuclear plant safety downstream of the blowdown isolation valves; therefore, the various components of the system are classified NNS and will be designed, fabricated, and tested in accordance with ASME Section VIII. The exceptions are the blowdown isolation valves and the associated piping between these valves and the steam generators. These items are classified ANS Safety Class 2A, and are designed, fabricated, tested, and inspected in accordance with ASME Section III.

10.4.8.2 System Description and Operation

Each reactor Unit has three steam generators and each generator has its own blowdown and sample lines.

The flow of blowdown fluid from each of the three steam generators is individually flowrate-controlled before the blowdown lines are manifolded outside of the containment barrier, as the blowdown requirements for each generator may not be the same. The system flow diagrams are shown in drawings D-175071, sheet 1; D-205071, sheet 1; D-175071, sheet 2; D-205071, sheet 2; D-175071, sheet 3; and D-205071, sheet 3. The flow diagrams show a typical series flow path with all four demineralizers bypassed. Although typically not used, if required, various combinations of two demineralizers, aligned in series, would be utilized as directed by plant procedures to process the blowdown fluid through the demineralizer processing portion of the system prior to being released to the environment. For the purpose of describing system operation, it is assumed that processing is initially not required and the demineralizers are therefore bypassed.

Fluid from the steam generator manifold enters under pressure into a shell and tube heat exchanger, where the fluid temperature is reduced by plant service cooling water. The cooling water flowrate is modulated to maintain a constant blowdown fluid exit temperature. The pressure is then reduced across a pressure control valve to the level required to overcome system resistance. The blowdown fluid is then directed through a radiation monitor and into a surge tank. From the surge tank, the fluid is pumped through a second radiation monitor to the discharge line by the discharge pumps. The rate of discharge is controlled by level instrumentation in the surge tank so that tank level is maintained at a nearly constant level.

For the path described above, the blowdown fluid receives no processing except cooling. In the event activity is transmitted to the secondary side of the steam generator, it will show up in the blowdown fluid. If the activity level is above 1.0×10^{-5} $\mu Ci/cm^3$, the radiation monitor located upstream of the surge tank will alarm in the control room and trip closed the control valve downstream of the heat exchanger, providing automatic isolation of the system. As the surge tank level decreases, the control valve will throttle down the discharge flow, and a low-surge tank level switch will shut off the pumps.

If the first radiation monitor fails to detect the activity, a redundant monitor is located on the discharge side of the surge tank that trips, isolating the system discharge. The system may also be automatically isolated by low service water dilution flow during normal plant operation. Plant procedures allow for bypass of the low dilution flow automatic isolation feature during certain operational conditions, such as plant outages. When system isolation is accomplished by closure of the discharge valve, the pumps are protected by mini flow lines.

The surge tank level will increase until a high-level switch trips, thereby terminating blowdown. Operator action can also shut off the pumps and operate the valves.

For the events described above, an amount of contaminated blowdown fluid may be in the surge tank which is unsuitable for discharge. This fluid can be processed through the processing portion of the system to provide the necessary decontamination to permit discharge.

All subsequent steam generator blowdown will be automatically processed through the processing system.

The processing portion of the system consists of four mixed bed demineralizers, a filter, and instrumentation that provides process-related information used to monitor system performance. After processing, the fluid can be recycled to the main condenser, but may be discharged through the discharge line when required.

The processing system is designed such that it can be operated continuously, if needed, provided the resin beds are periodically renewed. Resin bed exhaustion is detected by periodic sample analysis. Resin beds are normally series aligned with the fresher bed downstream. Sampling analysis may be used to determine the acceptability of using other configurations. Normally, various series combinations of two resin beds are used. If breakthrough of the upstream bed occurs, the downstream bed continues to process the flow. Normally, process flow will then be realigned through one of the other series flow paths available. Spent resin is transferred from the exhausted bed to the spent-resin storage tank and new resin installed as determined by plant scheduling. The new resin is now available as a new downstream bed. The spent resin in the storage tank is transferred to the solidification and dewatering facility as determined by plant scheduling.

The resin is removed from the storage tank by first loosening the resin by applying nitrogen gas to the bottom of the tank through six sparger pipes. The spent-resin sluice pump can also be used to fluidize or loosen the resin by taking water from the storage tank and pumping it back into the bottom of the tank through the six sparger pipes.

Nitrogen gas pressure is then applied to the top of the resin, and it is this pressure head that moves the fluidized resin to its disposal point. The system also incorporates provisions for backflushing the valves and piping with demineralized water or sluice water when this operation is completed.

Each plant unit has its own processing system (demineralizers, filters).

10.4.8.2.1 Component Description

10.4.8.2.1.1 Steam Generator Blowdown Heat Exchangers. One heat exchanger cools the steam generator blowdown before it is discharged from the plant or sent to the demineralizers for cleanup. The heat exchangers are shell and tube design, with blowdown water in the tubes being cooled by service water on the shell side.

10.4.8.2.1.2 Steam Generator Blowdown Inlet Filter. This filter removes particulate matter from the steam generator blowdown fluid before it flows to the demineralizers. This filter assures maximum utilization of the demineralizer resins.

10.4.8.2.1.3 Steam Generator Blowdown Surge Tank. The surge tank collects the blowdown water prior to its being discharged from the system. The tank provides the necessary suction head for the discharge pumps.

10.4.8.2.1.4 Steam Generator Blowdown Discharge Pumps. The horizontal, centrifugal pumps are provided to pump the treated blowdown water from the surge tank to the main condenser, for plant discharge, or to recycle the blowdown water through the demineralizer train. Only one pump is operated normally, with the second serving as an installed spare.

10.4.8.2.1.5 Deleted.

10.4.8.2.1.6 Steam Generator Blowdown Mixed Bed Demineralizer. Four flushable, mixed bed demineralizers are provided in the blowdown treatment system. Exhausted resin beds are replaced based upon periodic sample analysis and plant scheduling.

10.4.8.2.1.7 Steam Generator Blowdown Outlet Filter. This filter removes particulate matter that may be carried over from the demineralizer beds. This protects the discharge pumps and prevents accumulation buildup in the surge tank.

10.4.8.2.1.8 Steam Generator Blowdown Spent- Resin Storage Tanks. These tanks are used to collect and store the spent resin from the steam generator blowdown demineralizers until it is transferred to the solidification and dewatering facility.

10.4.8.2.1.9 Steam Generator Blowdown Spent-Resin Sluice Pump. This canned, centrifugal pump is provided to sluice the spent resin from the demineralizers to the spent-resin storage tanks. The pump draws water from either spent-resin storage tank through a screen and directs it to the demineralizers. A resin slurry is formed and directed to the spent-resin storage tank.

10.4.8.2.1.10 Steam Generator Blowdown Sluice Filter. This filter removes resin fines from the sluice water flow directed to the demineralizers.

10.4.8.3 Design Evaluation

10.4.8.3.1 Radioactivity Discharge Rates

When operating without steam generator leakage or when the system effluent is being recycled back to the main condenser, there will be essentially zero release of radioactivity from this system. When the system effluent is discharged to the environment while operating with concurrent fuel defects and steam generator leakage, radioactivity discharge rates will depend on the combinations of these parameters which are assumed. The system is designed to limit

average discharge concentrations under these conditions to 2 x 10^{-8} $\mu Ci/cm^3$ or less. This average has been taken as being the average quarterly and the average annual discharge concentration for release to the environment. For the conditions of 20-gal/day steam generator leakage and 0.2-percent fuel defects, the average discharge concentration will be considerably below the above limits (~1.1 x 10^{-9} $\mu Ci/cm^3$). If conditions of higher tube leakage are postulated, the system could meet the average quarterly release limits, assuming 2 months of operation at 20-gal/day steam generator leakage at 1-percent fuel defects, and 1 month of operation at 144-gal/day steam generator leakage at 1-percent fuel defects. Following this period, the plant would require shutdown for steam generator tube repair if such were the case.

The radiological evaluation analysis for normal operating conditions is given in subsection 12.1.6.

10.4.8.3.2 Failure Analysis of Components

The blowdown processing system can be isolated by the action of two isolation valves activated by two separate radiation monitors. Sample points located throughout the system can be used as a means of checking the activity level in the blowdown fluid if necessary.

Piping and valving inside and outside containment to the containment isolation valve are designed and fabricated to ANS Safety Class 2A requirements. As this system performs no function related to safe shutdown of the plant, all components downstream of the containment isolation valve are classified as NNS Safety Class. The rupture of components downstream of the containment isolation valve will generally require shutdown of the plant.

10.4.8.3.3 Analysis of Shell-Side Radioactivity Concentration During Blowdown Processing System Isolation

The operation criteria for the secondary-side blowdown system are dictated by the need for limiting the secondary-side buildup of dissolved solids.

Hence, it is unlikely that the plant may operate with the blowdown system isolated. However, assuming system isolation coincident with 1-percent fuel defects and 144-gal/d primary-to-secondary-side leakage, the secondary-side activity will build up to approximately 5 x 10^{-2} $\mu Ci/cm^3$ in one 24-h period.

10.4.8.4 Tests and Inspections

Periodic tests and recalibration will be required on the radiation monitors in the blowdown processing system as described in the technical specifications. Periodic tests of the blowdown isolation valve functioning will be performed to check operability. Periodic visual inspections and preventive maintenance can be conducted as necessary when all components are available for inspection.

10.4.8.5 Safety Evaluation

The limiting conditions for operation and surveillance requirements for secondary water monitoring as defined in the Farley Technical Specifications assure that steam generator tube integrity is not reduced below an acceptable level for adequate margins of safety.

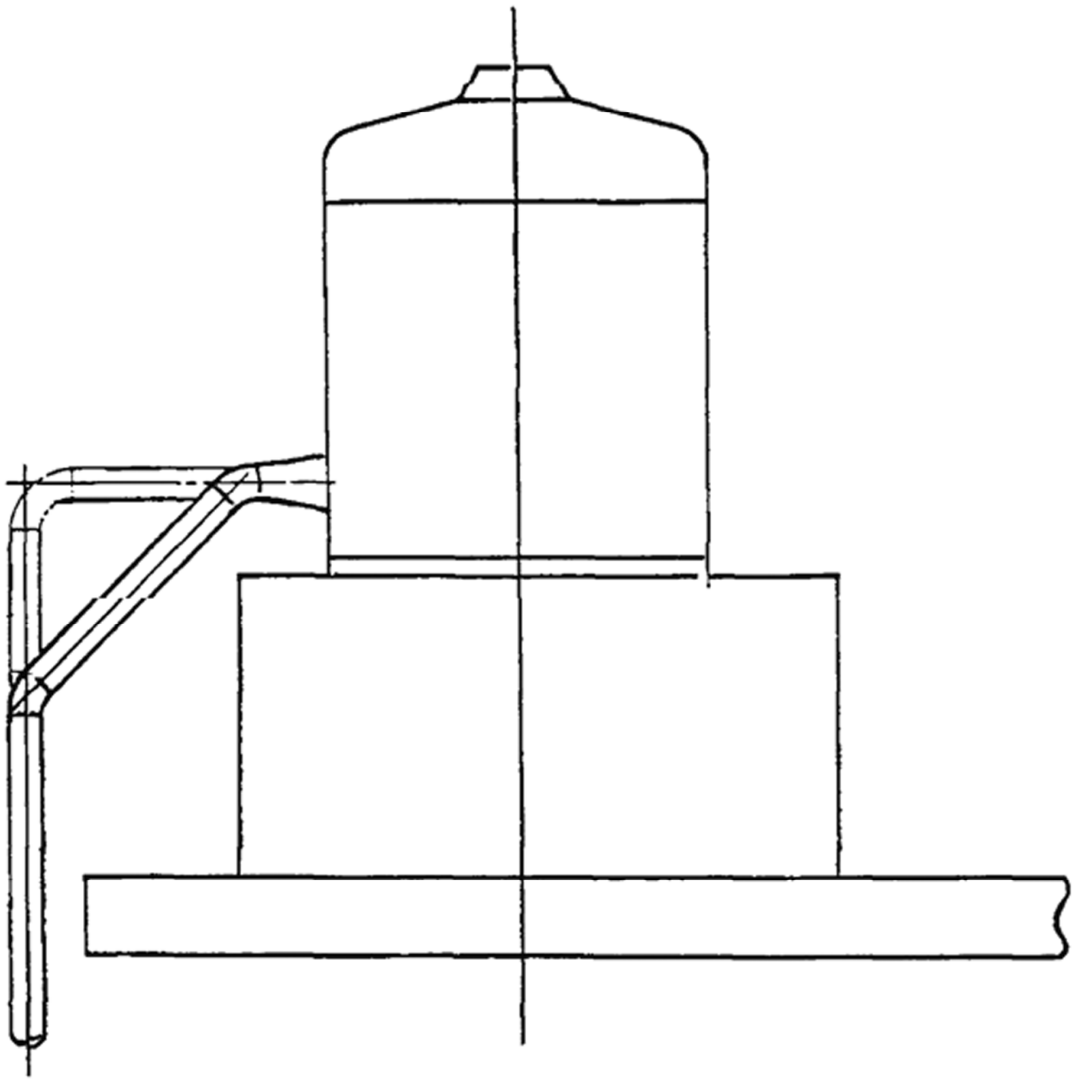

13

REV 21 5/08

SOUTHERN COMPANY
Energy to Serve Your World©

JOSEPH M. FARLEY
NUCLEAR PLANT
UNIT 1 AND UNIT 2

STEAM GENERATOR 1A, 1B, 1C, 2A,
AND 2C FEEDWATER CONNECTION

FIGURE 10.4-1

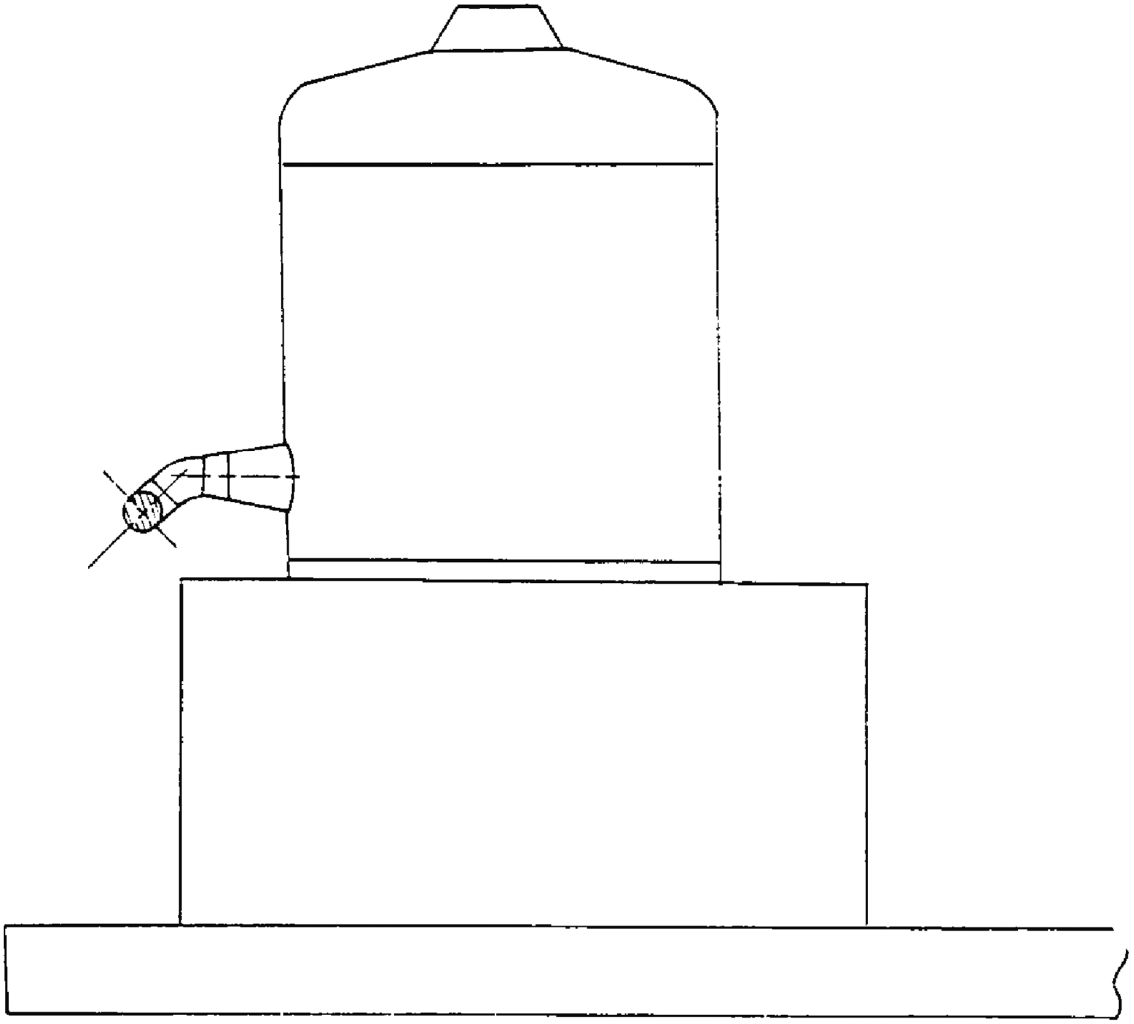

13

REV 21 5/08

SOUTHERN COMPANY
Energy to Serve Your World®

JOSEPH M. FARLEY
NUCLEAR PLANT
UNIT 1 AND UNIT 2

STEAM GENERATOR 2B
FEEDWATER CONNECTION

FIGURE 10.4-2

APPENDIX 10A

DYNAMIC ANALYSIS OF MAIN STEAM SWING DISC TRIP VALVE FOR FAULTED CONDITIONS

TABLE OF CONTENTS

TABLE OF CONTENTS

LIST OF TABLES

LIST OF FIGURES

LIST OF FIGURES

LIST OF FIGURES

APPENDIX 10A

DYNAMIC ANALYSIS OF MAIN STEAM SWING DISC TRIP VALVE FOR FAULTED CONDITIONS

10A.1 INTRODUCTION

Prior to performing the closure impact analysis described herein, Teledyne Materials Research (TMR) performed two preliminary closure impact analyses for the disc of a main steam swing-disc trip valve intended for service in the Joseph M. Farley Nuclear Plant. In both of the preliminary analyses, it was conservatively assumed that the valve body would remain rigid during impact. The objective of the preliminary analyses was to demonstrate the structural adequacy of the disc before proceeding with a more comprehensive analysis in which the valve body would be allowed to deform. The assumption of a rigid valve seat was considered to yield a conservative evaluation of the disc because of the implied requirement that the kinetic energy stored in the disc and swing arm would be dissipated solely through plastic-strain energy absorption in the disc. This report contains the final analysis in which both the disc and the body are allowed to deform during the closure impact.

Large impact-induced strains in the disc were predicted on the basis of the conservative results of the first preliminary analysis. This led to a decision to substitute a more ductile material for the disc. For this reason, the A516 Gr. 70 steel disc considered in the first preliminary analysis was replaced by a type 304 stainless steel disc in the second preliminary analysis. The choice of type 304 stainless steel was justified on the basis of available high-strain rate tensile test data for the temperature of interest (600°F). Data presented in reference 2 reveals that the material had excellent ductility at strain rates as high as 100 s^{-1}, both in terms of the uniform elongation at ultimate stress and the reduction of area at fracture. Therefore, this material was considered to have excellent energy absorption characteristics for impact conditions. Another consideration in the selection of the stainless steel was the ability to construct stress-strain diagrams for various rates of straining by means of information available from reference 3. This information originated from the same testing program described in reference 2.

To reduce the high strains predicted in the first preliminary analysis for the disc rim region, a disc geometry modification was introduced prior to performance of the second preliminary analysis. The modification consisted of adding material to the backside of the disc in the rim region. Because the material change and geometry change were made simultaneously, it was not possible to determine to what degree the geometry change was effective toward reducing high local strains in the contact region. However, the geometry change, if nothing more, reduced the shear strains averaged across the disc thickness. Therefore, the ability of the redesigned disc to resist gross shearing at the internal seat diameter was improved.

The final analysis reported here is an axisymmetric simulation of the problem. That is, the structure was modeled axisymmetrically and the swinging motion of the disc was replaced by a translational motion. The problem was solved for a disc impact velocity of 150 ft/s. This velocity was obtained by equating the kinetic energy of the translating disc to that of the swinging disc.

A pressure of 705 psig was assumed to act on the upstream side of the disc for the duration of the impact event and the temperature of the valve was assumed to be 600°F.

The computer program used for the final analysis of the impact problem under faulted conditions was the PISCES code. This Lagrangian finite-difference code permits the dynamic response of a structure to be analyzed as a function of time under conditions of substantial plastic deformation and gross geometric distortion.

Strain criteria are introduced in the report for evaluating the results of the impact analysis. On the basis of testing the results against these criteria, it is concluded in section 10A.2 that the valve body and disc are structurally adequate to withstand the postulated faulted-condition event.

To acquaint the reader with the general appearance of the valve under consideration, a sketch of the longitudinal cross-section is shown in figure 10A-1. The figure was obtained by tracing Atwood and Morrill drawing No. 21261-H and shows the disc in the closed position. Under normal operating conditions, the disc will be fully open and steam will flow from left to right. As indicated on figure 10A-1, the downstream and upstream surfaces of the disc will be referred to as the front surface and back surface, respectively.

Figure 10A-1 shows the component configurations considered for the final analysis reported herein. With this design, the disc is subjected to a concentrated load at its center at the time of impact. This load is due to the inertia of the disc arm, post, and nut. For the purpose of analysis, a conservative approach was taken whereby the kinetic energy in the disc arm was forced to be dissipated through plastic deformation of the disc and body. As discussed later, this was accomplished by adding the kinetic energy of the disc arm to the kinetic energy of the disc through an increase in the density of the material near the center of the disc.

Following completion of the analysis reported herein, the disc arm was redesigned to the configuration indicated in figures 10A-2 and 10A-3. For the redesigned disc arm, the kinetic energy of the arm is transferred to the disc via four points located along the disc rim. The modified arm design results in less severe disc loading than that presented in this report. Consequently, the analysis performed in the original arm design (as shown in figure 10A-1) may be viewed as a conservative evaluation for the modified disc arm design.

Table 10A-1 shows the nomenclature used in the report.

10A.2 SUMMARY AND CONCLUSIONS

The complete impact analysis of the disc required two tasks. Fluid dynamics were used to calculate the forces on the disc and the disc closing velocity (attachment D). The impact analysis was based on converting the angular velocity calculated in attachment D to an equivalent uniform translational velocity and evaluating the impact response by means of an axisymmetric representation of the disc and valve body.

10A.2.1 SUMMARY OF FLUID DYNAMICS RESULTS

Addendum 8 to Bechtel Inquiry SS-1102-32 (reference 1) specifies the initial steam pressure and quality for the two cases of main steam flow conditions to be considered in the swing-disc, trip-valve closure analysis. Denoting these as cases 1 and 2, the fluid flow states vary between saturated steam in case 1, and 4-percent quality steam in case 2. The flow conditions for case 1 and case 2 are outlined in attachment D.

The elapsed time from pipe break detection to dump valve actuation is 0.5 s, and an additional 1.0 s is required for the air cylinder to depressurize from the nominal 100-psig pressure to the disc balance pressure. During this 1.5-s delay, the 32-in. main steam line blows down and outflow is established by the upstream flow restrictor. Thus, the disc is not exposed to the initial blowdown through the 32-in. pipe.

Atwood and Morrill weight and center of gravity data were used to compute a moment of inertia for the disc assembly. Relations for the torques acting on the swing disc were formulated, including those due to gravity, pressure, and the closing spring. Also considered was a constant shaft counter torque due to gland packing friction and based on Atwood and Morrill data.

A calculation was made to determine the choking angle across the disc at which the dihedral area between the disc plane and the plane of the valve seat is exactly equal to the flow area across the valve seat. The choke angle was computed as 24.5 degrees, measured from the valve seat.

In computing flow conditions across the valve, the conservative assumption was made that the break occurs just downstream of the valve, resulting in a choked-flow condition across the valve seat. This determined the flow velocity to which the disc was subjected. A dynamic analysis of the disc motion was conducted for five angular segments between the normal "open" position (65 degrees) and the closed position. The net torque acting on the disc was computed for each included angular segment, and the results were used to solve the equations of motion. Included in each calculation were ΔP, torque (T), α, ω, Δ, and Σt.

Upon onset of choking at θ = 24.5 degrees, a static pressure of 995 psia was taken at the back of the disc. A critical pressure ratio of 0.578 applied to this yielded a valve throat pressure of 575 psia, and a ΔP across the disc of 419.9 psid. This pressure differential was held constant during the remaining 24.5 degrees of disc travel to impact. To account for the steam hammer specified for cases 1 and 2, the steam hammer was averaged with ΔP of 419.9 psid over the last 10 degrees of disc travel to impact, and the result then used in the torque calculation.

The results of the fluid flow analysis, as contained in attachment D, indicate a disc center impact velocity of 117 ft/s for case 1 (saturated steam), and a 102.7 ft/s disc center impact velocity for case 2 (x = 4 percent). Closure times were 0.146 s and 0.158 s, respectively.

Using the more conservative case 1 disc center impact velocity, a modified disc center velocity was determined by equating the kinetic energy for the assumed translational rotational mode (KE_t) to the kinetic energy computed for the actual rotational mode (KE_r). As shown in

attachment C, this computation gives the disc center a velocity of V_t = 150 ft/s used in the impact analysis. This approach to the choice of a uniform impact velocity was in accordance with the conservative assumption that the kinetic energy must be dissipated solely through plastic deformation of the valve body and disc.

10A.2.2 SUMMARY OF IMPACT ANALYSIS RESULTS

The dynamic solution formulated in section 10A.3 permitted the structural behavior of the valve under impact conditions to be investigated as a function of time. Both the disc and the valve body were allowed to deform plastically. Pertinent results obtained in the investigation are discussed in section 10A.4. Evaluation of the results against acceptance criteria is the subject of section 10A.5. The following is a summary of key results obtained in the analysis:

A. The duration of the impact event as measured by dissipation of the kinetic energy in the moving parts of the valve is approximately 1300 μs (1.3×10^{-3} s). The dynamic solution covers the first 1150 μs. Extrapolation to 1300 μs produces only minor changes in the results.

B. Following impact at 150 ft/s, the center of the disc continues to accelerate before it slows down. The highest velocity of 180 ft/s is reached 350 μs after impact.

C. Impact of the disc on the body seat results in substantial permanent geometric distortion of the valve, but not in the creation of a steam path past the disc. Consideration of the deformed shape shows rotation of the seating surfaces of both body and disc, as well as large-scale bending in the central portion of the disc. The center of the disc deflects 1.84 in., which is equivalent to a displacement of half the thickness of the disc (3.75 in.).

D. The largest value of the effective strain in the body is 15 percent. Because it is accompanied by a compressive hydrostatic stress state, an effective strain of up to 29 percent is considered acceptable. (Had the hydrostatic stress state been tensile, only 11-percent strain would have been acceptable.)

E. The largest value of the effective strain in the rim region of the disc is 17 percent. This is a localized strain for which an effective strain of 30 percent is considered acceptable (regardless of whether the hydrostatic stress state is tensile or compressive).

F. The largest value of the radial and hoop-bending strains in the disc which occur at the center of the front surface is 8.5 percent for both. Because of the constant volume conditions associated with plastic deformation, the bending strains are accompanied by a strain in the thickness direction of -17 percent. The effective strain for this state of strain is 17 percent. An effective strain of up to 18 percent is considered acceptable by a strain criterion for limiting geometric distortion by bending.

10A.2.3 CONCLUSIONS

A. The impact analysis shows that the body and disc are structurally adequate to withstand the dynamic forces produced by valve closure under the postulated faulted conditions.

B. The axisymmetric method of solution adopted for the dynamic analysis was confirmed as an acceptable analytical approach by the results obtained. That is, a sufficient margin exists between the imposed strain limits and maximum strains computed for the contact region of body and disc to provide protection against any deviations from the computed results attributable to the initially nonuniform impact velocity along the circumference of the disc.

C. The conclusions of A and B above are not invalidated by the redesign of the disc arm which followed the investigation.

10A.3 IMPACT ANALYSIS - FAULTED CONDITIONS

10A.3.1 METHOD OF ANALYSIS

The valve impact analysis reported herein is based on the method of solution incorporated in the PISCES computer code. This code permits the solution of stress-wave propagation problems by solving equations of motion and constitutive equations expressed in finite-difference form. Thus, the code is especially well suited for analyzing the response of structures to impact, and explosion and penetration conditions. Such response normally involves both elastic-plastic deformation of the material and gross distortion of the structural geometry. A solution is generated by calculating the response at each of many small time steps, also called cycles. The magnitude of the time step is automatically calculated within the program by means of a criterion that controls numerical stability.

Printout of the solution is available for any of the time steps. The user of the program preselects the times at which printout is desired. A standard output format is provided, but the user can also develop additional output by writing his own subroutine and appending it to the PISCES code. Because strain components, effective strain, and effective stress are not part of the standard output, TMR developed its own subroutine for the computation and printing of these variables. Plotting routines are available in PISCES for plotting the standard output, but TMR adapted its own plotting routines to PISCES to facilitate plotting of standard and nonstandard output.

References 4 through 6 are the manuals used in generating the PISCES solutions for the valve problem. They may be consulted for additional information on the computer code.

The following units used in the PISCES solutions are needed to interpret the printed and plotted results:

A. Unit of length = centimeter (cm).

B. Unit of time = microsecond (μs).

C. Unit of force = 10^{12} dyn.

D. Unit of pressure = mbar (1 mbar = 10^{12} dyn/cm^2).

E. Unit of mass = (g).

F. Unit of energy = 10^{12} dyn/cm.

Note that 1 psi is equal to 6.89 x 10^{-8} mbar.

10A.3.2 DISC MODEL

The overall disc dimensions used for constructing the PISCES model are given in figure 10A-4. The dimensions are shown in inches and in centimeters, the latter in parentheses. Attention is called to the undercut fillet at A. For reasons explained below, two fillet geometries were investigated. Figures 10A-5 and 10A-6 show the first PISCES model analyzed. The fillet in this model approximates the original design in that the outer radius of the fillet coincides with the inside diameter of the body seat. This coincidence led to computational difficulties with the PISCES code, apparently triggered by the local strain concentration in the disc resulting from indentation of the disc corner by the body seat corner. To circumvent this problem, the fillet geometry was changed to that shown in figures 10A-7 and 10A-8. The modification consists of increasing the outer radius of the fillet by 0.1 in. while leaving the outside diameter of the disc unchanged. As a consequence, the radial dimension of the contact face on the disc is reduced by the same amount, from 1.25 in. to 1.15 in.[(a)]

A dashed outline is used in figure 10A-4 to indicate the configuration of the original carbon steel disc which was considered in the first preliminary analysis. It was mentioned in section 10A.1 that when the disc material was changed from carbon steel to stainless steel, additional material was added to the disc backside to improve the shear strength of the disc. Because the chamfer at B has little bearing on the structural behavior of the disc, it was not included in the PISCES model.

---

a. This modification has been incorporated into the design of the stainless steel disc. After completion of the analysis reported herein, the fillet depth was increased by 0.1 in. The rationale for this later modification is discussed in section 10A.5.

It was mentioned in section 10A.1 that a fictitious higher-density material was assumed to occupy the central portion of the disc. As explained in subsection 10A.3.6, the value of this higher-density material is determined from the imposed requirement that the kinetic energy of the disc post, nut, and disc arm be transferred to the disc on impact. In section 10A.1 it was stated that subsequent to the performance of this analysis, the disc arm was redesigned to add four adjustable points of attachment between the disc arm, and the disc post was redesigned to become an integral part of the discs (figures 10A-2 and 10A-3). The modified disc arm and postarrangement facilitates the field replacement and alignment of the stainless steel disc in the valve body and simplifies the machining of the replacement disc. The modified disc arm design will create a more favorable impact loading on the disc so that the impact analysis reported herein will remain valid.

10A.3.3 BODY MODEL

The valve body has a complex three-dimensional geometry. Considerable geometric simplification was necessary to permit an axisymmetric representation of the body. Modeling was facilitated by the massive proportions of the body relative to the disc so that it could be predicted that plastic deformation would be confined to the immediate vicinity of the seat area. However, even in this region, the geometry is not axisymmetric apart from the seat itself. Therefore, the choice was made to model the body seat region in such a way that it would best simulate the structural response at the location where the impact velocity of the disc is highest during the swing motion.

This choice led to the body geometry seen in figures 10A-5 through 10A-8. The model dimensions are defined in figure 10A-9.

The PISCES model of the body consists of two cylinders of unequal diameters but equal wall thickness separated by a transition region that contains the valve seat. The wall thickness of the two cylinders was made equal to the valve's allowed minimum wall thickness. The most characteristic aspect of the geometry is the feature of having the inside diameter on the downstream side match the diameter of the seat opening. The resulting 90-degree angle between the shell wall and the valve seat is representative of the geometry immediately adjacent to the point of maximum impact velocity mentioned above. This will be evident by comparing the model geometry with the actual geometry sketched in figure 10A-10, obtained by tracing part of Atwood and Morrill drawing No. 21322-F.

Only part of the PISCES model is shown in figures 10A-5 through 10A-8. As indicated on figure 10A-9 the model is 200 in. long, 100 in. each way from the seating surface. This much length was included in the model to assure that elastic stress waves reflected at the ends of the model would not return to the contact region in less than 1000 μs. Based on the preliminary analyses, it had been estimated that the conversion of kinetic energy to plastic-strain energy would, for all practical purposes, be completed in this timespan. To limit the number of zones in the model, a transition from six zones across the wall to two zones was made 12 in. downstream and 5 in. upstream from the seat surface. Moreover, the length of the zones was increased to 10 in. starting at axial positions located 20 in. downstream and 10 in. upstream. At distances this far from the impact surface, the use of zones with an aspect ratio of 10 can be justified on the assumption of uniform wave fronts.

10A.3.4 DISC MATERIAL

The material properties employed for the disc, which are for type 304 stainless steel at 600°F, are summarized below:

A. Elastic Constants

For Young's modulus (E), the value provided in Appendix I of ASME Section III was selected. Poisson's ratio (ν) was assumed to be 0.3, and the shear modulus (G) and bulk modulus (K) were computed from E and ν. Thus,

1. $E = 25.4 \times 10^6$ psi = 1.75 mbar.

2. $\nu = 0.3$.

3. $G = (E/2)/(1 + \nu) = 0.673$ mbar.

4. $K = (E/3)/(1 - 2\nu) = 1.46$ mbar.

B. Stress-Strain Diagram

The Liquid Metal Fast Breeder Reactor Materials Handbook (reference 3) was the source for the stress-strain diagrams for different strain rates shown in figure 10A-11. The pertinent page of the reference cited is included as attachment A. It provides a transcendental equation that gives, as a function of temperature and strain rate, the relationship between the true stress (σ_t) and the true plastic strain (ε_p). The equation is valid to 25-percent strain and strain rates from 10^{-5} to 10^2 s^{-1}. Total true strain (ε_t) may be obtained by adding the elastic strain such that $\varepsilon_t = \varepsilon_p + \sigma_t/E$. The diagram for a strain rate of 10^3 s^{-1} was expected to be encountered in the solution.

The PISCES code permits the use of a bilinear stress-strain diagram together with a specified maximum on stress. Figure 10A-12 defines the diagram used in the analysis. It consists of an elastic portion, a strain-hardening elastic-plastic portion, and a perfectly-plastic portion. It is also superposed on the curves in figure 10A-11 to indicate the reasoning employed in defining figure 10A-12. That is, since the effect of strain rate could not be modeled in the PISCES computer solution, a diagram was selected which would approximate high-strain behavior at large strains and low-strain rate behavior at small strains. Because the yield strength at the low-strain rate of 10^{-5} s^{-1} was less than the specified minimum value in Appendix I of ASME Section III, no downward adjustment of the curve to account for minimum properties was needed.

Denoting the yield stress (or proportional limit), true ultimate stress and tangent modulus in the strain-hardening range by σ_y, σ_{ut} and E_t, respectively, the values of these parameters associated with figures 10A-11 and 10A-12 are:

1. σ_y = 25,000 psi = 1.72 x 10^{-3} mbar.

2. σ_{ut} = 80,000 psi = 5.51 x 10^{-3} mbar.

3. E_t = 0.314 x 10^6 psi = 0.0216 mbar.

C. Ductility Parameters

The results of the PISCES solution will be evaluated on the basis of strain criteria expressed in terms of the ductility parameters ε_{ut} and ε_f. Here, ε_{ut} is the true uniform elongation (the true strain at the maximum load in a tension test) and ε_f is the true fracture strain. If ε_u is the measured engineering strain at maximum load, and RA is the measured reduction of area at the fracture location, then ε_{ut} and ε_f may be computed with the relations $\varepsilon_{ut} = \ln(1+\varepsilon_u)^{ut}$ and $\varepsilon_f = \ln [1/(1-RA)]$.

Referring to the HEDL data reported in reference 2 and reproduced in attachment B, the uniform elongation (figure B.1 of attachment B) and the reduction of area (figure B.2 of attachment B) for type 304 stainless steel at 600°F are not very dependent on strain rate. Based on the information contained in the two diagrams, appropriate choices for ε_{ut} and RA are 30-percent and 65-percent true absolute strain, respectively. The value of RA yields $\varepsilon_f/3$ = 35-percent true absolute strain.

D. Stellite Overlay

The contact surface of the disc is protected against wear by a stellite overlay. This layer of different material was not modeled as a separate material in the present analysis. While it would have been possible to do so, omitting the layer is justifiable on the ground that larger strains will be predicted without the stellite and that this will lead to a conservative evaluation.

10A.3.5 BODY MATERIAL

The body material is A-216, Gr. WCB steel, which is listed in Appendix I of ASME Section III as a carbon steel for casting purposes. Because no published data were available pertaining to the effect of strain rate on the stress-strain characteristics of material, a number of tension tests were performed on specimens machined from a blank of the casting material (supplied to TMR by Atwood and Morrill).

The tests furnished the information on stress-strain diagrams and ductility summarized below. (A report on the test program will be issued separately.[7])

A. Elastic Constants

For Young's modulus (E), the value provided in Appendix I of ASME Section III was selected. Poisson's ratio (ν) was assumed to be 0.3, and the shear modulus (G) and bulk modulus (K) were computed from E and ν. Thus, at 600 F,

1. $E = 25.4 \times 10^6$ psi = 1.77 mbar.

2. $\nu = 0.3$.

3. $G = (E/2)/(1 + \nu) = 0.682$ mbar.

4. $K = (E/3)/(1 - 2\nu) = 1.48$ mbar.

B. Stress-Strain Diagram

Stress-strain diagrams obtained at different strain rates and in three orthogonal directions of the test blank are shown in figures 10A-13, 10A-14, and 10A-15. The testing conditions are summarized in table 10A-2, which gives the dimensions of the blank as well as the nominal strain rate and the direction of loading for each of 11 test specimens. The Z-direction is the thickness direction of the cast material, whereas the x and Y directions are arbitrary inplane directions, metallographic examination of samples normal to the three directions furnished evidence of a uniform grain structure without a preferred orientation.

Inspection of the stress-strain diagrams in figures 10A-13 through 10A-15 reveals only a minor dependence of the results on loading direction and strain rate. The material appears to soften slightly with increase in strain rate, but for analytical purposes, the material can be assumed to be isotropic and strain-rate insensitive.

Also depicted in figures 10A-13 through 10A-15 is the trilinear stress-strain diagram assumed for the PISCES solution. The reader will note that the diagram is chosen well below the measured diagrams. One reason for this choice was that the material characterization should be conservative in view of the fact that the tests were few in number and that strain rates as high as 1000 s-1 could not be achieved. Here it should be recognized that lowering the stress-strain curve will lead to increased strains. This, in turn, leads to a conservative evaluation because of the use of criteria that place limits on strain. A second reason for lowering the stress-strain curve was the need to compensate for a yield strength measured at room temperature that was higher than the minimum yield strength given in Appendix I of ASME Section III.

The assumed stress-strain diagram is also shown in figure 10A-12, where it can be compared to the diagram for the disc material. The values of σ_y, σ_{ut}, and E_t for the body material are:

1. $\sigma_y = 30{,}000$ psi = 2.07×10^{-3} mbar.

2. $\sigma_{ut} = 62{,}000$ psi = 4.28×10^{-3} mbar.

3. $E_t = 0.320 \times 10^6$ psi = 0.0221 mbar.

C. Ductility Parameters

As mentioned in the discussion of the disc material, the ductility parameters to be used in the evaluation of the PISCES solution are ε_{ut} and ε_f. Table 10A-2 furnishes the measured values of ε_u and RA, and also the values of ε_{ut} and ε_f derived from ε_u and RA. Inspection of the tabulated values reveals a slight tendency for increased ductility at higher strain rates. (The low value of ε_{ut} for specimen No. 14 appears to be a spurious result.)

By averaging the values from all 11 tests, the following result is obtained: ε_{ut} = 11-percent true absolute strain, and ε_f = 88-percent true absolute strain. The strain criteria for the body will be based on these averages.

D. Stellite Overlay

The contact surface of the body seat is protected against wear by a stellite overlay. This overlay was not modeled in the body as a separate material for the same reasons that it was not in the disc.

10A.3.6 INITIAL CONDITIONS AND BOUNDARY CONDITIONS

A. Initial Positions of Body and Disc

It is assumed in the PISCES solution that the moving disc will first contact the stationary body at time t = 0, the starting point of the solution. It is also assumed that the still undeformed contact faces will at that point in time meet in the plane defined by the axial position x = 0.

B. Constraint on Body Motion

During the impact event, axial motion of the body is rigidly constrained at the upstream end of the model (at x = 100 in.). No such constraint is imposed at the downstream end (at x = -100 in.) so that the total length of the model is permitted to change.

C. Initial Disc Velocity

The disc velocity at impact is 150 ft/s (4.58 cm/μs). This velocity was determined in attachment C by matching the kinetic energy of disc translation to the kinetic energy of disc rotation. The rotational energy was known from the fluid dynamics analysis reported in attachment D.

D. Pressure Loading

A constant pressure of 705 psig (4.86×10^{-5} mbar) is maintained on the upstream side of the valve for the duration of the impact event.

E. Initial Material Densities

The initial density of model materials in the PISCES code is entered as a relative density (the density relative to that of water). Hence, for the steels used in the disc and body, the relative density (ρ_s) is 7.85. In the analysis performed, the mass of the post, nut, and arm attached to the disc was accounted for by assuming that a higher-density material normally occupies the threaded hole in the center of the disc. The density of this material was selected such that its mass was equivalent to that of the post, nut, and arm combined. With reference to attachment C, the relative density of the equivalent material (ρ_e) is found from the relation $\rho_e = 14.6\ \rho_s$. The equivalent material is occupied by the first five rows of zones in the disc model. The higher density derived in attachment C pertains to the original disc arm design reflected in figure 10A-1. As stated in section 10A-1, the redesigned disc arm shown in figures 10A-2 and 10A-3 will result in less severe loading of the disc by the disc arm. That is, the disc arm load is now applied in the rim region where its contribution to disc loading is insignificant. Loading at the center of the disc has been reduced to that due to the mass of the post, which is integral with the disc in the modified disc arm design. The mass of the post is less than the equivalent mass of post, arm, and nut in the original arm design so that the analysis as performed will be conservative.

10A.3.7 PISCES SOLUTION

A trial solution with the full model provided the value of the stable step between computation cycles as 0.385 μs. The initial time step was specified as 0.025 μs, a value computed by means of a formula provided in the PISCES Input Manual (reference 5). Subsequent time steps are determined internal to the code to ensure numerical stability in the computation. The stable time step was reached in 13 cycles.

The final solution was executed for 3000 cycles. The associated elapsed time was 1150 μs. Standard computer output was printed at intervals of 200 cycles; nonstandard output was printed at intervals of 50 cycles. The nonstandard output was acquired by means of a specially-written subroutine (called EXOUT). It furnished the following results: effective strain ($\bar{\varepsilon}$), axial strain (ε_x), radial strain (ε_y), hoop strain (ε_z), shear strain (ε_{xy}), and effective stress ($\bar{\sigma}$). Effective stress and effective strain are computed from stress and strain components with the following formulas from plasticity theory:

$$\bar{\sigma} = \left(1/\sqrt{2}\right)\left[\left(\sigma_x - \sigma_y\right)^2 + \left(\sigma_y - \sigma_z\right)^2 + \left(\sigma_z - \sigma_x\right)^2 + 6\tau_{xy}^2\right]^{1/2}$$

$$\bar{\varepsilon} = \left(\sqrt{2}/3\right)\left[\left(\varepsilon_x - \varepsilon_y\right)^2 + \left(\varepsilon_y - \varepsilon_z\right)^2 + \left(\varepsilon_z - \varepsilon_x\right)^2 + 6\varepsilon_{xy}^2\right]^{1/2}$$

It should be noted that the geometry of the PISCES model is continually updated (following each computation cycle) so that the stress components σ_x, σ_y, σ_z, and τ_{xy} are true stresses and

the strain components ε_x, ε_y, ε_z, and ε_{xy} are true strains. Consequently, $\bar{\sigma}$ and $\bar{\varepsilon}$ are also true quantities. It should further be noted that ε_{xy} is the tensorial shear strain, which is twice the engineering shear strain.

10A.4 PISCES RESULTS

Pertinent information extracted from the PISCES solution is presented in this section of the report.

At this point, an introduction is needed to explain the convention employed in the PISCES code for identifying grid points and grid zones. The grid is defined by columns and rows, indexed I and J, respectively. Figures 10A-16 and 10A-17 show the column and row numbering schemes adopted for the disc and body. A particular grid point in the model is defined by the values of I and J of the row and column that intersect at that point. For instance, point 11, 31 refers to outermost point on the front face of the disc. A grid zone is bounded by two columns, I and J + 1 and by two rows J and J + 1. A zone is defined by the values of I + 1 and J + 1. Thus, as an example, zone 12, 31 is the outermost zone on the front side of the disc.

10A.4.1 DISSIPATION OF KINETIC ENERGY

In table 10A-3, the kinetic energy in the model is tabulated versus the time elapsed since impact. To facilitate the interpretation of the results, the kinetic energy is also given as a percent of its initial value. The latter results furnish the curve plotted in figure 10A-18. It is apparent from the diagram that the kinetic energy is dissipated at a rate that decreases with time from t = 0 to t = 300 μs, and again from t = 700 μs on. In the timespan from t = 300 μs to t 700 μs, the rate of energy dissipation is practically constant. At solution termination time, t = 1150 μs, 97.2 percent of the kinetic energy has been dissipated. The graphical extrapolation of the curve in figure 10A-18 indicates that for practical purposes the duration of the impact is approximately 1300 μs.

10A.4.2 MAXIMUM DEFLECTION OF DISC

The position of various points on the disc as a function of time is given in table 10A-17. The data tabulated for the axial position of the surface points on the disc centerline yield the axial displacement curves portrayed in figure 10A-19. At the extrapolated time of 1300 μs, the displacement (U_x) is 1.77 in. at the front surface and 1.84 in. at the back surface.

Also shown in figure 10A-19 is a straight line which depicts the axial displacement of the disc in free motion (no impact). Since the computed displacement curves are initially above the line, it is clear that following impact, the center of the disc accelerates before it slows down.

10A.4.3 MAXIMUM VELOCITY IN DISC

A plot of axial velocity versus time is shown in figure 10A-20 for the two surface points on the centerline of the disc. The axial velocity (x) reaches a maximum value of 175 ft/s at the front surface and 179 ft/s at the back surface.

10A.4.4 GEOMETRIC DISTORTION

The progressive geometric distortion of the valve model may be observed in figures 10A-21, 10A-22, and 10A-23 where grid plots obtained at 300, 700, and 1150 μs after impact are shown. Figure 10A-24 is a superposition of the distorted shape at the end of the solution (t = 1150 μs) on the undistorted shape (t = 0).

Inspection of the geometry plot in figure 10A-21 reveals that the disc fillet below the contact zone has flattened out. As a consequence, the corner of the body starts to indent the zone of the disc just opposite this corner. The PISCES code permits this to happen. Evidence of such indentation is evident in figures 10A-22 and 10A-23 where the body grid appears to overlap the disc grid. The overlap is not a physical reality. It is a consequence of the plotting routine, which is based on connecting grid points by straight lines and which does not recognize indentation of a zone located in a contact region. The actual geometric distortion is sketched in figure 10A-24.

In the PISCES code, penetration can occur only at contact surfaces. The contact surfaces have to be columns. The column on the stationary part of the model is usually the so-called master column, and the column on the moving part is the slave column. Grid points on the master column can indent the slave column, but grid points on the slave column cannot indent the master column. An optional feature of the master slave approach in the PISCES code permits the formation of voids between the contacting surfaces. While this option was demonstrated to work in a preliminary computer run and then exercised in the full PISCES solution, the results obtained produced no clear evidence that any separation between disc and body occurred in the contact zone.

10A.4.5 STRAIN HISTORY PLOTS

The accumulation of strain as time progresses is best illustrated by means of history plots. All plots to be presented contain four curves, each portraying the strain in a given zone. The applicable zones are identified by column and row numbers in the manner explained at the beginning of section 10A.4.

A. Body Strains

The largest body strains occur in the two columns of zones adjacent to the contact surface. Representative history plots for this region are shown in figures 10A-25 and 10A-26. They indicate that effective strains in the body reach stable values in about 900 μs. The maximum effective strain in the body is 14.7 percent and occurs at zone 9, 17.

B. Disc Strains

Effective strains in the rim region are largest in the four rows of zones for which the results are plotted in figures 10A-27 through 10A-30. It is seen that the strains tend to stabilize faster than in the body, although complete stabilization again requires about 900 μs. The maximum strain in the rim region is 17.4 percent and is found at zone 13, 27.

Results for the central portion of the disc are plotted in figures 10A-31 through 10A-38. Figures 10A-31 through 10A-34 give the effective strain ($\bar{\varepsilon}$), the axial strain (ε_x), the radial strain (ε_y), and the hoop strain (ε_z), respectively, for four zones spaced along the front surface of the disc. Likewise, figures 10A-35 through 10A-38 give the corresponding results for the back surface. The two sets of results show that the front surface is more severely strained than the back surface. A comparison with the results for the rim region indicates that strains in the central region do not begin to accumulate significantly until after most of the strain accumulation in the rim region is over. At solution termination time, the effective strain reaches a maximum of 14.3 percent at the center on the front side and 10.4 percent at the center on the back side. Extrapolation to time t = 1300 μs increases these values to 14.6 percent and 10.6 percent, respectively.

10A.4.6 STRESS HISTORY PLOTS

Because of the severe straining of the body and disc, strains are of considerably more interest and importance than stresses. For this reason, only two history plots were obtained. These pertain to the effective surface stress in the central region of the disc. Figures 10A-39 and 10A-40 show the results for the front surface and the back surface. The spikes in the curves below 200 μs are due to elastic unloading and reloading. In reality, there are many more spikes in the solution, but these are not seen because the results plotted are based on computer output saved at every 50th time step. After 200 μs, the stresses are observed to rise monotonically. Stresses remaining at the completion of the event will be the sum of the residual stresses brought about by plastic deformation, and the stresses that are in equilibrium with the pressure load on the upstream side of the disc.

10A.4.7 DISTRIBUTION OF STRAINS IN THE CONTACT REGION

The distribution of effective strain ($\bar{\varepsilon}$) at times of 300, 700, and 1150 μs is shown in figures 10A-41 through 10A-43. As observed in subsection 10A.4.5, strains in the contact zone of the body clearly do not rise as fast as in the contact zone of the disc. The diagrams are also instructive in showing that large strains in the body are confined to the immediate vicinity of the body seat. Furthermore, they show that the largest strains occur at some distances below the contact surface, a phenomenon not uncommon to contact problems.

At solution termination time, the distributions of strains ε_x, ε_y, ε_z, and ε_{xy} are as presented in figures 10A-44 through 10A-47. It will be noted that at the high-strain locations, the sum of ε_x,

ε_y, and ε_z is approximately zero. This is a consequence of the constant volume condition associated with plastic deformation.

10A.4.8 DISTRIBUTION OF STRAINS IN THE CENTRAL DISC REGION

Figures 10A-48 through 10A-50 provide insight into the distribution of the effective strain $\bar{\varepsilon}$ at times of 300, 700, and 1150 μs. Similar results, but limited to the time of 1150 μs, are shown in figures 10A-51 through 10A-54 for ε_x, ε_y, ε_z, ε_{xy}.

Along the centerline of the disc, ε_x, ε_y, and ε_z are distributed as shown in figure 10A-55. The extrapolated values at the front surface are -17, 8.5, and 8.5 percent, respectively. At the back surface they are 14.4, -7.2, and -7.2 percent. The sum of the strains is zero in each case, which is in accordance with the constant volume condition for plastic strain, elastic strains being small compared to the plastic strains at the two locations considered.

10A.4.9 DISTRIBUTION OF STRESSES IN THE CENTRAL DISC REGION

Distributions of $\bar{\sigma}$, σ_x, σ_y, σ_z, and τ_{xy} radial plane of the disc are presented in figures 10A-56 and 10A-60. The values shown are in ksi (1 ksi = 1000 psi). The diagram for $\bar{\sigma}$ is particularly useful in that it reveals the extent of plastic deformation, as yielding occurs when $\bar{\sigma}$ exceeds 25 ksi. The results are for time t = 1150 μs.

10A.4.10 STRAIN RATES

A tabulation of strain rates at several key locations is presented in tables 10A-5 and 10A-6. Table 10A-5 gives strain rates at various times for the highest strained zones in the body and disc, namely for zones 9, 17 and 13, 27. Strain rates as high as 500 s^{-1} are noted for the body, and as high as 800 s^{-1} for the disc.

Table 10A-6 gives strain rates for zones 12, 2 and 19, 2, which are located at the front surface and back surface of the disc. Strain rates as high as 300 s^{-1} and 200 s^{-1} are noted for these locations. The peak values are reached at time t = ~ 600 μs. This observation agrees with the observation of maximum slopes in the strain time plots (figures 10A-31 through 10A-38).

10A.5 EVALUATION

The impact event associated with valve closure under faulted conditions constitutes an energy dissipation problem. Thus, valve components will deform progressively until the kinetic energy accumulated in the disc, disc post, and disc arm during closure has been dissipated through plastic-strain energy absorption. In the analysis described in this report, it has been assumed, conservatively, that all the kinetic energy is absorbed by the body and disc.

Because the structure must absorb kinetic energy through plastic deformation, meaningful acceptance criteria by which to judge the structural adequacy of the valve should consist of limits placed on geometric distortion (to ensure proper functioning of the valve) and on strain (to preclude fracture).

10A.5.1 DEFORMATION CONSIDERATIONS

The obvious criterion for limiting deformation is that geometric distortion caused by the impact shall not prevent the proper closure of the valve. Application of this criterion requires a qualitative appraisal of the results of the PISCES solution.

Consideration of the deformed shape presented in figure 10A-24 shows that, in spite of considerable geometric distortion, closure is unimpaired. In fact, as evident from the distorted grid plots in figures 10A-21 through 10A-23, the contact surface on the disc has moved radially outward rather than inward, while the radius of the body seat opening has decreased slightly.

Figures 10A-23 and 10A-24 show that the body seat corner has indented the disc below the stellite overlay. This condition is likely to cause higher strains than the PISCES solution is capable of showing. However, such a condition can be circumvented by deepening of the fillet in the disc by 0.1 in. This modification has been incorporated into the disc design. Since it is a minor geometry change, the results of the PISCES solution will remain valid.

With reference to subsection 10A.4.2, the maximum deflection at the center of the disc is 1.84 in. Since any axial displacement of the shaft about which the disc rotates can be assumed to be negligible, the large deflection of the disc could cause binding of the disc post in the collar of the disc arm in the configuration analyzed. However, this concern has been eliminated by the redesign of the disc arm mentioned earlier.

10A.5.2 EVALUATION AGAINST STRAIN CRITERIA

The strain criteria presented below are intended to prevent fracture initiation caused by large local strains in the contact region of body and disc, and excessive bending distortion in the central portion of the disc. Each of the criteria is expressed in terms of the uniform elongation ε_{ut} and the fracture strain ε_f. Section 10A.3 furnishes the following values of these ductility parameters:

A. Disc (type 304 stainless steel) - $\varepsilon_{ut} = 30\%$, $\varepsilon_f/3 = 35\%$.

B. Body (type A-216 grade WCB steel) - $\varepsilon_{ut} = 11\%$, $\varepsilon_f/3 = 29\%$.

10A.5.2.1 Local Strain Limits for Contact Region

The strain criteria adopted for limiting local strain are as follows:

A. Rule 1

If the hydrostatic stress component $(\sigma_x + \sigma_y + \sigma_z)/3$ at the location of maximum effective strain is tensile, $\bar{\varepsilon}$ shall be limited to the smaller of ε_{ut} and $\varepsilon_f/3$.

B. Rule 2

If the hydrostatic stress component $(\sigma_x + \sigma_y + \sigma_z)/3$ at the location of maximum effective strain is compressive, $\bar{\varepsilon}$ shall be limited to the larger of ε_{ut} and $\varepsilon_f/3$.

The first rule is justified on the basis that it would have been effective in preventing fracture in burst experiments on clamped discs which had a circumferential structural discontinuity near the clamped edge. The results of the burst tests conducted on special disc specimens were reported in reference 8 and analyzed in reference 9.[(a)] In the tests, the specimens were rigidly clamped along the rim and subjected to pressure on one face. Three materials with different degrees of ductility were used, one of which was type 304 stainless steel. Depending on the material and the disc dimensions, the discs failed in tension either at the rim fillet or in the center. The rim failures resulted from strain concentration, the center failures resulted from strain instability. By applying rule 1 to the maximum equivalent strain in the rim fillet, it was ascertained that no rim failures would have occurred in the tests had they been interrupted when the true strain reached the lesser of ε_u and $\varepsilon_f/3$ of the materials involved.

Because fracture initiation is unlikely when the hydrostatic stress component is compressive, the second rule must be viewed as conservative from a fracture prevention point of view. However, the rule also serves as a useful limit for preventing excessive local distortion of the structure.

It is noted that for both the body and the disc, ε_{ut} is smaller than $\varepsilon_f/3$. For the body, ε_{ut} = 11 percent, and $\varepsilon_f/3$ = 29-percent true absolute strain; for the disc, ε_{ut} = 30 percent, and $\varepsilon_f/3$ = 35-percent true absolute strain.

Considering the body first, inspection of the strain distribution in figure 10A-43 shows that ε_{ut} is exceeded only in three locations. At zone 9, 17, $\bar{\varepsilon}$ = 15 percent, and at zones 9, 16 and 10, 18, $\bar{e}$ = 12 percent. For each of these locations, the PISCES solution shows that the hydrostatic stress component is compressive, so that an effective strain as high as 29 percent is allowed. Hence, the effective strains at the three locations are well within the limit provided by rule 2. Therefore, the body is judged structurally adequate.

---

a. A copy of reference 9 is included in the report as attachment E.

Inspection of figure 10A-43 also shows that $\bar{\varepsilon}$ does not exceed ε_{ut} in the rim region of the disc. That is, the maximum value of $\bar{\varepsilon}$ is 17 percent, whereas $\bar{\varepsilon}_{ut}$ = 30 percent. Consequently, since the disc meets the limit provided by rule 1, examination of the hydrostatic stress component is unnecessary.

10A.5.2.2 Strain Limit for Central Region of Disc

The criterion adopted for qualifying the central portion of the disc is the following:

A. Rule 3

The value of $\bar{\varepsilon}$ along the surfaces of the disc shall not exceed 60 percent of ε_{ut}; i.e., $\bar{\varepsilon} \leq 0.6\ \varepsilon_{ut}$.

Basis for this criterion is the observation gleaned from reference 10 that in an internally-pressurized thin-walled sphere, the uniform circumferential strain at maximum pressure will not be less than 0.3 ε_{ut}, for materials whose strain-hardening exponent (n) is less than 0.3. (The precise formula given in reference 10 states that the ratio of the circumferential strain at maximum pressure and the uniform elongation = $(2/3)^n$). By neglecting elastic strains as being very small, it follows that $\bar{\varepsilon}$ is equal to twice the circumferential strain for such a sphere. Since n is less than 0.3 for most steels, limiting $\bar{\varepsilon}$ to 0.6 ε_{ut} would ensure that the maximum pressure in the sphere is not reached. Unstable progressive distortion is thereby prevented.

Invoking rule 3 for the disc evaluation is a conservative procedure because pressure loading of the thin-walled sphere produces membrane loading only, while the loading mode of the disc is primarily bending. However, a conservative rule on $\bar{\varepsilon}$ is desirable from the viewpoint that it places an indirect limit on gross geometric distortion.

The maximum value of $\bar{\varepsilon}$ is found at the center of the front surface, where it is 17 percent. This is less than 0.6 ε_{ut} (18 percent), so that the central portion of the disc is also structurally adequate.

REFERENCES

1. Southern Company Services, Inc., for Alabama Power Company, "Special Conditions Main Steam Isolation Valves - Joseph M. Farley Nuclear Plant, Unit No. 1,"Inquiry No. SS-1102-32, Addendum 8," November 9, 1973.

2. Steichen, J. M., "High Strain Rate Mechanical Properties of Types 304 and 316 Stainless Steel," Technical Document HEDL-TMF 71-164, Hanford Engineering Development Laboratory, November 1971.

3. "Liquid Metal Fast Breeder Reactor Materials Handbook," Technical Document HEDL-TMR 71-32, Hanford Engineering Development Laboratory, Current.

4. "General Description of Finite-Difference Equations," Version 3, Revision 3, PISCES 2DL, Manual A, Physics International Company, 1972.

5. "Input Manual," Version 3, Revision 2, PISCES 2DL, Manual B, Physics International Company, 1973.

6. "Non-Standard Options," Version 3, Revision 3, PISCES 2DL, Manual C, Physics International Company, 1972.

7. "High Strain Rate Tensile Properties of SA-216, GR WCB Steel Casting and SA-182, GR. F304 Stainless Steel Forging Materials," Technical Report No. TR-1901, May 30, 1975.

8. Cooper, W. E., Kottcamp, E. H., and Spiering, G. A., "Experimental Effort on Bursting of Constrained Discs as Related to the Effective Utilization of Yield Strength," ASME 71-PVP-49, American Society of Mechanical Engineers, May 1971.

9. Riccardella, P. C., "Elastic-Plastic Analysis of Constrained Disc Burst Tests," ASME 72-PVP-12, American Society of Mechanical Engineers, June 1972.

10. Cooper, W. E., "The Significance of the Tensile Test of Pressure Vessel Design," Welding Journal, Research Supplement, pp 49-s - 56-s, January 1957.

TABLE 10A-1 (SHEET 1 OF 2)

NOMENCLATURE

Word	Abbreviation or Letter Symbol
time (from initial impact)	t
temperature	T
axial coordinate	x
radial coordinate	y
hoop coordinate	z
velocities	$\dot{x}, \dot{y}$
displacements	U_x , U_y
effective stress (defined as follows)	$\bar{\sigma}$
effective strain (defined as follows)	$\bar{\varepsilon}$
stresses	$\sigma_x, \sigma_y, \sigma_z, \tau_{xy}$
strains	$\varepsilon_x, \varepsilon_y, \varepsilon_z, \varepsilon_{xy}$
strain rates	$\dot{\varepsilon}_x, \dot{\varepsilon}_y, \dot{\varepsilon}_z, \dot{\varepsilon}_{xy}$
Young's modulus	E
shear modulus	G
bulk modulus	K
Poisson's ratio	ν
relative density	D
pressure	P
kinetic energy	KE
Teledyne Materials Research	TMR
Atwood and Morrill Company	A & M

TABLE 10A-1 (SHEET 2 OF 2)

Definitions

$$\bar{\sigma} = (1/\sqrt{2})\left[(\sigma_x - \sigma_y)^2 + (\sigma_y - \sigma_z)^2 + (\sigma_z - \sigma_x)^2 + 6\tau_{xy}^2\right]^{1/2}$$

$$\bar{\varepsilon} = (\sqrt{2}/3)\left[(\varepsilon_x - \varepsilon_y)^2 + (\varepsilon_y - \varepsilon_z)^2 + (\varepsilon_z - \varepsilon_x)^2 + 6\varepsilon_{xy}^2\right]^{1/2}$$

TABLE 10A-2 (SHEET 1 OF 2)

TENSION TEST RESULTS

Test blank dimensions:
a = 14 in.
b = 14 in.
c = 2 in.

Test temperature = 600°F

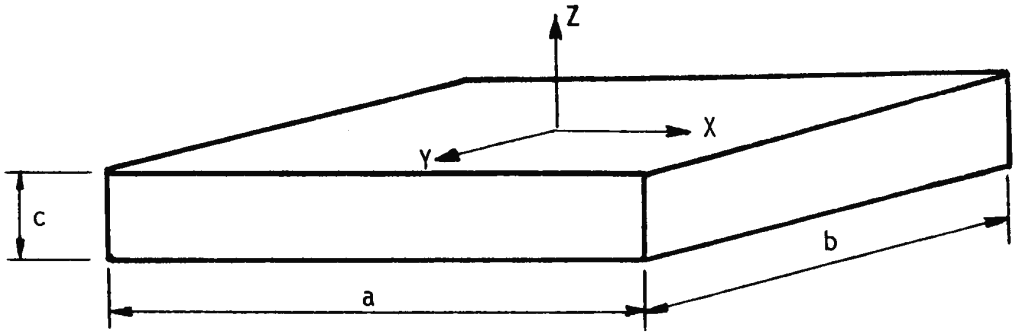

Specification Number	Loading Direction	$\dot{\varepsilon}$ S^{-1}	ε_u %	ε_{ut} %	RA %	ε_f %
2	X	0.092	13.5	12.7	54.0	78
5	X	0.90	12.0	11.3	57.4	85
4	X	6.0	14.0	13.1	59.9	91
6	X	13.0	15.0	14.0	62.0	97
11	Y	0.097	11.0	10.4	51.7	73
13	Y	0.96	12.0	11.3	56.6	83
14	Y	6.0	9.0	8.6	59.2	90
9	Y	13.0	14.0	13.1	62.0	97
19	Z	0.11	8.5	8.2	58.9	89
20	Z	1.1	10.5	10.0	61.5	95

TABLE 10A-2 (SHEET 2 OF 2)

Specification Number	Loading Direction	$\dot{\varepsilon}$ s^{-1}	ε_u %	ε_{ut} %	RA %	ε_f %
15	Z	9.8	10.5	10.0	60.9	94
Average Values:		-	11.8	11.2	58.6	88

Legend

$\dot{\varepsilon}$ = nominal strain rate (based on ram velocity of testing machine)

ε_u = uniform elongation (engineering strain at maximum load)

ε_{ut} = $\ln(1 + \varepsilon_u)$ = true uniform elongation

RA = reduction of area at fracture

ε_f = $\ln[1/(1 - RA)]$ = true fracture strain

TABLE 10A-3

KINETIC ENERGY IN MODEL VERSUS TIME

Time (t/μs)	Kinetic Energy (KE(t), eu)[(a)]	Kinetic Energy (KE(T), 10 in.^{6}/lb)	KE(t)/KE(0) (%)
0	3.404	3.009	1.000
36	3.119	2.757	0.916
74	2.828	2.500	0.831
151	2.318	2.049	0.681
228	1.994	1.763	0.586
304	1.759	1.555	0.517
381	1.574	1.391	0.462
458	1.372	1.213	0.403
534	1.167	1.032	0.343
611	0.993	0.878	0.292
688	0.809	0.715	0.238
765	0.613	0.542	0.180
841	0.451	0.399	0.132
918	0.332	0.293	0.098
995	0.230	0.203	0.068
1072	0.155	0.137	0.046
1148	0.097	0.086	0.028

a. 1 energy unit (eu) = 1 x 10^{12} dyn/cm = 8.84 x 10^5 in/lb.

TABLE 10A-4

DISC LOCATIONS VERSUS TIME

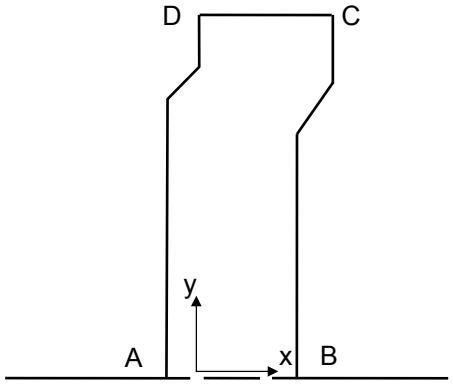

Time (t/μs)	X_A (cm)	X_B (cm)	X_C (cm)	X_D (cm)	Y_C (cm)	Y_D (cm)
0	-2.86	6.67	9.53	0.00	34.93	34.92
36	-3.02	6.51	9.38	-0.02	34.92	35.04
74	-3.20	6.33	9.26	-0.05	34.89	35.14
151	-3.56	5.96	9.13	-0.09	34.82	35.24
228	-3.95	5.57	9.12	-0.12	34.69	35.28
304	-4.35	5.16	9.12	-0.13	34.57	35.29
381	-4.75	4.74	9.14	-0.13	34.46	35.29
534	-5.53	3.94	9.16	-0.14	34.26	35.27
688	-6.22	3.22	9.16	-0.15	34.12	35.26
841	-6.75	2.65	9.15	-0.16	34.06	35.26
995	-7.09	2.27	9.14	-0.17	33.92	35.24
1148	-7.27	2.08	9.11	-0.20	33.89	35.24
change(cm)	-4.41	-4.59	-0.42	-0.20	-1.04	0.32
change(in.)	-1.74	-1.81	-0.17	-0.08	-0.41	0.13

TABLE 10A-5

STRAIN RATES AT HIGHEST-STRAINED ZONES OF BODY AND DISC

Time (μs)	Zone I, J	$\dot{\varepsilon}_x$ (s^{-1})	$\dot{\varepsilon}_y$ (s^{-1})	$\dot{\varepsilon}_z$ (s^{-1})	$\dot{\varepsilon}_{xy}$ (s^{-1})
37	9, 17	-373	488	-21	123
74		-238	280	-13	79
151		-124	124	-2	52
228		-104	104	-2	53
304		-162	175	-5	128
381		-130	122	-5	117
534		-43	46	0	51
841		-43	46	-4	46
1148		-2	-3	1	-4
37	13, 27	-793	785	25	509
74		-765	746	17	602
51		-107	94	19	159
228		-19	11	5	42
304		-11	4	3	31
381		-4	-3	-1	12
534		-3	0	-3	0
841		-7	8	-2	33
1148		-2	0	0	-4

TABLE 10A-6

STRAIN RATES AT CENTERLINE OF DISC

Time (μs)	Zone I, J	$\dot{\varepsilon}_x$ (s^{-1})	$\dot{\varepsilon}_y$ (s^{-1})	$\dot{\varepsilon}_z$ (s^{-1})
37	12, 2	0	-2	-2
74		31	-96	-96
151		-76	46	44
228		-43	23	26
304		-44	13	12
381		-101	58	58
534		-232	119	117
688		-272	138	137
841		-181	92	91
1148		-55	28	28
37	19, 2	-4	5	5
74		36	-94	-93
151		133	-76	-77
228		-50	-82	-75
304		-24	-20	-18
381		88	-59	-57
534		207	-106	-105
688		187	-96	-95
841		106	-56	-53
1148		15	-12	-7

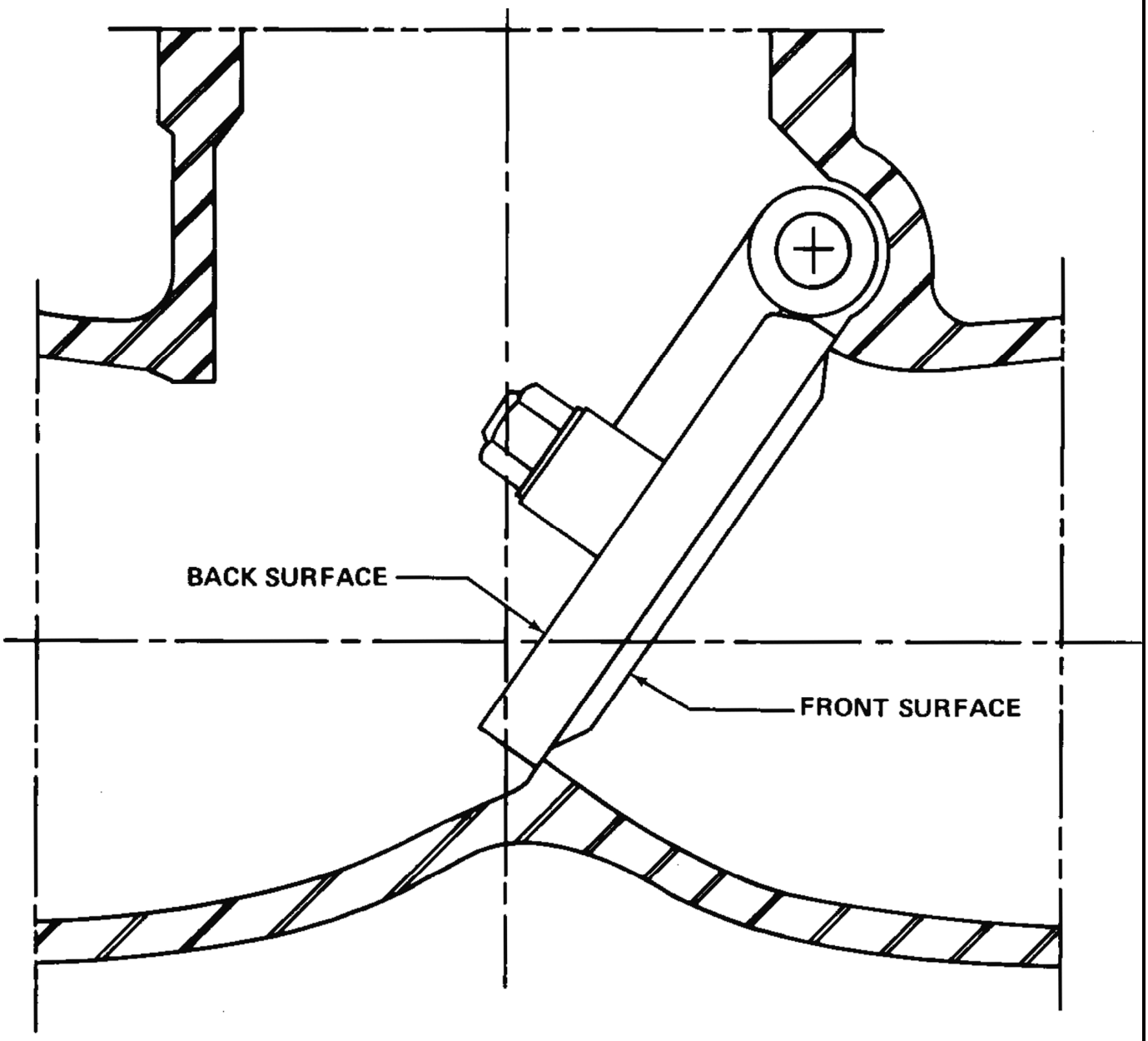

REV 21 5/08

SOUTHERN COMPANY
Energy to Serve Your World©

JOSEPH M. FARLEY
NUCLEAR PLANT
UNIT 1 AND UNIT 2

ISOLATION VALVE
IN CLOSED POSITION

FIGURE 10A-1

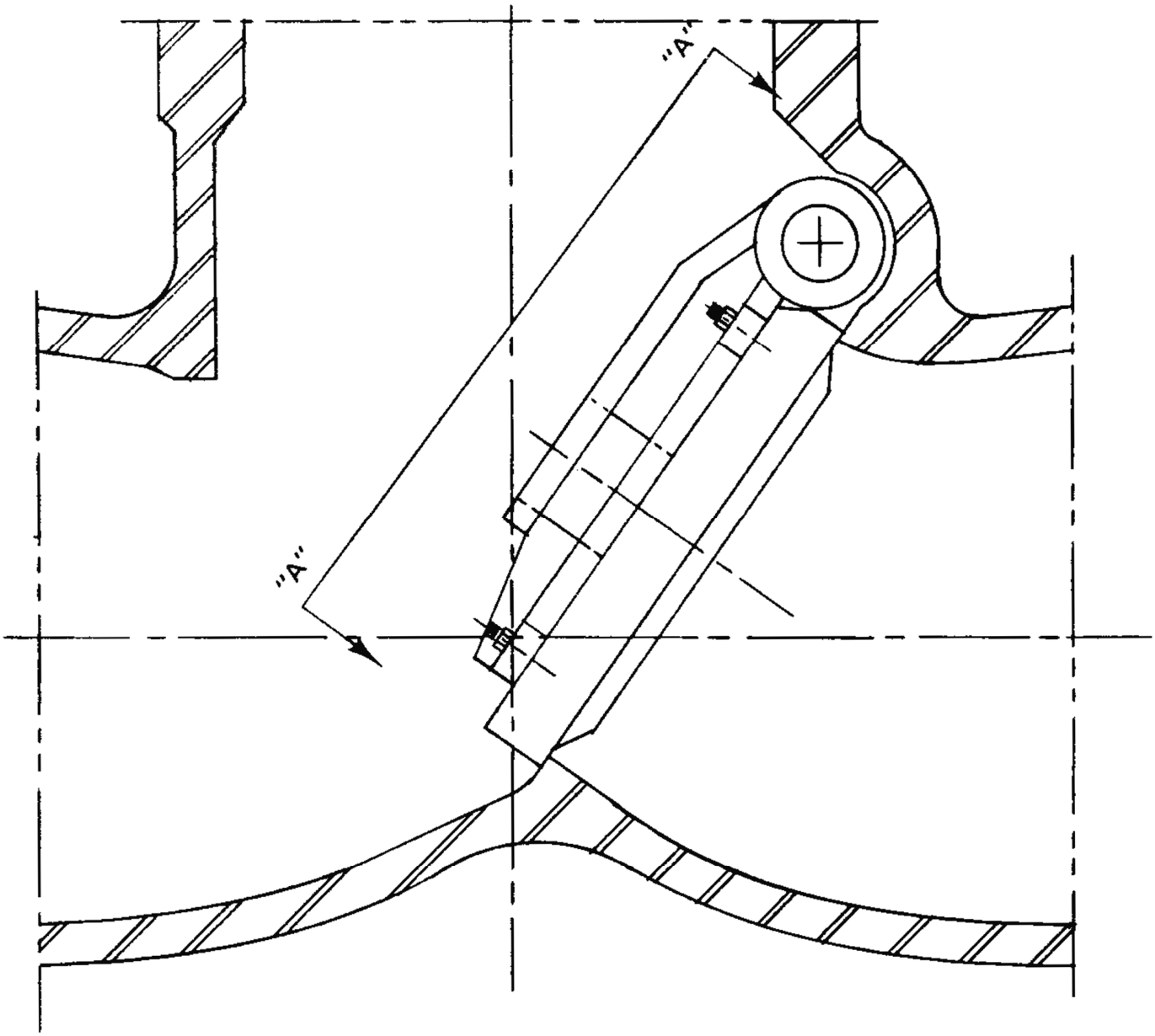

REV 21 5/08

SOUTHERN COMPANY *Energy to Serve Your World®*	**JOSEPH M. FARLEY NUCLEAR PLANT UNIT 1 AND UNIT 2**	ISOLATION VALVE WITH MODIFIED DISC ARM
		FIGURE 10A-2

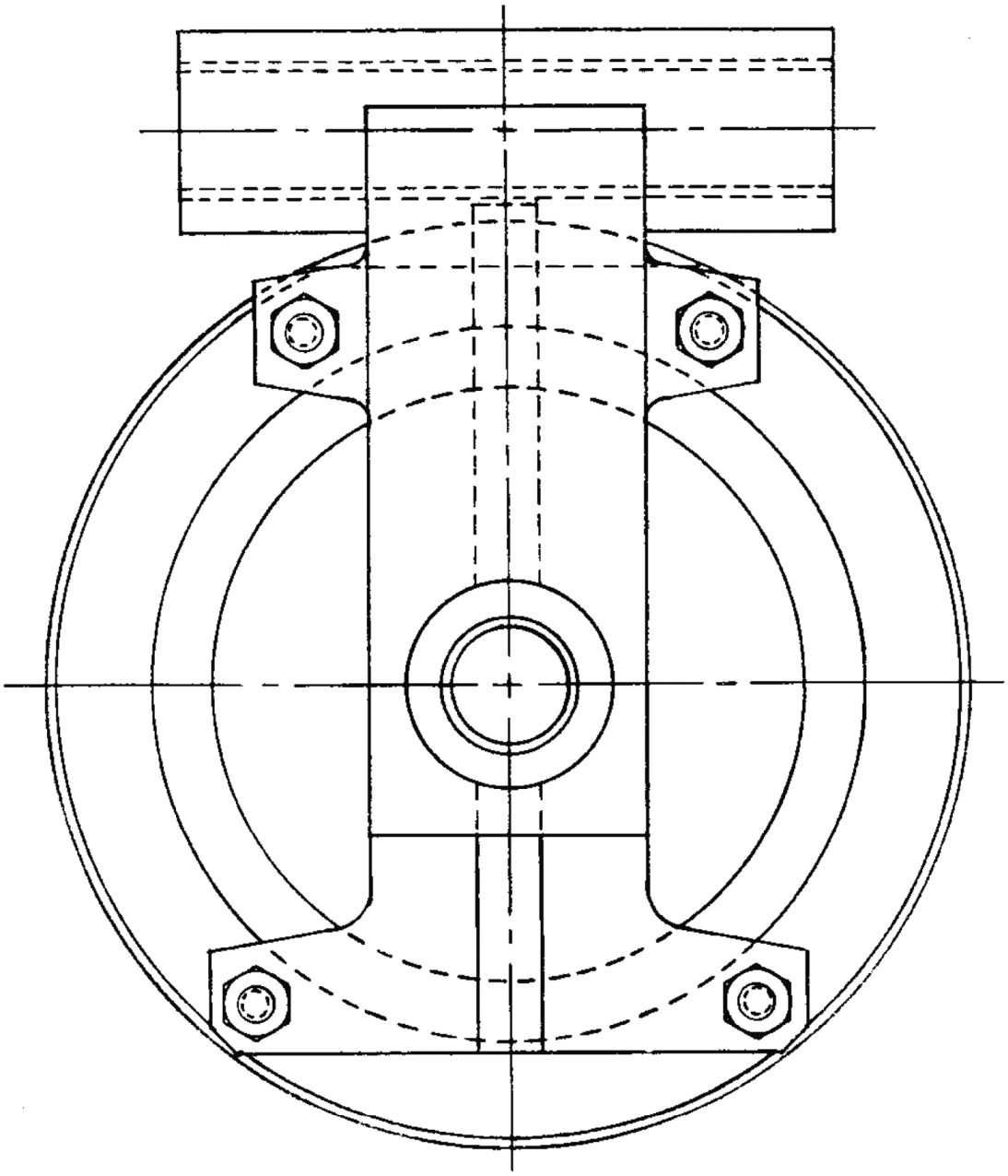

NOTE: SEE SHEET 2 OF THIS FIGURE FOR THE FINAL AS-BUILT CONFIGURATION SHOWING DETAILS OF LOCKING DEVICES USED ON THE DISC ARM STUDS AND NUTS.

REV 21 5/08

SOUTHERN COMPANY
Energy to Serve Your World®

JOSEPH M. FARLEY NUCLEAR PLANT UNIT 1 AND UNIT 2

SECTION "A-A" FROM FIGURE 10A-2 TOP VIE W OF MODIFIED DISC ARM ASSEMBLY

FIGURE 10A-3 (SHEET 1 OF 2)

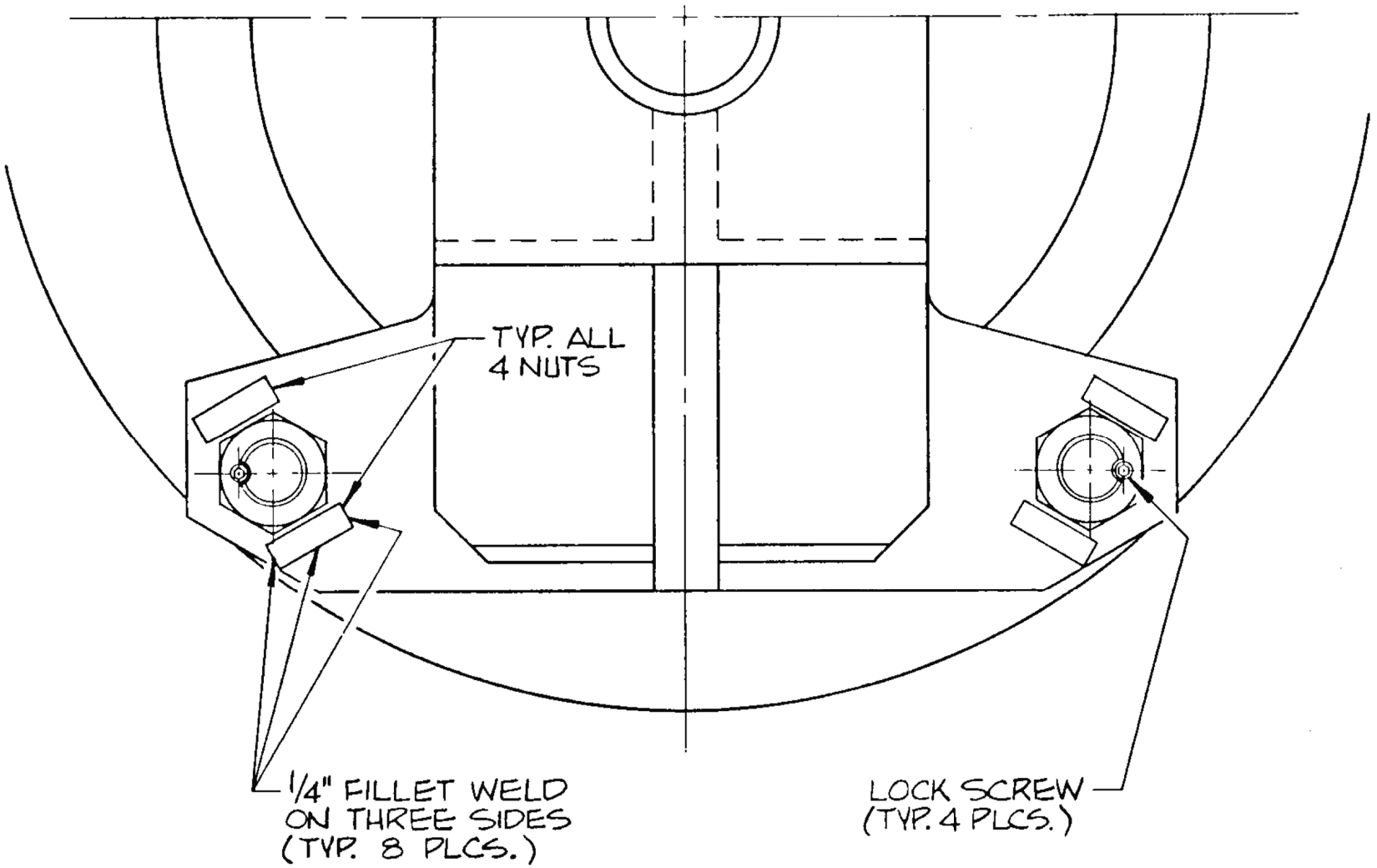

REV 21 5/08

SOUTHERN COMPANY
Energy to Serve Your World®

JOSEPH M. FARLEY
NUCLEAR PLANT
UNIT 1 AND UNIT 2

DETAIL OF MODIFIED DISC ARM
ASSEMBLY SHOWING LOCKING DEVICES
USED ON STUDS AND NUTS

FIGURE 10A-3 (SHEET 2 OF 2)

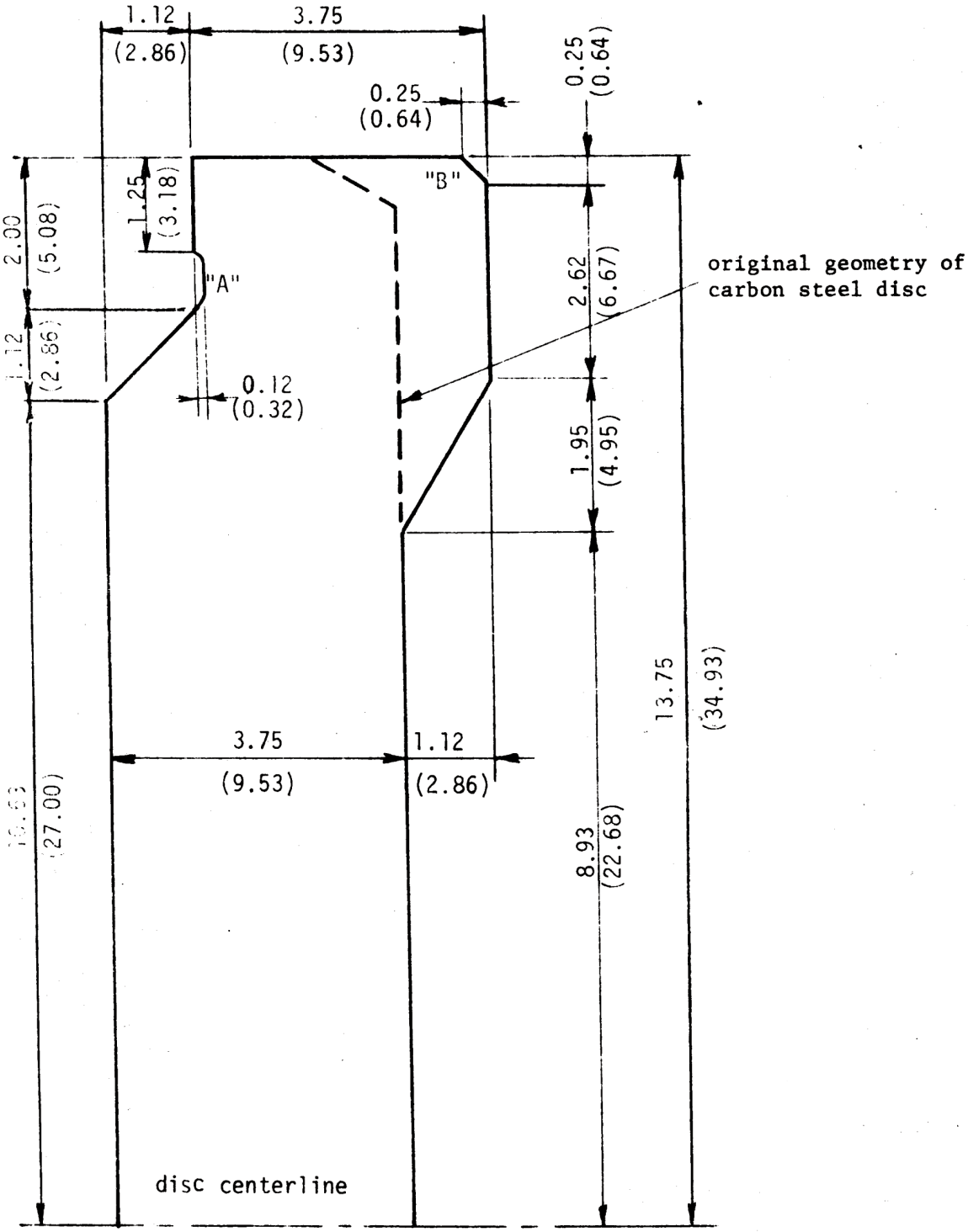

REV 21 5/08

SOUTHERN COMPANY *Energy to Serve Your World®*	**JOSEPH M. FARLEY NUCLEAR PLANT UNIT 1 AND UNIT 2**	BASIC DISC DIMENSIONS IN INCHES AND IN CENTIMETERS
		FIGURE 10A-4

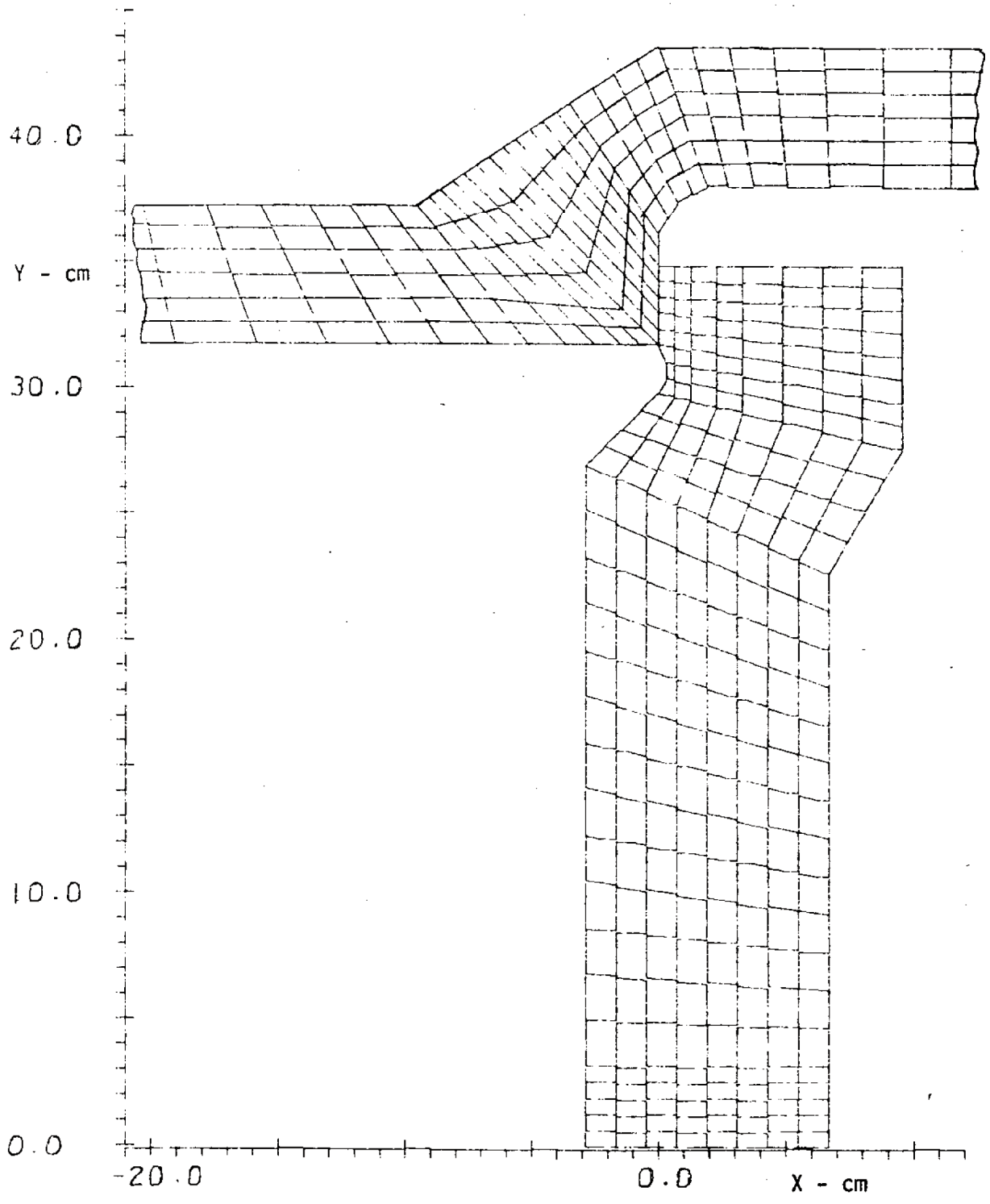

REV 21 5/08

SOUTHERN COMPANY
Energy to Serve Your World®

JOSEPH M. FARLEY NUCLEAR PLANT UNIT 1 AND UNIT 2

FIRST PISCES MODEL
(BODY SHOWN IN PART)

FIGURE 10A-5

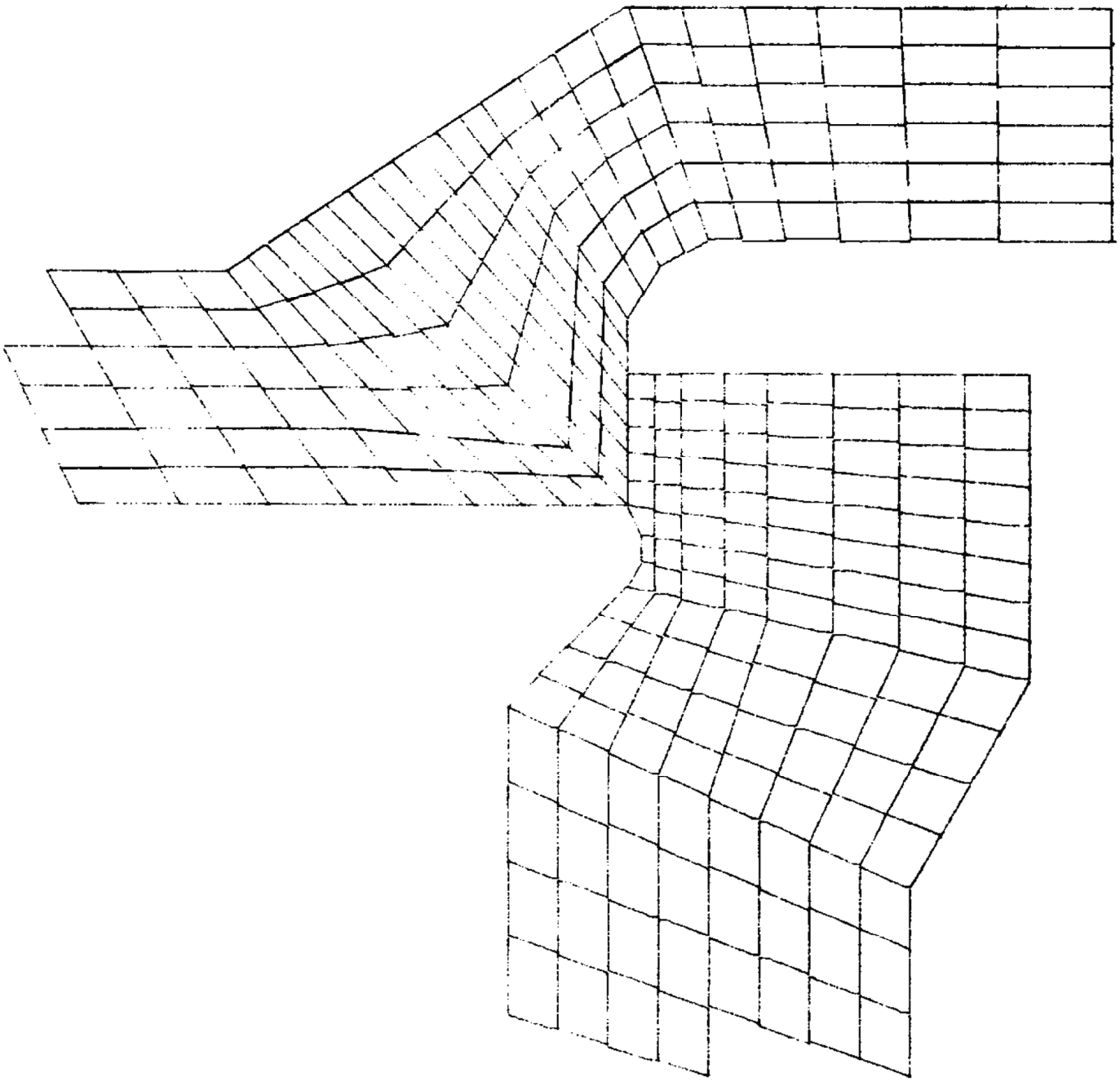

REV 21 5/08

SOUTHERN COMPANY
Energy to Serve Your World®

JOSEPH M. FARLEY
NUCLEAR PLANT
UNIT 1 AND UNIT 2

FIRST PISCES MODEL
(CLOSEUP OF CONTACT REGION)

FIGURE 10A-6

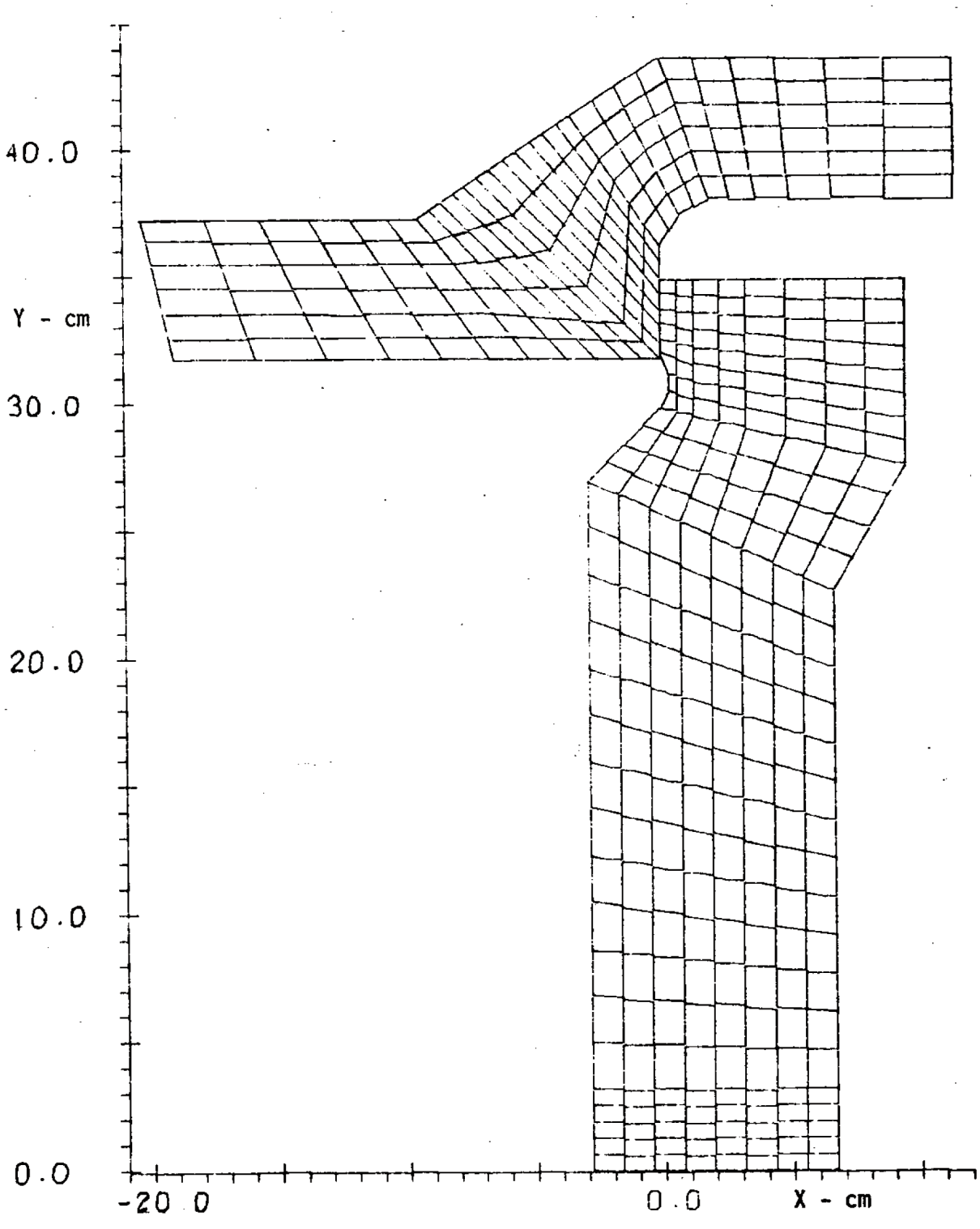

REV 21 5/08

SOUTHERN COMPANY
Energy to Serve Your World®

JOSEPH M. FARLEY
NUCLEAR PLANT
UNIT 1 AND UNIT 2

SECOND PISCES MODEL
(BODY SHOWN IN PART)

FIGURE 10A-7

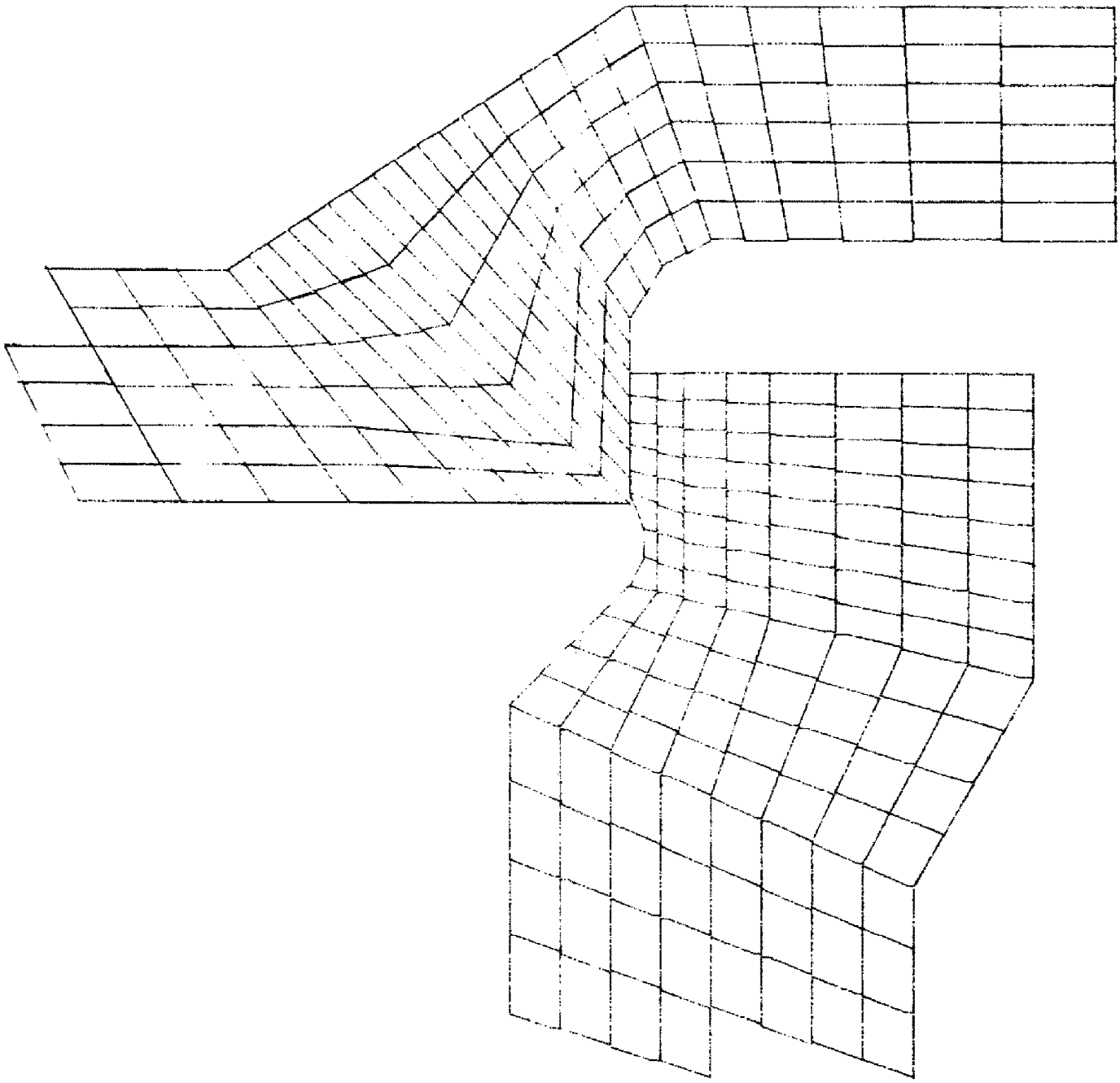

REV 21 5/08

SOUTHERN COMPANY
Energy to Serve Your World©

JOSEPH M. FARLEY
NUCLEAR PLANT
UNIT 1 AND UNIT 2

SECOND PISCES MODEL
(CLOSEUP OF CONTACT REGION)

FIGURE 10A-8

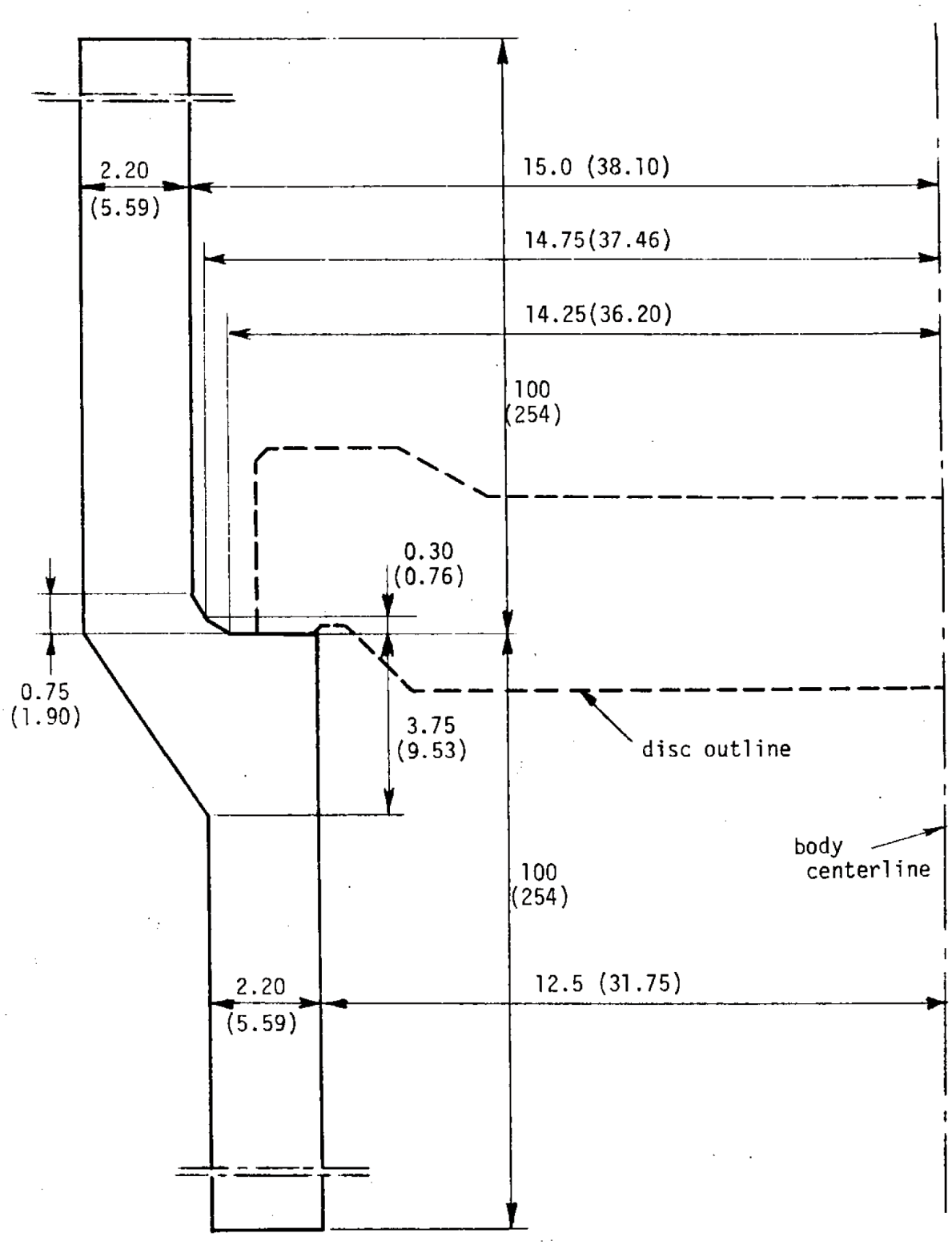

REV 21 5/08

SOUTHERN COMPANY
Energy to Serve Your World©

JOSEPH M. FARLEY NUCLEAR PLANT UNIT 1 AND UNIT 2

BODY DIMENSIONS ASSUMED FOR PISCES MODEL (IN INCHES AND IN CENTIMETERS)

FIGURE 10A-9

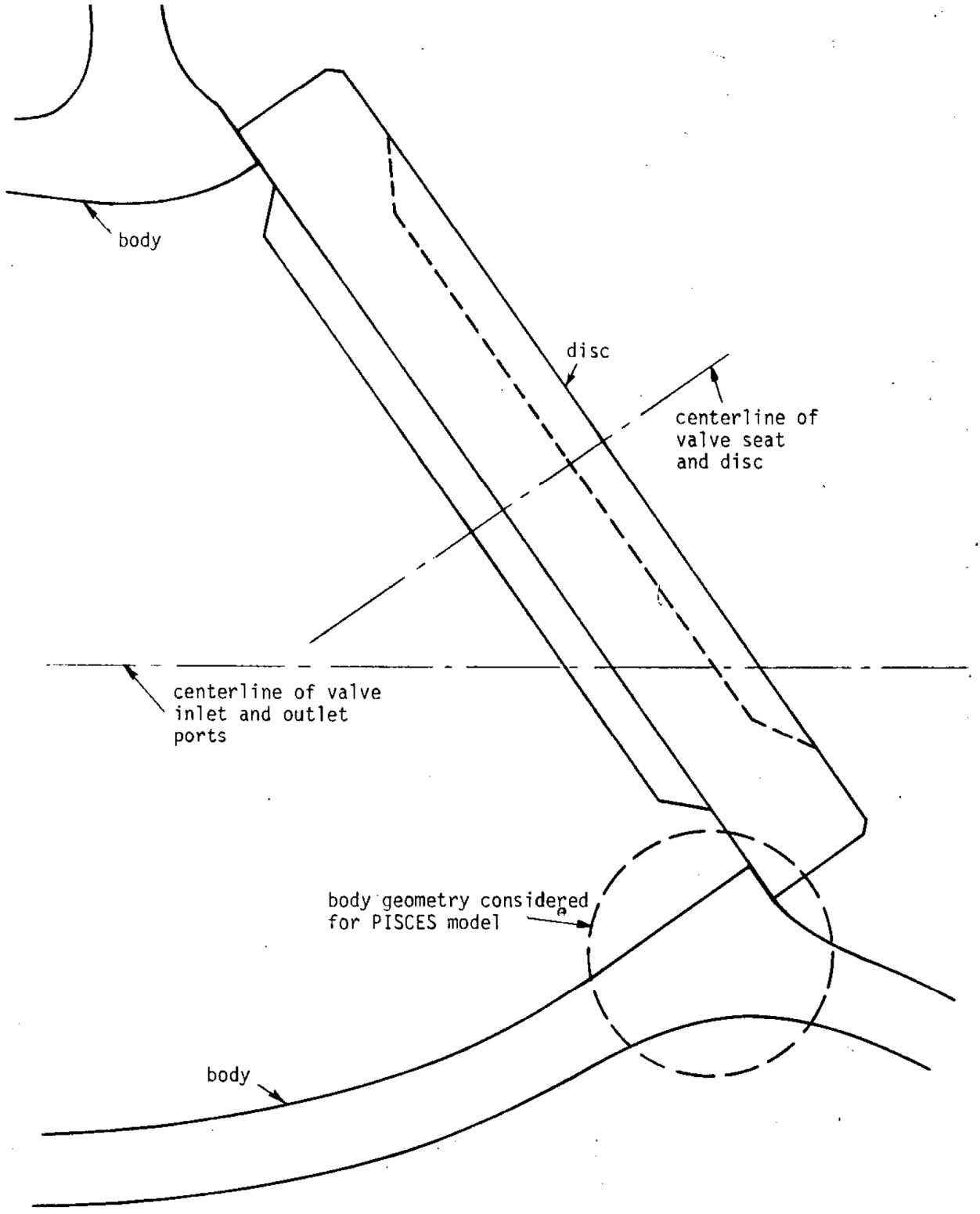

REV 21 5/08

SOUTHERN COMPANY
Energy to Serve Your World©

JOSEPH M. FARLEY
NUCLEAR PLANT
UNIT 1 AND UNIT 2

VALVE SEAT REGION OF
ISOLATION VALVE

FIGURE 10A-10

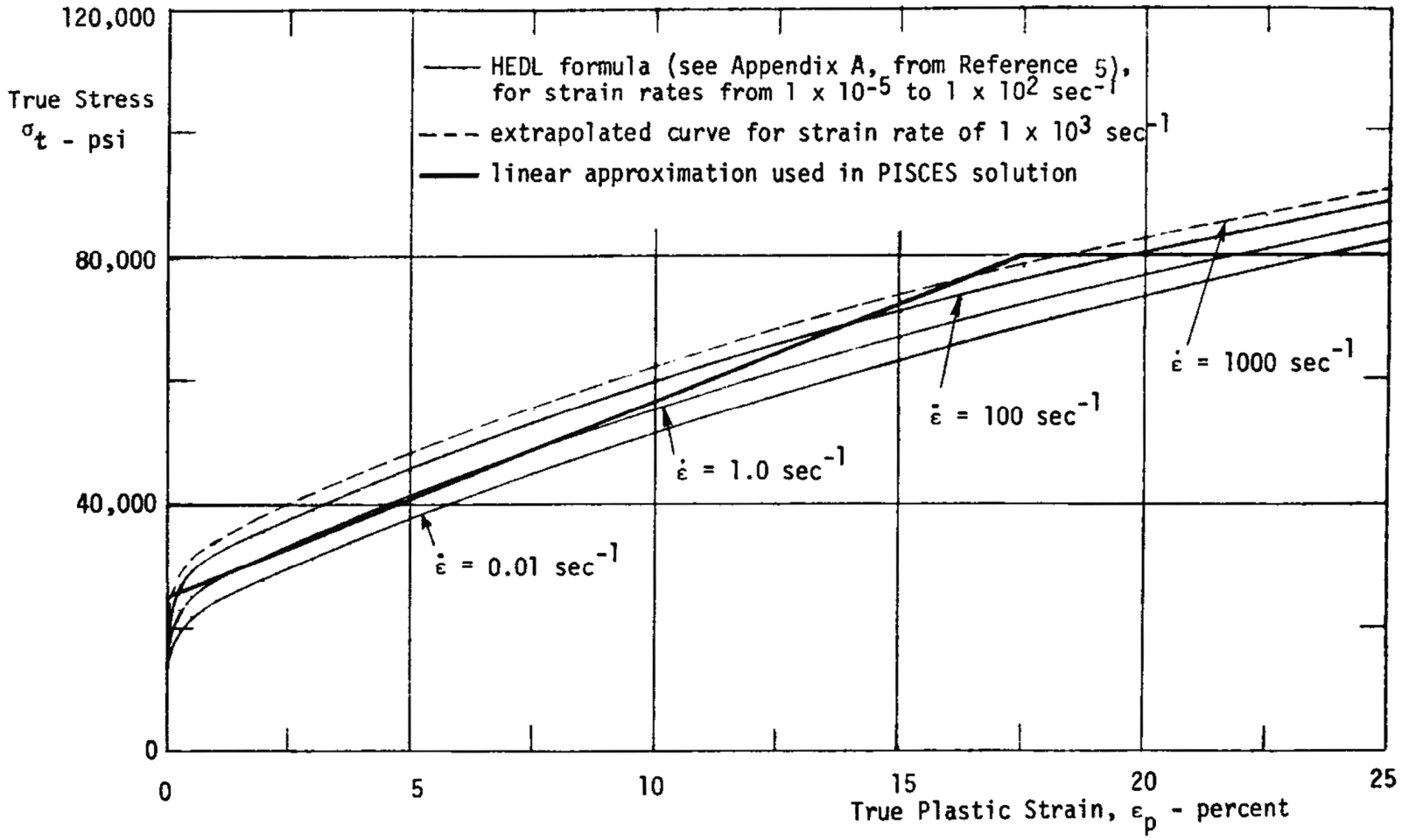

REV 21 5/08

SOUTHERN COMPANY
Energy to Serve Your World®

JOSEPH M. FARLEY
NUCLEAR PLANT
UNIT 1 AND UNIT 2

TYPICAL STRESS – TRUE STRAIN DIAGRAMS FOR AISI 304 STAINLESS STEEL

FIGURE 10A-11

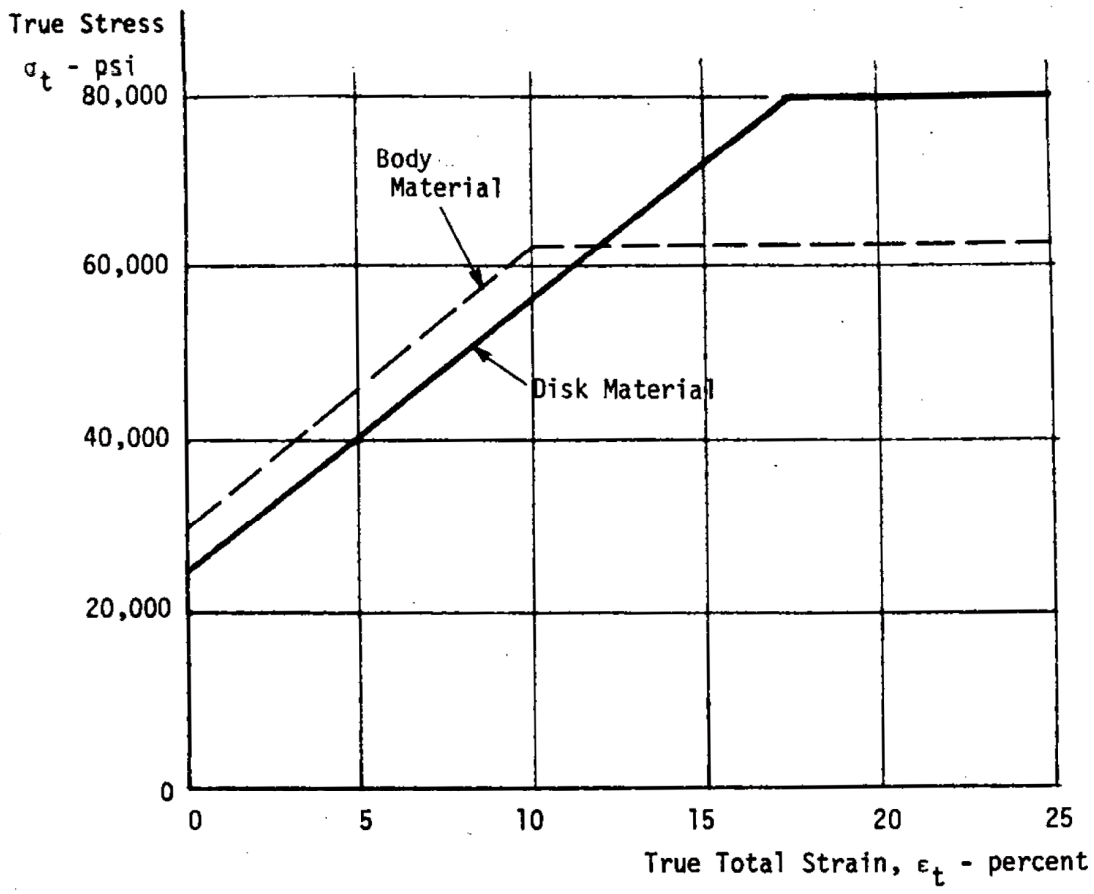

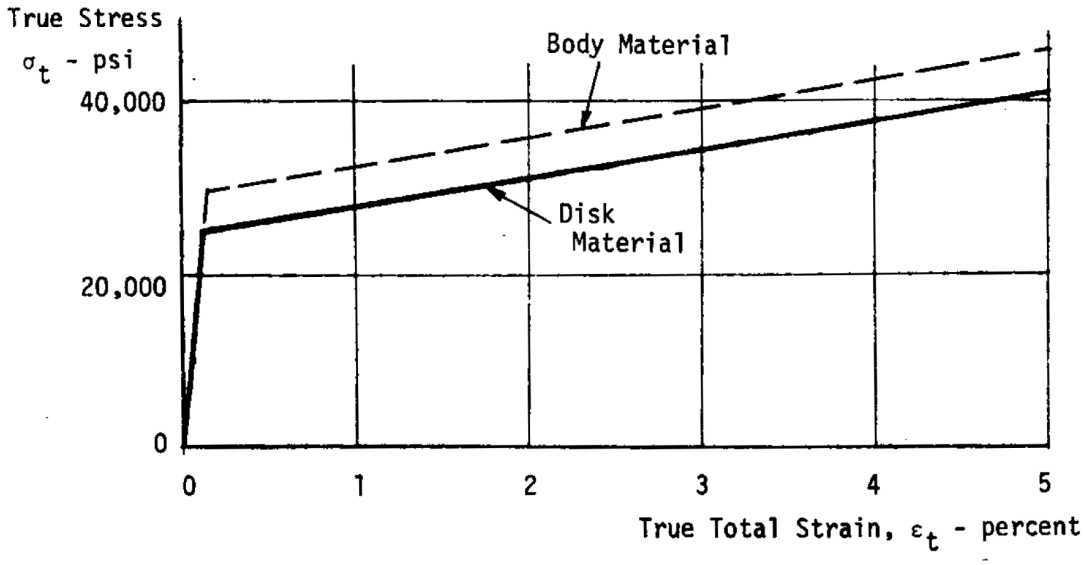

SOUTHERN COMPANY
Energy to Serve Your World©

JOSEPH M. FARLEY
NUCLEAR PLANT
UNIT 1 AND UNIT 2

STRESS-STRAIN DIAGRAMS USED IN PISCES SOLUTION

FIGURE 10A-12

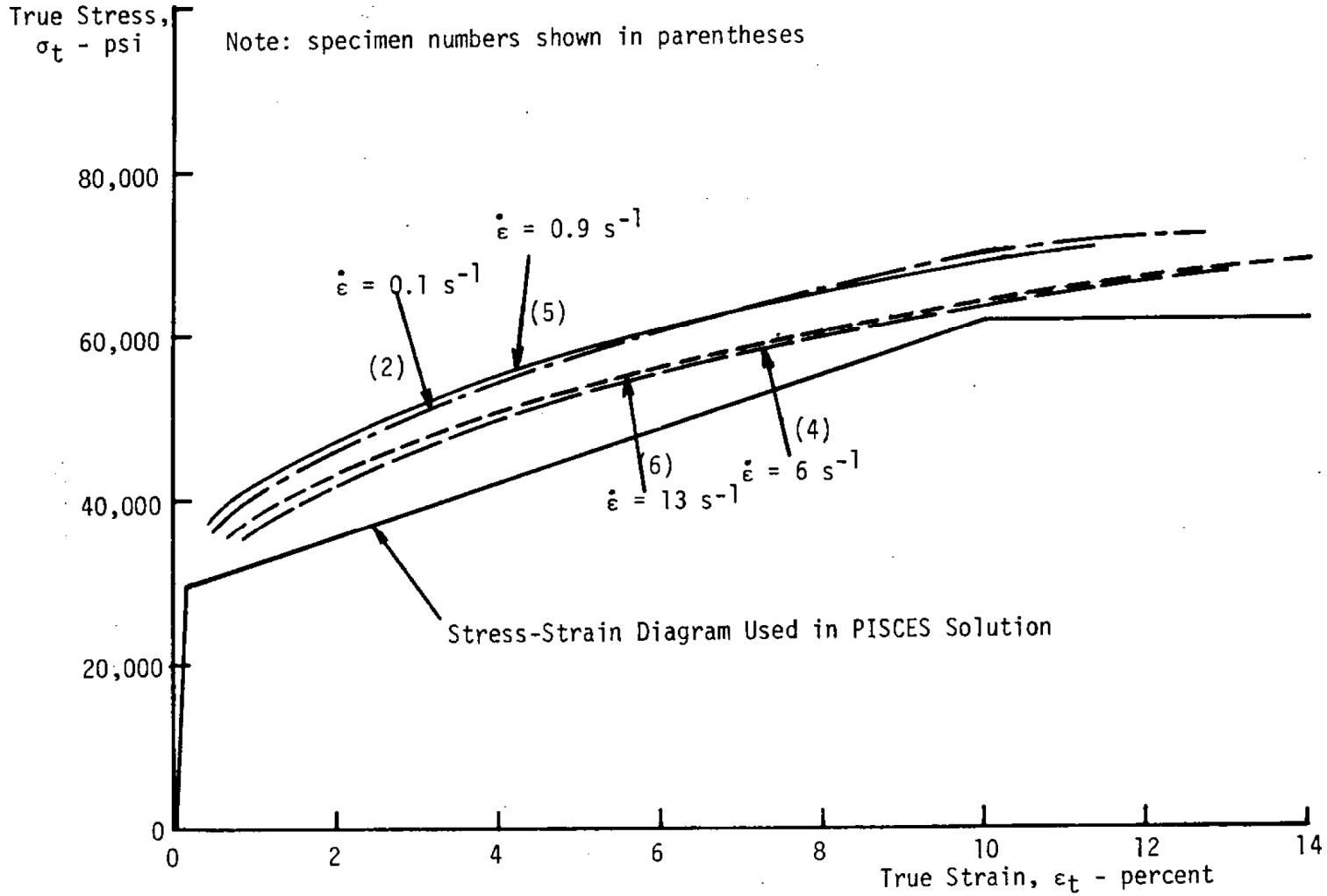

REV 21 5/08

SOUTHERN COMPANY
Energy to Serve Your World®

JOSEPH M. FARLEY
NUCLEAR PLANT
UNIT 1 AND UNIT 2

TYPICAL STRESS-STRAIN DIAGRAMS FOR
A-216 GRADE WCB STEEL
(X-DIRECTION, SEE TABLE 10A-2)

FIGURE 10A-13

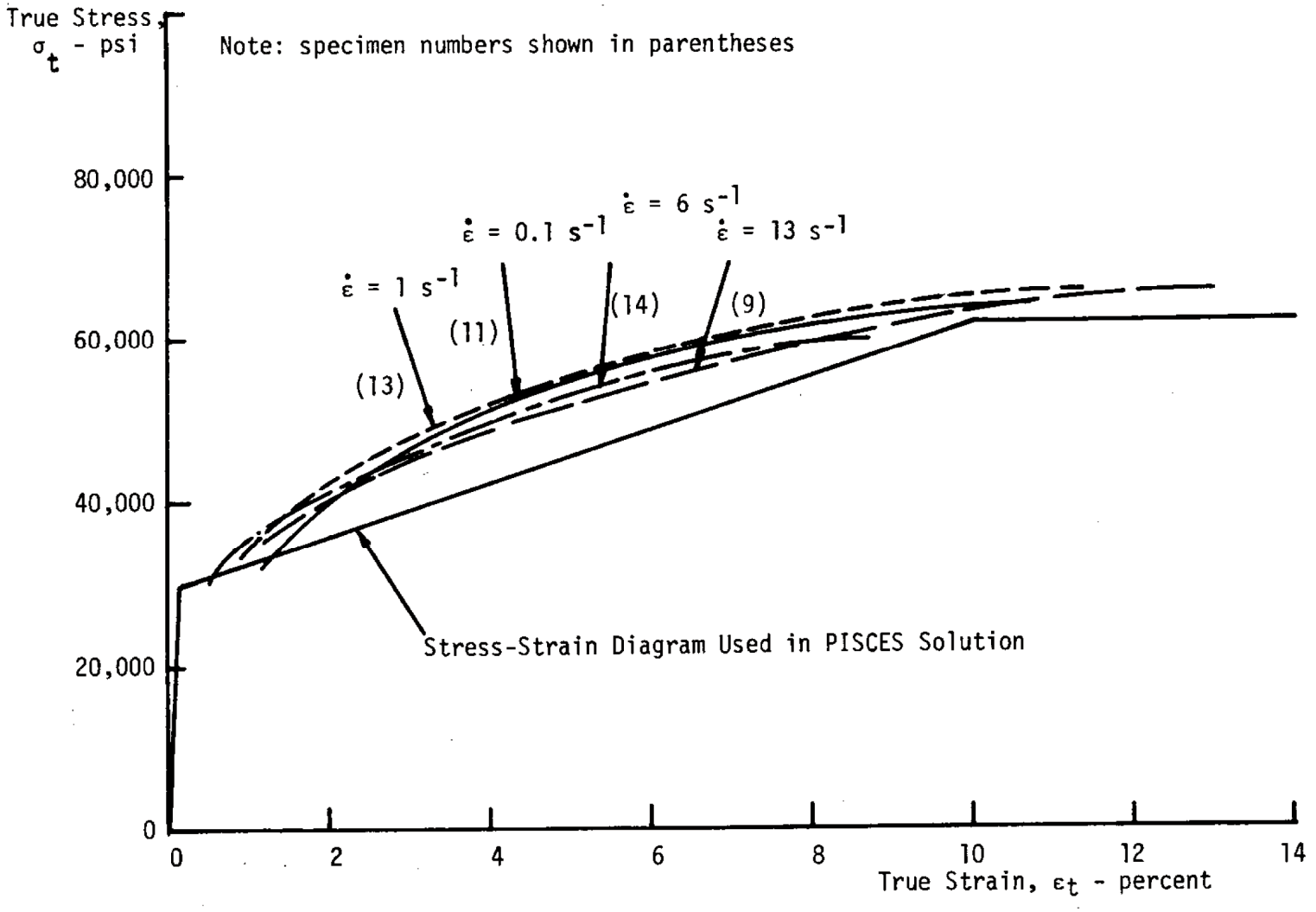

REV 21 5/08

SOUTHERN COMPANY
Energy to Serve Your World®

JOSEPH M. FARLEY NUCLEAR PLANT UNIT 1 AND UNIT 2

TYPICAL STRESS-STRAIN DIAGRAMS FOR A-216 GRADE WCB STEEL (Y-DIRECTION, SEE TABLE 10A-2)

FIGURE 10A-14

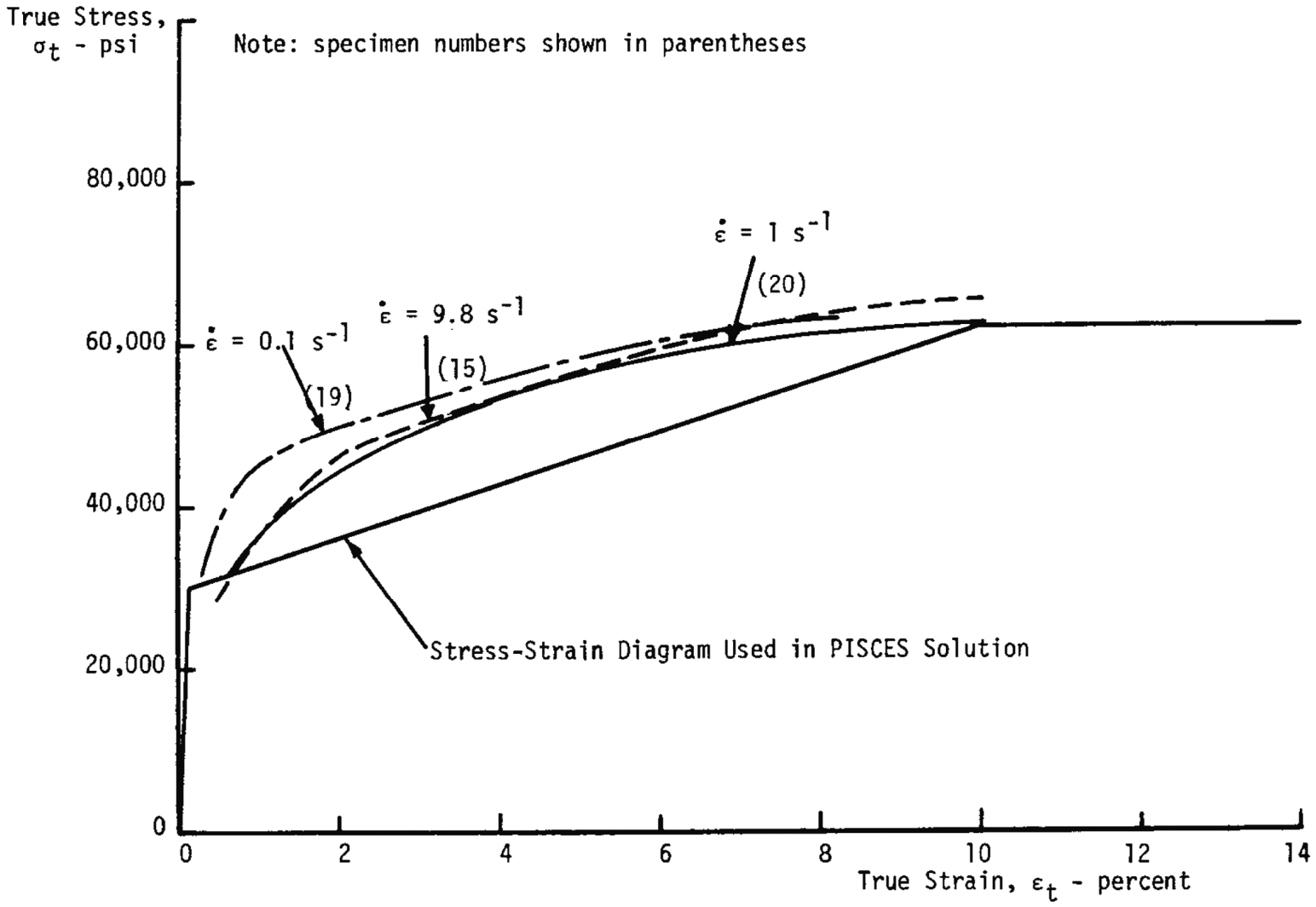

REV 21 5/08

SOUTHERN COMPANY
Energy to Serve Your World®

JOSEPH M. FARLEY
NUCLEAR PLANT
UNIT 1 AND UNIT 2

TYPICAL STRESS-STRAIN DIAGRAMS FOR
A-216 GRADE WCB STEEL
(Z-DIRECTION, SEE TABLE 10A-2)

FIGURE 10A-15

I = Column Number

J = Row Number

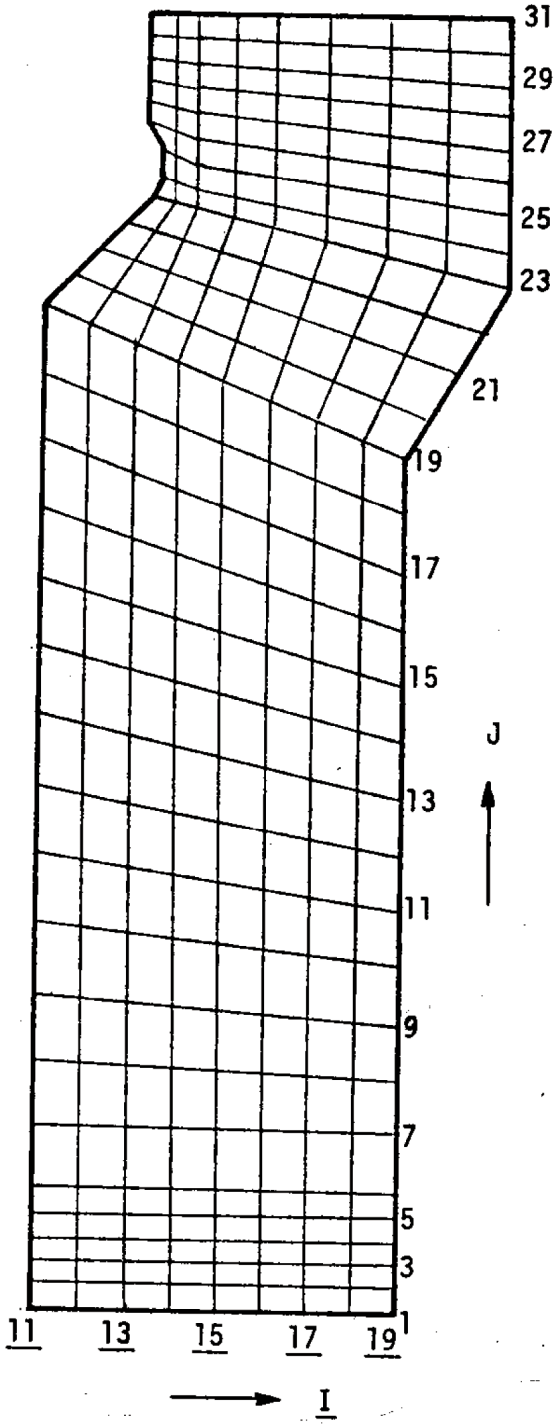

REV 21 5/08

SOUTHERN COMPANY *Energy to Serve Your World®*	JOSEPH M. FARLEY NUCLEAR PLANT UNIT 1 AND UNIT 2	COLUMN AND ROW NUMBERS OF DISC REGION
		FIGURE 10A-16

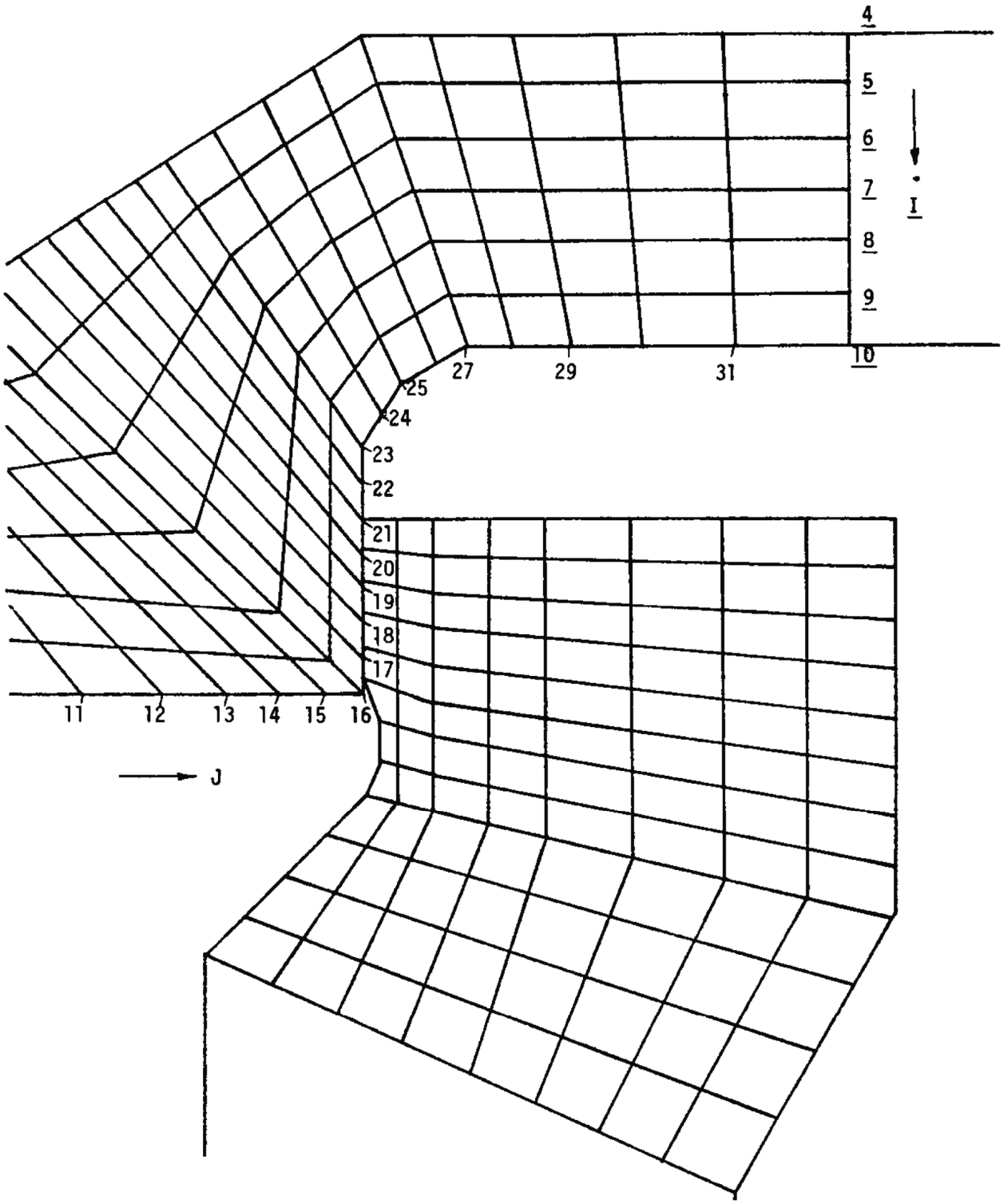

REV 21 5/08

SOUTHERN COMPANY
Energy to Serve Your World©

JOSEPH M. FARLEY NUCLEAR PLANT UNIT 1 AND UNIT 2

COLUMN AND ROW NUMBERS OF BODY REGION

FIGURE 10A-17

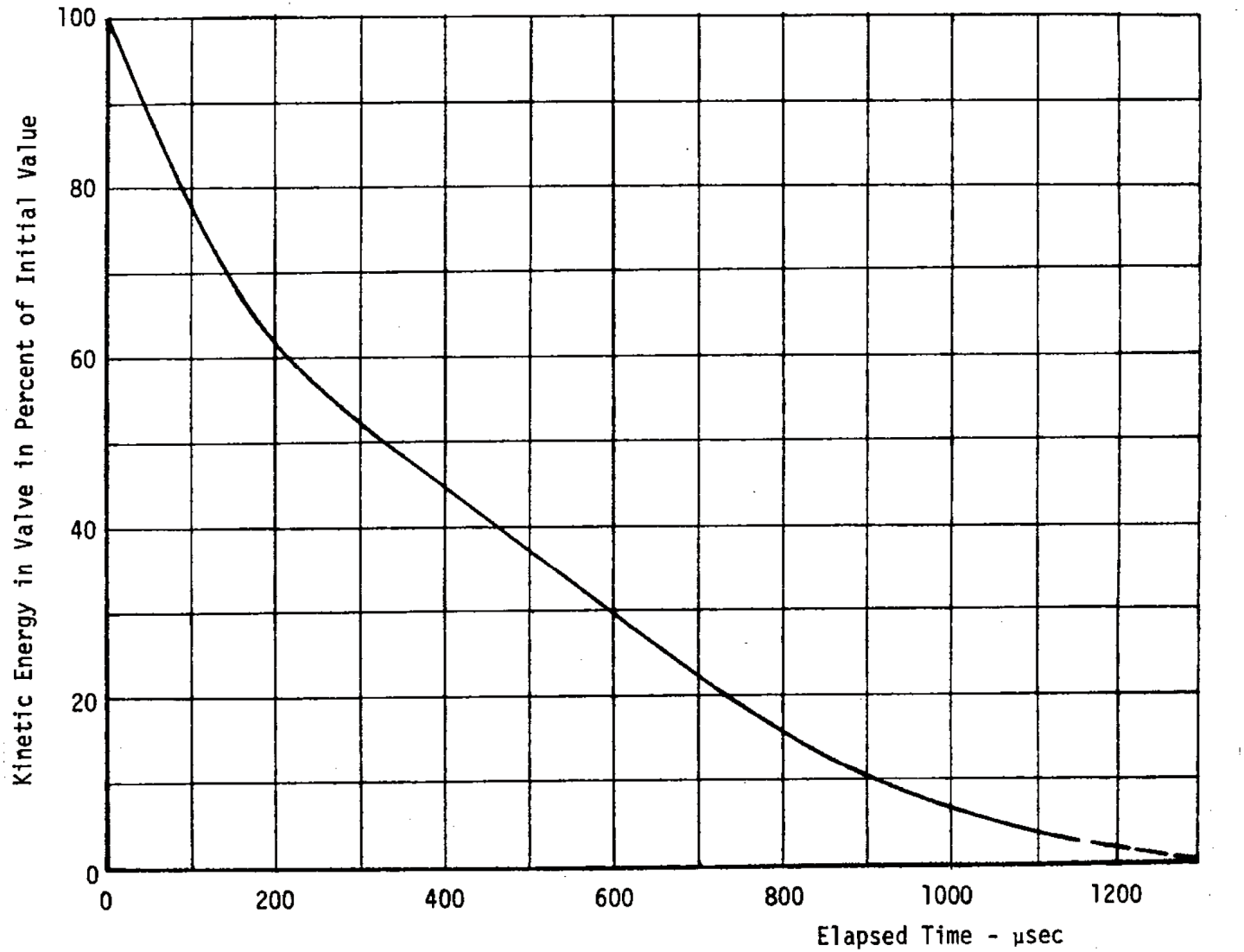

REV 21 5/08

SOUTHERN COMPANY
Energy to Serve Your World©

JOSEPH M. FARLEY
NUCLEAR PLANT
UNIT 1 AND UNIT 2

KINETIC ENERGY IN VALVE
VERSUS TIME SINCE IMPACT

FIGURE 10A-18

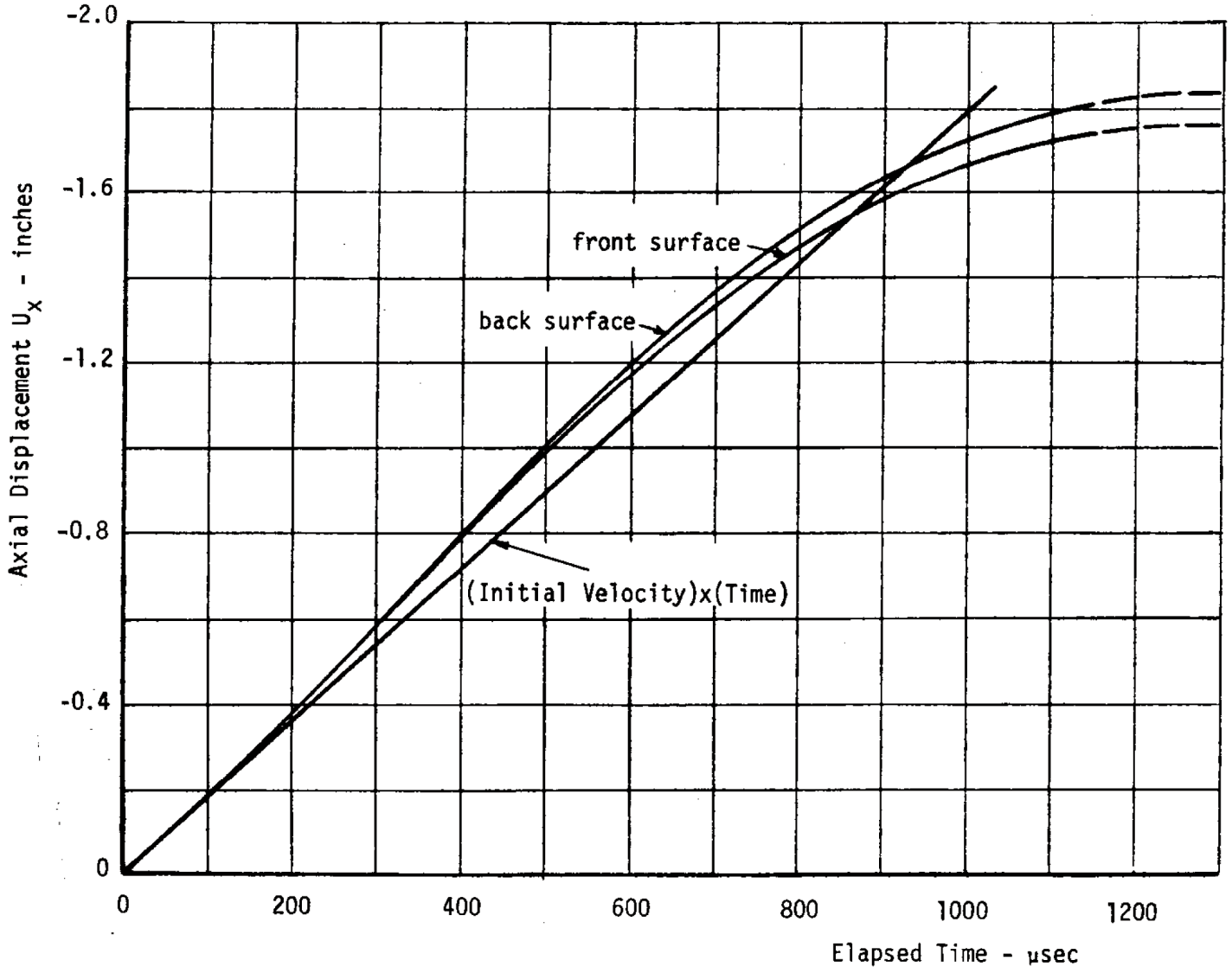

REV 21 5/08

SOUTHERN COMPANY
Energy to Serve Your World®

JOSEPH M. FARLEY
NUCLEAR PLANT
UNIT 1 AND UNIT 2

AXIAL DISPLACEMENTS AT
CENTERLINE OF DISC VERSUS TIME
SINCE IMPACT

FIGURE 10A-19

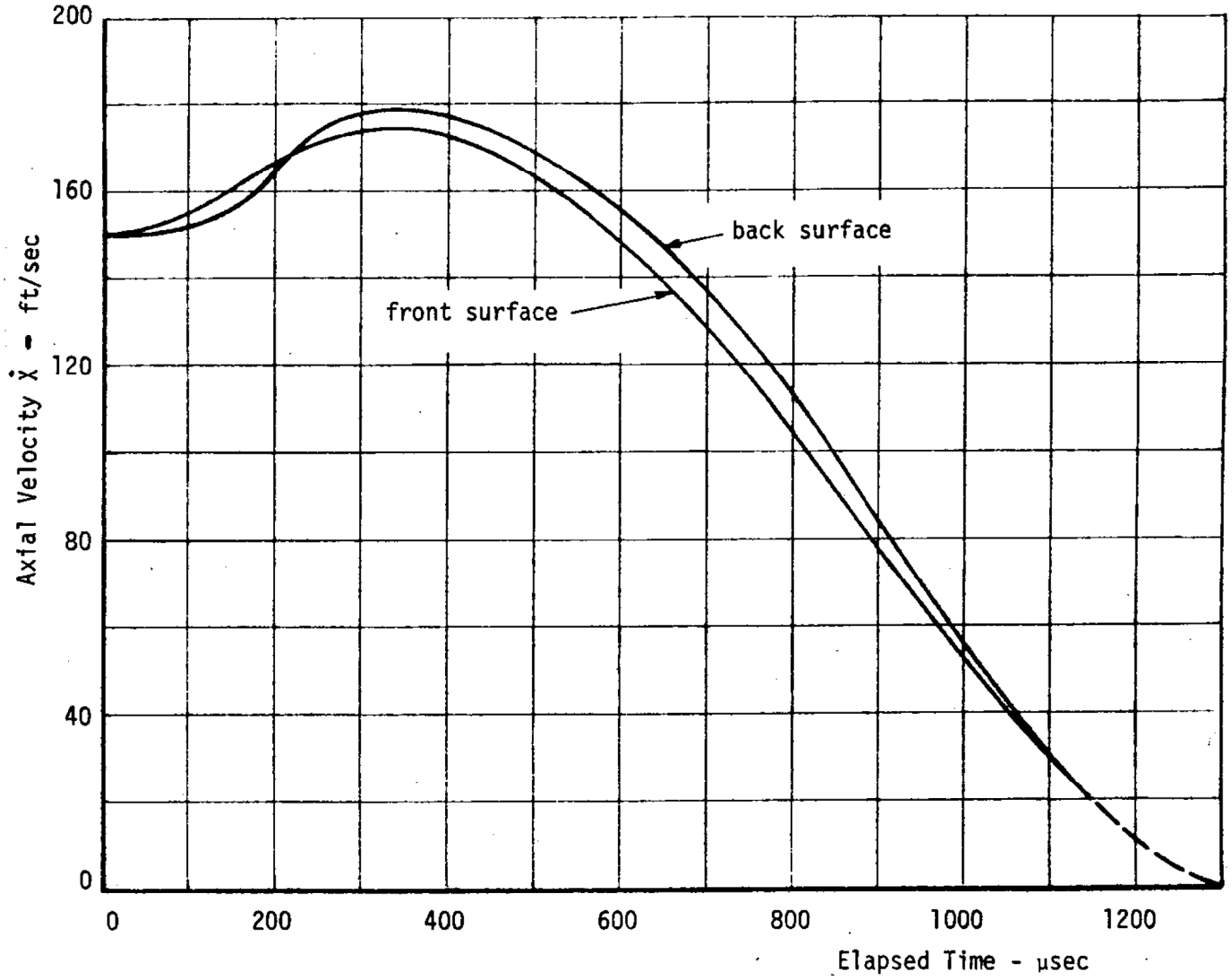

REV 21 5/08

SOUTHERN COMPANY
Energy to Serve Your World©

JOSEPH M. FARLEY NUCLEAR PLANT UNIT 1 AND UNIT 2

AXIAL VELOCITY AT CENTERLINE OF DISC VERSUS TIME SINCE IMPACT

FIGURE 10A-20

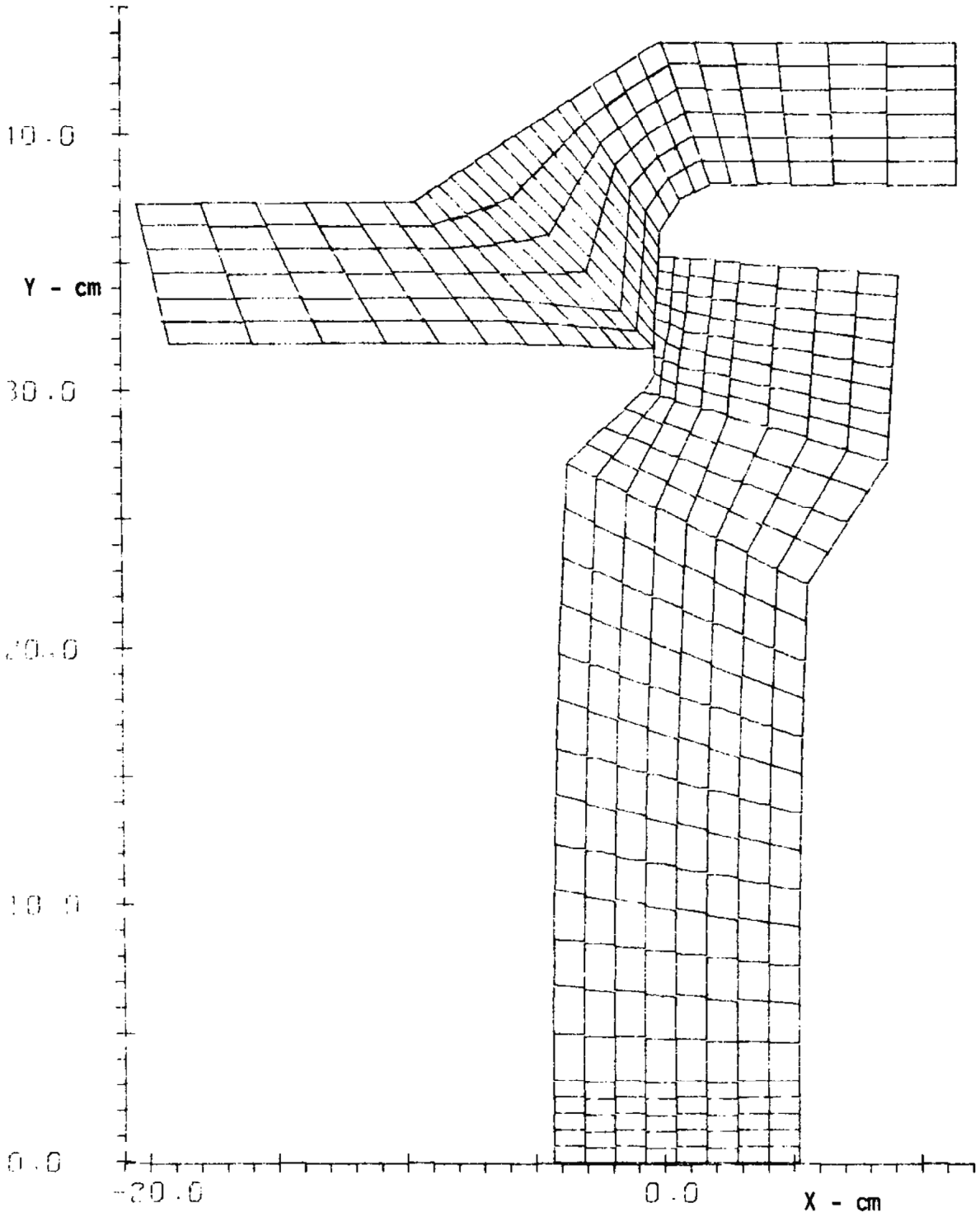

REV 21 5/08

SOUTHERN COMPANY
Energy to Serve Your World®

JOSEPH M. FARLEY
NUCLEAR PLANT
UNIT 1 AND UNIT 2

DISTORTED GEOMETRY AT TIME
t = 300 μS

FIGURE 10A-21

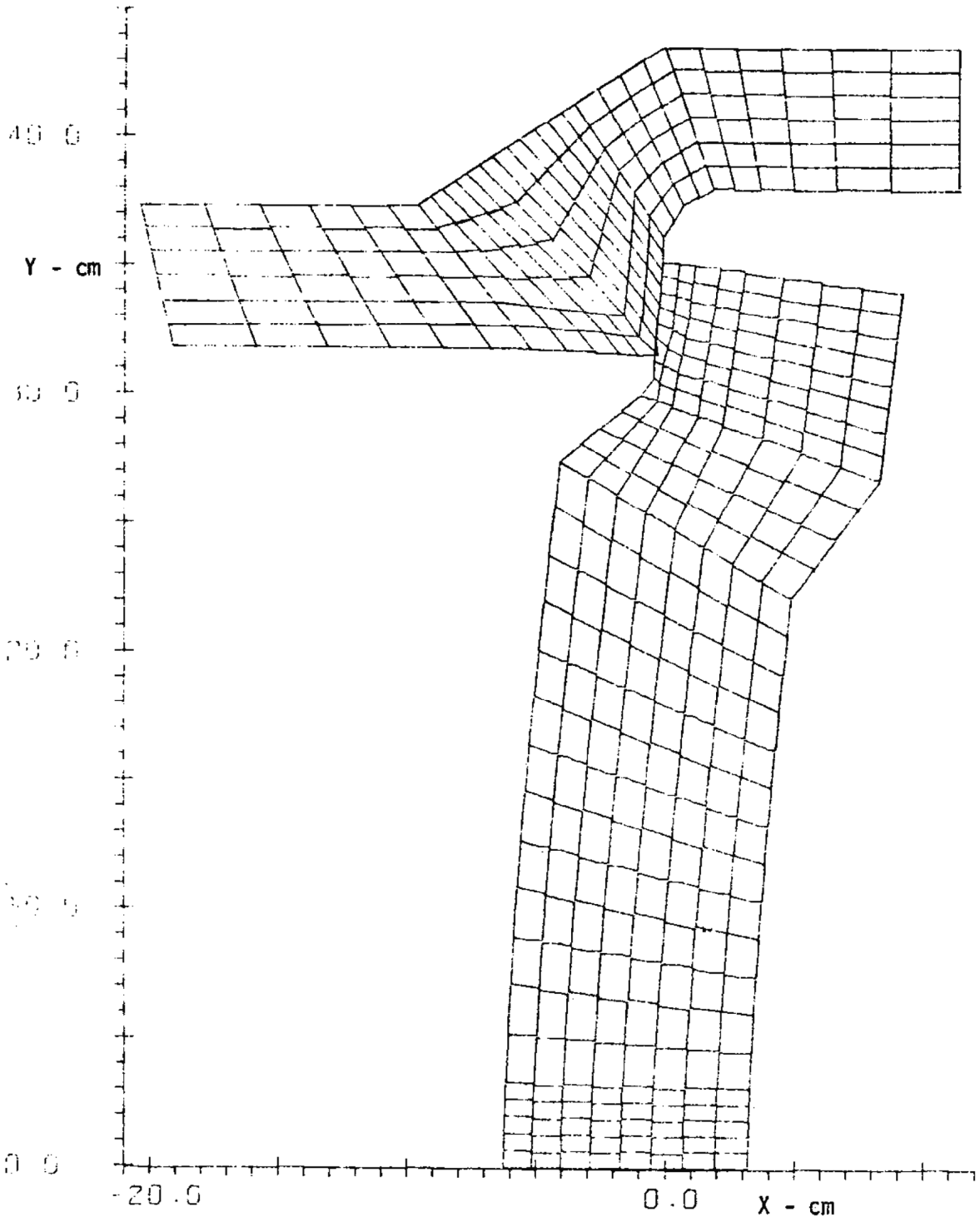

REV 21 5/08

SOUTHERN COMPANY
Energy to Serve Your World®

JOSEPH M. FARLEY
NUCLEAR PLANT
UNIT 1 AND UNIT 2

DISTORTED GEOMETRY AT TIME
t = 700 µS

FIGURE 10A-22

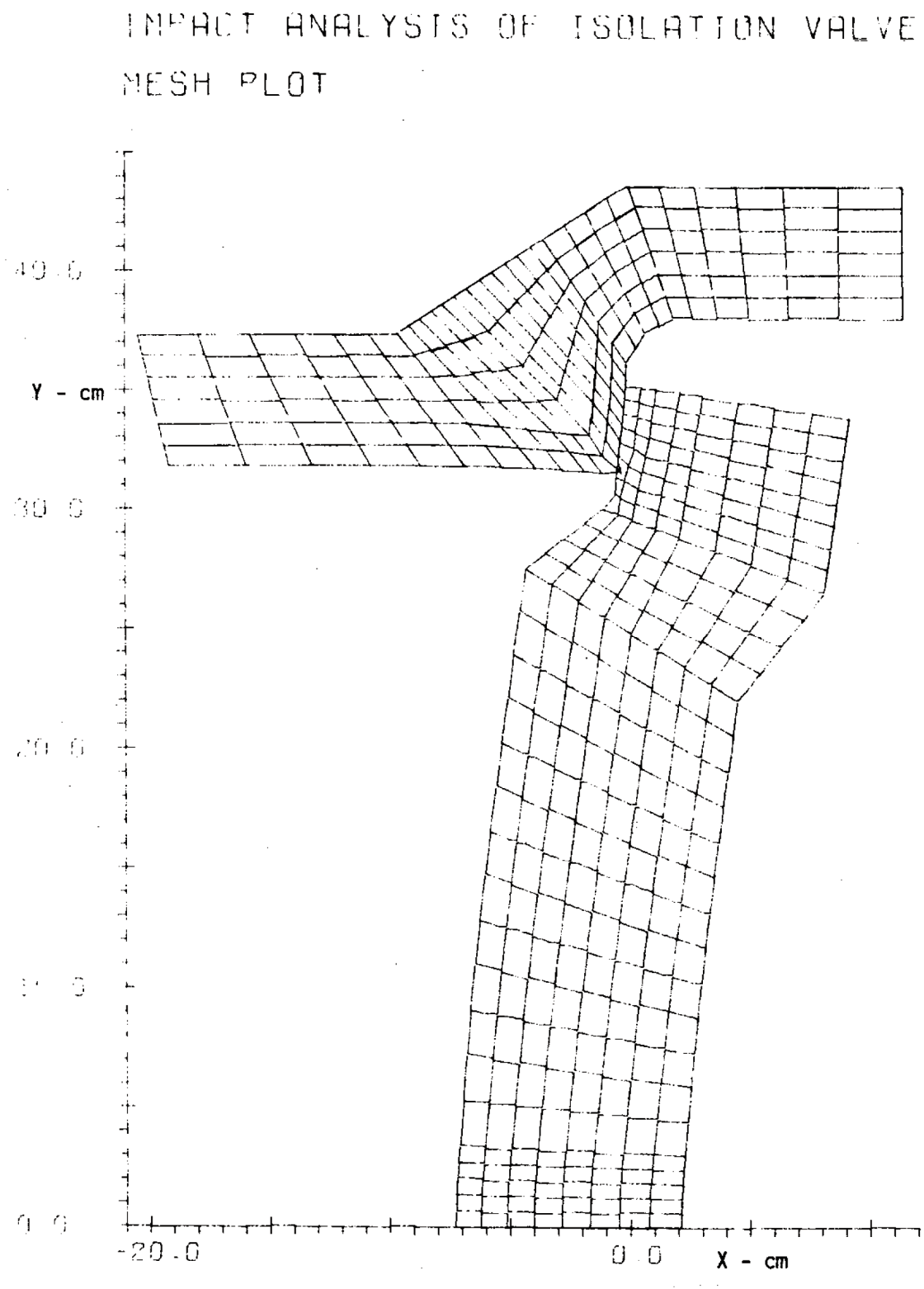

REV 21 5/08

SOUTHERN COMPANY
Energy to Serve Your World®

JOSEPH M. FARLEY NUCLEAR PLANT UNIT 1 AND UNIT 2

DISTORTED GEOMETRY AT TIME
t = 1150 µS

FIGURE 10A-23

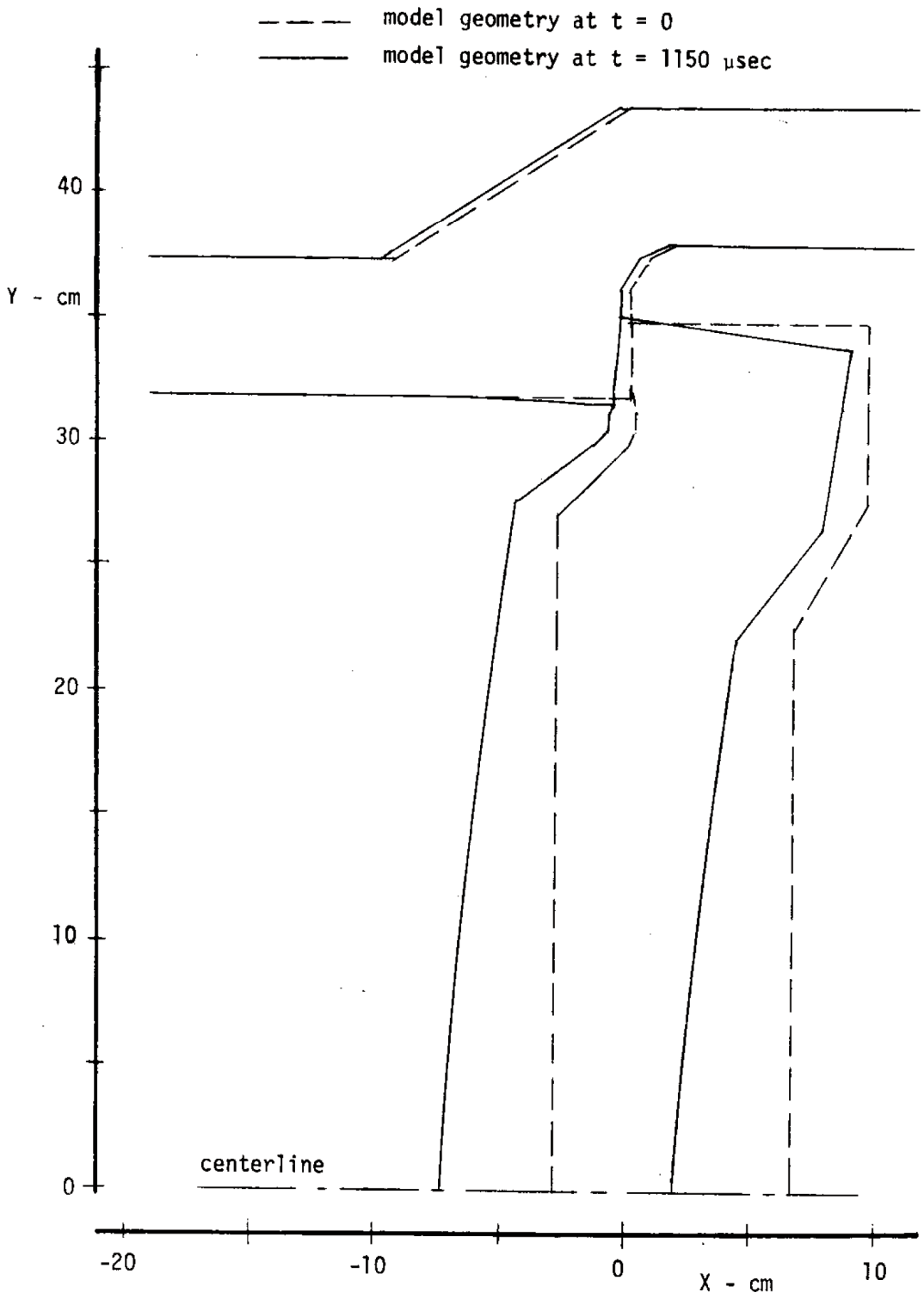

REV 21 5/08

SOUTHERN COMPANY
Energy to Serve Your World®

JOSEPH M. FARLEY NUCLEAR PLANT UNIT 1 AND UNIT 2

SHAPE OF MODEL BEFORE AND AFTER IMPACT

FIGURE 10A-24

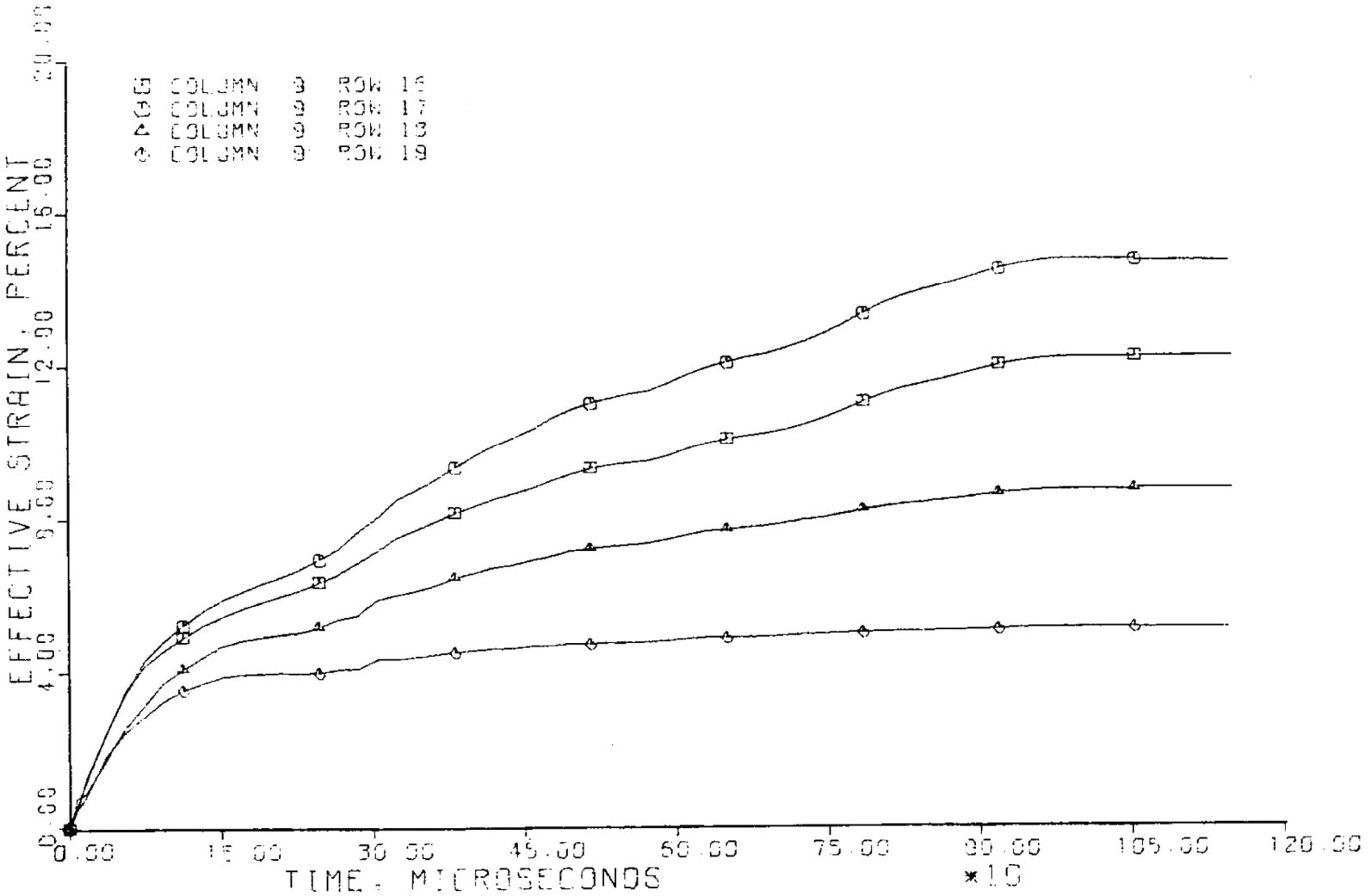

REV 21 5/08

SOUTHERN COMPANY
Energy to Serve Your World®

JOSEPH M. FARLEY
NUCLEAR PLANT
UNIT 1 AND UNIT 2

EFFECTIVE STRAINS IN BODY VERSUS TIME SINCE IMPACT

FIGURE 10A-25

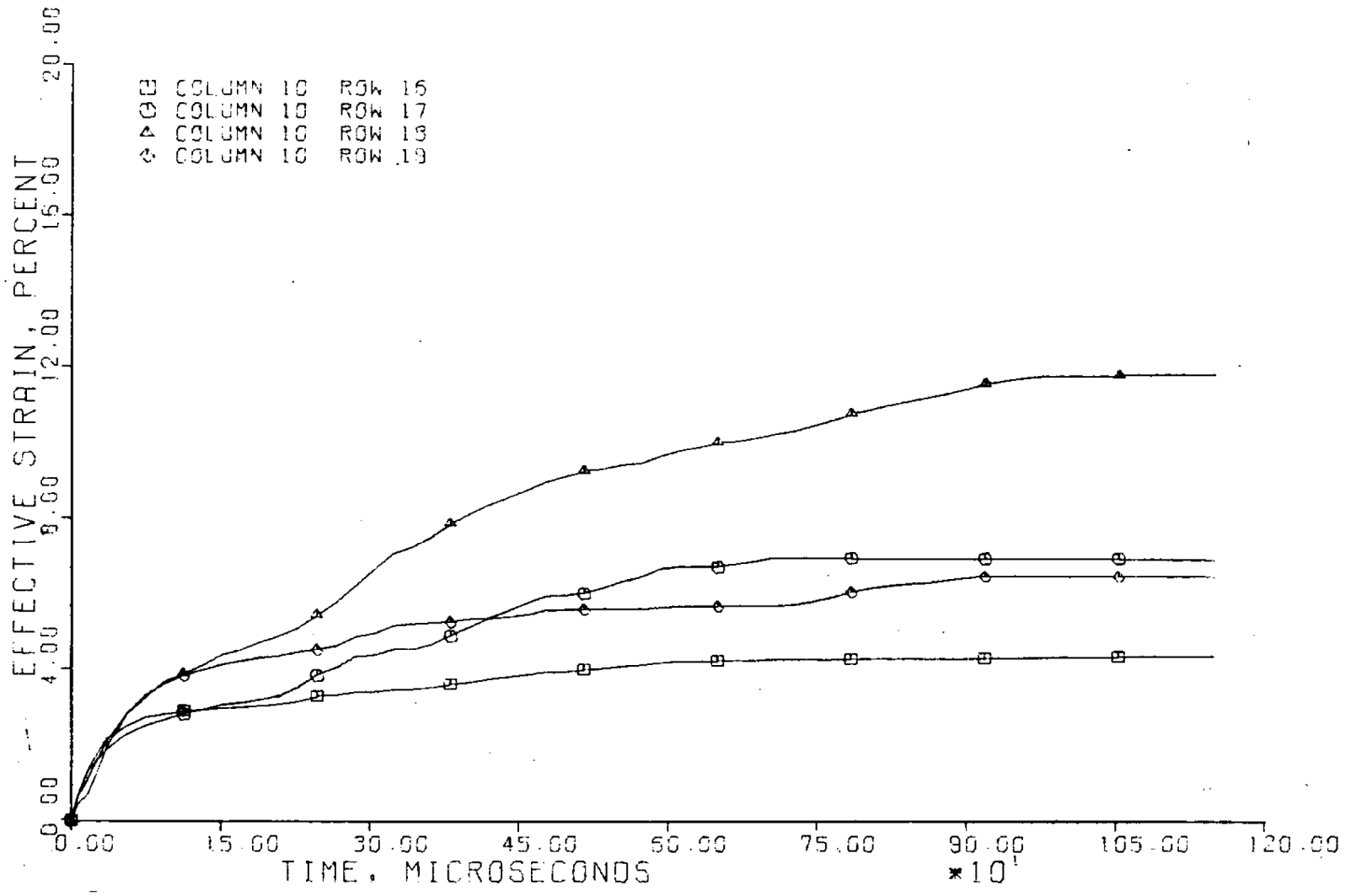

REV 21 5/08

SOUTHERN COMPANY
Energy to Serve Your World©

JOSEPH M. FARLEY
NUCLEAR PLANT
UNIT 1 AND UNIT 2

EFFECTIVE STRAINS IN BODY VERSUS TIME SINCE IMPACT

FIGURE 10A-26

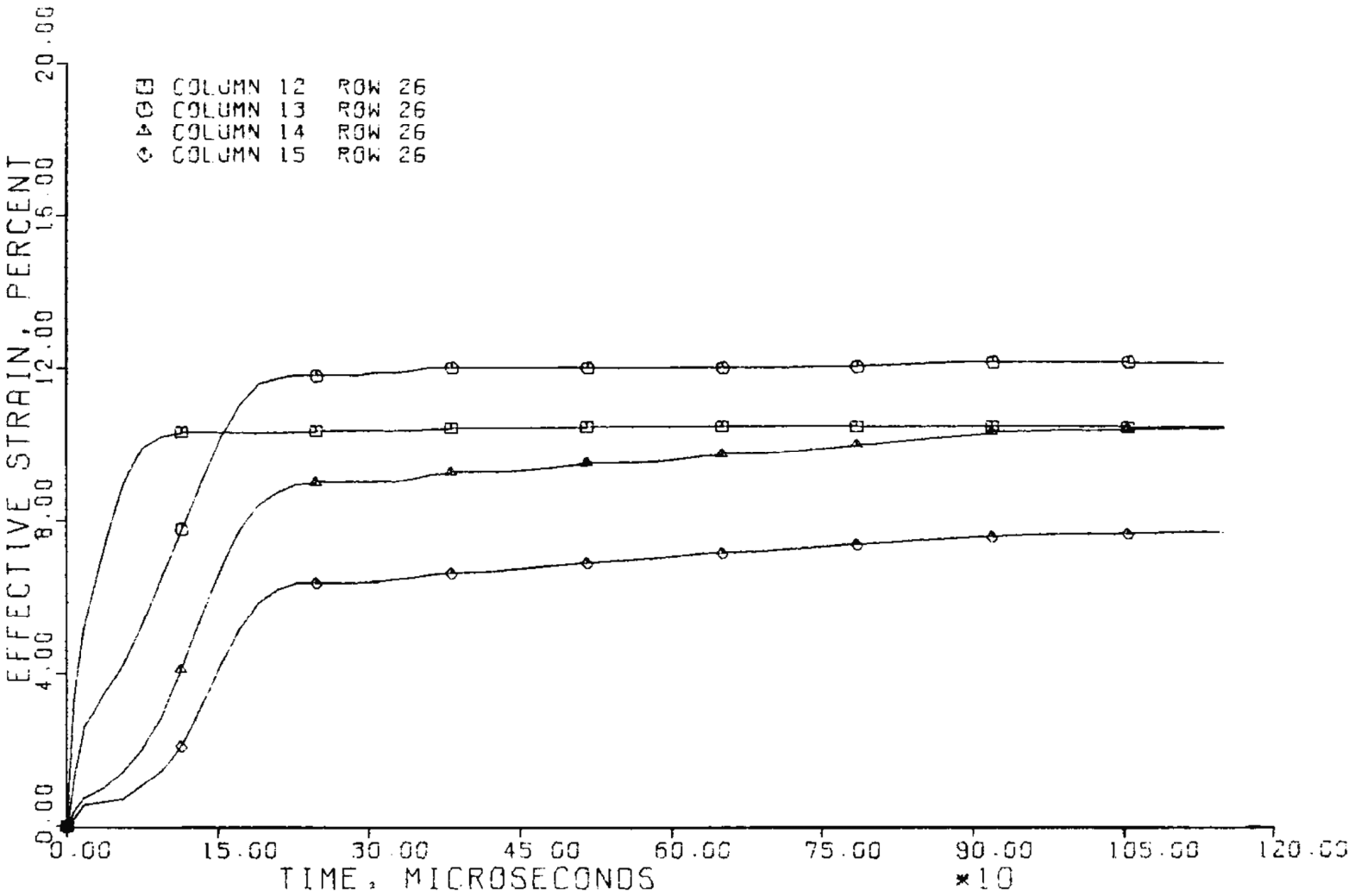

REV 21 5/08

SOUTHERN COMPANY
Energy to Serve Your World©

JOSEPH M. FARLEY
NUCLEAR PLANT
UNIT 1 AND UNIT 2

EFFECTIVE STRAINS IN DISC VERSUS TIME SINCE IMPACT

FIGURE 10A-27

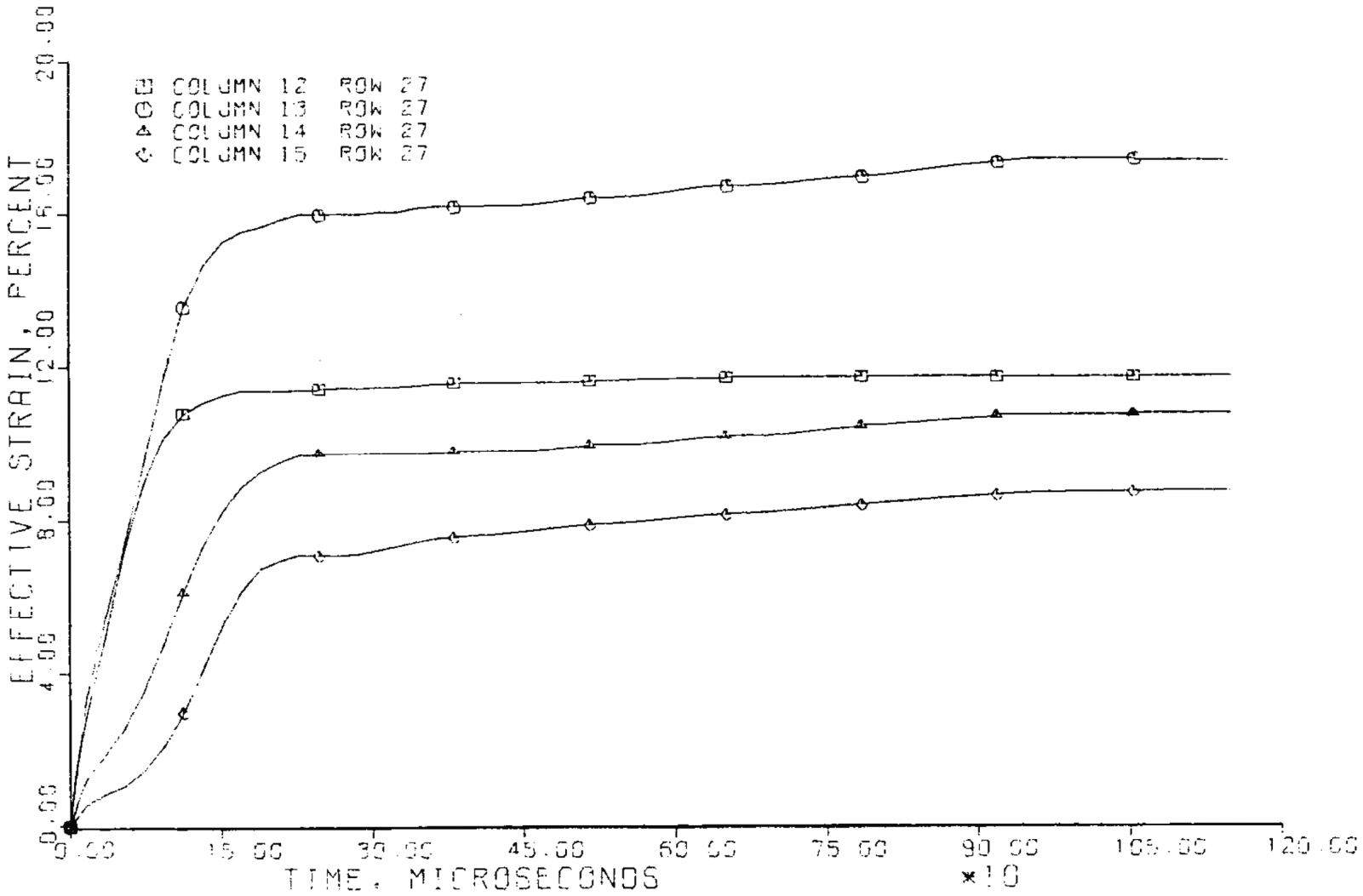

REV 21 5/08

SOUTHERN COMPANY
Energy to Serve Your World©

JOSEPH M. FARLEY NUCLEAR PLANT UNIT 1 AND UNIT 2

EFFECTIVE STRAINS IN DISC VERSUS TIME SINCE IMPACT

FIGURE 10A-28

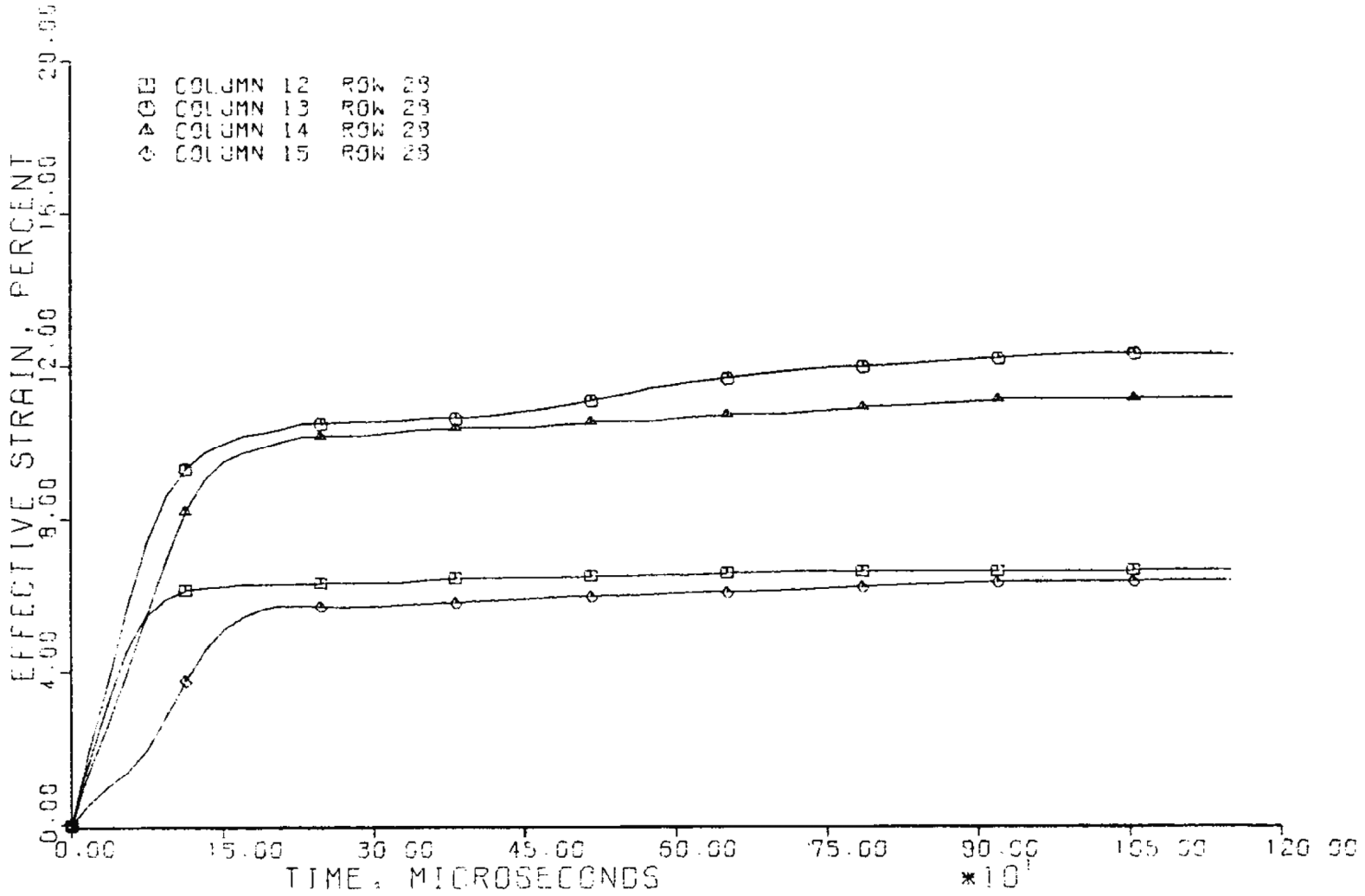

REV 21 5/08

SOUTHERN COMPANY
Energy to Serve Your World®

JOSEPH M. FARLEY
NUCLEAR PLANT
UNIT 1 AND UNIT 2

EFFECTIVE STRAINS IN DISC VERSUS TIME SINCE IMPACT

FIGURE 10A-29

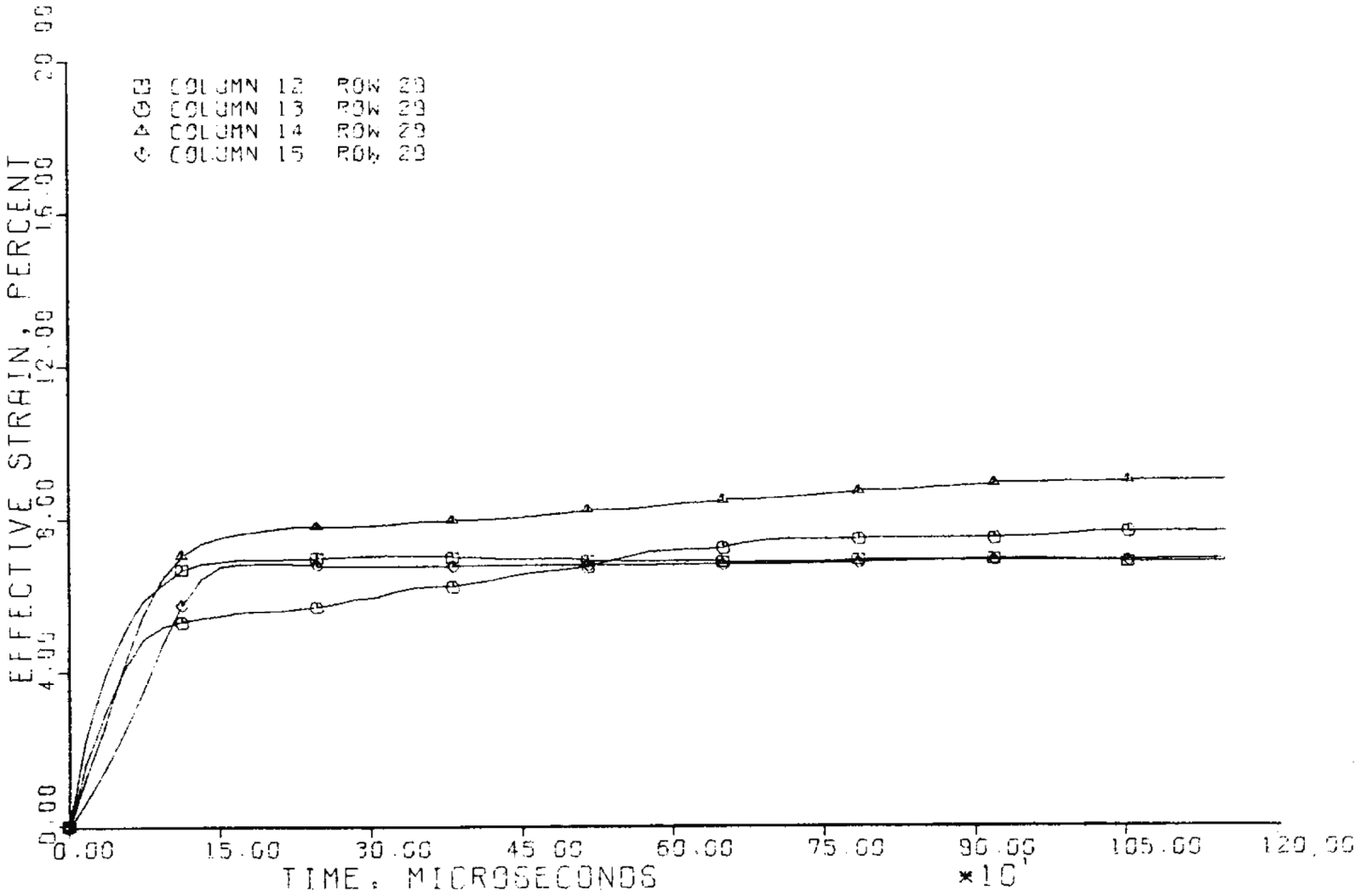

REV 21 5/08

SOUTHERN COMPANY
Energy to Serve Your World©

JOSEPH M. FARLEY
NUCLEAR PLANT
UNIT 1 AND UNIT 2

EFFECTIVE STRAINS IN DISC VERSUS TIME SINCE IMPACT

FIGURE 10A-30

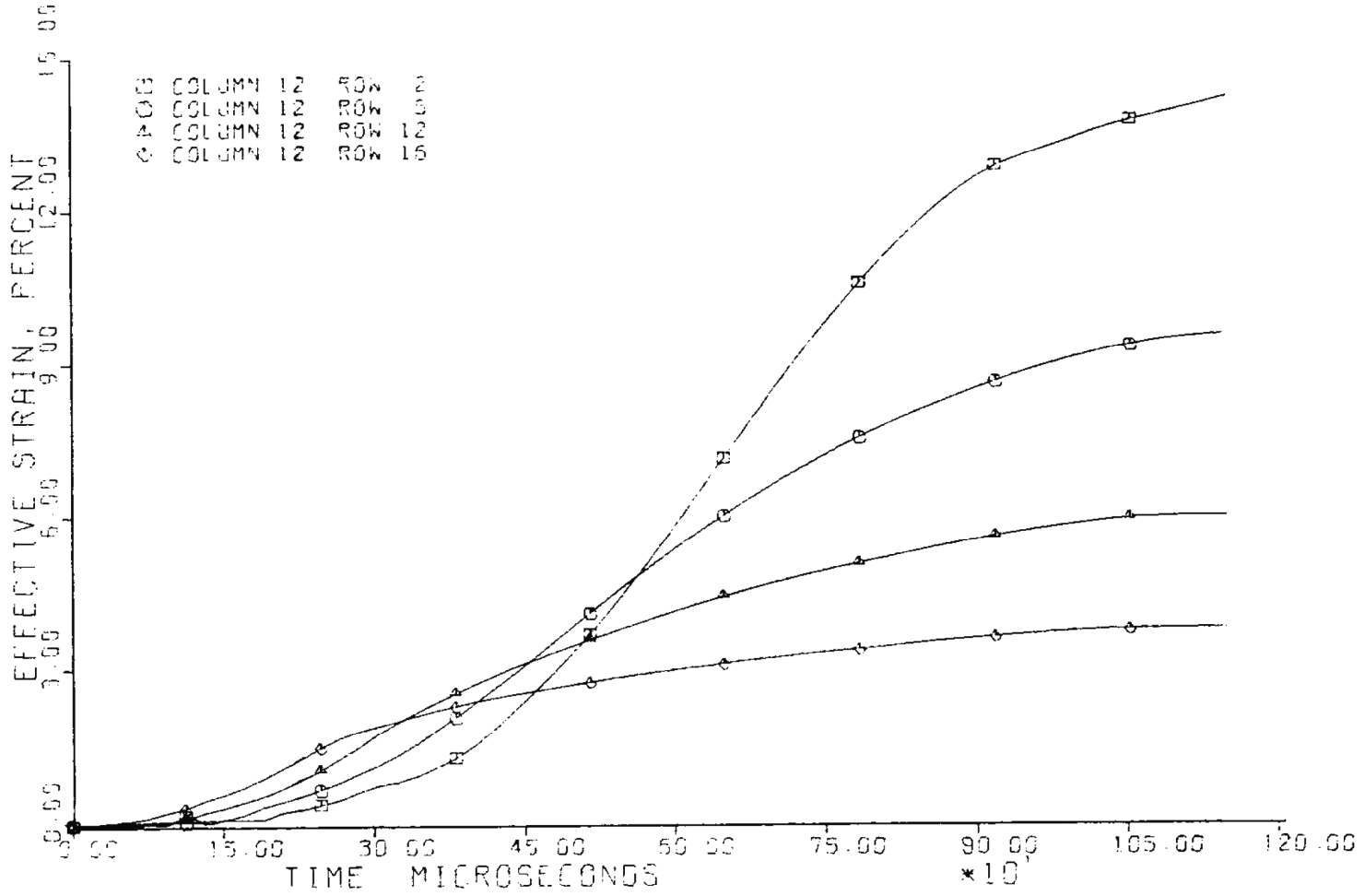

REV 21 5/08

SOUTHERN COMPANY
Energy to Serve Your World©

JOSEPH M. FARLEY
NUCLEAR PLANT
UNIT 1 AND UNIT 2

EFFECTIVE STRAINS IN DISC VERSUS TIME SINCE IMPACT

FIGURE 10A-31

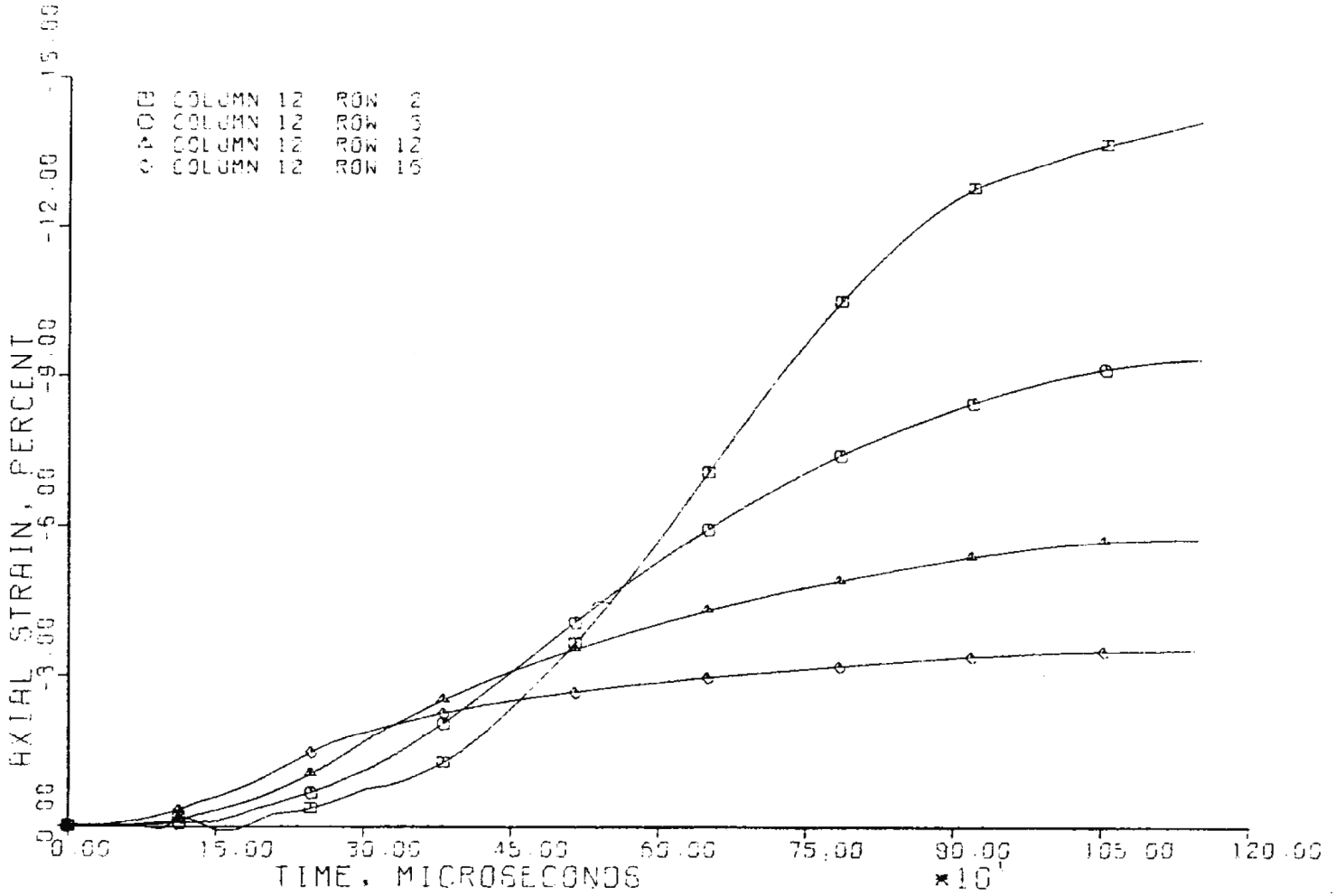

REV 21 5/08

SOUTHERN COMPANY
Energy to Serve Your World®

JOSEPH M. FARLEY
NUCLEAR PLANT
UNIT 1 AND UNIT 2

AXIAL STRAINS IN DISC VERSUS
TIME SINCE IMPACT

FIGURE 10A-32

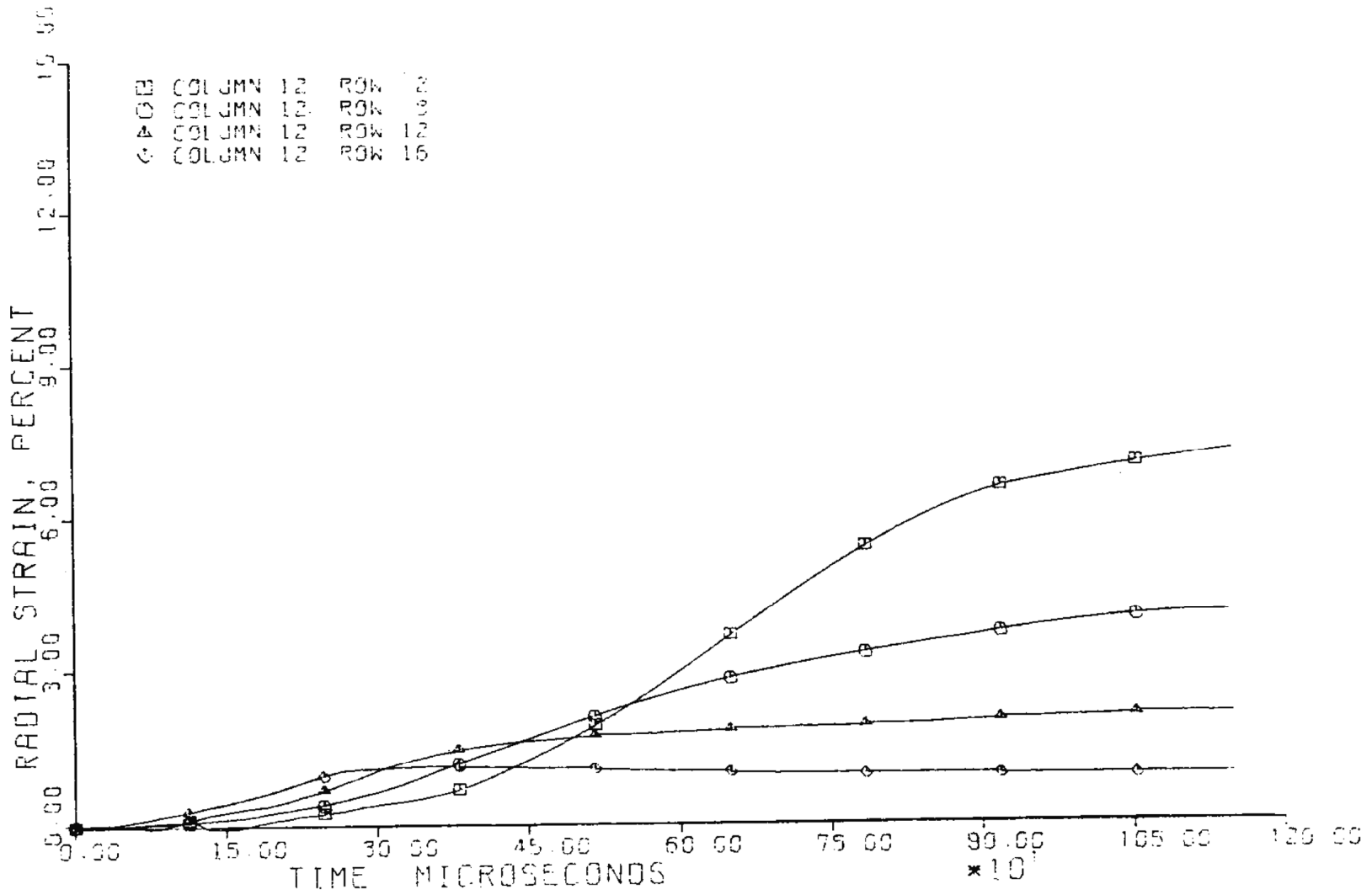

REV 21 5/08

SOUTHERN COMPANY
Energy to Serve Your World©

JOSEPH M. FARLEY
NUCLEAR PLANT
UNIT 1 AND UNIT 2

RADIAL STRAINS IN DISC VERSUS TIME SINCE IMPACT

FIGURE 10A-33

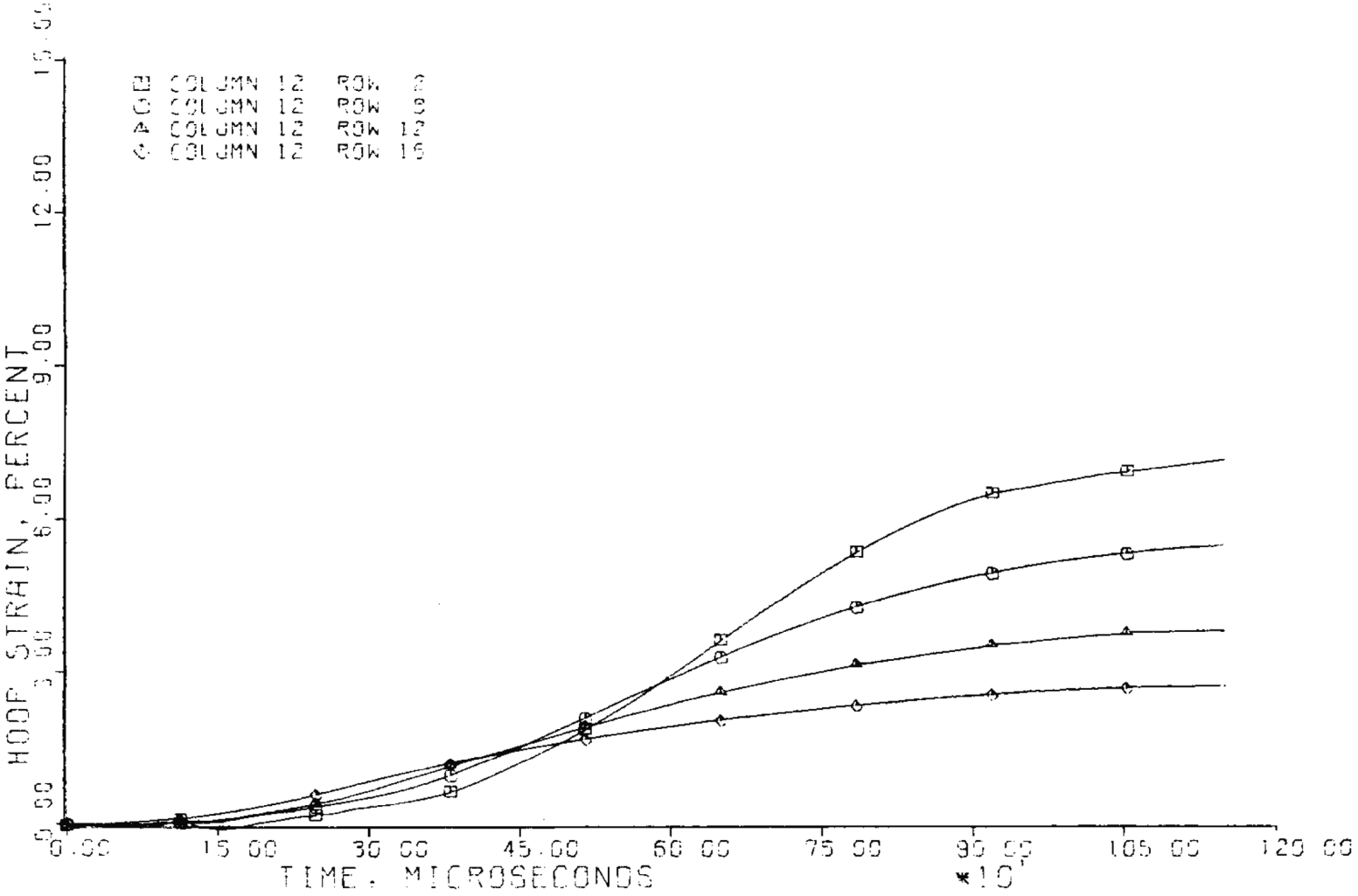

REV 21 5/08

SOUTHERN COMPANY
Energy to Serve Your World©

JOSEPH M. FARLEY
NUCLEAR PLANT
UNIT 1 AND UNIT 2

HOOP STRAINS IN DISC VERSUS
TIME SINCE IMPACT

FIGURE 10A-34

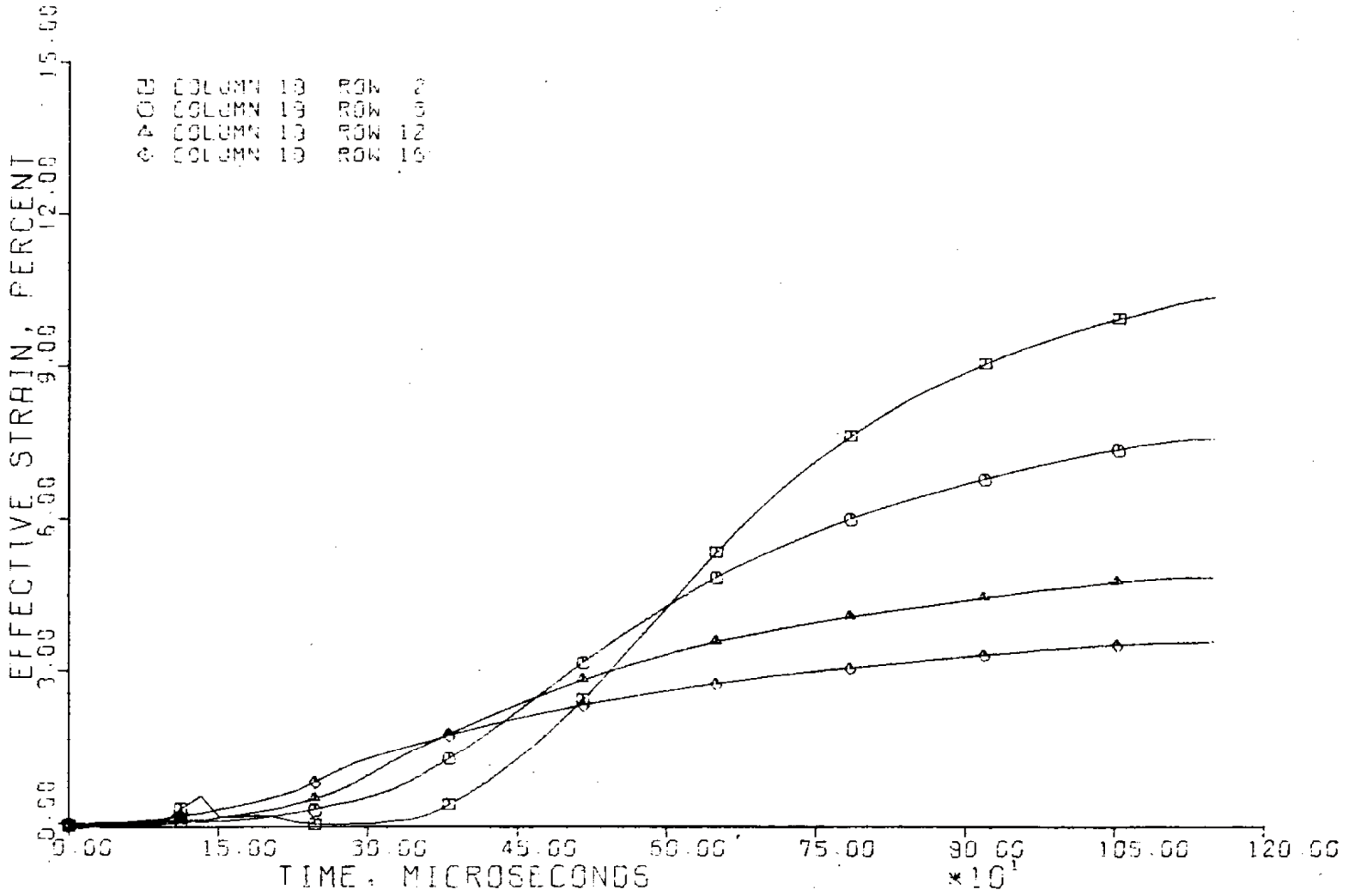

REV 21 5/08

SOUTHERN COMPANY
Energy to Serve Your World®

JOSEPH M. FARLEY
NUCLEAR PLANT
UNIT 1 AND UNIT 2

EFFECTIVE STRAINS IN DISC VERSUS TIME SINCE IMPACT

FIGURE 10A-35

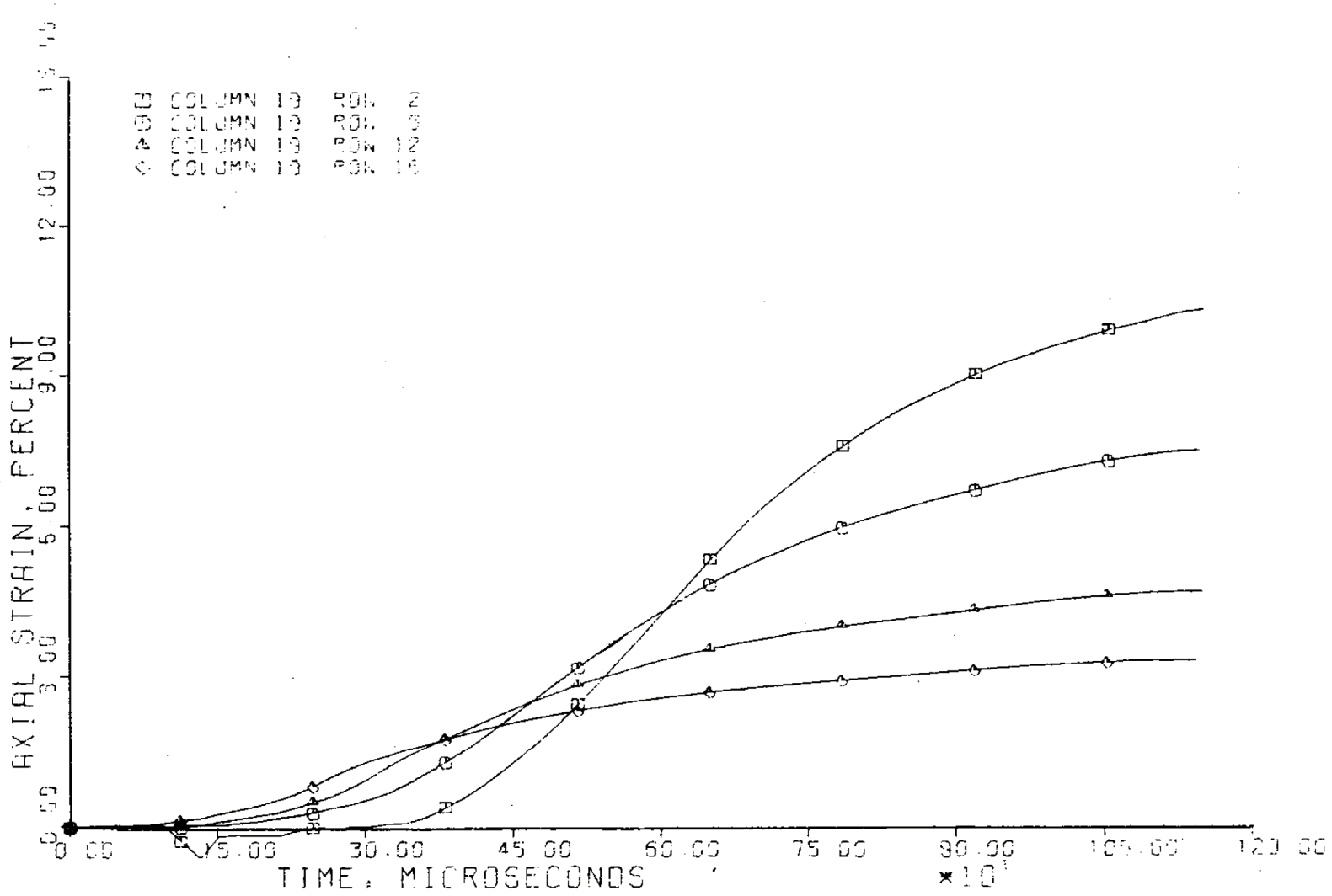

REV 21 5/08

SOUTHERN COMPANY
Energy to Serve Your World®

JOSEPH M. FARLEY NUCLEAR PLANT UNIT 1 AND UNIT 2

AXIAL STRAINS IN DISC VERSUS TIME SINCE IMPACT

FIGURE 10A-36

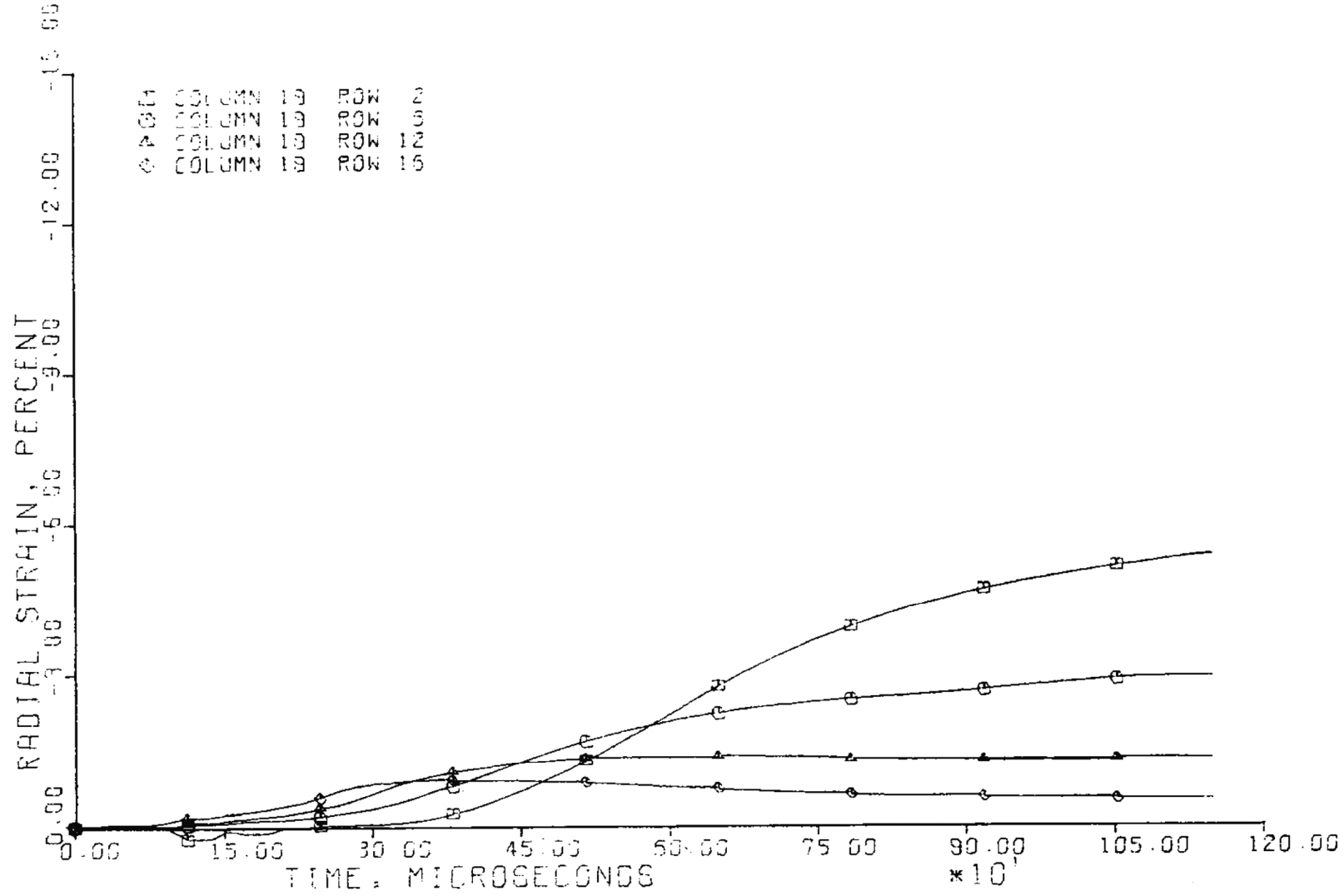

REV 21 5/08

SOUTHERN COMPANY
Energy to Serve Your World©

JOSEPH M. FARLEY
NUCLEAR PLANT
UNIT 1 AND UNIT 2

RADIAL STRAINS IN DISC VERSUS TIME SINCE IMPACT

FIGURE 10A-37

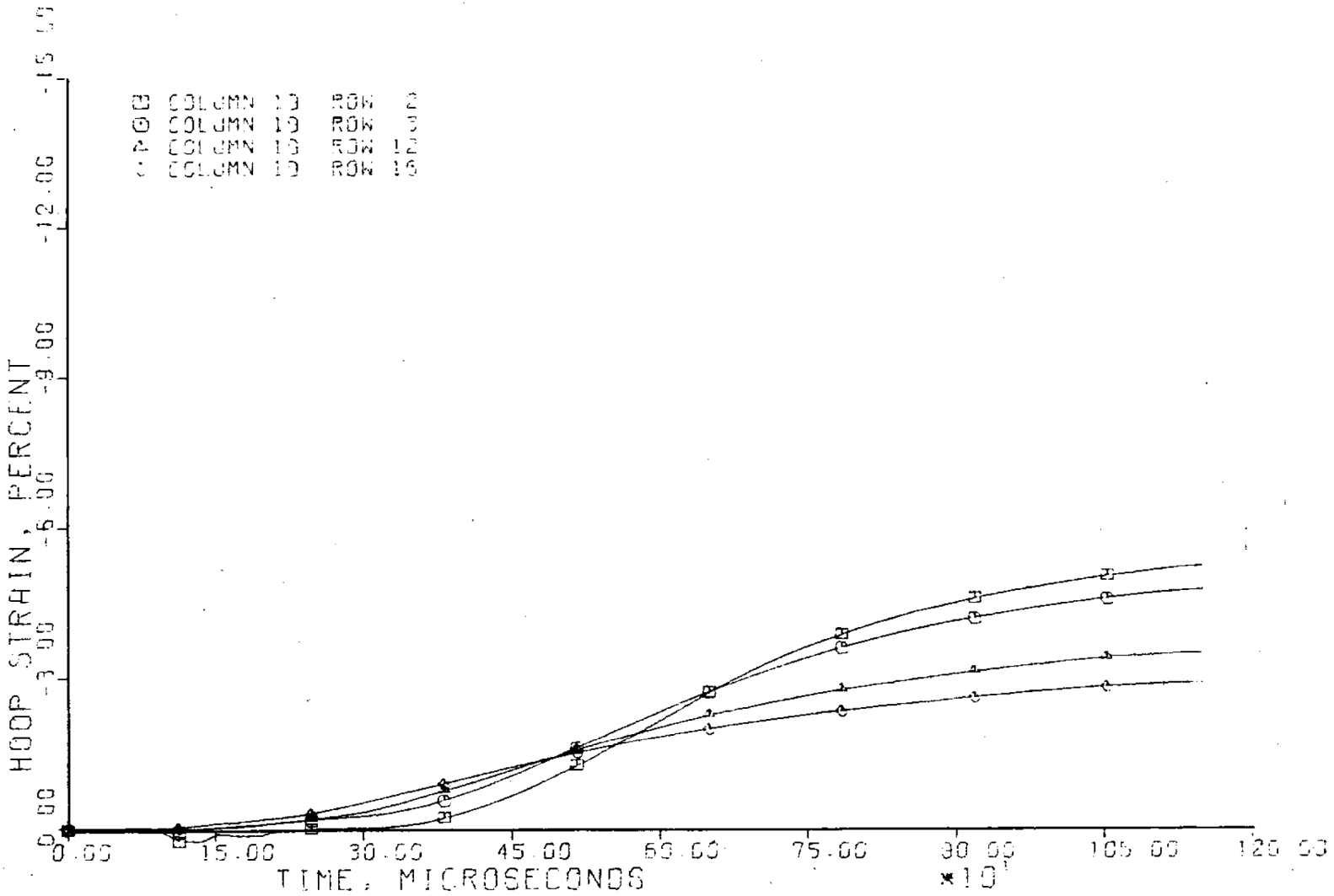

REV 21 5/08

SOUTHERN COMPANY
Energy to Serve Your World®

JOSEPH M. FARLEY
NUCLEAR PLANT
UNIT 1 AND UNIT 2

HOOP STRAINS IN DISC VERSUS TIME SINCE IMPACT

FIGURE 10A-38

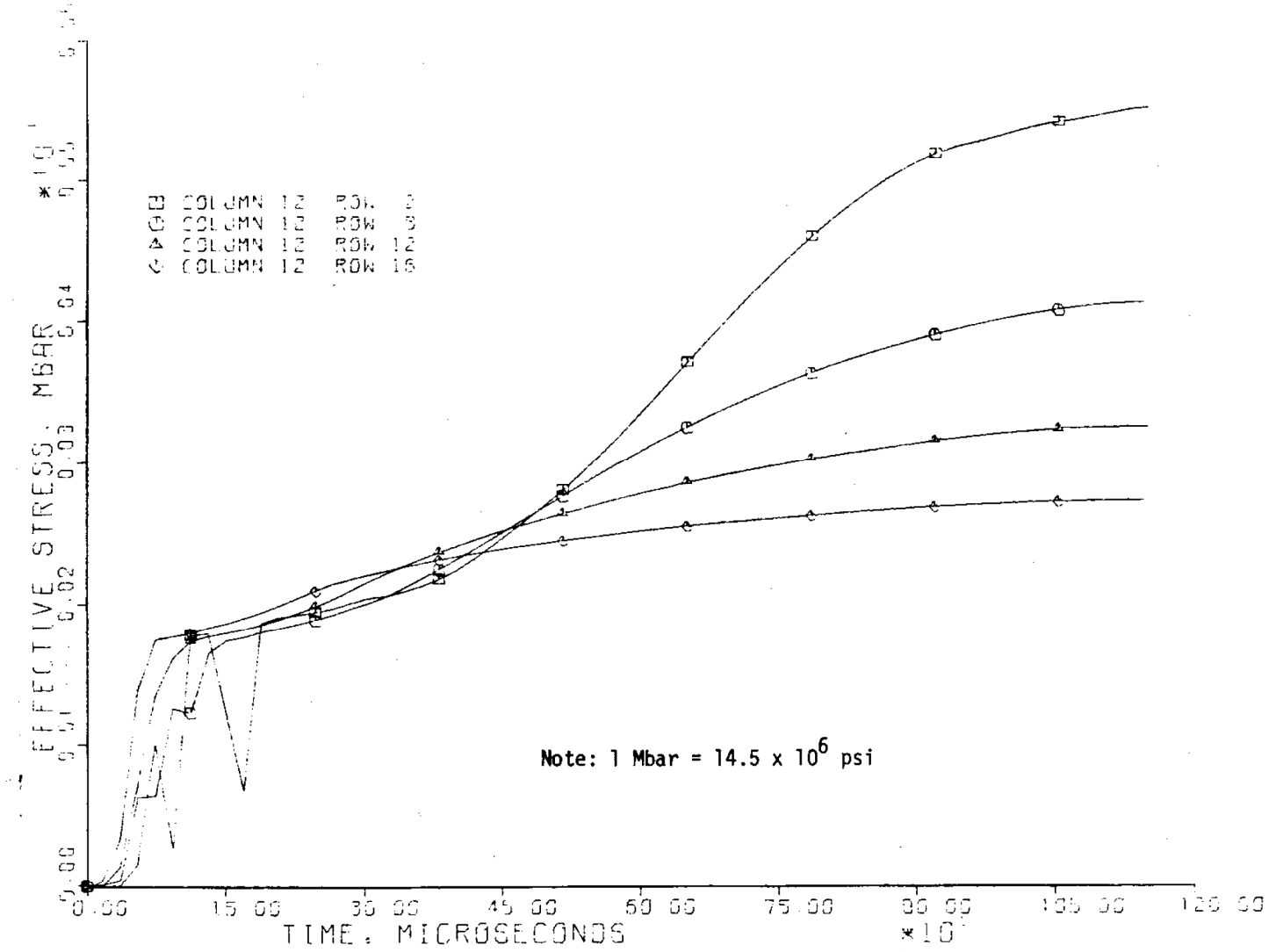

REV 21 5/08

SOUTHERN COMPANY
Energy to Serve Your World®

JOSEPH M. FARLEY NUCLEAR PLANT UNIT 1 AND UNIT 2

EFFECTIVE STRESSES IN DISC VERSUS TIME SINCE IMPACT

FIGURE 10A-39

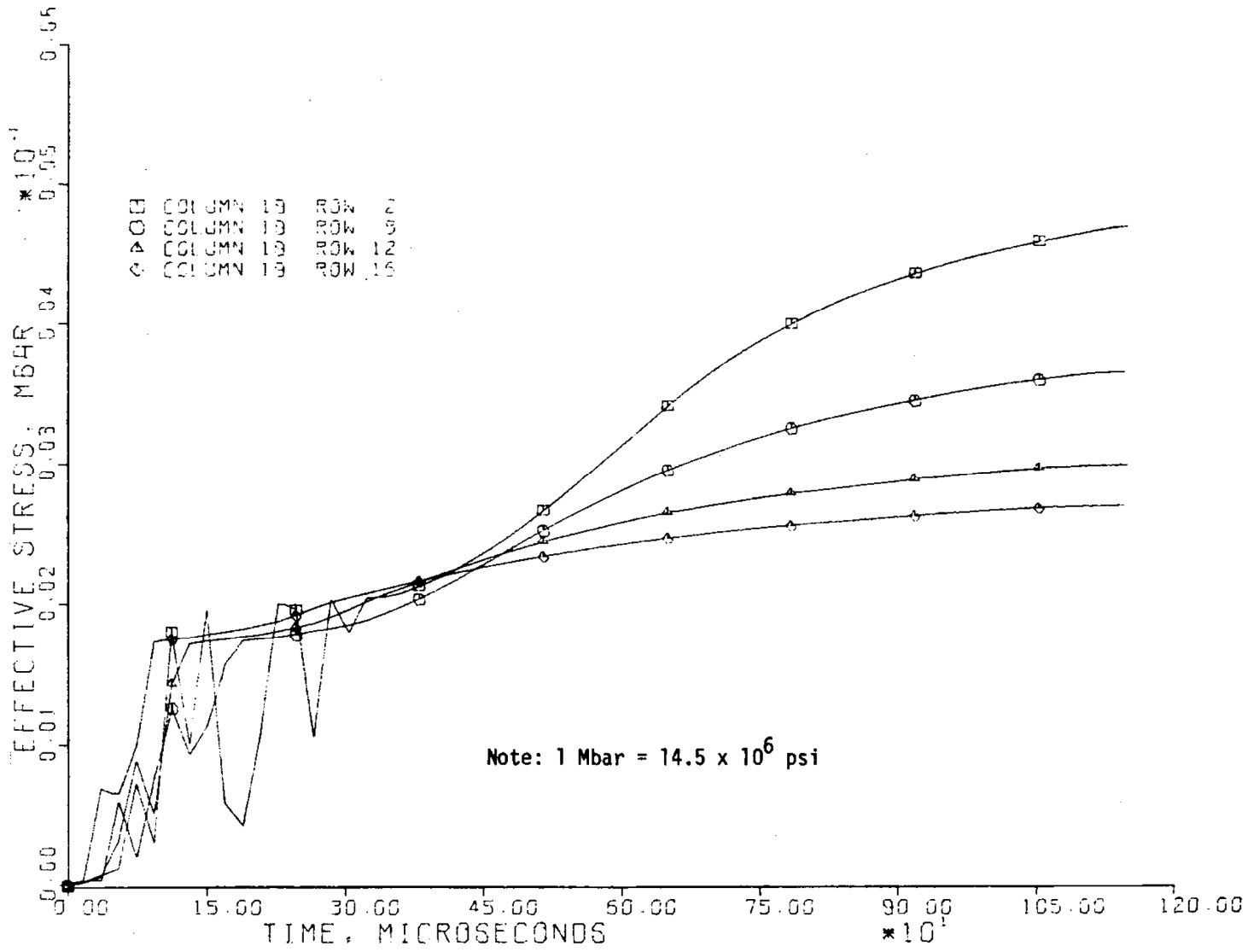

REV 21 5/08

SOUTHERN COMPANY
Energy to Serve Your World®

JOSEPH M. FARLEY
NUCLEAR PLANT
UNIT 1 AND UNIT 2

EFFECTIVE STRESSES IN DISC VERSUS TIME SINCE IMPACT

FIGURE 10A-40

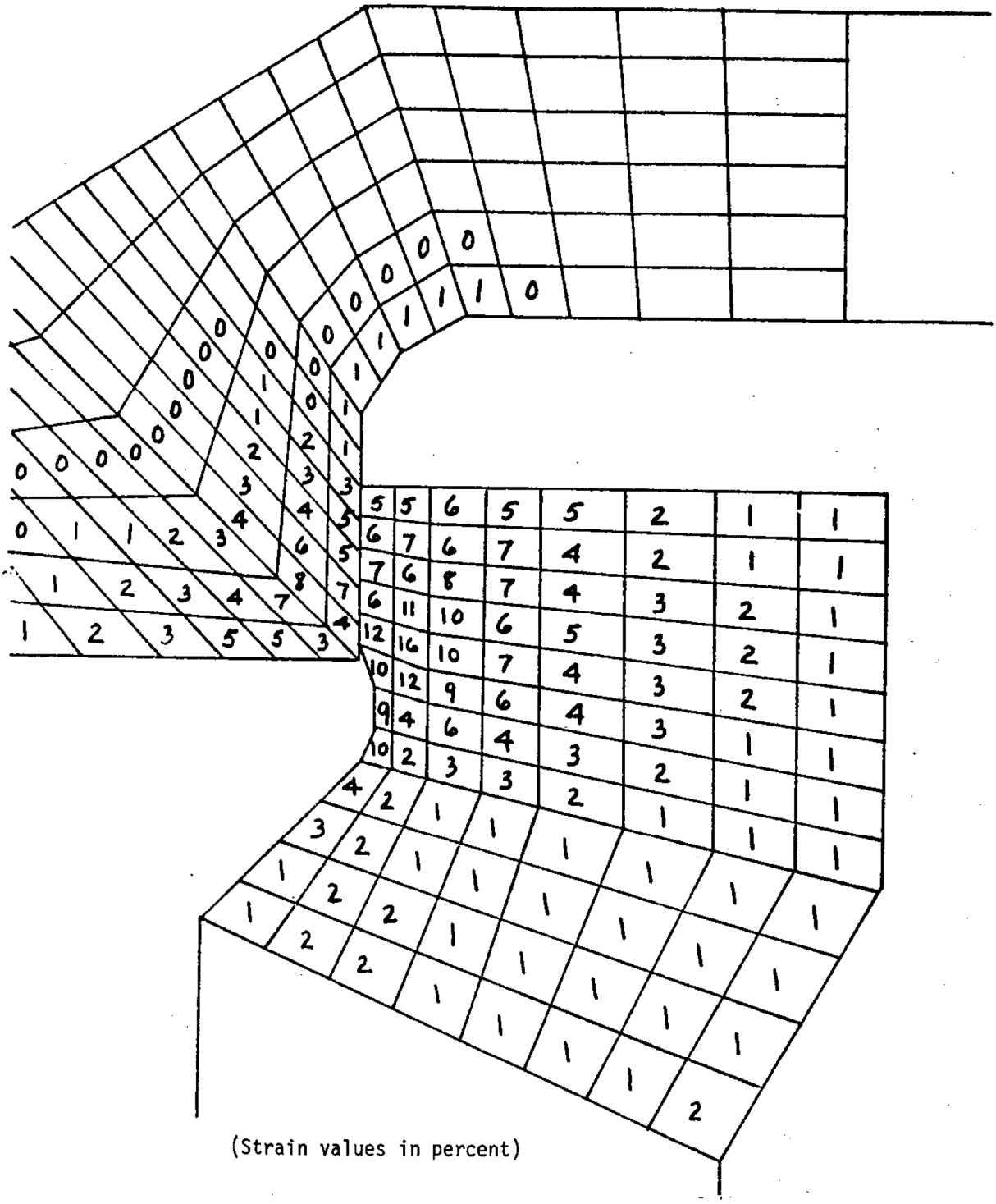

REV 21 5/08

SOUTHERN COMPANY *Energy to Serve Your World©*	JOSEPH M. FARLEY NUCLEAR PLANT UNIT 1 AND UNIT 2	DISTRIBUTION OF EFFECTIVE STRAIN $\bar{\varepsilon}$ AT TIME t = 300 μS
		FIGURE 10A-41

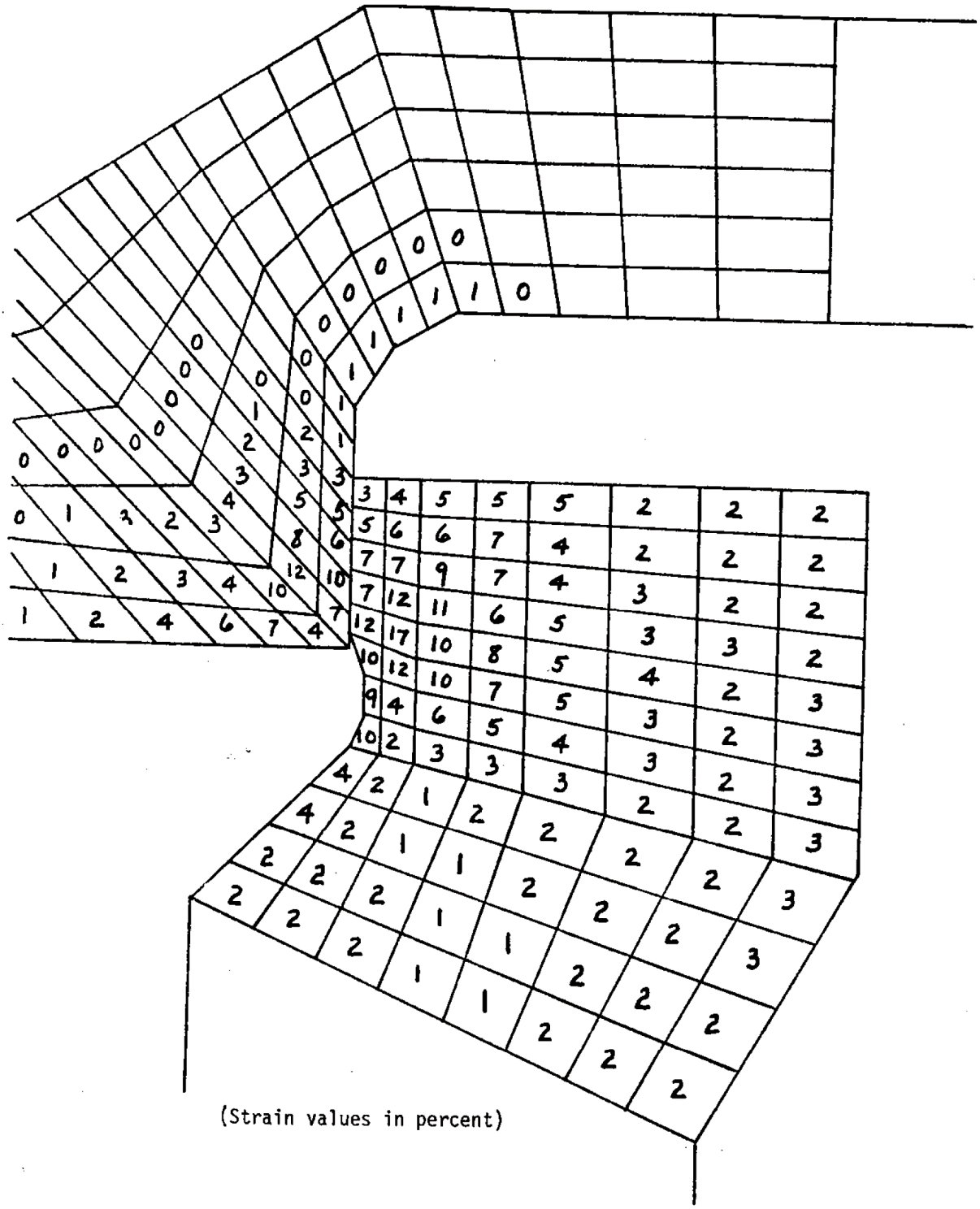

REV 21 5/08

SOUTHERN COMPANY *Energy to Serve Your World®*	JOSEPH M. FARLEY NUCLEAR PLANT UNIT 1 AND UNIT 2	DISTRIBUTION OF EFFECTIVE STRAIN $\bar{\varepsilon}$ AT TIME t = 700 μS
		FIGURE 10A-42

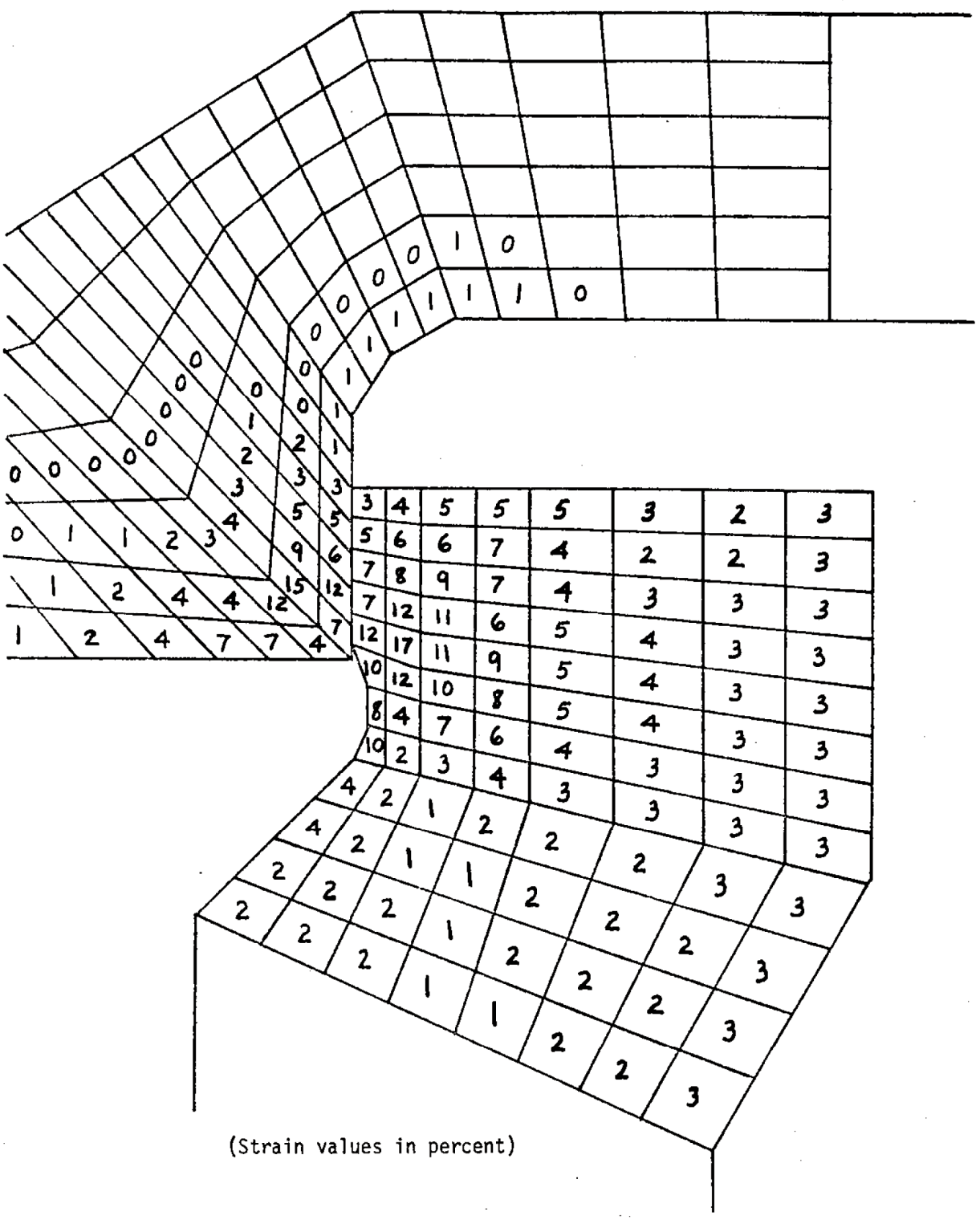

REV 21 5/08

SOUTHERN COMPANY *Energy to Serve Your World©*	JOSEPH M. FARLEY NUCLEAR PLANT UNIT 1 AND UNIT 2	DISTRIBUTION OF EFFECTIVE STRAIN $\bar{\varepsilon}$ AT TIME t = 1150 μS FIGURE 10A-43

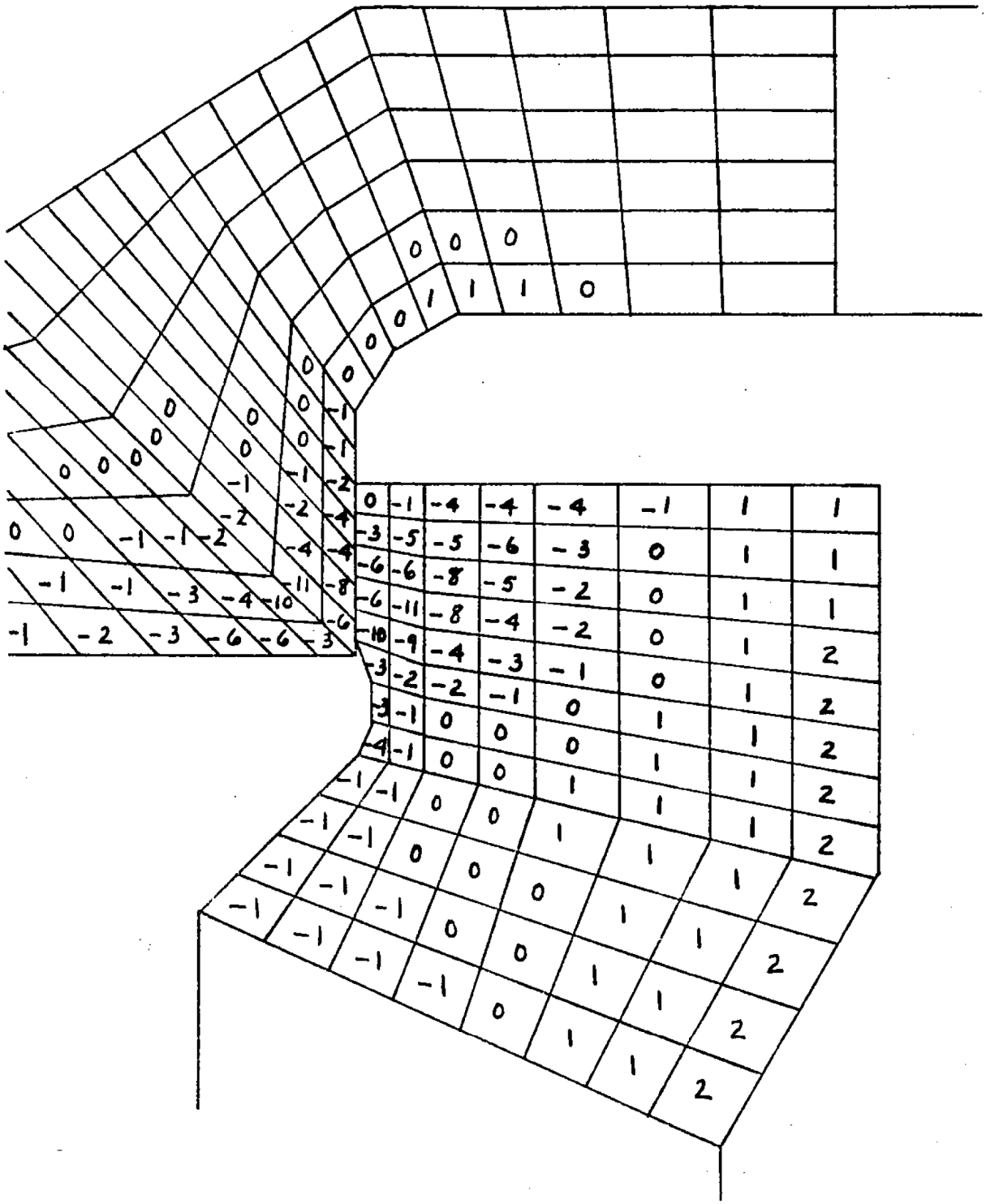

REV 21 5/08

SOUTHERN COMPANY
Energy to Serve Your World®

JOSEPH M. FARLEY NUCLEAR PLANT UNIT 1 AND UNIT 2

DISTRIBUTION OF AXIAL STRAIN ε_X
$\bar{\varepsilon}$ AT TIME t = 1150 μS

FIGURE 10A-44

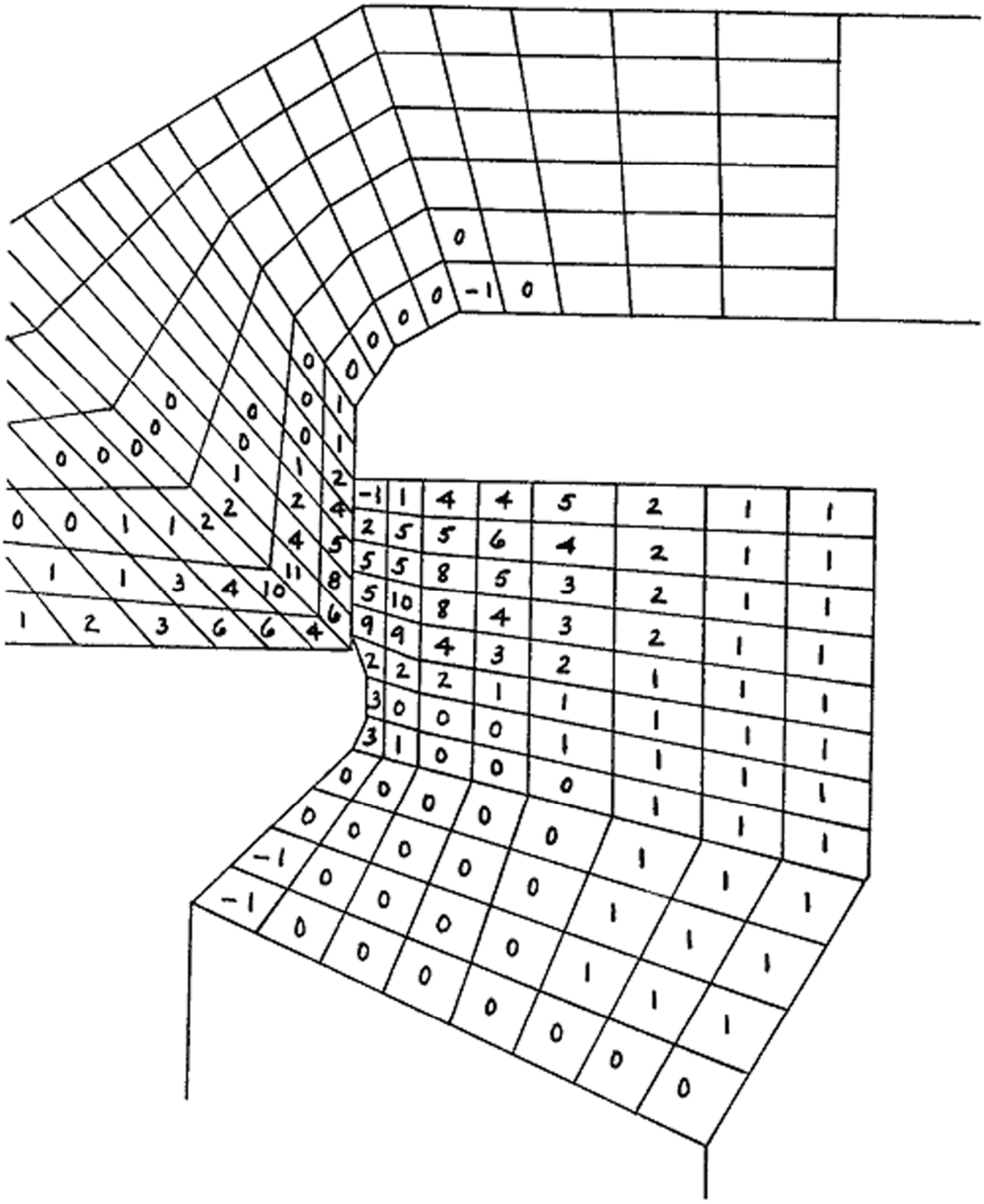

REV 21 5/08

SOUTHERN COMPANY
Energy to Serve Your World©

JOSEPH M. FARLEY
NUCLEAR PLANT
UNIT 1 AND UNIT 2

DISTRIBUTION OF RADIAL STRAIN
ε_y AT TIME t = 1150 μS

FIGURE 10A-45

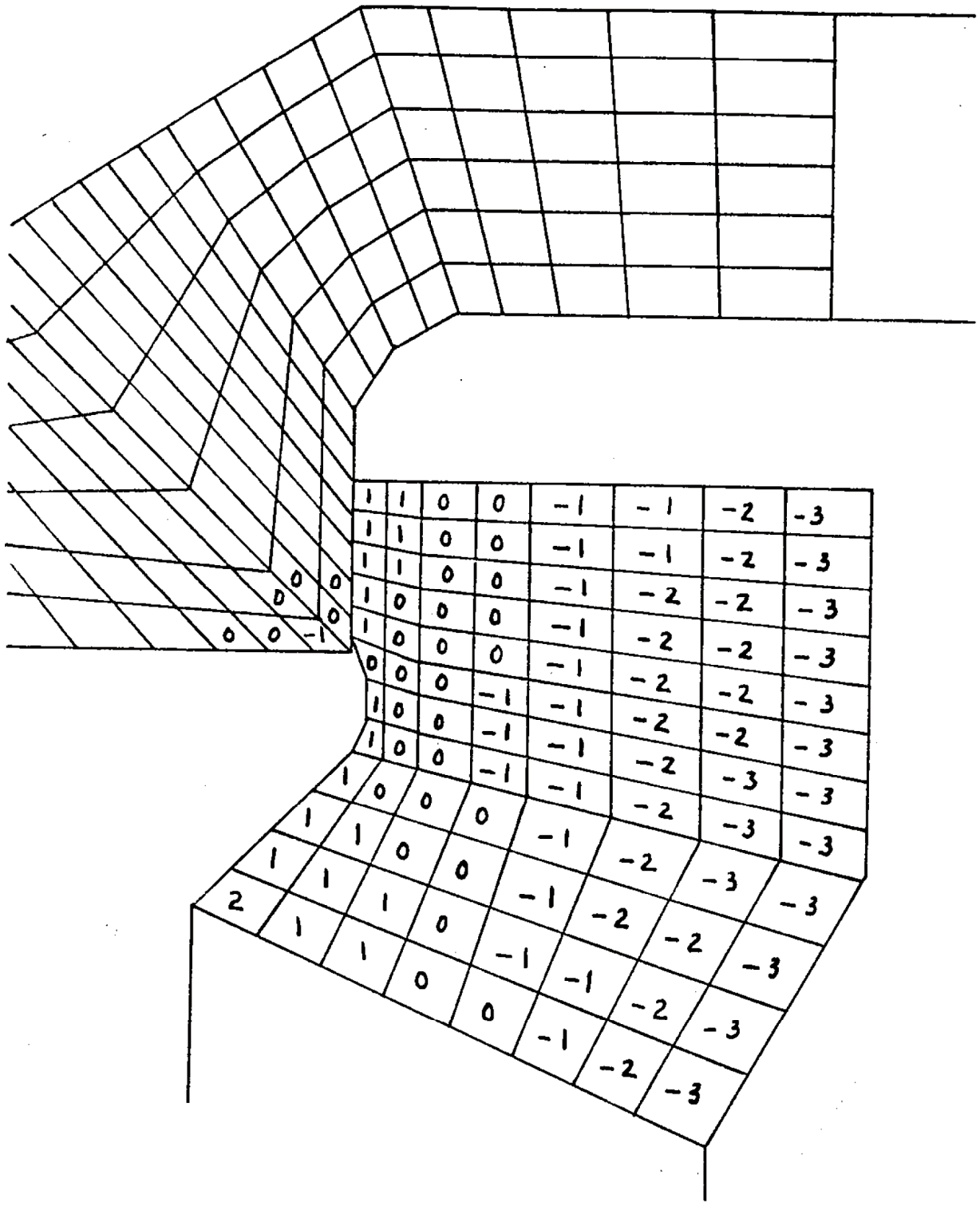

REV 21 5/08

SOUTHERN COMPANY
Energy to Serve Your World®

JOSEPH M. FARLEY NUCLEAR PLANT UNIT 1 AND UNIT 2

DISTRIBUTION OF HOOP STRAIN
ε_z AT TIME t = 1150 μS

FIGURE 10A-46

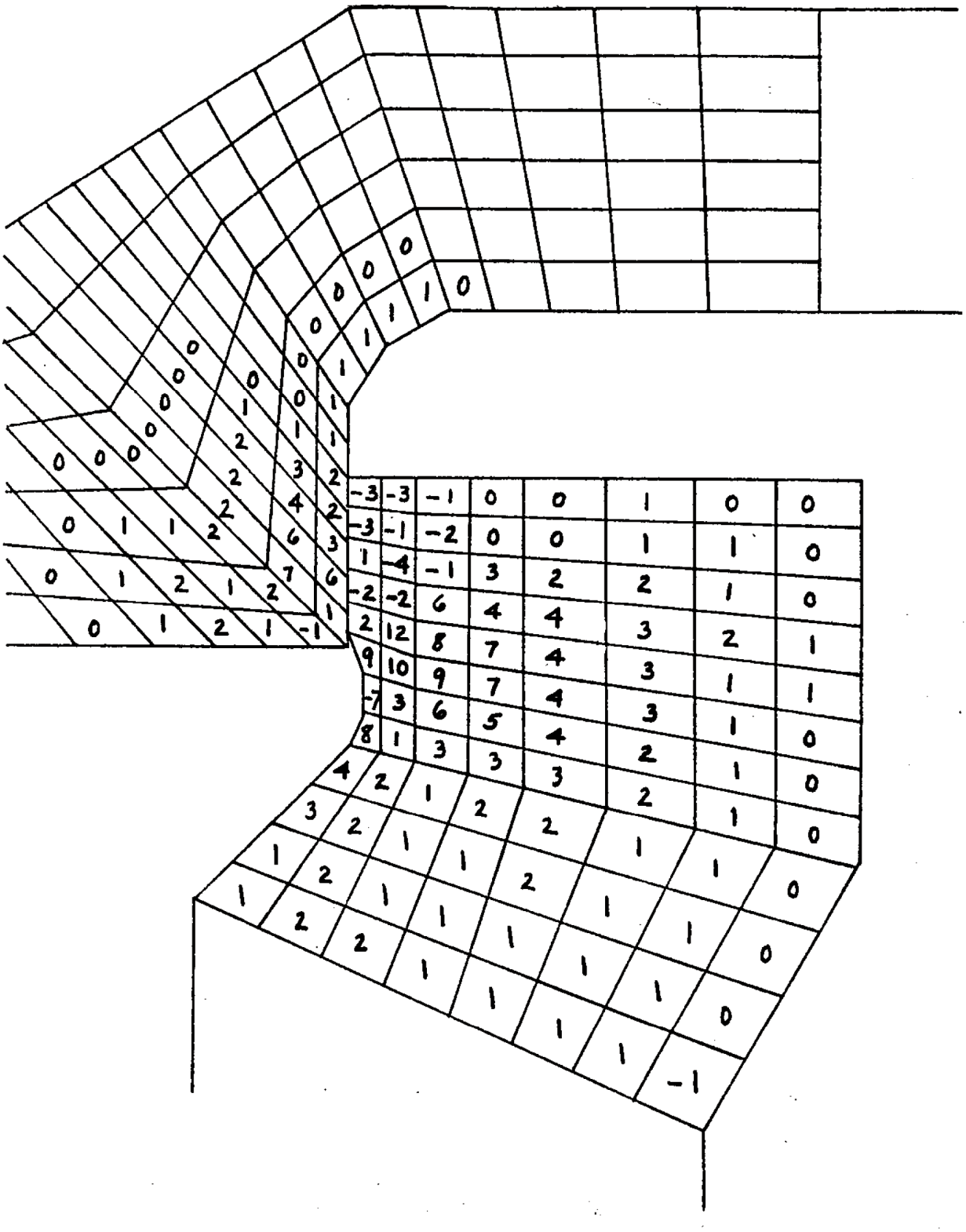

REV 21 5/08

SOUTHERN COMPANY *Energy to Serve Your World©*	**JOSEPH M. FARLEY NUCLEAR PLANT UNIT 1 AND UNIT 2**	DISTRIBUTION OF SHEAR STRAIN ε_{XY} AT TIME t = 1150 μS
		FIGURE 10A-47

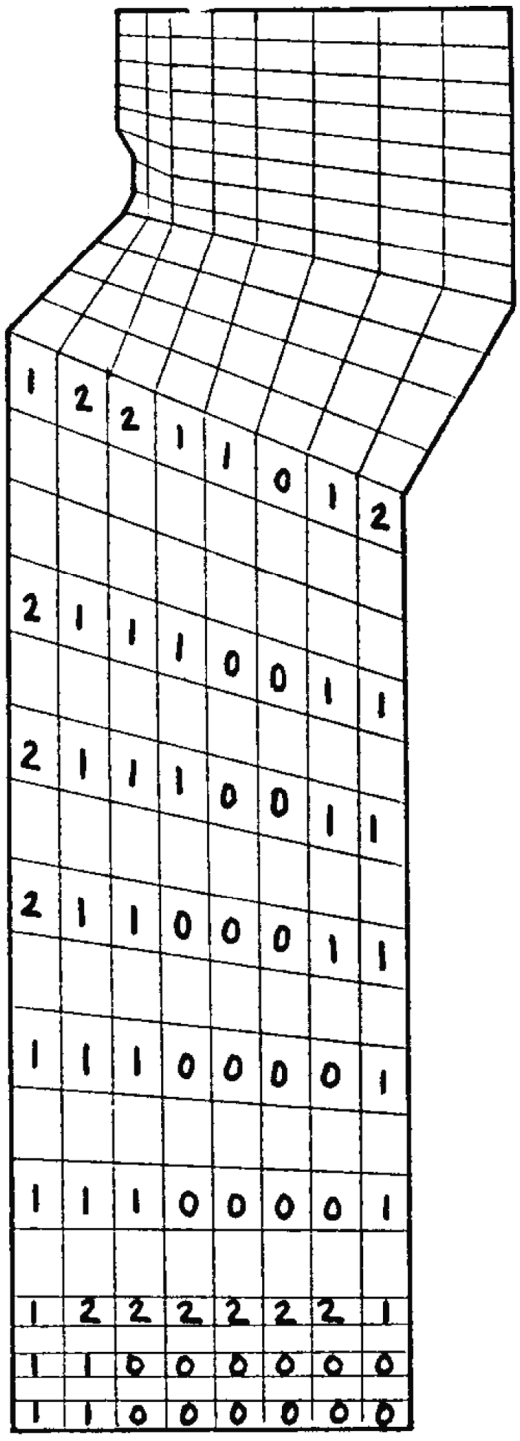

REV 21 5/08

SOUTHERN COMPANY *Energy to Serve Your World®*	**JOSEPH M. FARLEY NUCLEAR PLANT UNIT 1 AND UNIT 2**	DISTRIBUTION OF EFFECTIVE STRAIN $\bar{\varepsilon}$ AT TIME t = 300 μS
		FIGURE 10A-48

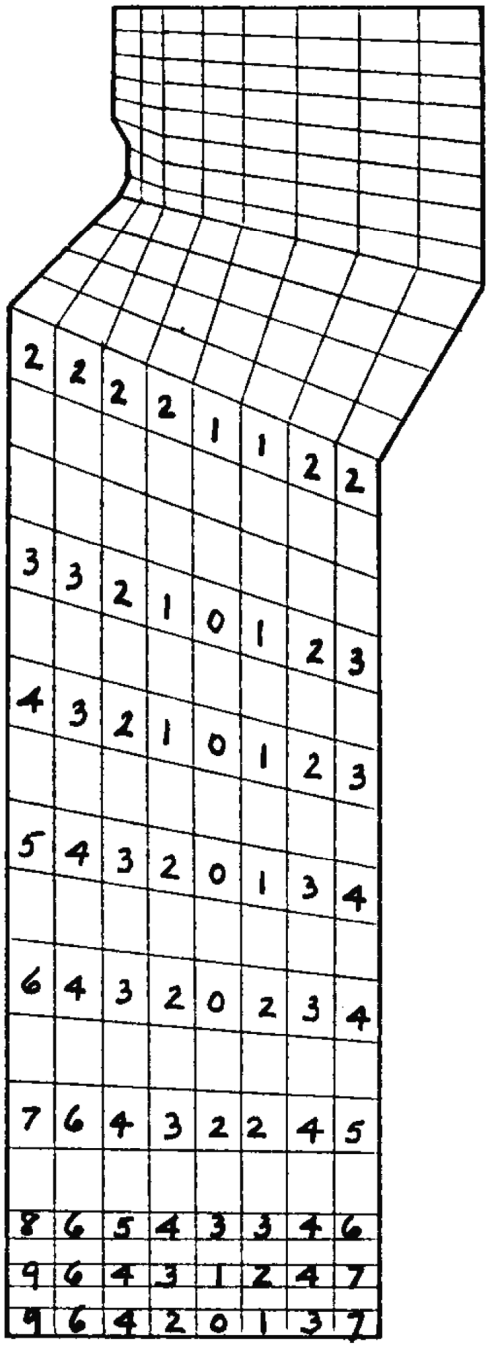

REV 21 5/08

SOUTHERN COMPANY
Energy to Serve Your World®

JOSEPH M. FARLEY NUCLEAR PLANT UNIT 1 AND UNIT 2

DISTRIBUTION OF EFFECTIVE STRAIN
$\bar{\varepsilon}$ AT TIME t = 700 μS

FIGURE 10A-49

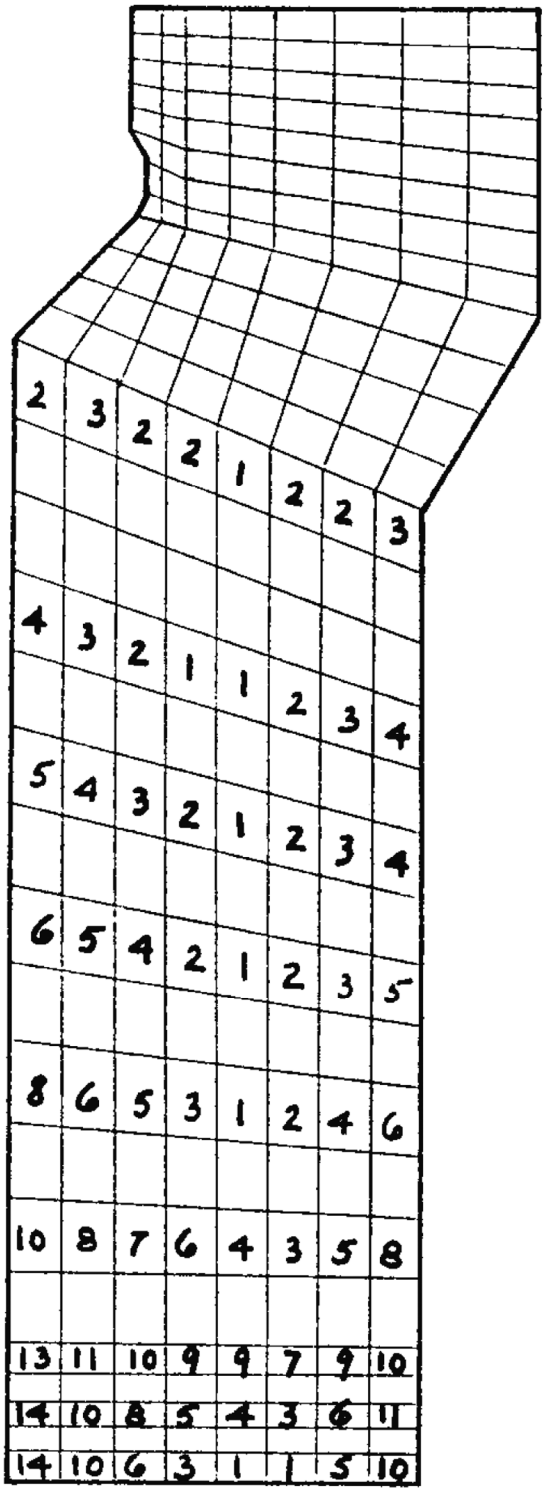

REV 21 5/08

SOUTHERN COMPANY
Energy to Serve Your World®

JOSEPH M. FARLEY NUCLEAR PLANT UNIT 1 AND UNIT 2

DISTRIBUTION OF EFFECTIVE STRAIN
$\bar{\varepsilon}$ AT TIME t = 1150 μS

FIGURE 10A-50

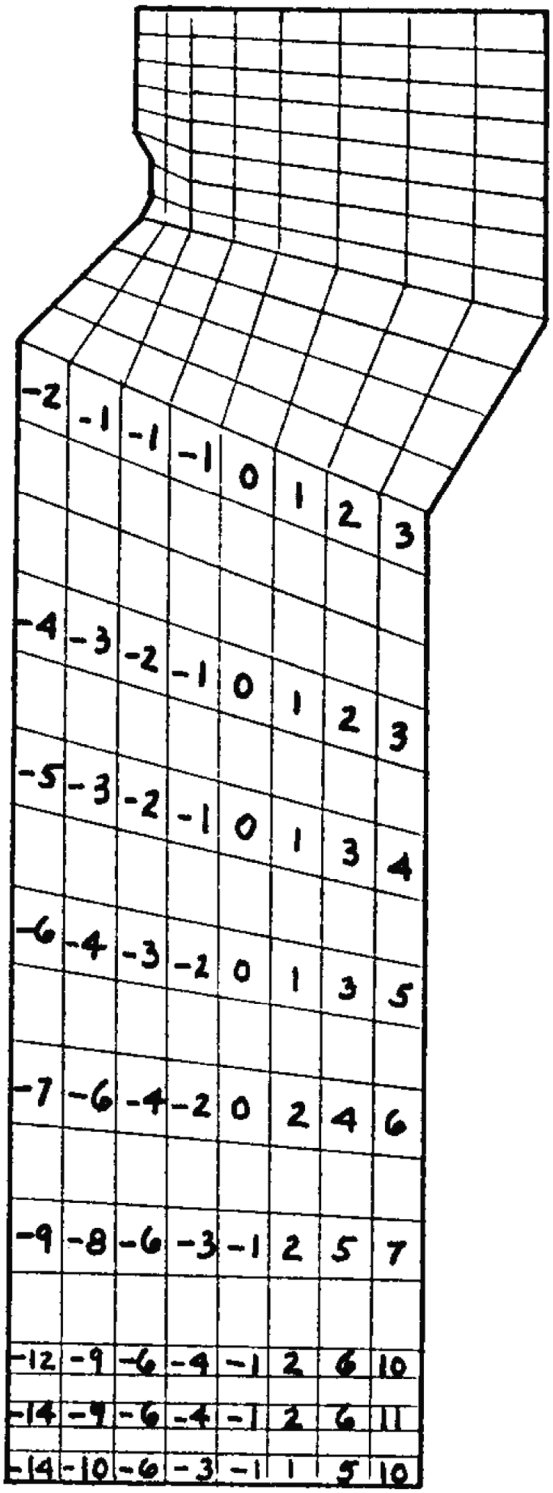

REV 21 5/08

SOUTHERN COMPANY
Energy to Serve Your World®

JOSEPH M. FARLEY NUCLEAR PLANT UNIT 1 AND UNIT 2

DISTRIBUTION OF AXIAL STRAIN
ε_x AT TIME t = 1150 μS

FIGURE 10A-51

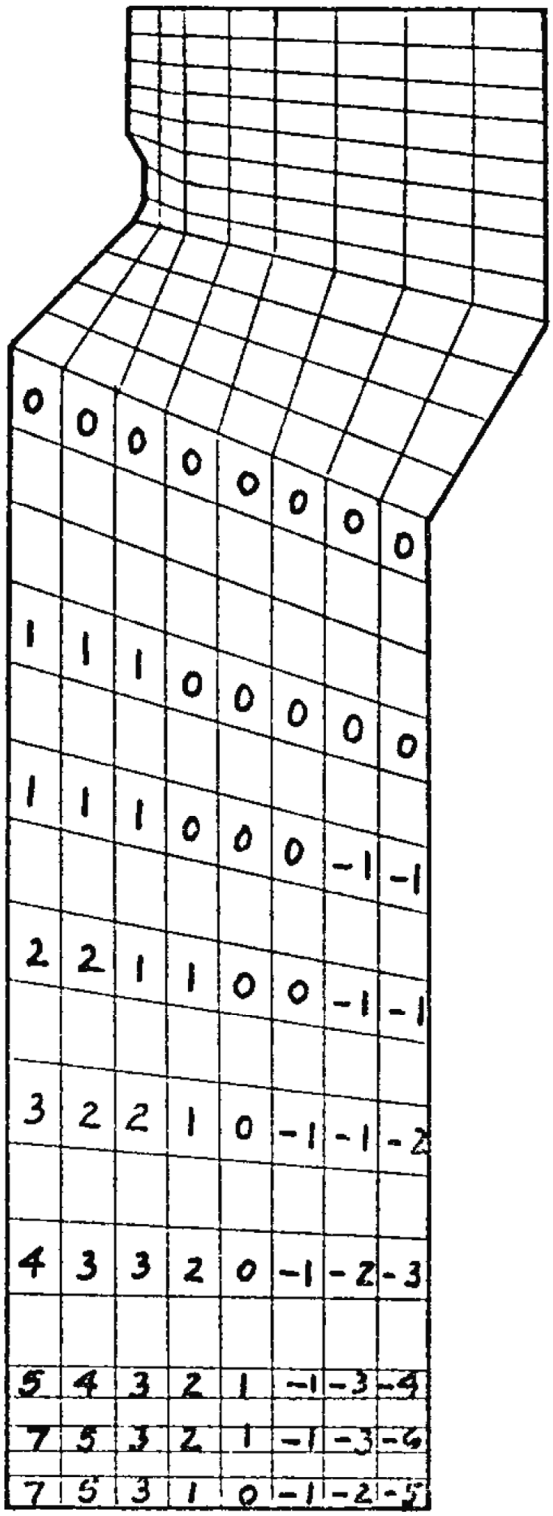

REV 21 5/08

SOUTHERN COMPANY
Energy to Serve Your World®

JOSEPH M. FARLEY NUCLEAR PLANT UNIT 1 AND UNIT 2

DISTRIBUTION OF RADIAL STRAIN
ε_y AT TIME t = 1150 μS

FIGURE 10A-52

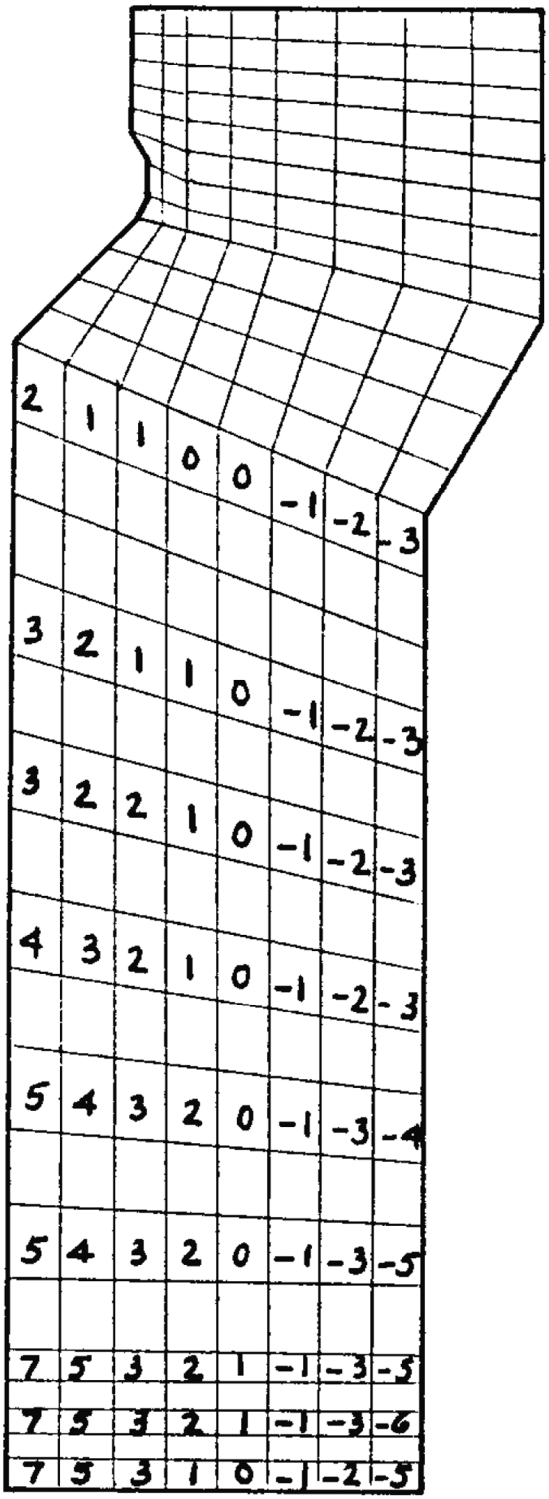

REV 21 5/08

SOUTHERN COMPANY
Energy to Serve Your World®

JOSEPH M. FARLEY NUCLEAR PLANT UNIT 1 AND UNIT 2

DISTRIBUTION OF HOOP STRAIN
ε_z AT TIME t = 1150 μS

FIGURE 10A-53

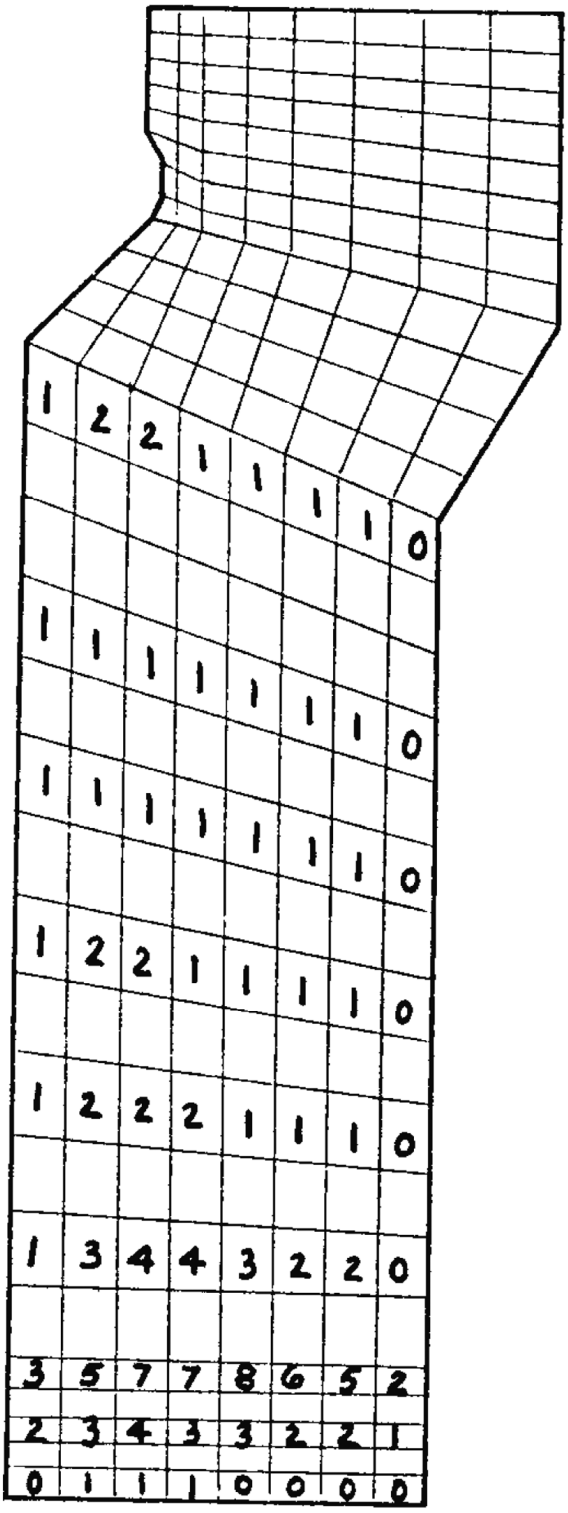

REV 21 5/08

SOUTHERN COMPANY
Energy to Serve Your World®

JOSEPH M. FARLEY NUCLEAR PLANT UNIT 1 AND UNIT 2

DISTRIBUTION OF SHEAR STRAIN
ε_{XY} AT TIME t = 1150 μS

FIGURE 10A-54

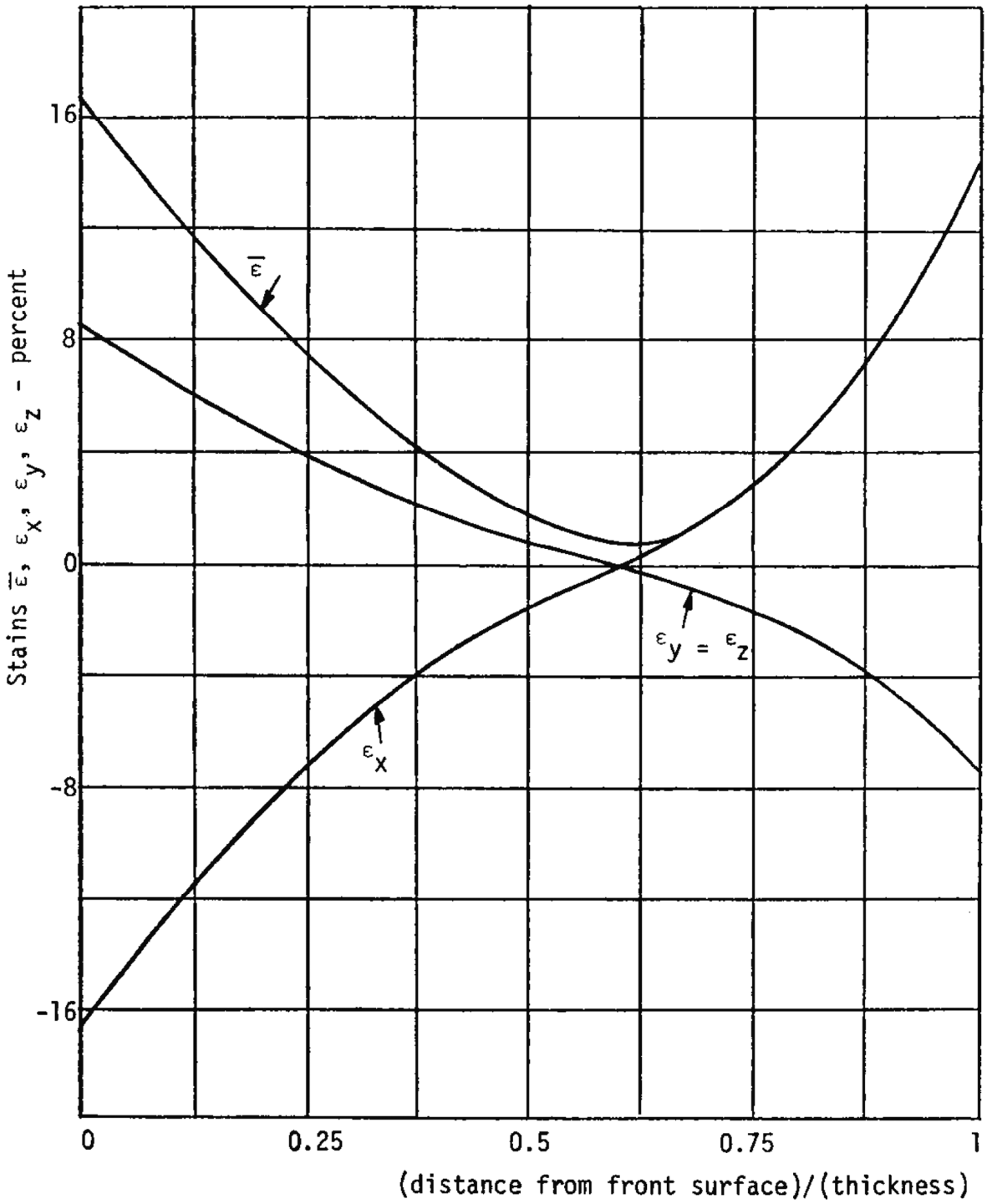

REV 21 5/08

SOUTHERN COMPANY
Energy to Serve Your World©

JOSEPH M. FARLEY NUCLEAR PLANT UNIT 1 AND UNIT 2

DISTRIBUTION OF STRAINS ALONG CENTERLINE OF DISC

FIGURE 10A-55

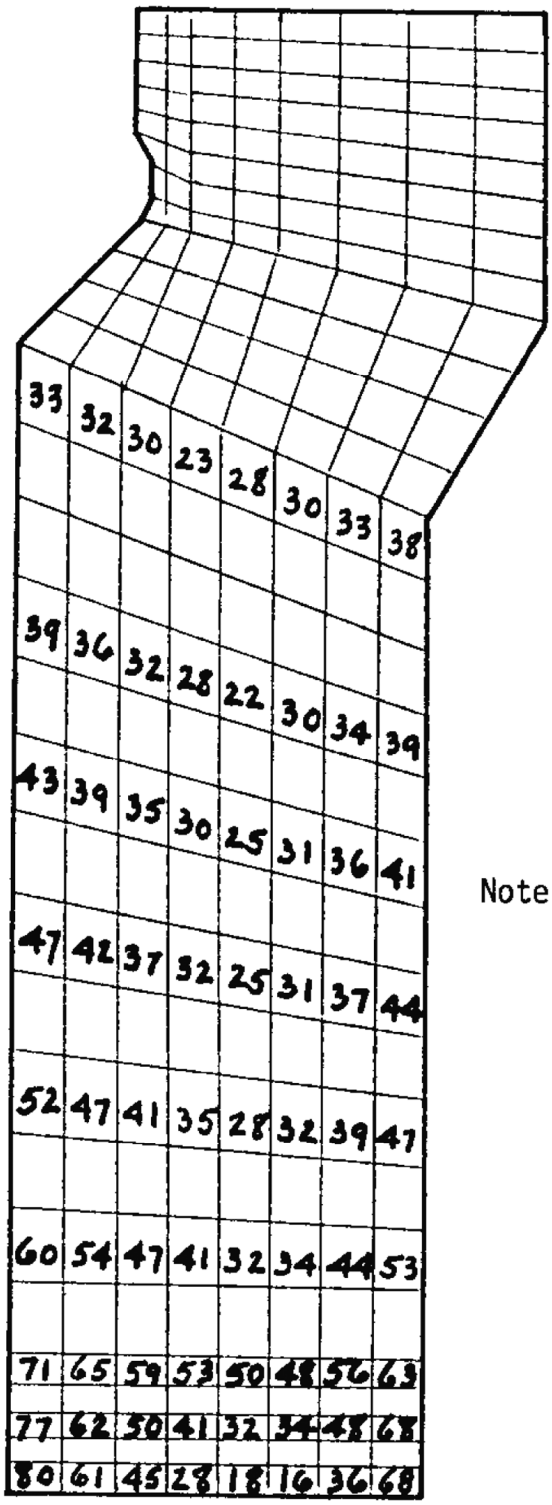

Note: stresses in ksi

REV 21 5/08

SOUTHERN COMPANY
Energy to Serve Your World©

JOSEPH M. FARLEY
NUCLEAR PLANT
UNIT 1 AND UNIT 2

DISTRIBUTION OF EFFECTIVE STRESS $\bar{\sigma}$
AT TIME t = 1150 μS

FIGURE 10A-56

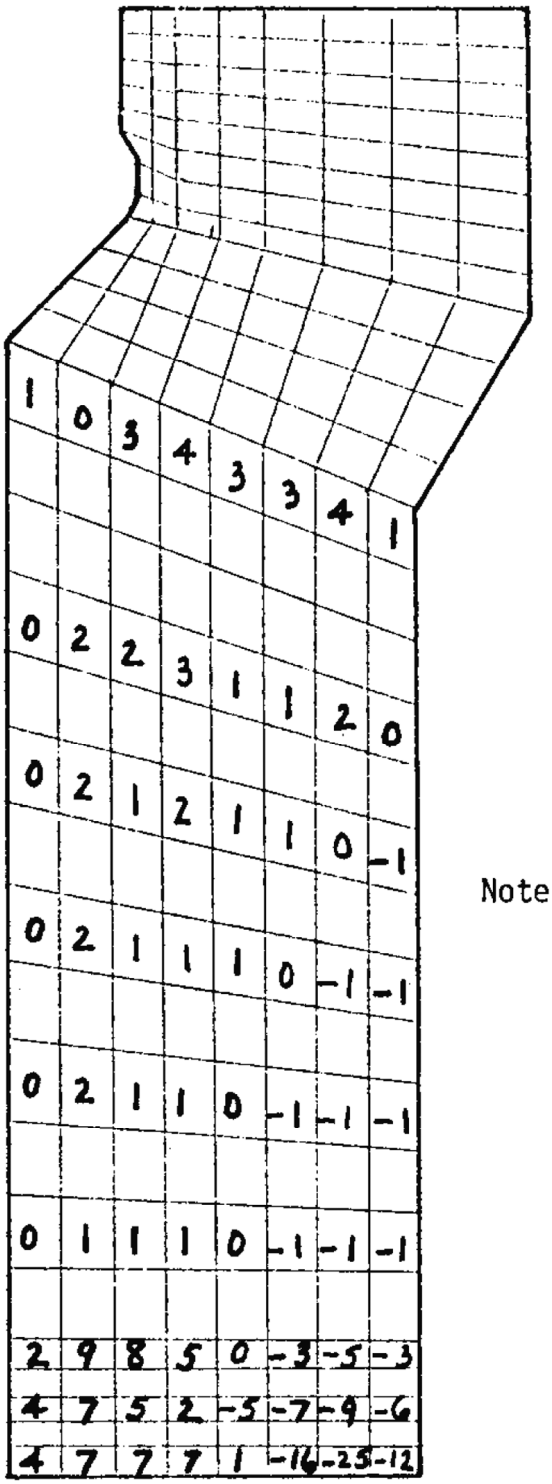

Note: stresses in ksi

REV 21 5/08

SOUTHERN COMPANY
Energy to Serve Your World®

JOSEPH M. FARLEY NUCLEAR PLANT UNIT 1 AND UNIT 2

DISTRIBUTION OF AXIAL STRESS
σ_x AT TIME t = 1150 μS

FIGURE 10A-57

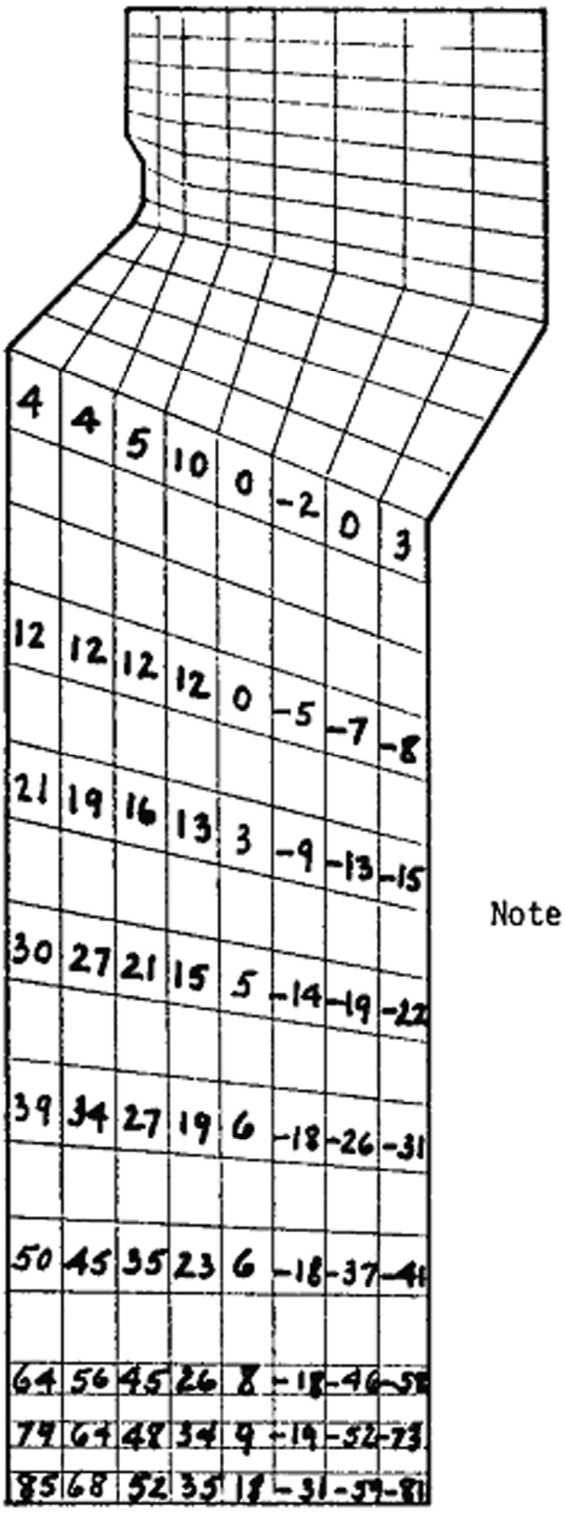

Note: stresses in ksi

REV 21 5/08

SOUTHERN COMPANY
Energy to Serve Your World®

JOSEPH M. FARLEY NUCLEAR PLANT UNIT 1 AND UNIT 2

DISTRIBUTION OF RADIAL STRESS
σ_y AT TIME t = 1150 μS

FIGURE 10A-58

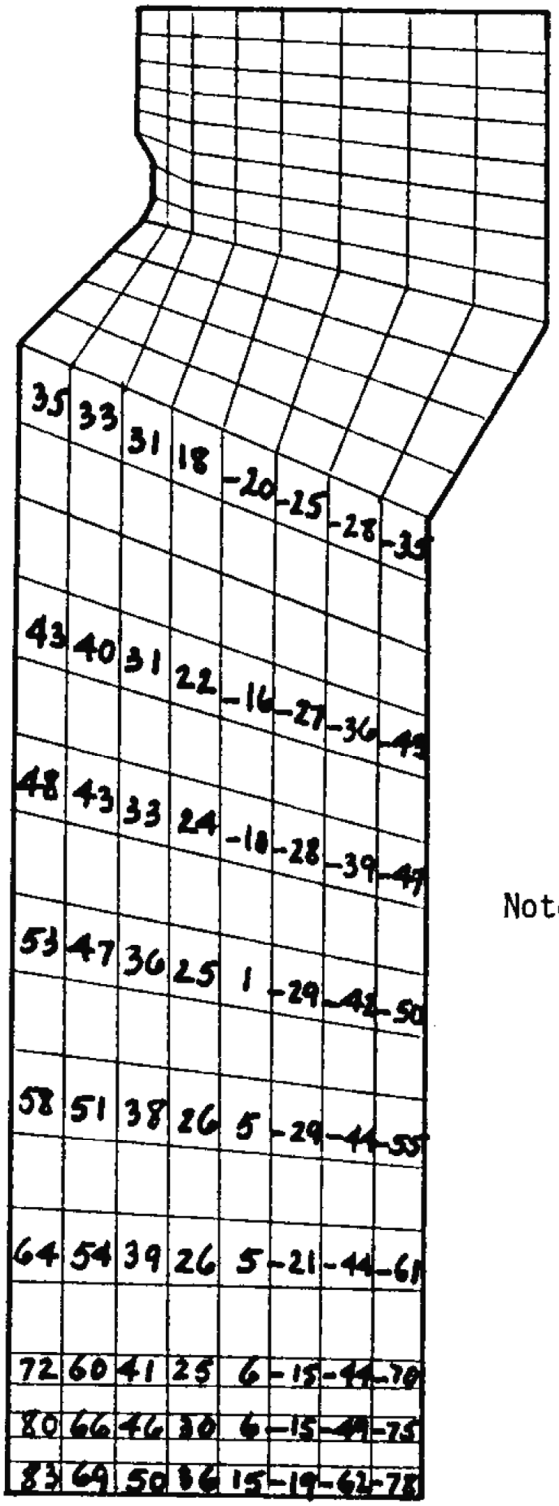

Note: stresses in ksi

REV 21 5/08

SOUTHERN COMPANY
Energy to Serve Your World®

JOSEPH M. FARLEY NUCLEAR PLANT UNIT 1 AND UNIT 2

DISTRIBUTION OF HOOP STRESS
σ_z AT TIME t = 1150 μS

FIGURE 10A-59

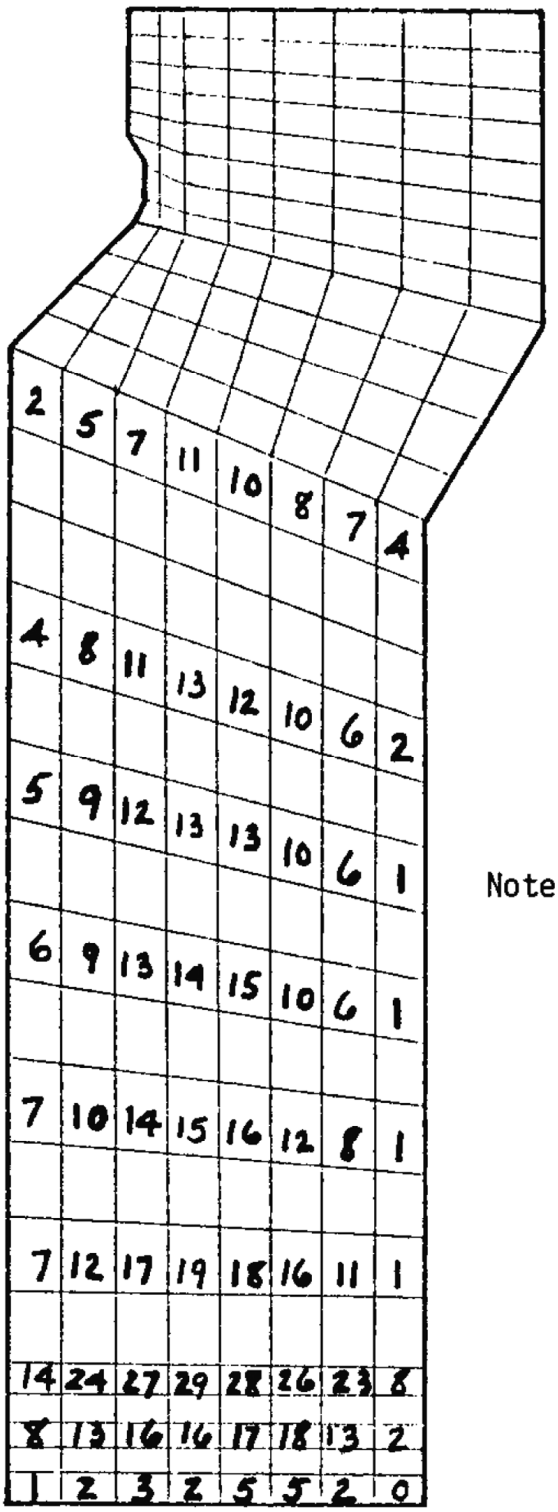

Note: stresses in ksi

REV 21 5/08

SOUTHERN COMPANY
Energy to Serve Your World®

JOSEPH M. FARLEY NUCLEAR PLANT UNIT 1 AND UNIT 2

DISTRIBUTION OF SHEAR STRESS
τ_{xy} AT TIME t = 1150 μS

FIGURE 10A-60

ATTACHMENT A

EFFECT OF STRAIN RATE ON STRESS-STRAIN BEHAVIOR OF TYPE 304 STAINLESS STEEL[3]

LMFBR	MATERIALS HANDBOOK	Type 304 Stainless Steel*
DATE 1-18-73 SUPERSEDES New		Effect of Strain Rate on Stress - Strain Behavior

EFFECT OF STRAIN RATE ON AVERAGE TRUE STRESS-TRUE STRAIN BEHAVIOR OF TYPE 304 STAINLESS STEEL*

$$\sigma_T = K_1 \varepsilon_p^{n_1} + e^{(K_2 + n_2 \varepsilon_p)}$$

σ_T = average true stress, ~~ksi~~ *psi*

ε_p = average true plastic strain, in/in

K_1, n_1, K_2, and n_2 = constants

For 600°F	For 800°F	For 1000°F	For 1200°F
$n_1 = 0.473 - 0.023 \log \dot{\varepsilon}$	$n_1 = 0.508 - 0.013 \log \dot{\varepsilon}$	$n_1 = 0.490 - 0.005 \log \dot{\varepsilon}$	$n_1 = 0.475 + 0.006 \log \dot{\varepsilon}$
$K_1 = 164{,}640 - 2{,}150 \log \dot{\varepsilon}$	$K_1 = 164{,}220 + 1{,}930 \log \dot{\varepsilon}$	$K_1 = 155{,}070 + 2{,}070 \log \dot{\varepsilon}$	$K_1 = 133{,}260 + 5{,}270 \log \dot{\varepsilon}$
$n_2 = -51.23 - 3.18 \log \dot{\varepsilon}$	$n_2 = -50.45 - 4.28 \log \dot{\varepsilon}$	$n_2 = -68.94 - 4.48 \log \dot{\varepsilon}$	$n_2 = -94.50 + 3.45 \log \dot{\varepsilon}$
$K_2 = 9.641 + 0.052 \log \dot{\varepsilon}$	$K_2 = 9.583 + 0.063 \log \dot{\varepsilon}$	$K_2 = 9.347 + 0.028 \log \dot{\varepsilon}$	$K_2 = 9.125 + 0.008 \log \dot{\varepsilon}$

Where: $\dot{\varepsilon}$ = strain rate, sec^{-1}.

Constants for 600-1000°F valid for nominal strain rates from 1×10^{-5} to 1×10^{2} sec^{-1}.

Constants for 1200°F valid for nominal strain rates from 5×10^{-3} to 1×10^{2} sec^{-1}.

Constants valid for nominal strains up to 25%.

For any level of strain, accuracy of stress is $\pm$ 7.5%.

Ref: 71-5
72-4

*Bar Only

PREPARED BY JH Steichen — Hanford Engineering Development Laboratory

Approved By: James G. Irwin

ATTACHMENT B

EFFECT OF STRAIN RATE ON UNIFORM ELONGATION AND REDUCTION OF AREA[2]

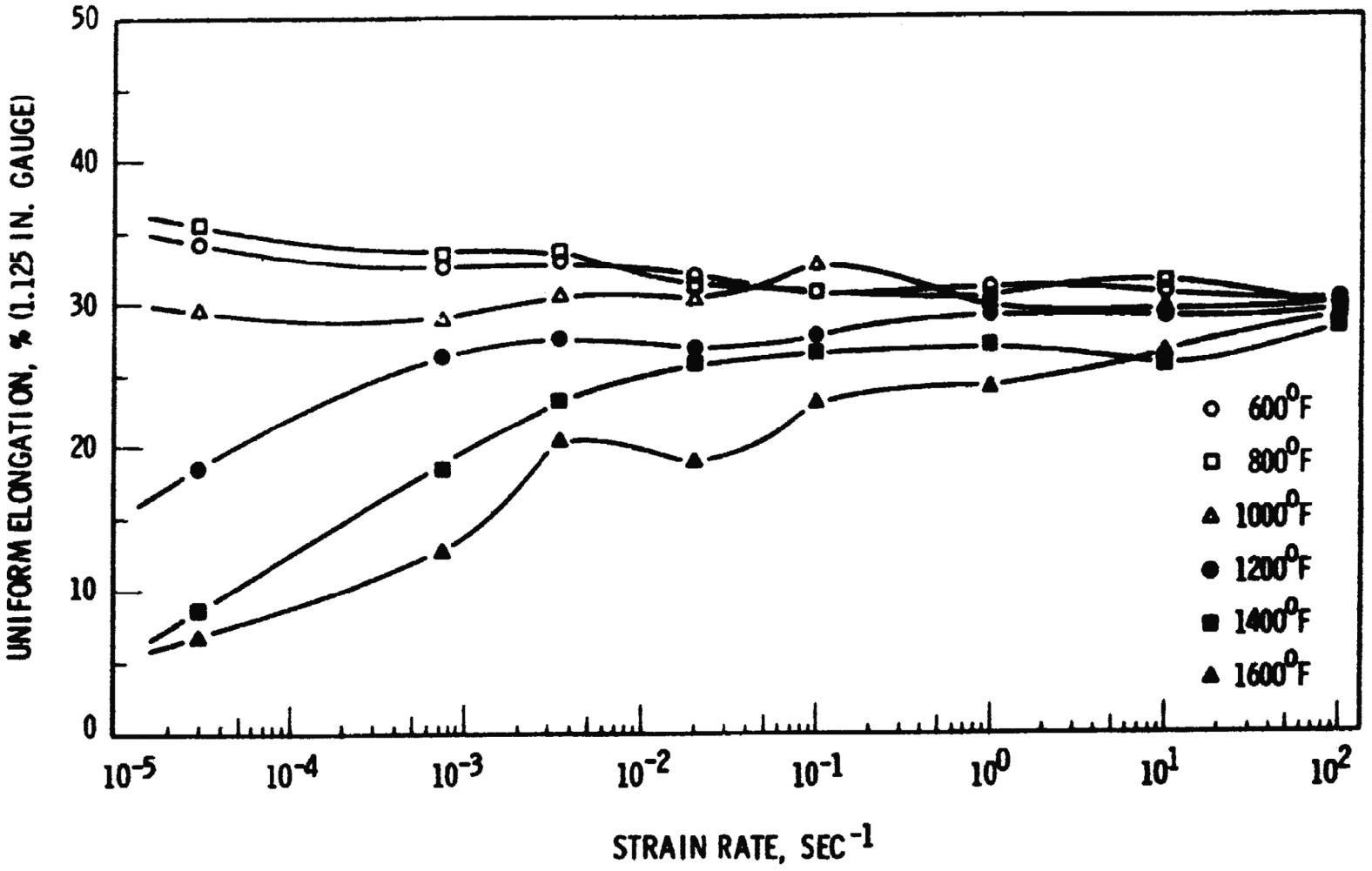

REV 21 5/08

SOUTHERN COMPANY
Energy to Serve Your World©

JOSEPH M. FARLEY
NUCLEAR PLANT
UNIT 1 AND UNIT 2

EFFECT OF STRAIN RATE AND TEMPERATURE ON THE UNIFORM ELONGATION OF 304 SS

FIGURE B-1

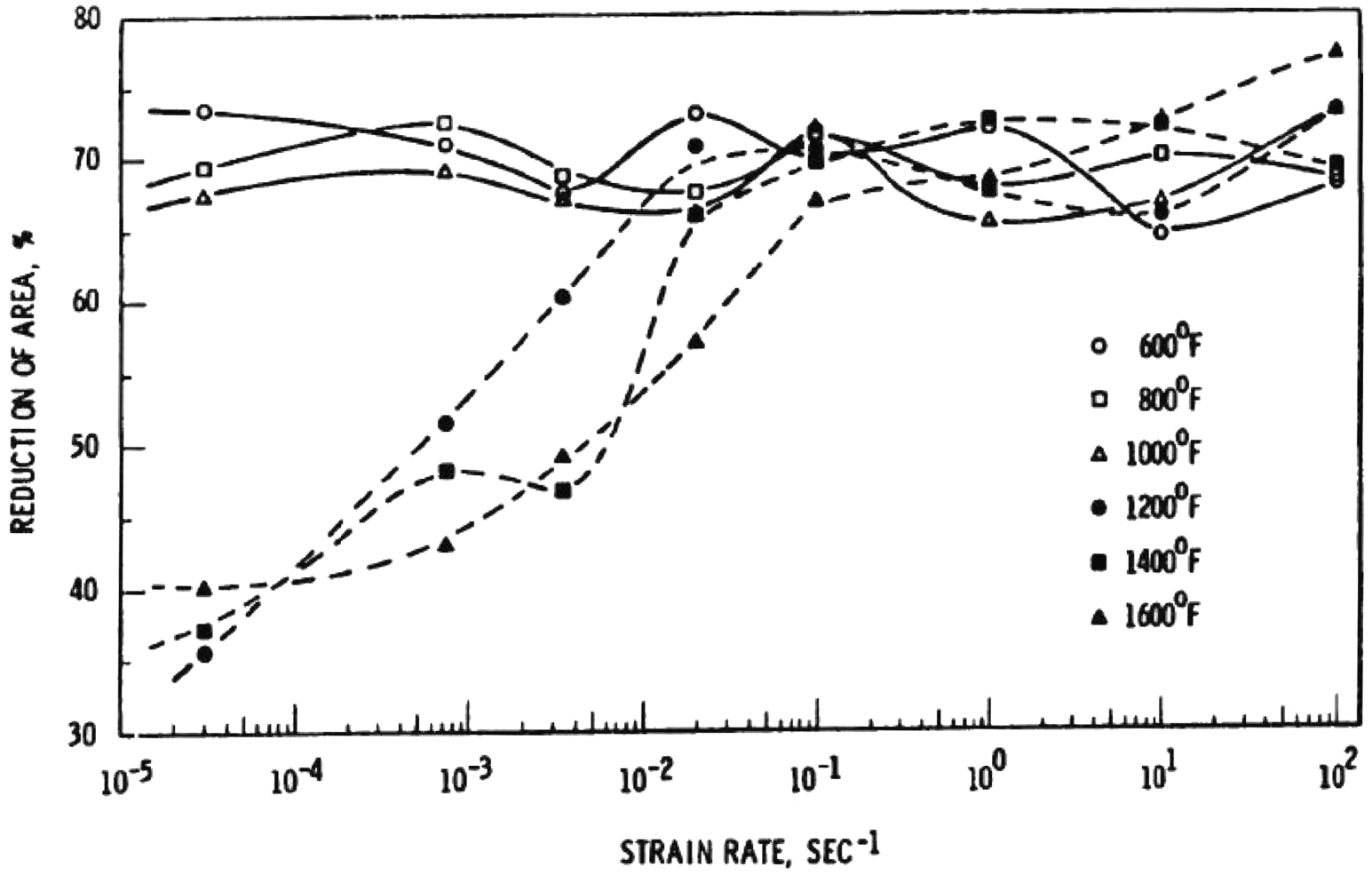

REV 21 5/08

SOUTHERN COMPANY
Energy to Serve Your World©

JOSEPH M. FARLEY
NUCLEAR PLANT
UNIT 1 AND UNIT 2

EFFECT OF STRAIN RATE AND TEMPERATURE ON THE REDUCTION OF AREA OF 304 SS

FIGURE B-2

ATTACHMENT C

MASS SIMULATION OF DISC ARM, POST, AND NUT DETERMINATION OF TRANSLATIONAL IMPACT VELOCITY

Mass Simulation of Disc Arm, Post And Nut

(a) Equivalent Weight of Disc Arm

Approximated geometry:

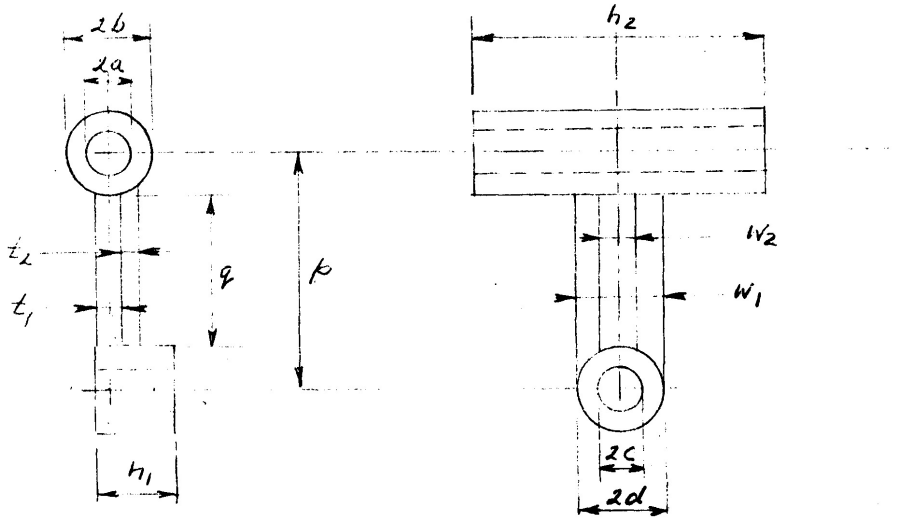

dimensions (inches)

2a = 3.5	p = 16.5	W_1 = 6.0
2b = 6.0	q = 10.0	W_2 = 2.0
2c = 3.28	h_1 = 5.5	t_1 = 1.5
2d = 6.0	h_2 = 19.5	t_2 = 1.75

Reference Dwgs (Atwood & Morrill): 30666-405-C, 22751-C

$M = 152 \times 7.35 \times 10^{-4} = 0.112$ slugs

Let W = weight of equivalent mass

$W = Mg = 43.1$ lb

(b) Weight of Post And Nut

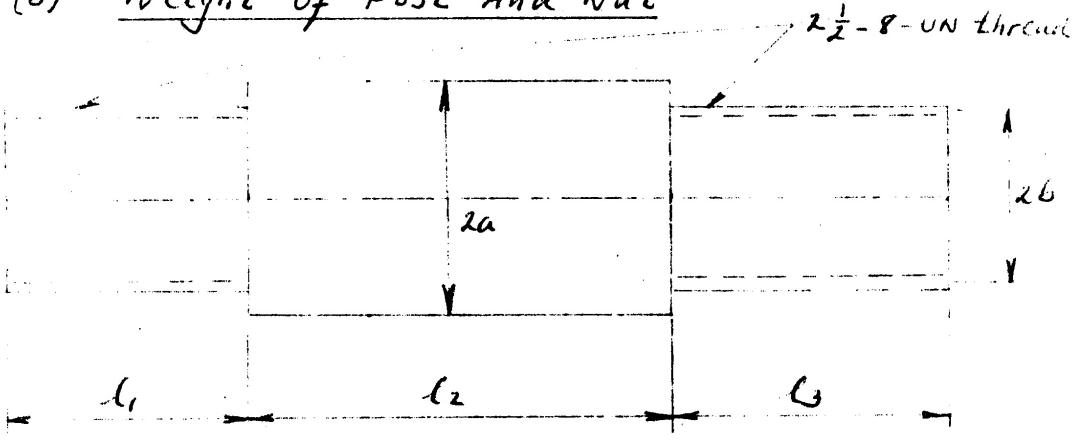

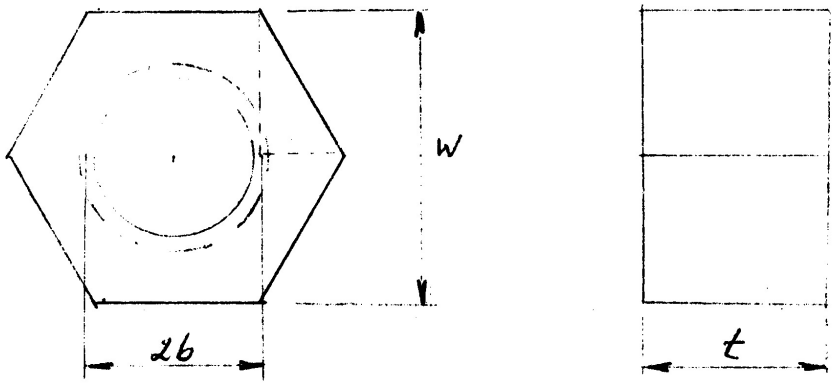

V_1 = Volume of post, V_2 = Volume of nut

$V_1 = \pi b^2(\ell_1 + \ell_3) + \pi a^2 \ell_2$

$V_2 = (12 \times \frac{1}{2} \times \frac{W}{2} \times \frac{W}{2} \tan 30 - \pi b^2)t$

$= (1.5 W^2 \tan 30 - \pi b^2)t$

dimensions (inches)

$2a = 3.25$	$\ell_1 = 3.44$	$W = 3.88$
$2b = 2.43$	$\ell_2 = 5.81$	$t = 2.55$
	$\ell_3 = 3.15$	

Substitution:

$V_1 = 81.5 \text{ in}^3$

$V_2 = 21.4 \text{ in}^3$

$\Big\}\ V = V_1 + V_2 = 102.9 \text{ in}^3$

W = weight of post and nut = $V\rho$

$= 102.9 \times 0.284 = \underline{29.2}$ lb

(c) Simulation

Assume central cavity of disc occupied by material having density such that weight matches that of arm, post and nut.

W_t = total weight = $43.1 + 29.2 = 72.3$ lb

V_c = cavity volume = $\frac{\pi}{4}(2.43)^2 3.75 = 17.4 \text{ in}^3$

Equivalent specific weight ρ_e = $Wt/V_c = 4.16$ lb/in^3

For steel, $\rho_s = 0.284$

Conclusion: $\rho_e/\rho_s = \rho_e/\rho_s = 14.6$

Determination of Translational Impact Velocity

The uniform impact velocity for the disc is determined by matching the kinetic energy for the assumed translational mode (Ke_t) to the kinetic energy computed for the actual rotational mode (Ke_r).

Let, R_c = distance from pivot point to disc center of gravity

ω = angular velocity of disc

$V_c = \omega R_c$ = velocity at center of gravity

I = mass moment of inertia of disc about pivot point

M = mass of disc

V_t = impact velocity

Then, $KE_r = I\omega^2/2$

$KE_t = Mv_t^2/2$

Equating KE_t to KE_r gives $V_t/V_c = (1/R_c)\sqrt{I/M}$

Velocity V_t can be determined with sufficient accuracy by simplifying the disc to one with flat surfaces, 3.75 in. apart, and by assuming the center of gravity to be located on the disc centerline. Denoting the outside diameter, inside diameter and thickness of the disc by D, d and t, respectively, one has

$$I = I_p + Mr_c^2$$

where $$I_p = \left[\pi t/64\right]\left[D^4\rho_s + d^4\left(\rho_e - \rho_s\right)\right]$$

$$M = \left[\pi t/4\right]\left[D^2\rho_s + d^2\left(\rho_e - \rho_s\right)\right]$$

Therefore,

$$\left(V_t/V_c\right)^2 = 1 + \left[D^4 + \mu d^4\right]/\left[16R_c^2\left(D^2 + \mu d^2\right)\right]$$

where $\mu = \rho_e/\rho_s - 1$

Substitution of D = 27.5 in., d = 2.432 in., ρ_e/ρ_s = 14.6, and V_c = 117.0 ft/sec. (Attachment D), gives the result

$V_t = 1.081\, V_c = 126.4$ ft/sec. $= 3.853 \times 10^{-3}$ cm/μsec.

For conservatism, a V_t of 150 ft/sec will be assumed.

ATTACHMENT D

FLUID DYNAMICS ANALYSIS

D. Fluid Dynamics

Impact Analysis of Main Steam Swing Disk Trip Value

The main steam swing disk trip valve, located in the main steam line outside containment, prevents total blowdown of the steam generator following a downstream pipe rupture.

In operation, the swing disk assembly, consisting of the disk, disk post, and disk arm, is held in an open position some 65° from its seat. Valve positioning is accomplished by means of a pneumatically actuated air cylinder. One hundred (100)-psig air applied to the air cylinder displaces a piston upward, and this motion is transmitted by linkage to the trip valve shaft as rotary motion, raising the disk to its open position. In this position the disk is clear of the main stream of flow through the valve. In displacing the air cylinder upward, the pressurizing air also compresses a return spring located beneath the air cylinder, which is coupled axially to the displaced piston.

Upon rupture of the downstream steam line, a signal is transmitted to the air cylinder dump solenoid valves which are actuated, thereby initiating depressurization of the air cylinder. Elapsed time from break to dump valve operation is 0.500 s. Prior to disk motion, the 100-psig air cylinder pressure must decay to approximately 35 psig at which pressure the disk assembly is just maintained in its open position (65°). As choked flow conditions exist at the dump valve exhaust to ambient, outflow is limited, and the pressure decay occurs over approximately 1.0 s. Thus onset of disk motion occurs some 1.5 s following pipe rupture.

During downward motion of the disk, the disk is initially under the influence of only gravity and spring tension. After traversing an arc of 17.5°, it enters the edge of the main steam flow and induces an ever-increasing ΔP as it swings across the final 47.5° of arc toward closure at the valve seat.

Flow Conditions to be Analyzed

Two steam generator hot standby conditions will be evaluated for disk impact. The flow characteristics for each are summarized as follows:

Case	P_0, PSIA	P_{THROAT}, PSIA	Quality, %	Flow, $\frac{LBM}{SEC}$	Stm. Hammer PSI
1	1020	995	Dry & Sat.	2300	300
2	1020	995	4%	7800	150

Upon rupture of the main steam line, choke flow occurs at the break and, concurrently, a pressure rarefaction wave travels upstream, at the local speed of sound, acceleration the initially-stagnant steam toward the break. Initial steam outflow is that which occurs from a 32-in. O.D. pipe at identical initial conditions.

As the rarefaction wave ($C_0 \approx 1771$ ft/s) reaches the 14-in. ∅ flow restrictor, choked flow is established at its throat, limiting steam generator outflow to those flow rates noted above. Because the transition time to choking at the flow restrictor, ≈ 0.12 s, is considerably less than the 1.5-s delay until onset of disk motion, the closing disk will be exposed to only those choked flow rates noted, and not to the initial flow rate in the 32-in. pipe.

D.1 Swing Disk Trip Valve Characteristics

The following data describe the trip valve:

Weight: Combined weight of the disk, disk post, nut, and disk arm (excluding cyl. segment about rock shaft) is 969 LBM (per A. & M.)

Radius of Gyration, K:

The C.G. of the disk assembly is 16.0 in. from the rockshaft ℄, at an angle of 29.876° to the vertical (per A. & M.)

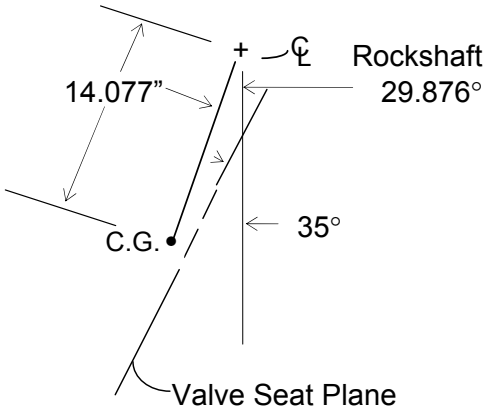

Moment of Inertia:

$$I = MK^2 \quad (8)$$

$$I = (969 \text{ LBM})(14.077 \text{ IN})^2 = 192{,}019 \text{ LBM-IN}^2$$

D.2 Relations for Dynamic Analysis During Disk Swing

D.2.1 Disk Equations of Motion

Angular Acceleration:

The angular acceleration of the disk at a given angular displacement is given:

$$\propto = \frac{\Sigma T_{OPCN \bullet \theta}}{I} \tag{1}$$

Angular Velocity:

The angular velocity of the disk at time interval $(t+\Delta t)$ is:

$$W_{t+\Delta t} = W_0 + \propto \Delta t \tag{2}$$

Angular Position:

The angular position of the disk at time t is given:

$$\Delta\theta = W_t \Delta t + \frac{\propto_t \left(\Delta t^2\right)}{2} \tag{3}$$

The disk impact analysis will consider the following disk displacement intervals:

1.	65°	→	47.5°	
2.	47.5°	→	35°	
3.	35°	→	24.5°	(CHOKE ∢)
4.	24.5°	→	10°	} CHOKED FLOW
5.	10°	→	IMPACT	} CHOKED FLOW

For these intervals, average valves of θ, T_{SPRING}, K_θ, & T_{FR} will be used.

D.2.2 Torques Acting on Swing Disk

During angular rotation from its open position (65°) to impact on its seat, the disk is exposed to:

1) Gravitational Torque tending to accelerate the disk to its closed position.

2) Fluid Torque due to the ΔP of steam flowing past the inclining disk.

3) Closing-spring Torque due to compressive load on returning spring.

4) Frictional Torque due to rock shaft rotation within the graphite/asbestos gland packing.

The net torque for various disk angular positions is written:

$65° < \theta < 47.5°$ (4)

$$T_{NET} = I_{\infty} = [(M,LBM)(L,IN)]\frac{g}{g_o} \sin(\theta + 29.876) + T_{SPRING} - T_{fr}$$

Where:

g = accel of gravity 32 $\frac{FT}{SEC}$

g_o = gravitational constant, 32.2 $\frac{LBM\ FT}{LBF\ SEC^2}$

L = moment arm to C.G., 16. IN

T_{SPRING} = spring load, LBF

T_{fr} = frictional torque, 47.70 in LBF

$47.5° > \theta > 0'$

$$T_{NET} = I_{\infty} = [(M,LBM)(L,IN)]\frac{g}{g_o} \sin(\theta + 29.876) + T_{SPRING} + \Delta P \bullet A \bullet L - T_{fr} \quad (5)$$

Where

ΔP = pressure drop across disk

A = surface area of disk MSD normal to $\mathbb{C}$

Figure D-1 illustrates the variation of the closing-spring torque for disk displacement angle from its seat.

Choke Angle

During initial descent of the disk from its open position, choked flow is assumed at the valve seat. At some choke angle, the choke suddenly translates upstream from the valve seat plane to that flow area described between the planes of the disk and seat. Calculations of the choke angle are described in the sheets following.

D.2.3 CALCULATION OF ANGLE FOR ONSET OF CHOKED FLOW DURING CLOSURE OF THE SWING DISK VALVE

An attitude angle for the swing disk trip valve is computed for the onset of choked flow across the closing valve. This condition begins at that instant when the effective orifice area, i.e., that dihedral area between the disk plane and the plane of the valve seat, is exactly equal to the cross-sectional area of flow across the valve seat. As we consider the effective flow area, we must consider the elliptical surface area defined by the intercepting “chords” as shown below.

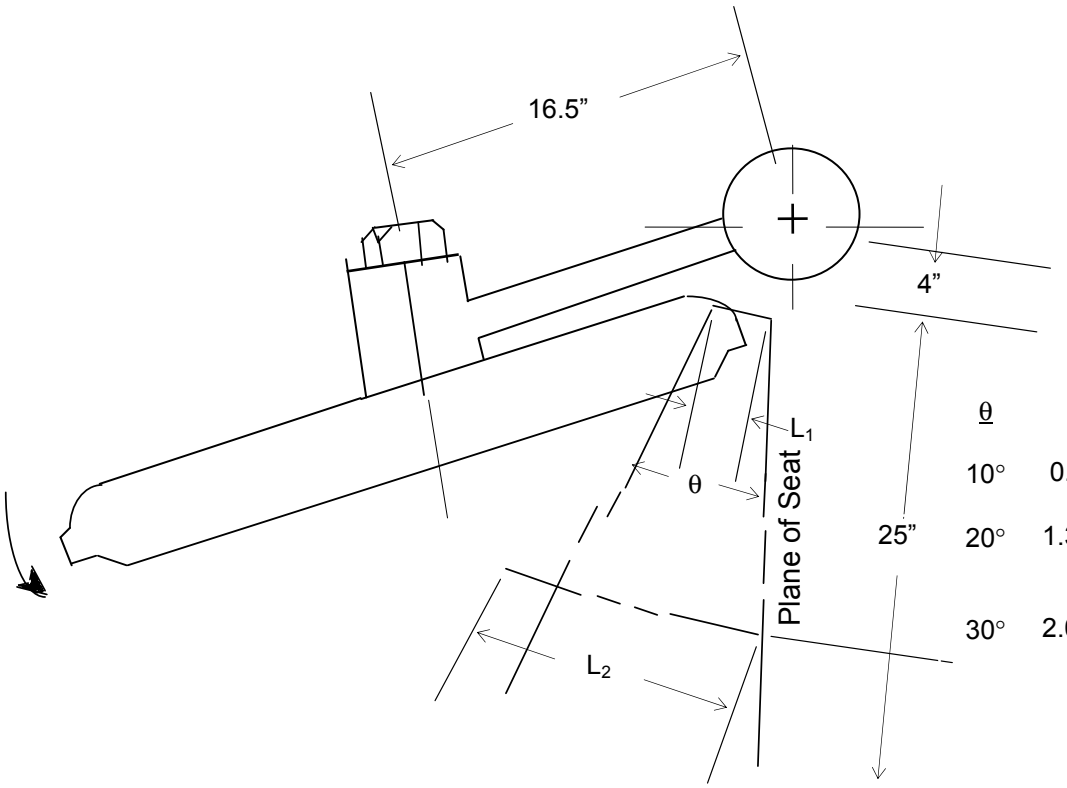

θ	L_1	L_2
10°	0.697”	5.055”
20°	1.3892”	10.0716”
30°	2.0706”	15.012”

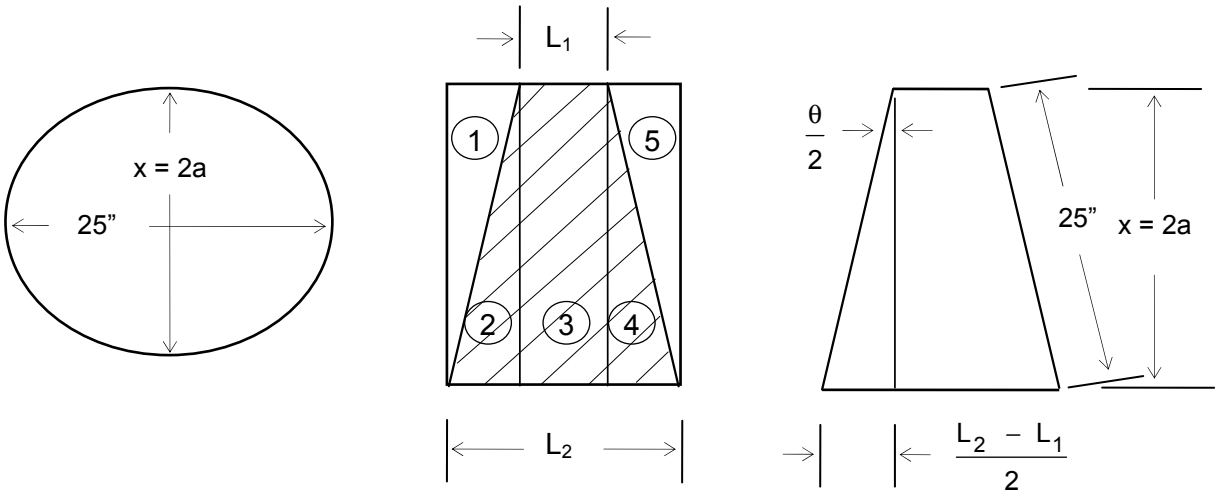

<u>θ = 10° From Seat</u>

$$\cos\frac{\theta}{2}=\frac{x}{25}$$

$$x = 25\cos 5^\circ = 24.905”$$

$$A_T = C \times L_2$$

$$= 2\pi\sqrt{\frac{a^2+6^2}{2}}\times L2 = 2\pi\sqrt{\frac{12.452^2+12.5^2}{2}}\times 5.055$$

$$A_T = (78.391)(5.055) = 396.26 \text{ in.}^2$$

Now: $A_3 = C \times L_1 = (78.391)(0.697) = 54.639 \text{ in.}^2$

$$\therefore A_{1,2,4,5} = \frac{396.26 \text{ IN}^2 - 54.639 \text{ in.}^2}{4} = 85.405 \text{ in.}^2$$

$$\therefore A_{2+3+4} = 54.639 + 2(85.405) = \underline{225.45} \text{ in.}^2$$

20° From Seat

$$\cos \frac{\theta}{2} = \frac{x}{25}$$

$$x = 25 \cos 10^\circ = 24.62''$$

$$A_T = c \times L_2 = 2\pi \sqrt{\frac{12.31^2 + 12.5^2}{2}} \times 10.072$$

$$A_T = (77.945)(10.072) = 785.06 \text{ in.}^2$$

NOW: $A_3 = (77.945)(1.3892) = 108.28 \text{ in.}^2$

$$A_{1,2,4,5} = \frac{785.06 - 108.28}{4} = 169.194 \text{ in.}^2$$

$$\therefore A_{2+3+4} = 108.28 + 2(169.194) = \underline{446.67} \text{ in.}^2$$

30° From Seat

$$x = 25 \cos 15^\circ = 24.148''$$

$$A_T = 2\pi \sqrt{\frac{12.074^2 + 12.5^2}{2}} \times 15.012$$

$$A_T = (77.213)(15.012) = 1159.123 \text{ in.}^2$$

$$A_3 = C \times L_1 = (77.213)(2.0706) = 159.88 \text{ in.}^2$$

$$A_{1,2,4,5} = \frac{1159.123 - 159.88}{4} = 249.81 \text{ in.}^2$$

$$\therefore A_{2+3+4} = 159.88 + 2(249.81) = \underline{659.50} \text{ in.}^2$$

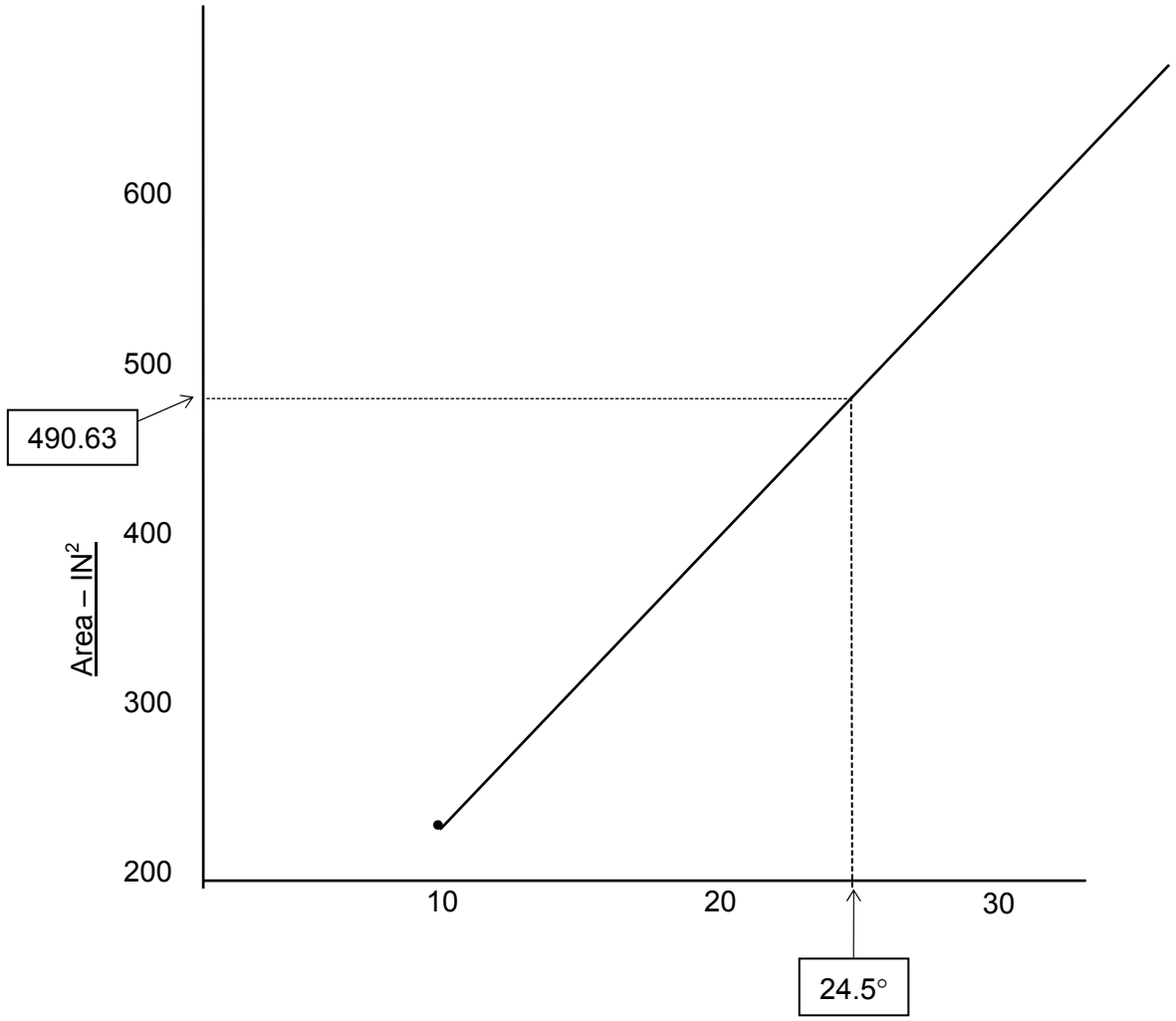

DIHEDRAL ANGLE θ ~ DEGREES

A_{seat} = $0.785(25)^2$ = 490.63 in^2

From the above we conclude that the choking angle is 24.5°.

D.3 Fluid Flow Equations/Dynamic Analysis

D.3.1 Case 1

Initial condition is Hot Standby, zero flow in the main steam line. Valve disk is held at 65° open-position by 100-psig cylinder air. The steam generator and 32-in. piping upstream of the valve are taken as an infinite reservoir at 1020 psia.

Steam Properties are[1]:

P_o = 1020 PSIA (Dry Saturated Steam)

T_o = 546.95 °F

$W_o = 0 \ \frac{LBM}{SEC}$

$h_g = 1191.6 \ \frac{BTU}{LBM}$

$s_g = 1.3879 \ \frac{BTU}{LBM^2}$

$\upsilon_g = 0.4361 \ \frac{FT^3}{LBM}$

$\gamma = 1.13$[2]

Sonic Velocity:

$$C_o = \sqrt{KRTg} \qquad (6)$$

$$C_o = \sqrt{(1.13)(85.6)(546.95 + 460)(32.2)} = \underline{1770.9} \ \frac{FT}{SEC}$$

1. J.Keenan & F.Keyes, Thermodynamic Properties of Steam, John Wiley & Sons, First Edition, 31st Printing, N.Y.

$\therefore$ The velocity of propagation of the pressure rarefaction wave is 1770.9 $\frac{ft}{sec}$.

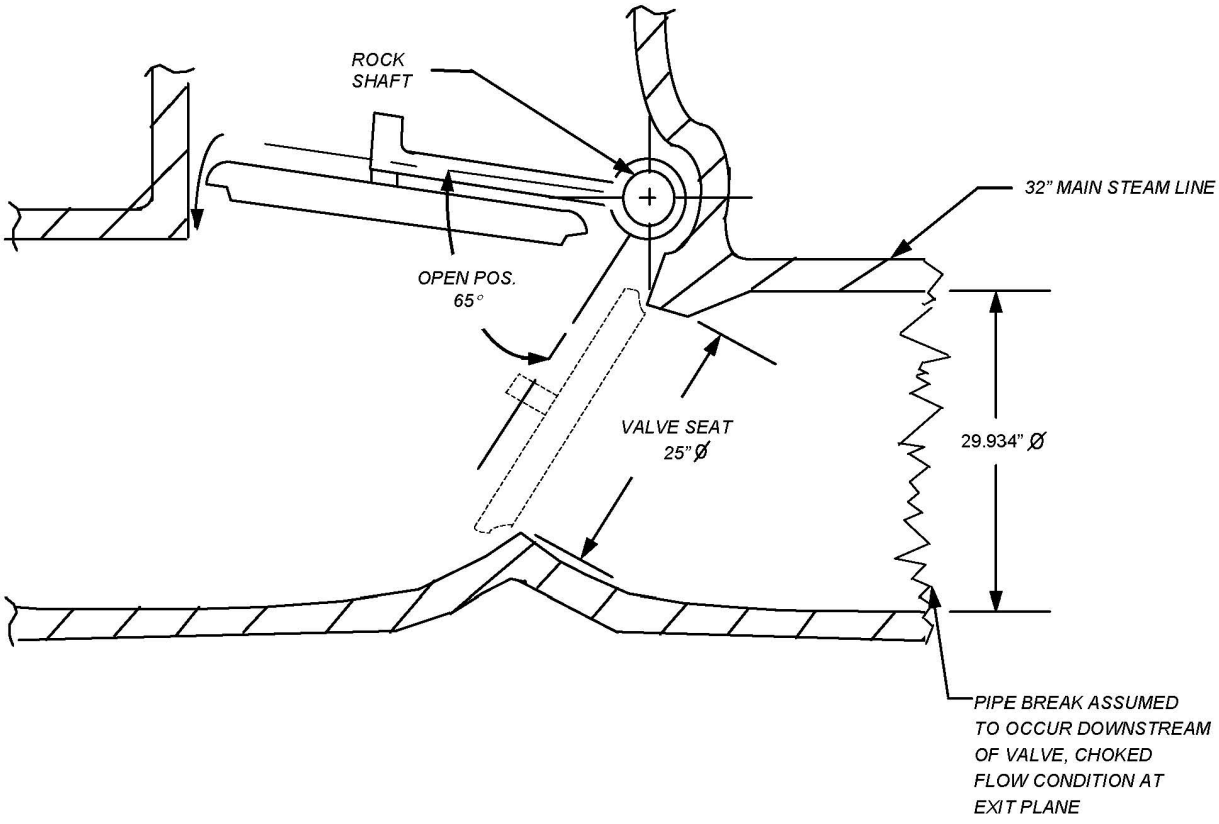

Upon rupture of the pipe, choked flow is established immediately at the break plane. This continues during travel of the pressure rarefaction (at 1771 $\frac{FT}{SEC}$) to the flow restrictor which then limits the steam outflow to the break. To determine flow conditions at the valve we must consider the flow path between the flow restrictor and valve such that all flow characteristics are considered. Steady state flow conditions are assumed at onset of disk.

Hall and Orme[3] have investigated the flow of compressible fluid thru sudden enlargements, and the effects of friction upon M (mach no.), P, T, and m. As a first approximation we may consider the nozzle/pipe junction a sudden enlargement, and use the results of this analysis to establish steam flow conditions at the valve.

Consider the following pipe configuration:

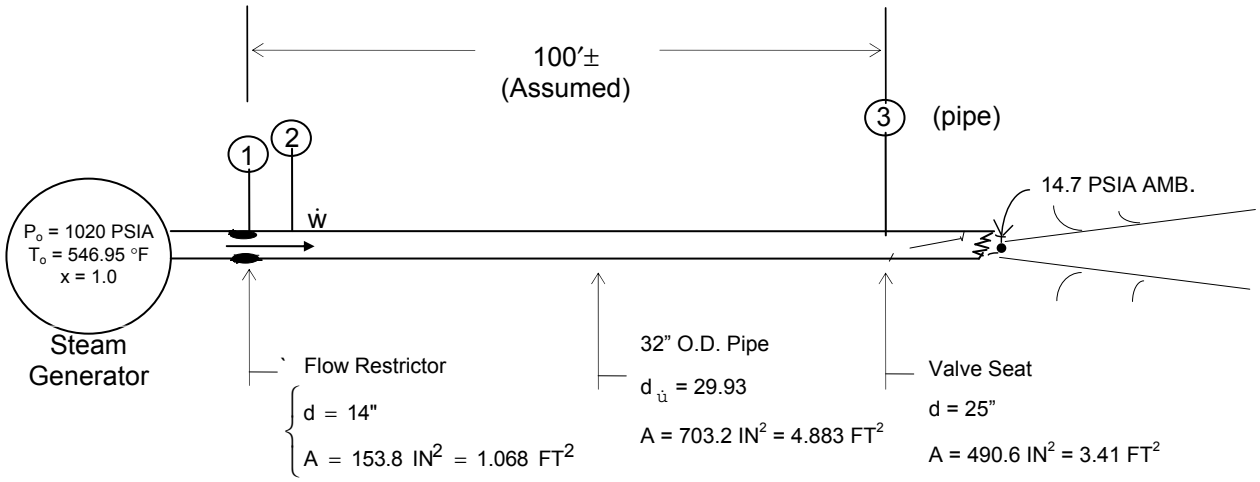

To determine flow conditions at each location, ①, ②, and ③, we start at the steam generator, progressing downstream toward the valve.

2. Ichoro Nishiwaki, " On a new theory for Adiabatic Index of Wet Steam," Proc. of 11th Japan National Congress for Appl. Mechs, 1961.

3. W. B. Hall, E. M. Orme, "Flow of a Compressible Fluid Through a Sudden Enlargement in a Pipe," Proc. of Inst. of Mech. Engrs., 1955, Vol. 169, No. 49, pp. 1007-1020.

Mach Numbers, M

As choked flow is established across the nozzle, $M_1 = 1$. Using FIG 7 of ref. 3, and an area ratio, ϕ, where:

$$\frac{A_{nozz}}{A_{pipe}} = \phi = \frac{153.8\ IN^2}{703.2\ IN^2} = 0.219 \quad (7)$$

we obtain $M_2 = 0.2$.

The friction loss between sections ② and ③ along the constant diameter pipe is given:

$$F_f = \frac{f \gamma x}{d_H} \quad (8)$$

Where f = Friction Factor - for turbulent flow conditions in 32" pipe- use 0.01

γ = Ratio specific heats = 1.13

x = Pipe length ≈ 100 FT

d_H = Hydraulic D/A = 29.93" = 2.494′

Solving EQ.(2):

$$F_f = \frac{(0.01)(1.13)(100\ FT.)}{2.494\ FT} = 0.453$$

Entering Fig 8 at $M_2 = 0.2$, with $F_f = 0.453$, we obtain $M_3 = 0.21$.

Pressure Distribution

Using M_1, P_o, and γ and by assuming adiabatic, frictionless flow into the nozzle we compute P_1 (Eq. 12)[3]:

$$\frac{P_o}{P_1} = \left[\frac{\gamma - 1}{2} M_1^2 + 1 \right]^{\frac{\gamma}{\gamma - 1}} \quad (9)$$

$$\frac{P_o}{P_1} = \left[\frac{1.13-1}{2}(1)^2 + 2\right]^{\frac{1.13}{1.13-1}} = 1.729$$

$\therefore P_1 = 0.578\ P_o = 590$ PSIA

Using EQ.(9)[3] we now compute P_2:

$$\frac{P_2}{P_1} = \phi\frac{M1}{M2}\sqrt{\frac{(\gamma-1)M_1^2+2}{(\gamma-1)M_2^2+2}} \qquad (10)$$

Substituting:

$$\frac{P_2}{P_1} = 0.219\frac{1.0}{0.2}\sqrt{\frac{(1.13-1)(1)^2+2}{(1.13-1)(0.2)^2+2}}$$

$$\frac{P_2}{P_1} = 1.13$$

$\therefore P_2 = (1.13)(.590) = \underline{665.9}$ PSIA

Again using EQ.(9)[3] compute P_3 : (ϕ = 1)

$$\frac{P_3}{P_2} = 1\frac{0.2}{0.21}\sqrt{\frac{(1.13-1)(0.2)^2+2}{(1.13-1)(0.21)^2+2}}$$

$$\frac{P_3}{P_2} = 0.952$$

$\therefore P_3$ (0.952)(665.9) = $\underline{634}$ PSIA

For a pipe rupture in close proximity to the valve, the flow chokes at the break, flowing at local sonic velocity. The pressure at the exit plane must correspond to the local sonic conditions.

If, in a limiting case, the break occurs downstream and adjacent to the valve seat, the flow chokes at the valve seat, and M = 1.0, rather than 0.21 as calculated above. In this case EQ. 11 of REF. 3 may be used to solve for the critical pressure at the seat.

Solving:

$$\left(\frac{\gamma-1}{2}\right)M^4 + M^2 - \frac{T\sigma\left(W/A\right)^2 R}{\gamma P^2} = 0 \qquad (11)$$

$$\frac{(1.13-1)(1)^4+1^2}{2} - \frac{(1007^\circ R)\left(\frac{2300}{3.41}\frac{LBM}{SEC\,FT^2}\right)^2\left(85.6\frac{FT-LBF}{LBM-^\circ R}\right)}{(1.13)\left(P\frac{LBF}{FT^2}\right)^2\left(32.2\frac{LBM\,FT}{LBF\,SEC^2}\right)\left(144^2\frac{IN^4}{FT^4}\right)}$$

$$1.065 - \frac{51974.6}{P^2} = 0$$

$$P = 220.9 \text{ or } \underline{\underline{221}} \text{ PSIA}$$

From steam tables, at x = 10

$$\nu_g = 2.096\ \frac{FT^3}{LBM}$$

Solving for flow velocity:

$$V = \frac{Q}{A} = \frac{\left(2300\frac{LBM}{SEC}\right)\left(2.096\frac{FT^3}{LBM}\right)}{3.41 FT^2}$$

$$V = \underline{\underline{1414}}\ \frac{FT}{SEC}$$

This velocity is now used in ΔP calculations up thru onset of choking.

Summarizing Flow Conditions

$$P = 221 \text{ PSIA}$$

$$\nu = 2.096\ \frac{FT^3}{LBM}$$

$$x = 1.0$$

$$W = 2300 \frac{LBM}{SEC}$$

$$V = 1414 \frac{FT}{SEC}$$

Pressure Drop Across Disk

Pressure drop across the closing disk varies as a function of the included angle between the disk plane and the plane of the valve seat.

For a given θ, pressure drop across the valve is:

$$\Delta P = K_\theta \frac{\int v^2}{2g} \qquad (12)$$

Where K_θ = Empirical value dependent upon θ (per A. & M. data), Fig 3-2

$\int$ = Fluid density, taken as $\frac{1}{v} = \frac{1}{0.7271 FT^3/LBM} = 1.375 \frac{LBM}{FT^3}$

V = Steam velocity upstream of valve seat = $1414 \frac{FT}{SEC}$

Solving EQ. (6):

$$\Delta P = K_\theta \frac{\left(\frac{1}{2.096}\frac{LBM}{FT^3}\right)\left(1414\frac{FT}{SEC}\right)^2}{(2)\left(32.2\frac{LBM\,FT}{LBF\,SEC^2}\right)\left(144\frac{IN^2}{FT^2}\right)}$$

$$\underline{\Delta P = 102.9\, K_\theta} \qquad (13)$$

Atwood & Morrill data for K_θ are shown in FIG. 3-2.

1. $65° > \theta > 47.5°$ (Free Fall w/Spring Friction)

$$\Delta P = 0$$

T_1, From EQ. (9):

$$T_1 = [(969\ \text{LBM})(14.077\ \text{IN})]\frac{32\ \text{FT}}{\text{SEC}^2} \times \frac{\text{LBF SEC}^2}{32\ \text{LBM FT}} \sin(56.25^\circ + 29.876^\circ)$$

$$+ 10658\ \text{IN. LBF} - 4770\ \text{IN. LBF}$$

$$T_1 = 13609 + 10658 - 4770 = 19{,}497\ \text{IN. LBF}$$

α_1:

$$\alpha_1 = \frac{T_1}{I} = \frac{19{,}497\ \text{IN.LBF}}{192{,}019\ \text{LBM} - \text{IN.}^2} \times \frac{32\ \text{LBM} - \text{FT}}{\text{LBF SEC}^2} \times \frac{12\ \text{IN.}}{\text{FT}}$$

$$\alpha_1 = 39.2\ \frac{\text{RAD}}{\text{SEC}^2}$$

t_1: Since disk is accelerated from W = 0_9 by EQ.13:

$$\Delta\theta = \frac{\alpha_1 t_1^2}{2}$$

$$t_1 = \sqrt{\frac{2\Delta\theta}{\alpha_1}} = \sqrt{\frac{(2)}{39.2}\frac{(17.5)}{57.3}} = 0.125\ \text{SEC}$$

W_1:

$$W_1 = \alpha_1 t_1$$

$$W_1 = \left(39.2\frac{\text{RAD}}{\text{SEC}^2}\right)(0.125\ \text{SEC}) = 4.90\frac{\text{RAD}}{\text{SEC}}$$

2. $47.5^\circ > \theta > 35^\circ$ ("Caught in Breeze" @ $\theta = 47.5^\circ$)

$$\alpha_1 = 39.2\ \frac{\text{RAD}}{\text{SEC}^2},\ t_1 = 0.125\ \text{SEC},\ W_1 = 4.90\ \frac{\text{RAD}}{\text{SEC}}$$

ΔP_2:

$$\Delta P = 102.9\ K_{\bar{\theta}} = (102.9)(1.41) = \underline{145.1}\ \text{PSI}$$

T_2:

$$T_2 = [(969\ \text{LBM})(14.077\ \text{IN})]\frac{32}{32}\sin(41.25 + 29.876)$$

$$+\left(145.1\frac{\text{LBF}}{\text{IN}^2}\right)(490.6\ \text{IN}^2)(16.5\ \text{IN}) + 9128\ \text{IN. LBF}$$

$$- 4770\ \text{IN LBF}$$

T_2 = 12,996 + 1,174,481 + 9128 - 4770 = 1,191,835 IN - LBF

$\propto_2$: $\propto_2 = \frac{T_2}{I} = \frac{1{,}191{,}835 \text{ IN} - \text{LBF}}{192{,}019 \text{ LBM} - \text{IN}^2} \times \frac{32 \text{ LBM FT}}{\text{LBF SEC}^2} \times \frac{12 \text{ IN}}{\text{FT}}$

$\propto_2 = \underline{2398} \frac{\text{RAD}}{\text{SEC}^2}$

Δt_2: $\Delta\theta_2 = W_1 \Delta t_2 + \frac{\propto_2 (\Delta t_2)^2}{2}$

$\frac{12.5}{57.3} = 4.90 \Delta t_2 + \frac{2398 \Delta t_2^2}{2}$

Solving:

$\Delta t_2^2 + 0.00409 \Delta t_2 - 0.00018 = 0$

$\Delta t_2 = \frac{-0.00409 + \sqrt{(0.00409)^2 + 4(1)(0.00018)}}{2}$

$\Delta t_2 = \underline{0.0116}$ SEC.

$\therefore$ Disk travels thru ARC 47.5° $\rightarrow$ 35° IN. 0.0116 SEC

W: $W_2 = W_1 + \propto_2 \Delta t_2$

$W_2 = 4.90 \frac{\text{RAD}}{\text{SEC}} + \left(2398 \frac{\text{RAD}}{\text{SEC}^2} \right) (0.0112 \text{ SEC}) = \underline{32.7} \frac{\text{RAD}}{\text{SEC}}$

$\sum t$: $\sum t = t_1 + \Delta t_2 = 0.125 + 0.0116 = \underline{0.1364}$ SEC.

3. 35° $\rightarrow$ 24.5°

$\propto_2 = 2398 \frac{\text{RAD}}{\text{SEC}^2} W_2 = 32.7 \frac{\text{RAD}}{\text{SEC}} \Sigma t = 0.1364 \text{ SEC}$

ΔP_3: $\Delta P_3 = 102.9\ K_{\bar{\theta}} = (102.9)(3.5) = \underline{360.2}$ PSI

T_3: $T_3 = \left[(969\ \text{LBM})(14.077\ \text{IN})\right]\frac{32}{32}\sin(29.75 + 29.876) +$

$$\left(360.2\frac{\text{LBF}}{\text{IN}^2}\right)\left(490.6\ \text{IN}^2\right)(16.5\ \text{IN}) + 7955\ \text{IN LBF} - 4770\ \text{IN LBF}$$

$T_3 = 11{,}813 + 2{,}915{,}378 + 7955 - 4770 = \underline{2{,}930{,}376}$ IN -LBF

α_3: $\alpha_3 = \frac{T_3}{I} = \frac{2{,}930{,}376\ \text{IN} - \text{LBF}}{192{,}019\ \text{LBM} - \text{IN}^2} \times \frac{32\ \text{LBM FT}}{\text{LBF SEC}^2} \times \frac{12\ \text{IN}}{\text{FT}}$

$\alpha_3 = \underline{\underline{5898}}\ \frac{\text{RAD}}{\text{SEC}^2}$

Δt_3: $\Delta\theta_3 = W_2\Delta t_3 + \frac{\alpha_3\left(\Delta t_3\right)^2}{2}$

$$\frac{10.5}{57.3} = 32.7\ \Delta t_3 + \frac{5898\Delta t_3^{\,2}}{2}$$

$\Delta t_3^2 + 0.0111\ \Delta t_3 - 0.000062 = 0$

$$\Delta t_3 = \frac{-0.0111 + \sqrt{(0.0111)^2 + 4(1)(0.000062)}}{2}$$

$\Delta t_3 = 0.00409$ SEC. $(35^\circ \rightarrow 24.5^\circ)$

$\therefore \Sigma t = 0.1364 + 0.00409 = \underline{0.1405}$ SEC.

W_3: $W_3 = W_2 + \alpha_3\ \Delta t_3$

$$W_3 = 32.7\ \frac{\text{RAD}}{\text{SEC}} + \left(5898\frac{\text{RAD}}{\text{SEC}^2}\right)(0.00409\ \text{SEC})$$

$W_3 = \underline{56.8}\ \frac{\text{RAD}}{\text{SEC}}$

4. $24.5° \rightarrow 10°$

Onset of choking (across the Dihedral Angle between the disk and seat) occurs at $\theta_c = 24.5°$. Prior to reaching θ_c, the closing disk has caused considerable pressure regain in the line. Add. 9 to Bechtel Inquiry SS-1102-32 specifies that, for case 1, the static pressure at the valve minimum flow area, with atmospheric pressure downstream, is 995 PSIA. Since choking occurs, we conservatively compute ΔP across the disk.

$$\Delta P_{CHOKE} = P_U - 0.578\ P_U$$

$$\Delta P_{CHOKE} = 995 - 0.578\ (995) = \underline{\underline{419.9}}\ \text{PSID}$$

T_4: $$T_4 = [(969\ \text{LBM})(14.077\ \text{IN})]\frac{32}{32}\sin(17.25 + 29.876) + \left(419.9\frac{\text{LBF}}{\text{IN}^2}\right)(490.6\ \text{IN}^2)(16.5\ \text{IN}) + 6680\ \text{IN LBF} - 4770\ \text{IN LBF}$$

$$T_4 = 9996 + 3{,}399{,}049 + 6680 - 4770 = 3{,}410{,}955\ \text{IN LBF}$$

α_4: $$\alpha_4 = \frac{T_4}{I} = \frac{3{,}410{,}955\ \text{IN LBF}}{192{,}019\ \text{LBM} - \text{IN}^2} \times \frac{32\ \text{LBM FT}}{\text{LBF SEC}^2} \times \frac{12\ \text{IN}}{\text{FT}}$$

$$\alpha_4 = \underline{\underline{6863.9}}\ \frac{\text{RAD}}{\text{SEC}^2}$$

Δt_4: $$\Delta\theta_4 = W_3\Delta t_4 + \frac{\alpha_4 (\Delta t_4)^2}{2}$$

$$\frac{14.5}{57.3} = 56.8\Delta t_4 + \frac{6863\Delta t_4{}^2}{2}$$

Solving:

$$\Delta t_4{}^2 + 0.0166\ \Delta t_4 - 0.000074 = 0$$

$$\Delta t_4 = \frac{-0.0166 + \sqrt{(0.0166)^2 + 4(1)(0.0000674)}}{2}$$

$$\Delta t_4 = 0.0036\ \text{SEC} \qquad (24.5° \rightarrow 10°)$$

$\Sigma t = 0.1405 + 0.0036 = \underline{0.1441}$ SEC

W_4 $W_4 = W_3 + \alpha_4 \Delta t_4$

$W_4 = 59.5 + (7539.6)(0.0035)$

$W_4 = \underline{81.9} \frac{\text{RAD}}{\text{SEC}}$

5. $10° \rightarrow$ IMPACT

As noted above, the ΔP across the disk during choke conditions is 419.9 PSID. Addendum #8 also specifies a pressure rise due to steam hammer on the disk of +300 PSI. At the moment of impact, then, the instantaneous pressure on the disk is:

$\Delta P_{IMPACT} = 419.9 + 300 = 719.9$ PSI

The average ΔP during the last 10° of motion is:

$$P_{AVG} = \frac{419.9 + 719.9}{2} = \underline{569.9} \text{ PSI}$$

T_5: $$T_5 = [(969 \text{ LBM})(14.077 \text{ IN})]\frac{32}{32}\sin(5 + 29.876) +$$

$$\left(569.9 \frac{\text{LBF}}{\text{IN}^2}\right)(490.6 \text{ IN}^2)(16.5 \text{ IN}) + 5430 \text{ IN} - \text{LBF} - 4770 \text{ IN LBF}$$

$T_5 = 6203 + 4,613,284 + 5430 - 4770 = 4,621,743$ IN LBF

α_5: $$\alpha_5 = \frac{T_5}{I} = \frac{4,621,743 \text{ IN LBF}}{192,019 \text{ LBM} - \text{IN}^2} \times \frac{32 \text{ LBM FT}}{\text{LBF SEC}^2} \times 12 \frac{\text{IN}}{\text{FT}}$$

$\alpha_5 = 9,300 \frac{\text{RAD}}{\text{SEC}^2}$

Δt_5: $$\Delta\theta_5 = W_4 \Delta t_5 + \frac{\alpha_5 (\Delta t_5)^2}{2}$$

$$\frac{10}{57.3} = 81.9\Delta t_5 + \frac{(9{,}300)(\Delta t_5)^2}{2}$$

$$\Delta t_5^2 + 0.0176\ \Delta t_5 - 0.0000375 = 0$$

$$\Delta t_5 = \frac{-0.0176 + \sqrt{(0.0176)^2 + 4(1)(0.0000375)}}{2}$$

Δt_5 = 0.0019 SEC.

Σt = 0.1441 +0.0019 = <u>0.1460</u> SEC.

W_5: $W_5 = W_4 + \alpha_5\ \Delta t_5$

W_5 = 81.9 + (9,300)(0.0019)

$$W_5 = \underline{\underline{99.8}}\ \frac{\text{RAD}}{\text{SEC}}$$

Summarizing, upon disk impact:

$$\alpha_{IMP} = \underline{\underline{9{,}300}}\ \frac{\text{RAD}}{\text{SEC}^2}$$

$$W_{IMP} = \underline{\underline{99.8}}\ \frac{\text{RAD}}{\text{SEC.}}$$

Σt_{IMP} = 0.1460 SEC.

$$V_{IMP} = \frac{99.8\ \text{RAD}}{\text{SEC}} \times 14.077\ \text{IN} = \underline{\underline{1404}}\ \frac{\text{IN}}{\text{SEC}} = \underline{\underline{117.0}} = \frac{\text{FT}}{\text{SEC}}$$

D.3.2 <u>Case 2</u>

Case 2 differs from Case 1 in that a 4% steam-water mixture, rather than dry saturated steam, flows at 7800 LBM/SEC. This represents a 2-phase blowdown across the valve. In this case the initial fluid condition is taken as saturated water at 1020 PSIA. During passage of the water through the pipe, the pressure drop results in reduced temperature and enthalpy. The reduction in enthalpy is manifested as latent heat of vaporization of the water, resulting in vapor formation within the liquid. The mixture quality on crossing the valve is 4%.

The critical pressure at the break exit plane is given by Griffith[4] as a function of pipe L/D ratio. Taking L = 100 FT, and D = 29.93 inches, we obtain:

$$\frac{L}{D} = \frac{100\ FT}{29.93/12\ FT} = 40$$

Referring to Fig. III - 2 of Ref. 4, we obtain:

$$\frac{P_c}{P_o} = 0.55$$

$\therefore P_c$ = 0.55 (1020 PSIA) = 561 PSIA.

Summarizing flow conditions:

P_c = 561 PSIA

T_c = 479 °F

x = 0.04

$$\nu = \nu_f + x\nu_{fg} = 0.020 + (0.04)(0.8250) = 0.053\ \frac{FT^3}{LBM}$$

$$w = 7800\ \frac{LBM}{SEC}$$ (assumed choked by flow restrictor)

Since the break location is unspecified, we may work upstream to estimate the pressure variation. Assume L = 10; D = 29.93″, f = 0.011; solve for V and ΔP:

$$V = \frac{Q}{A} = \frac{\left(7800\frac{LBM}{SEC}\right)\left(0.053\frac{FT^3}{LBM}\right)}{4.883\ FT^2} = 84.7\frac{FT}{SEC}$$

$$\Delta P = f\frac{L}{D}\frac{\rho V^2}{2g} \qquad (14)$$

4. P. Griffith, “Choked Two Phase Flow,” Mass. Inst. of Technology, Cambridge, Mass. Unpublished Report.

$$\Delta P = (0.011)\left(\frac{10\ FT}{\frac{29.93}{12}FT}\right)\frac{\left(\frac{LBM}{0.053\ FT^3}\right)\left(84.7\frac{FT}{SEC}\right)^2}{(2)\left(32.2\frac{LBM\ FT}{LBF\ SEC^2}\right)\left(144\frac{IN^2}{FT^2}\right)}$$

$$\Delta P = 0.64\ PSI \qquad \text{(Does not include density variation)}$$

Therefore for a short length between the break and valve, the pressure may conservatively be taken as P_c of 561 PSIA.

As in Case 1, we again use the valve seat area as the representative valve flow area.

$$\therefore V = \frac{Q}{A} = \frac{\left(7800\frac{LBM}{SEC}\right)\left(0.053\frac{FT^3}{LBM}\right)}{3.41\,FT^2}$$

$$V = \underline{\underline{121.2}}\ \frac{FT}{SEC}$$

For Case 2 we use identical relations for torques, inertia, weight, and equations of motion. EQ. (12) is used to obtain a new ΔP relation:

$$\Delta P = K_\theta \frac{\rho V^2}{2g}$$

$$\Delta P = \frac{K_\theta\left(\frac{LBM}{0.053\ FT^3}\right)\left(121.2\frac{FT}{SEC}\right)^2}{(2)\left(32.2\frac{LBM FT}{LBF\ SEC^2}\right)\left(144\frac{IN^2}{FT^2}\right)}$$

$$\therefore \Delta P = \underline{\underline{29.9K_\theta}}$$

As earlier, A. & M. data in Fig. 3-2 are used for K_θ.

1. $65° > \theta > 47.5°$ (Free fall w/spring, friction)

$\Delta P = 0$

As all disk mass, spring and friction constants are identical to those used for Case 1, we use those results directly.

$T_1 = 19{,}497$ IN LBF

$\alpha_1 = 39.2 \frac{RAD}{SEC^2}$

$t_1 = 0.125$ SEC

$W_1 = 4.90 \frac{RAD}{SEC}$

2. $47.5° > \theta > 35°$ (Caught in "Breeze" at $\theta = 47.5°$)

ΔP_2: $\Delta P_2 = 29.9\ K_{\bar{\theta}} = (29.9)(1.41) = \underline{\underline{42.2}}$ PSI

T_2:
$$T_2 = \left[(969\ \text{LBM})(14.077\ \text{IN})\right]\frac{32}{32}\sin(41.25 + 29.876) + \left(42.2\frac{\text{LBF}}{\text{IN}^2}\right)(490.6\ \text{IN}^2)(16.5\ \text{IN}) + 9128\ \text{IN - LBF} - 4770\ \text{IN LBF}$$

$T_2 = 13{,}239 + 341{,}273 + 9128 - 4770$

$T_2 = \underline{\underline{358{,}870}}$ IN - LBF

α_2:
$$\alpha_2 = \frac{T_2}{I} = \frac{358{,}850}{192{,}019} \times \frac{32\ \text{LBM FT}}{\text{LBF SEC}^2} \times \frac{12\ \text{IN}}{\text{FT}}$$

$\alpha_2 = \underline{\underline{722.2}} \frac{RAD}{SEC^2}$

Δt_2:
$$\Delta\theta_2 = W_1\,\Delta t_2 + \frac{\alpha_2 (\Delta t_2)^2}{2}$$

$$\frac{12.5}{57.3} = 4.90\Delta t_2 + \frac{722.2(\Delta t_2)^2}{2}$$

Solving

$$\Delta t_2^2 + 0.0136\,\Delta t - 0.00060 = 0$$

$$\Delta t_2 = \frac{-0.0136 + \sqrt{(0.0136)^2 + 4(1)(0.00060)}}{2}$$

$$\Delta t_2 = \underline{0.0187}\ \text{SEC}$$

W_2: $W_2 = W_1 + \alpha_2\,\Delta t_2$

$$W_2 = 4.90 + (722.2)(0.0187) = 18.4\ \frac{\text{RAD}}{\text{SEC}}$$

Σt: $\Sigma t = 0.125 + 0.0187 = \underline{0.1435}$ SEC

3. $35^\circ \rightarrow 24.5^\circ$

$$\alpha_2 = 722.2\ \frac{\text{RAD}}{\text{SEC}^2} W_2 = 18.4\ \frac{\text{RAD}}{\text{SEC}} \Sigma t_2 = 0.1435\ \text{SEC}.$$

ΔP_3: $\Delta P_3 = 29.9\ K_\theta = (29.9)(3.5) = 104.7$ PSI

T_3:

$$T_3 = [(969\ \text{LBM})(14.077\ \text{IN})]\frac{32}{32}\sin(29.75 + 29.876)$$
$$+$$
$$\left(104.7\ \frac{\text{LBF}}{\text{IN}^2}\right)(490.6\ \text{IN}^2)(16.5\ \text{IN}) + 7955\ \text{IN LBF} - 4770\ \text{IN LBF}$$

$$T_3 = 12{,}173 + 847{,}131 + 7955 - 4770 = \underline{862{,}489}\ \text{IN LBF}$$
$$-4770\ \text{IN LBF}$$

α_3:

$$\alpha_3 = \frac{T_3}{I} = \frac{862{,}489\ \text{IN LBF}}{192{,}019\ \text{LBM} - \text{IN}^2} \times 32\ \frac{\text{LBM FT}}{\text{LBF SEC}^2} \times \frac{12\ \text{IN}}{\text{FT}}$$

$$\alpha_3 = \underline{1736}\ \frac{\text{RAD}}{\text{SEC}^2}$$

Δt_3:

$$\Delta\theta_3 = W_2\,\Delta t_3 + \frac{\alpha_3\,(\Delta t_3)^2}{2}$$

$$\frac{10.5}{57.3} = 18.9\Delta t_3 + \frac{(1736)\Delta t_3^{\,2}}{2}$$

$$\Delta t_3^{\,2} + 0.02\ \Delta t_3 - 0.000211 = 0$$

$$\Delta t_3 = \frac{-0.02 + \sqrt{(0.02)^2 + 4(1)(0.000211)}}{2}$$

Δt_3 = 0.0074 SEC

$\therefore \Sigma t$ = 0.1435 + 0.0074 = 0.1509 SEC

W_3: $W_3 = W_2 + \alpha_3\ \Delta t_3$

W_3 = 18.4 + (1736)(0.0074)

W_3 = 31.2 $\frac{\text{RAD}}{\text{SEC}}$

4. $24.5° \rightarrow 10°$

As discussed in Case 1, onset of choking across the disk occurs at $\theta = 24.5°$. Addendum 9 states (as for Case 1) that the static pressure at the valve minimum flow area, with atmospheric pressure downstream, is 995 PSIA. Repeating the Case 1 calculation with $\frac{P_c}{P_o}$ = 0.55

ΔP_{CHOKE} = P_u - 0.55 P_u

ΔP_{CHOKE} = 995 - 0.55 (995) = 448 PSID

$$\alpha_3 = 1736\ \frac{\text{RAD}}{\text{SEC}^2} W_3 = 31.2 \frac{\text{RAD}}{\text{SEC}} \Sigma t_3 = 0.1509 \text{ SEC.}$$

T_4

$$T_4 = [(969\ \text{LBM})(14.077\ \text{IN})]\frac{32}{32}\sin(17.25 + 29.876) + 448\left(490.6\ \text{IN}^2\right)(16.5\ \text{IN}) + 6680\ \text{IN-LBF} - 4770\ \text{IN LBF}$$

T_4 = 9996 + 3,626,515 + 6680 - 4770

T_4 = 3,638,421 IN LBF

α_4: $$\alpha_4 = \frac{T4}{I} = \frac{3{,}638{,}421\ \text{IN LBF}}{192{,}019\ \text{LBM} - \text{IN}^2} \times 32 \frac{\text{LBM FT}}{\text{LBF SEC}^2} \times \frac{12\ \text{IN}}{\text{FT}}$$

$$\alpha_4 = \underline{7{,}321} \frac{\text{RAD}}{\text{SEC}^2}$$

Δt_4: $$\Delta\theta_4 = W_3\ \Delta t_4 + \frac{\alpha_4 (\Delta t_4)^2}{2}$$

$$\frac{14.5}{57.3} = (31.23)\Delta t_4 + \frac{7321(\Delta t_4)^2}{2}$$

$$\Delta t_4^{\,2} + 0.0085\ \Delta t_4 + 0.000069 = 0$$

$$\Delta t_4 = \frac{-0.0085 + \sqrt{(0.0085)^2 + 4(1)(0.000069)}}{2}$$

$$\Delta t_4 = \underline{\underline{0.0051}}\ \text{SEC}$$

$$\Sigma t_4 = 0.1509 + 0.0051 = \underline{\underline{0.1560}}\ \text{SEC}$$

W_4: $$W_4 = W_3 + \alpha_4\ \Delta t_4 = 31.23 + (7321)(0.0051) = 68.4\ \frac{\text{RAD}}{\text{SEC}}$$

5. $10^\circ \rightarrow$ IMPACT

Addendum 9 specifies a fluid hammer at disk impact of 150 PSI. At the moment of impact the total ΔP acting on the disk is:

$$\Delta P_{IMPACT} = 448 + 150 = 598\ \text{PSID}$$

The avg. ΔP during the last 10° of motion is:

$$\Delta P_{AVG} = \frac{448 + 598}{2} = 523\ \text{PSID}$$

T_5: $$T_5 = [(969\ \text{LBM})(14.077\ \text{IN})]\frac{32}{32}\sin(5 + 29.876) +$$

$$\left(523\frac{\text{LBF}}{\text{IN}^2}\right)\left(490.6\ \text{IN}^2\right)\left(16.5\ \text{IN}\right) + 5430\ \text{IN-LBF} - 4770\ \text{IN-LBF}$$

$T_5 = 7799 + 4{,}233{,}633 + 5430 - 4770$

$T_5 = \underline{4{,}242{,}092}\ \text{IN-LBF}$

α_5: $$\alpha_5 = \frac{T_5}{I} = \frac{4{,}242{,}092\ \text{IN LBF}}{192{,}019\ \text{LBM} - \text{IN}^2} \times 32.2\frac{\text{LBM FT}}{\text{LBM SEC}^2} \times \frac{12\ \text{IN}}{\text{FT}}$$

$$\alpha_5 = \underline{\underline{8536}}\ \frac{\text{RAD}}{\text{SEC}^2}$$

Δt_5: $$\Delta\theta_5 = W_4\,\Delta t_5 + \frac{\alpha_5\left(\Delta t_5\right)^2}{2}$$

$$\frac{10}{57.3} = 68.4\Delta t_5 + \frac{8536\left(\Delta t_5\right)^2}{2}$$

$$\Delta t_5^{\,2} + 0.0160\,\Delta t_5 + 0.000041 = 0$$

$$\Delta t_5 = \frac{-0.0160 + \sqrt{(0.0160)^2 + 4(1)(0.000041)}}{2}$$

$\Delta t_5 = \underline{\underline{0.0022}}\ \text{SEC}$

$\Sigma t_5 = 0.1560 + 0.0022 = \underline{\underline{0.1582}}\ \text{SEC}$

W_5: $W_5 = W_4 + \alpha_5\,\Delta t_5$

$W_5 = 68.4 + (8536)(0.0022)$

$$W_5 = \underline{\underline{87.5}}\ \frac{\text{RAD}}{\text{SEC}}$$

Summarizing, upon disk impact:

$$\alpha_{IMP} = 8536\ \frac{\text{RAD}}{\text{SEC}^2}$$

W_{IMP} = 87.5 $\frac{RAD}{SEC}$

Σt_{IMP} = 0.1582 SEC

V_{IMP} = 87.5 $\frac{RAD}{SEC} \times 14.077\ IN = \underline{\underline{1232}}\ \frac{IN}{SEC} = \underline{\underline{102.7}}\ \frac{FT}{SEC}$

D.4 Impact Conditions

The following summarize the disk impact conditions for Cases 1 and 2:

	Case 1	Case 2
Angular acceleration - $\propto, \frac{RAD}{SEC^2}$	9,300	8,536
Angular velocity - W, $\frac{RAD}{SEC}$	99.8	87.5
Closure time ~ SEC	0.146	0.158
Tip velocity - $^{FT}/_{SEC}\,(r = 30.25")$	251.5	220.6
Impact energy E = $\frac{Iw_{MAX}^{\ 2}}{2}, FT - LBF$	206,254	158,759

CLOSING TORQUE ON SWING DISK
DUE TO COMPRESSION OF SPRING

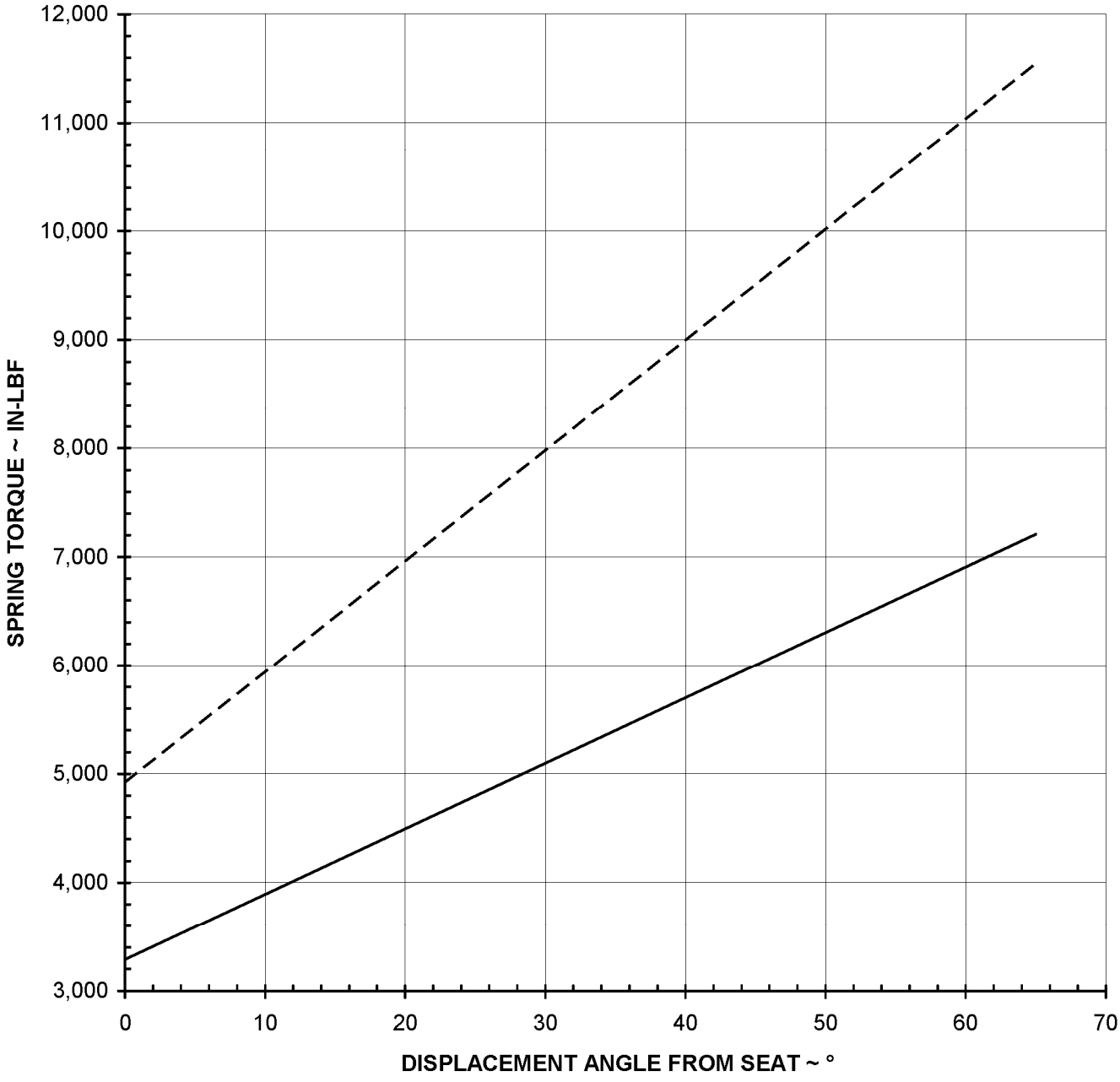

REV 23 5/11

SOUTHERN COMPANY
Energy to Serve Your World©

JOSEPH M. FARLEY NUCLEAR PLANT UNIT 1 AND UNIT 2

CLOSING TORQUE ON SWING DISC
DUE TO COMPRESSION OF SPRING

FIGURE D-1

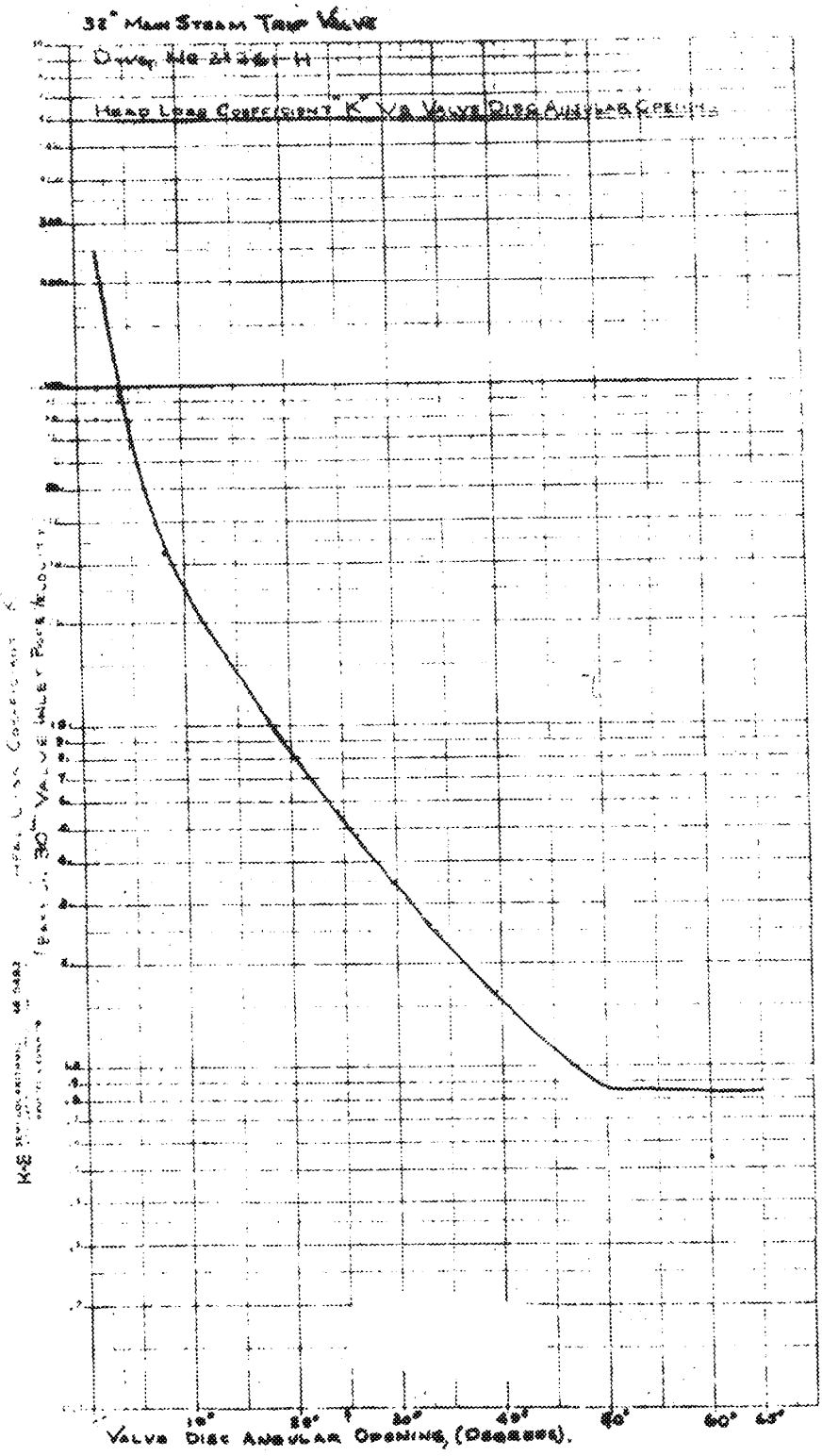

REV 21 5/08

SOUTHERN COMPANY *Energy to Serve Your World®*	**JOSEPH M. FARLEY NUCLEAR PLANT UNIT 1 AND UNIT 2**	HEAD LOSS COEFFICIENT K VERSUS VALVE DISC ANGULAR OPENINGS
		FIGURE D-2

ATTACHMENT E

ASME PAPER NO. 72-PVP-12[9]

P. C. RICCARDELLA
Materials and Stress Analysis,
Westinghouse Nuclear Energy Systems,
Pittsburgh, Pa.

Elasto-Plastic Analysis of Constrained Disk Burst Tests

The PVRC Subcommittee on Effective Utilization of Yield Strength has conducted an extensive series of pressurized burst tests on constrained disk specimens of seven steels. Elasto-plastic analyses have been performed for nine of these tests and the results are presented in this report. Good agreement between the analytical and experimental results all the way to failure pressure is illustrated by a comparison of centerline deflections. Interpretation of the analytical data indicates that both edge type and centerline type of failures are correlated reasonably well by the conventional reduction in area from a uniaxial tensile test once triaxiality is accounted for.

Introduction

THE PVRC Subcommittee on Effective Utilization of Yield Strength has conducted a series of constrained disk burst tests [1][1] using the disk specimen and test setup illustrated in Fig. 1. In order to interpret these tests and their relation to the safety margins which exist in the components of a Westinghouse nuclear steam supply system, elasto-plastic analyses have been performed on three disk geometries with three materials each. The three materials considered were type 304 stainless steel, ASTM A533B low-alloy steel, and ABS-C carbon steel. These materials are representative of reactor core support structures and piping, the reactor pressure vessel, and plant component supports, respectively. A summary of the mechanical properties from uniaxial tensile tests performed on the actual disk materials is given in Table 1.

Extensive data from the disk tests, including burst pressures and experimental pressure versus deflection curves have been reported in references [1] and [2]. Some of the disks failed at the disk centerlines, while others failed along the edge of the disks at the fillet between the thin and thick regions. Table 2 summarizes the failure data for the disks considered in this analysis, which include three centerline failures and six edge failures. The details of the three disk geometries are tabulated in Fig. 1.

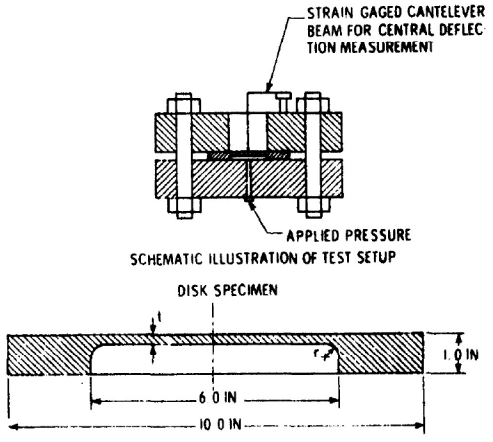

GEOMETRY	THICKNESS (t)	FILLET RADIUS (r)
A	0.25 IN	0.375 IN
B	0.125 IN	0.125 IN
C	0.125 IN	0.375 IN

Fig. 1 PVRC disk test details

[1] Numbers in brackets designate References at end of paper.

Contributed by the Pressure Vessels and Piping Division and presented at the Petroleum Mechanical Engineering Conference with Pressure Vessels and Piping Conference, New Orleans, La., September 17-21, 1972, of THE AMERICAN SOCIETY OF MECHANICAL ENGINEERS. Manuscript received at ASME Headquarters, June 6, 1972. Paper No. 72-PVP-12.

Table 1 Material properties

Material	.2% Y.S. (PSI)	$S_{ult.}$ (PSI)	$\epsilon_{ult.}$ (in/in)	Reduction in area	A* (PSI)	n*
Type 304 Stainless Steel	30,000.	85,000.	.54	.74	193,000.	.494
A-533B Low Alloy Steel	70,000.	95,000.	.17	.68.	146,000.	.161
ABS-C Carbon Steel	30,000.	64,000.	.31	.66	115,130.	.242

* Stress-strain curve assumed to be of form $\sigma = A\,\epsilon^n$

Table 2 Experimental failure data

Material	Geometry	Burst Pressure (PSI)	Type of Failure
304 S.S.	A	15,000.	Edge
	B	6,800.	Center
	C	7,700.	Center
A-533 B	A	11,000.	Edge
	B	5,300.	Edge
	C	6,700.	Center
ABS-C	A	9,800.	Edge
	B	3,750.	Edge
	C	4,940.	Edge

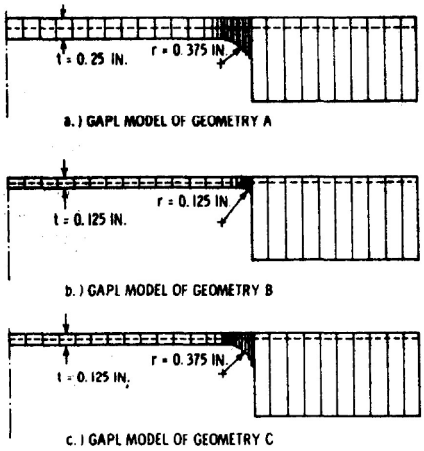

Fig. 2 Computer models of PVRC disks

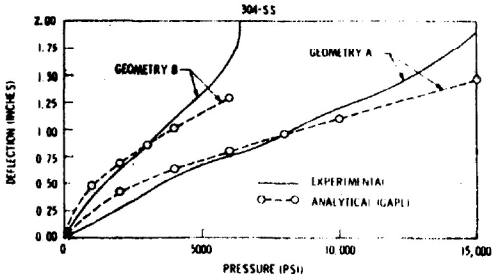

Fig. 3(a) PVRC disk tests—centerline deflection versus pressure (experimental and analytical results for 304 stainless steel disks)

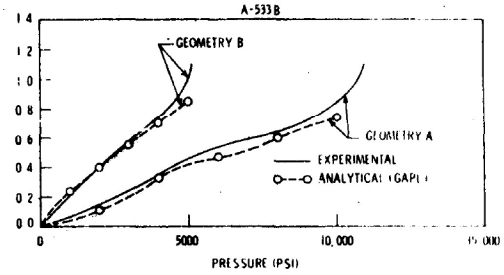

Fig. 3(b) PVRC disk tests—centerline deflection versus pressure (experimental and analytical results for A-533 B low alloy steel disks)

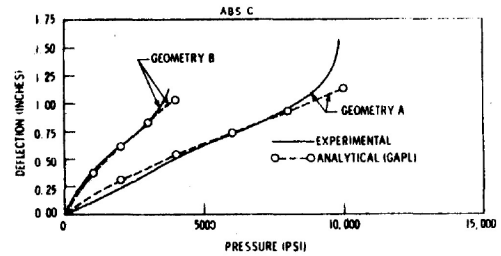

Fig. 3(c) PVRC disk tests—centerline deflection versus pressure (experimental and analytical results for ABS-C carbon steel disks)

Fig. 3

Analysis

The analysis of the disks was performed using the computer program GAPL-3 [3]. This program performs elasto-plastic, large-deformation analysis for stresses, strains, loads, and deflections of thin plates or axially symmetric shells with pressure loading and deflection restraints. The discrete element method employed in GAPL-3 requires fewer elements than conventional finite element techniques to adequately describe structures with high stress gradients because it makes use of a two-layered system of elements: one layer for the strain-displacement field, and a second layer for the stress field. The body is first divided into constant thickness, finite length strain-displacement elements along the axis of the body. The deflections in the elements are represented by a bending type polynomial along the axis and by a linear variation through the thickness. Each element is then further subdivided into constant stress regions in which the stresses are found as a function of the strains in the region. It is the deflection elements, however, which dictate the size of the problem.

The pressure loading is applied in steps and an equilibrium solution is found at each step by iterating for both geometric and material nonlinearities. The choice of incremental or deformation theory of plasticity is made by the user according to the size of the load steps he chooses. Since the program must iterate at each load step, the finer the load steps, the more costly the problem becomes.

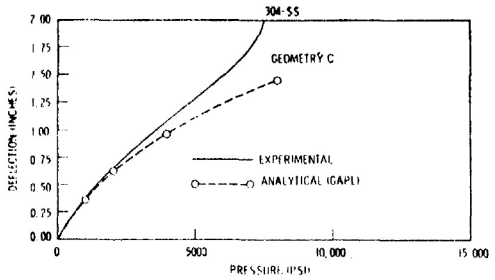

Fig. 4(a) PVRC disk tests—centerline deflection versus pressure (experimental and analytical results for 304 stainless steel disks)

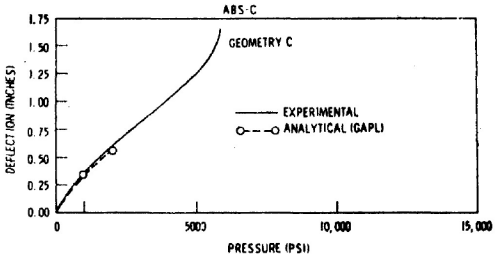

Fig. 4(c) PVRC disk tests—centerline deflection versus pressure (experimental and analytical results for ABS-C carbon steel disks)

Fig. 4

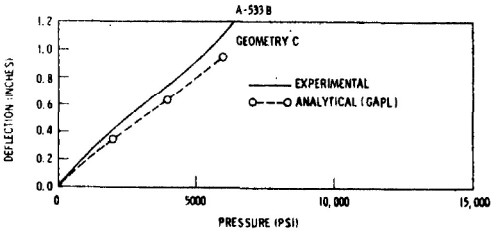

Fig. 4(b) PVRC disk tests—centerline deflection versus pressure (experimental and analytical results for A-533 B low alloy steel disks)

The three PVRC disk geometries were represented by the discrete strain-displacement element models shown in Fig. 2. In the thin portion of the disks, eight stress regions were specified for each strain-displacement element, while in the fillet regions twelve stress regions per element were used. Material properties for the three steels analyzed were input in terms of a power hardening law, using the constants A and n listed in Table 1. Both fine and crude load steps were tested to evaluate the effect of deformation versus incremental theories of plasticity, and the results were practically identical which indicates that the problem is a proportional loading situation. The production runs were then made using five load steps per case so that a reasonable representation of stresses and displacements as a function of applied pressure could be obtained.

Results

A comparison of the experimental and analytical centerline deflections at various pressures is given for geometries A and B in Fig. 3 and for geometry C in Fig. 4. The agreement is excellent all the way to failure pressure in eight of the nine cases considered. In the ninth case (ABS-C, geometry C) some difficulty was experienced in getting convergence at high pressures, although the experimental-analytical agreement was good at low pressures. In all cases the experimental data shows a tailing up as the pressure approaches burst pressure which the analytical results fail to predict. Since the GAPL program does not account for reduction in thickness, it can not be expected to predict tensile instability which the experimental tailing up represents.

Since the analytical prediction of centerline deflection was so good, it is expected that the stress and strain distributions predicted by GAPL are reasonable estimates of what occurred in the actual test specimens. Some reservation is called for in the fillet region, however, since the thin shell approximations of the GAPL program are not strictly valid there. The GAPL analysis includes plastic hinge type of strain redistribution, but the strain concentration effect due to fillet radius is not accounted for since the predicted strain distribution in the cross section of the fillet is linear there by assumption.

Table 3 Strain concentration factors

Material	Exponent	K_ϵ	GAPL RESULTS					
			Geometry A		Geometry B		Geometry C	
	(n)	$(1/n)$	ϵ_{GAPL}	$K_\epsilon/\epsilon_{GAPL}$	ϵ_{GAPL}	$K_\epsilon/\epsilon_{GAPL}$	ϵ_{GAPL}	$K_\epsilon/\epsilon_{GAPL}$
A-533 B	.141	7.1	7.2	.98	7.5	.94	8.3	.86
ABS-C	.242	4.1	5.3	.77	6.1	.68	6.6	.62
304-SS	.494	2.0	3.6	.56	4.5	.45	5.2	.38

As the pressure increased, the computed stresses at the disk centerlines approached a state of uniform biaxial membrane stress with negligible bending stress. In the fillet, the membrane stresses were lower than at the disk centerline, but the peak stresses on the inside surface of the fillet were the highest in the disk. Figs. 5, 6, and 7 summarize the computed stress and strain data for the fillet and centerline regions of the disks for the 304 SS, the A-533 B, and the ABS-C, respectively. The curves give maximum values of von Mises equivalent stress and strain in the two locations.

Several authors [4, 5, 6] have noted that the strain concentration (or redistribution) in the fillet in tests such as this should increase as the strain hardening exponent (n) decreases. As a first approximation, use of a strain concentration factor (K_ϵ) which is inversely proportional to n has been suggested [7]. In Fig. 8, the maximum radial fillet strains from the GAPL analysis have been cross-plotted against centerline deflections from Figs. 3 and 4 in order to study the effect of hardening exponent upon strain redistribution. The trend of increasing strain concentration with decreasing strain hardening is evident in this figure for all three geometries.

A simple elastic analysis has been performed on the disks in order to test the simple inverse proportion rule mentioned previously. The resulting maximum stresses in the fillet have been divided by Young's modulus and the results are given by the elastic lines in Fig. 8. Strain concentration factors have been computed at three discrete values of centerline deflection (0.6 in., 0.8 in., and 1.0 in.) by dividing the strains from the elasto-plastic GAPL analysis by the elastically computed strains at each deflection. The resulting strain concentration factors were then averaged over the three deflections, and these average values are listed in Table 3. This table shows that while the $(1/n)$ approximation is quite good for the lowest strain hardening exponent ($n = 0.141$), it tends to get worse as n increases. The inverse

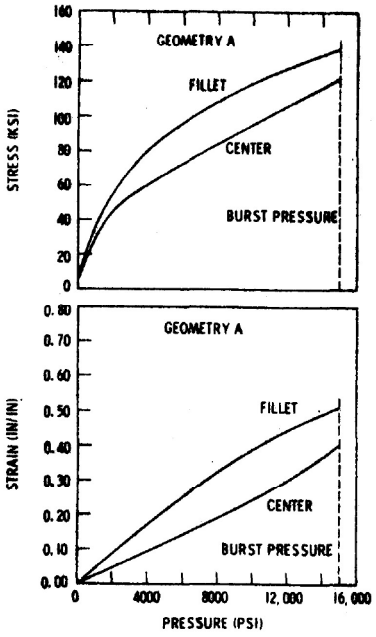

Fig. 5(a) Stress and strain data for 304 stainless steel disks

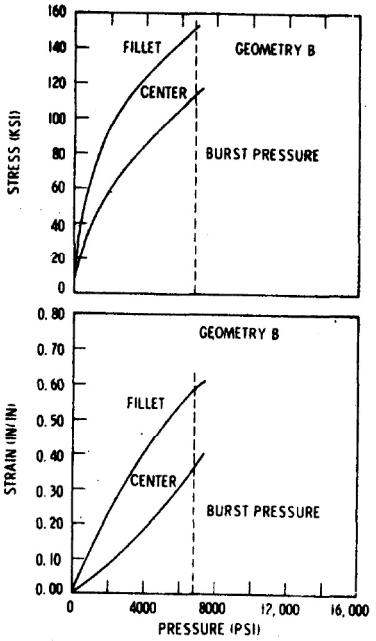

Fig. 5(b) Stress and strain data for 304 stainless steel disks

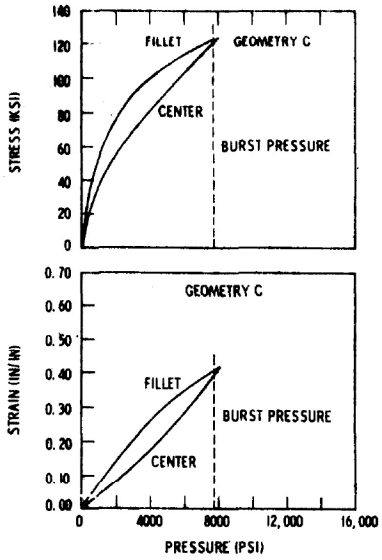

Fig. 5(c) Stress and strain data for 304 stainless steel disks

Fig. 5

proportion rule substantially underestimates the strain concentration for the stainless steel disks ($n = 0.494$).

Interpretation of Results

An interesting interpretation of this work arises when the equivalent strain levels at failure shown in Figs. 5, 6, and 7 are tabulated. All of the edge failures occurred at approximately the same strain level (~50 percent) and all of the centerline failures occurred at approximately the same strain level (~35 percent). (See Table 4). This seems surprising at first, since the ultimate or uniform strains for the three materials are 54 percent for the stainless steel, 17 percent for the low alloy steel, and 31 percent for the carbon steel as indicated in Table 1. However, the ultimate or uniform strain in a tensile test is somewhat artificial as a material property since it is really a measure of incipient tensile instability, and as such is geometry dependent.

Inspection of the material data in Table 1 indicates that the only tensile property which is approximately constant for all three materials is the reduction in area (R.A.). This suggests that reduction in area might be a good property for correlation of the test data. Before doing so, however, it is convenient to introduce the concept of triaxiality factor (TF) [8].

$$TF = 3\sigma_{mean}/\sigma_{eq}$$

$$\sigma_{mean} = \frac{(\sigma_1 + \sigma_2 + \sigma_3)}{3} \tag{1}$$

$$\sigma_{eq} = \frac{1}{\sqrt{2}}[(\sigma_1 - \sigma_2)^2 + (\sigma_2 - \sigma_3)^2 + (\sigma_3 - \sigma_1)^2]^{1/2}$$

$\sigma_1, \sigma_2, \sigma_3$ = principal stresses

Note that for uniaxial tension $TF = 1$, for pure biaxial tension $TF = 2$, and for pure triaxial tension $TF = \infty$.

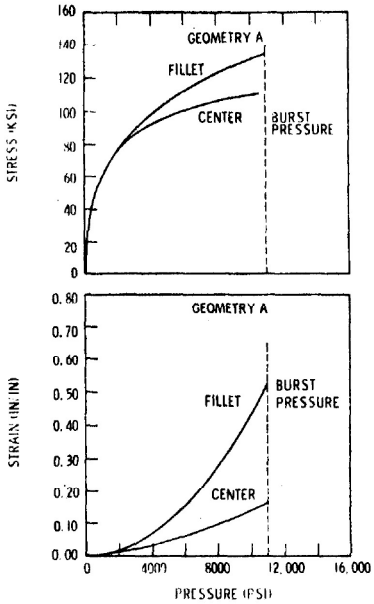

Fig. 6(a) Stress and strain data for A-533 B low alloy steel disks

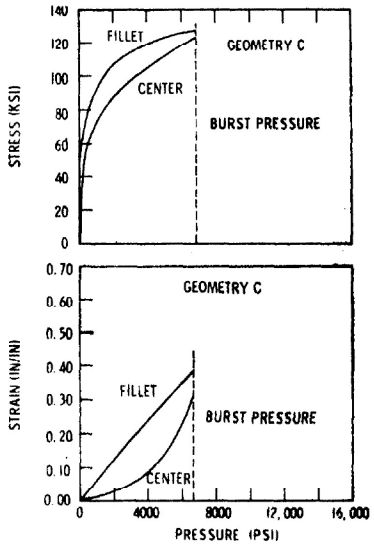

Fig. 6(c) Stress and strain data for A-533 B low alloy steel disks

Fig. 6

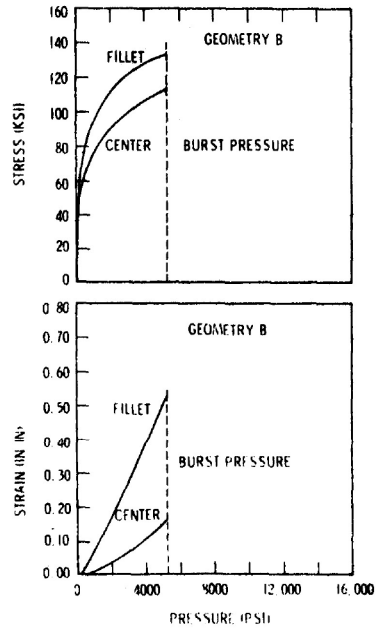

Fig. 6(b) Stress and strain data for A-533 B low alloy steel disks

Generally, the amount of strain that a material can withstand before fracture is expected to decrease with increasing triaxiality of the imposed stress state. Davis and Connelly [8] have suggested that the triaxiality factor as defined previously might be an effective parameter with which to study the reduction in ductility due to multiaxial state of stress. That is:

$$\epsilon_{\substack{crit \\ multiaxial}} = \epsilon_{\substack{crit \\ uniaxial}} \times f(TF) \tag{2}$$

Where $f(TF)$ is a monotonically decreasing function.

Investigation of failure data from several sources [9, 10, 11, 12] indicates that, in the absence of severe anisotropy, the following expression is not a bad first approximation of the influence of triaxiality upon ductility:

$$f(TF) = 1/TF \tag{3}$$

The triaxiality factors for the disk tests at failure were 2.0 for the centerline region and about 1.65 for the fillet based upon the computed stresses in those regions. The tensile tests used to measure reduction in area can be assumed to have had a triaxiality factor of 1.0. In addition, the tensile tests were performed for both longitudinal and transverse tensile specimens indicating very little anisotropy in the disk materials, so that the approximation of equation [3] should apply. Thus, as a first approximation of multiaxial ductility, the reduction in area values for the three materials have been divided by the appropriate triaxiality factors and listed in Table 4. The final column of Table 4 lists the ratios of equivalent strain in the failure location to the multiaxial ductility at that location. The correlation is always better than 30 percent, and the average error is about 16 percent.

Casting this same information in a slightly different format, the question of how well the foregoing scheme predicts failure pressure can be answered. Using the postulate that failure occurs whenever the value of equivalent strain exceeds the re-

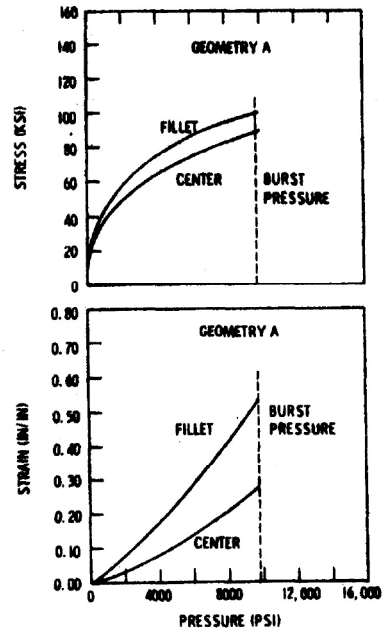

Fig. 7(a) Stress and strain data for ABS-C carbon steel disks

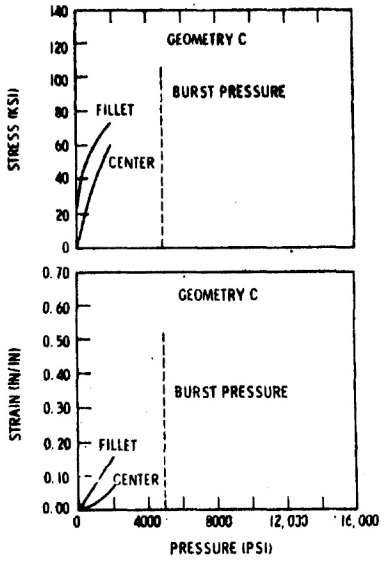

Fig. 7(c) Stress and strain data for ABS-C carbon steel disks

Fig. 7

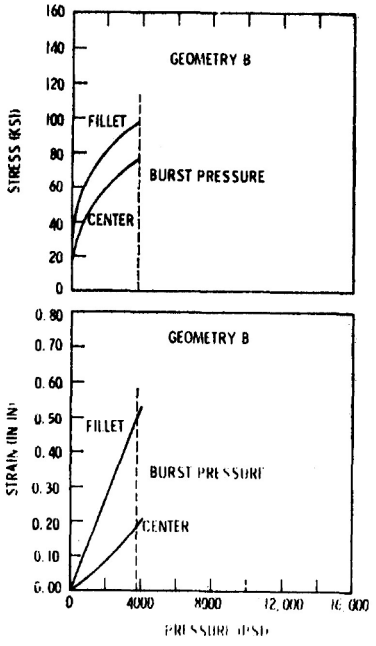

Fig. 7(b) Stress and strain data for ABS-C carbon steel disks

duction in area divided by the triaxiality ratio (multiaxial ductility) at any point in the disk, burst pressures as well as failure locations can be predicted from the analytical strain versus pressure curves of Figs. 5, 6, and 7. Table 5 presents such predictions for the test cases considered here. The predicted burst pressures give reasonably accurate estimates of the actual burst pressures, and the predicted location of failure was correct in all cases but one (304 S.S.—geometry B).

Summary and Conclusions

Results of an elasto-plastic, finite-deformation analysis of selected PVRC disk tests are presented and, in general, there is good agreement between experiment and analysis, which is illustrated by a comparison of the predicted and actual deflections at the disk centerlines as a function of applied pressure. A definite trend of increasing strain concentration in the fillet of the disks as the strain hardening decreases is apparent in the data for all three geometries analyzed. The order of magnitude of this trend supports the assumption of Section 3 of the ASME Boiler and Pressure Vessel Code that plastic strain concentration is inversely proportional to the strain hardening exponent, at least for low values of this exponent.

A scheme for predicting burst pressure from the analytical stress and strain data using the reduction in area from a conventional uniaxial tensile test as a critical strain parameter is suggested. Failure is posited when the computed equivalent strain in the disks exceeds the reduction in area property of the material adjusted by the triaxiality of the stress state. The scheme is shown to be reasonably consistent for the limited number of cases considered.

This analysis demonstrates that it is possible to predict failure loads for material and hardware similar to those used in commercial nuclear power plants, provided that a reasonably accurate

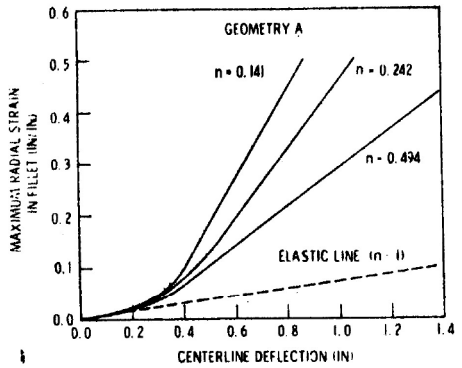

Fig. 8(a) Strain concentration in fillet for various strain hardening exponents

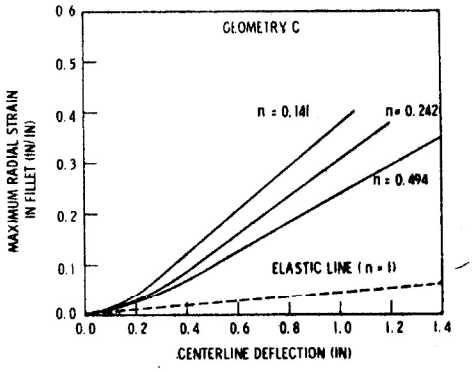

Fig. 8(c) Strain concentration in fillet for various strain hardening exponents

Fig. 8

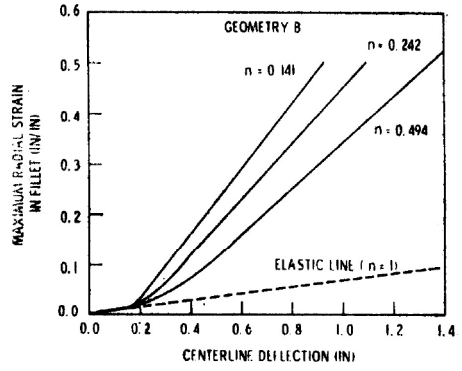

Fig. 8(b) Strain concentration in fillet for various strain hardening exponents

elasto-plastic analysis can be performed. Extension of such an analysis to the more complex loading and geometric conditions which exist in actual plant components will allow accurate evaluations of the margins of safety which exist in these components.

Acknowledgments

The author would like to thank Mr. G. A. Spiering of Teledyne Materials Research Company for his help in interpreting the test data and Dr. A. L. Thurman of Westinghouse Bettis Atomic Power Laboratory for the use of his computer program, without which the analysis could not have been performed.

References

1 Cooper, W. E., Kottcamp, E. H., and Spiering, G. A., "Experimental Effort on Bursting of Constrained Disks as Related to the Effective Utilization of Yield Strength," ASME, 71-PVP-49, May 1971.

2 *P.V.R.C. Subcommittee on Effective Utilization of Yield Strength Experimental Report of Pilot Program and Phase II Effort on Bursting of Constrained Discs*, Teledyne Materials Research Co., Technical Report No. E-1178(b).

3 Thurman, A. L., *GAPL-S-A Computer Program for the Inelastic Large Deflection Stress Analysis of a Thin Plate or Axially Symmetric Shell With Pressure Loading and Deflection Restraints*, WAPD-TM-791, Bettis Atomic Power Laboratory, Pittsburgh, Pa., June 1969.

4 Radomski, M., and White, D. J., "Some Theoretical Considerations Relating to Strain Concentration in Elasto-Plastic Bending of Beams," *Journal of Strain Analysis*, Vol. 3, No. 4, 1968, pp. 304–312.

5 White, D. J., and Radomski, M., "Strain Concentration in Beams Under Cyclic Plastic Straining," *Journal of Strain Analysis*, Vol. 3, No. 4, 1968, pp. 313–324.

Table 4 Computed strains at failure

Material	Geometry	Type of Failure	CENTERLINE DATA: Strain At Failure	Triaxiality Factor (TF)	Multiaxial Ductility ($\frac{\epsilon_f}{TF}$)	EDGE DATA: Strain At Failure	Triaxiality Factor (TF)	Multiaxial Ductility ($\frac{\epsilon_f}{TF}$)	RATIOS: Failure Strain Ductility
304 S.S.	A	Edge	.40	2.0	.37	.51	1.56	.65	1.12
	B	Centr	.37	2.0	.37	.58	1.65	.45	1.0
	C	Centr	.38	2.0	.37	.61	1.69	.45	1.05
A-533 B	A	Edge	.16	2.0	.36	.62	1.67	.41	1.27
	B	Edge	.17	2.0	.36	.53	1.67	.41	1.29
	C	Centr	.33	2.0	.36	.36	1.66	.41	.37
ABS-C	A	Edge	.27	2.0	.33	.52	1.66	.40	1.30
	B	Edge	.18	2.0	.33	.54	1.68	.40	1.26
	C	Edge	#	#	.33	#	#	.40	#

Solution did not converge at failure pressure

ATTACHMENT F

JUSTIFICATION OF VELOCITY USED IN VALVE IMPACT ANALYSIS

VELOCITY JUSTIFICATION FOR THE DYNAMIC ANALYSIS OF A SWING-DISK VALVE*

Introduction

The purpose of this section is to justify equating the kinetic energy of translation to the kinetic energy of rotation in an axisymmetric simulation of the rotational motion of the disk during valve closure.

The disk involved is essentially flat and of uniform thickness. It is sufficient for justification purposes to treat the disk as a thin circular plate and to ignore the mass of the support arm. Hence, the problem will be considered as defined in the attached diagram, where the Y-axis is the axis of rotation.

Derivation of Translational Velocity

Rotation: $KE_r = \frac{1}{2} I\omega^2$ Translation: $KE_t = \frac{1}{2} M V_t^2$

Let $KE_t = KE_r$, then $V_t^2 = (I/M)\ \omega^2$

$I = \rho t \left(\pi R^4/4 + \pi R^2 R_c^2\right)$ $M = \rho t \left(\pi R^2\right)$

$V_t = \omega \sqrt{R^2/4 + R_c^2}$ = equivalent translational velocity

$V_c = \omega R_c$ = centerline velocity

Ratio $R_1 = V_t/V_c = \sqrt{R^2/4 + R_c^2}/R_c$

$R = 13.75$ in., $R_c = 16.5$ in., $R_1 = 1.08$

* Nomenclature is defined at end of section.

Tip Velocity vs. Translational Velocity

$$V_{max} = \omega\left(R_c + R\right) = \text{tip velocity}$$

$$\text{Ratio } R_2 = V_{max}/V_t = \left(R_c + R\right)\sqrt{R^2/4 + R_c^2}$$

$$R_2 = 1.69$$

Consideration of Kinetic Energy per Unit Volume

Rotation at tip: $q_{max} = \frac{1}{2}\rho V_{max}^2$

Translation: $q_t = \frac{1}{2}\rho V_t^2$

$$\text{Ratio } R_3 = q_{max}/q_t = \left(V_{max}/V_t\right)^2 = R_2^2$$

$$R_3 = 2.86$$

Radial Distribution of Kinetic Energy

The distribution of the kinetic energy along the X-axis can be obtained with sufficient accuracy by subdividing the disk in 20 regions bounded by equidistant lines parallel to the Y-axis. For a given region, it is first required to obtain the area, moment of inertia, and center-of-gravity location of the two-disk segments bounded by straight edges on the left. Denoting these two sets by A_1, I_1, X_1, and A_2, I_2, X_2, respectively, and denoting the set for the region considered by A_i, I_i, and X_i, the latter can be obtained from the relationships:

$$A_i = A_1 - A_2 \qquad X_i = \left(A_1X_1 - A_2X_2\right)A_i \qquad I_i = \rho t\, A_i\, X_i^2$$

Neglected in this computation of I_i is the moment of inertia of A_i about the line $X = X_i$, but the resulting error is negligible. Summing of I_i for all the regions shows that the total is within 0.05 percent of the exact value obtained with the formula $I = \rho t\left(\pi R^4/4 + \pi R^2 R_c^2\right)$.

The above procedure leads to results given in the diagram. It is noted that the kinetic energy of rotation peaks at $X = R_c + 0.65\ R$. At this location, the ratio of rotational and translational energy is 2.03.

Justification

1. An axisymmetric dynamic plasticity analysis was performed to determine the structural response of the swing-disk valve to impact closure under faulted conditions. At impact, the kinetic energy per unit volume was uniform throughout the disk. The kinetic energy was dissipated in 1.3 milliseconds through plastic strain energy absorption. Energy absorption started in the contact region of the body and disk and ended in the central portion of the disk. This result shows that the impact velocity was low enough to permit redistribution of the dynamic loading.

2. The kinetic energy distributions in the translational mode and the rotational mode, as shown in the diagram, are sufficiently close in view of Item 1 above to permit the assumption that redistribution of nonaxisymmetric to axisymmetric dynamic loading will occur early in the impact event and that the resulting body seat and disk deformation will be essentially axisymmetric at the end of the event. Taken into account in this statement is the fact that the disk is not rigidly connected to the support arm and that the tip velocity is not more than 1.69 times the translational velocity assumed in the analysis.

3. At the location of maximum rotational velocity, the kinetic energy of rotation per unit volume is 2.86 times the translational kinetic energy per unit volume. While the possibility therefore exists that initially locally severe deformation will result, the progression of such preferential deformation will be arrested because it is incompatible with the deformation of the rest of the structure and the seating adjustment provided by the clearance between disk and disk arm. Furthermore, the kinetic energy at the tip is still small compared with the capacity of the material for absorbing energy. A conservative estimate for this capacity, per unit volume, is $\sigma_u \varepsilon_f$. For the body material, $\sigma_u \varepsilon_f$ is approximately 50,000 in.-lb/in.^{3}; for the disk material, $\sigma_u \varepsilon_f$ is approximately 80,000 in.-lb/in.^{3}. The kinetic energy per unit volume at the tip is:

$\frac{1}{2} \rho V_{max}^2 = \frac{1}{2} \left(0.284/386\right)\left(1.69\ V_t\right)^2$. In the analysis, V_t = 150 ft/sec, so that $\frac{1}{2} \rho V_{max}^2$ = 3400 in.-lb/in.^{3}.

Nomenclature

KE_r = kinetic energy of rotation
KE_t = kinetic energy of translation
M = mass of disk
I = moment of inertia of disk about axis of rotation
ω = angular velocity
V_t = translational velocity
V_c = centerline velocity
V_{max} = tip velocity
R = radius of disk
R_c = distance from center of disk to axis of rotation
t = thickness of disk
ρ = mass density of disk
q = kinetic energy per unit volume
σ_u = true ultimate stress
ε_f = true fracture strain

TABLE F-1

DISTRIBUTION OF KINETIC ENERGY

$$C = \left[\rho t V_c^2 \, R_c^2 / 2\right]^{-1}$$

X_i = distance to c.g

I	II	III	II/III
$\frac{X_i - R_c}{R}$	$\frac{cdKE/dx}{Rotation}$	$\frac{cdKE/dx}{Translation}$	Ratio
-0.940	0.0019	0.0479	0.040
-0.847	0.0063	0.0854	0.074
-0.749	0.0130	0.1076	0.121
-0.649	0.0222	0.1237	0.179
-0.549	0.0341	0.1360	0.251
-0.450	0.0485	0.1455	0.333
-0.350	0.0653	0.1526	0.428
-0.250	0.0843	0.1577	0.535
-0.150	0.1051	0.1611	0.652
-0.050	0.1274	0.1627	0.783
0.050	0.1504	0.1627	0.924
0.150	0.1737	0.1611	1.078
0.250	0.1962	0.1577	1.244
0.350	0.2169	0.1526	1.421
0.450	0.2342	0.1455	1.610
0.549	0.2463	0.1360	1.811
0.649	0.2503	0.1237	2.023
0.749	0.2417	0.1076	2.246
0.847	0.2118	0.0854	2.480
0.940	0.1297	0.0479	2.708
	Sum = 2.559	Sum = 2.560	

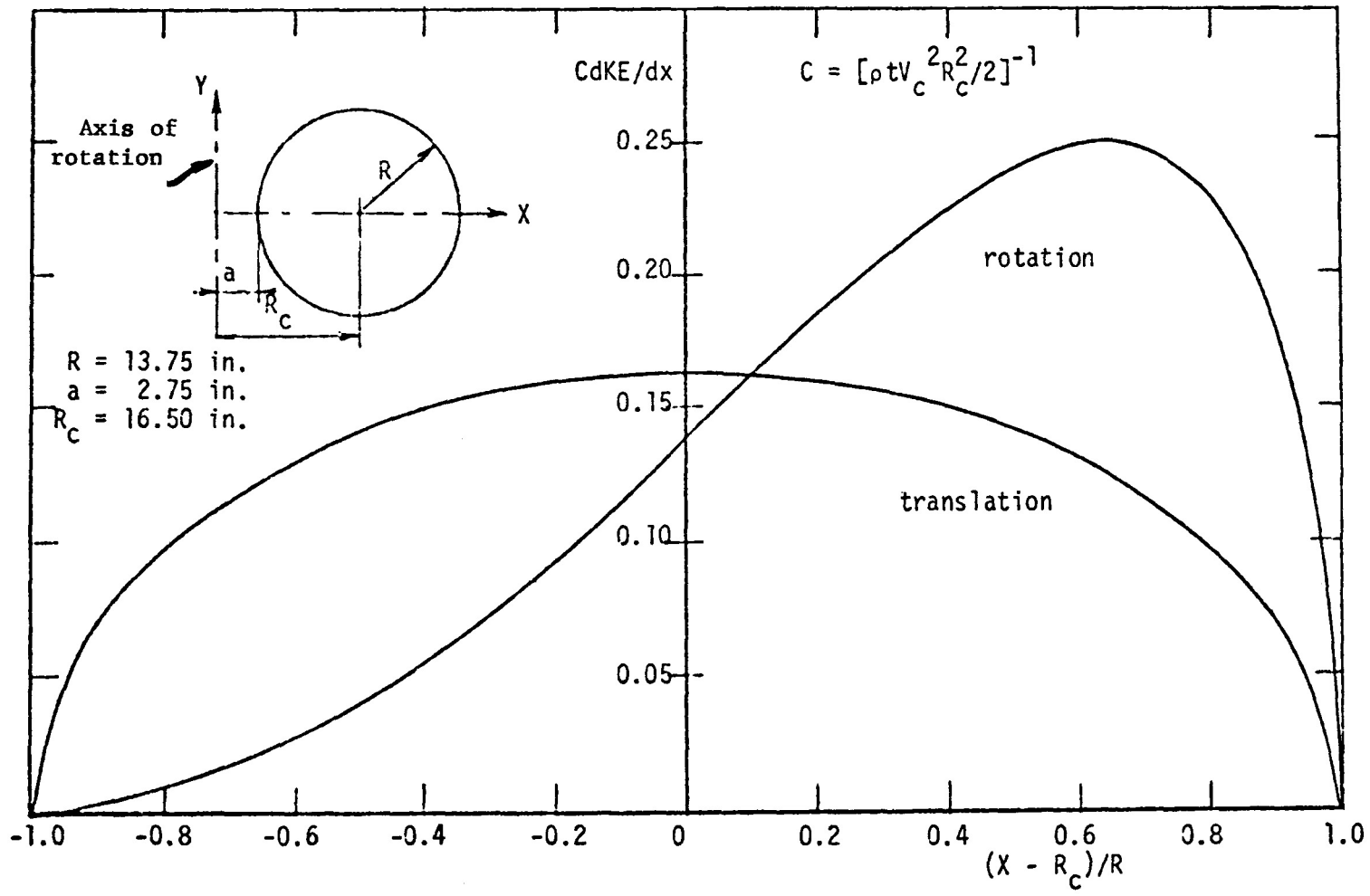

REV 21 5/08

SOUTHERN COMPANY
Energy to Serve Your World®

JOSEPH M. FARLEY NUCLEAR PLANT UNIT 1 AND UNIT 2

ROTATIONAL AND TRANSLATIONAL KINETIC ENERGY DISTRIBUTION IN DISC

FIGURE F-1

ATTACHMENT G

CONVERSION OF TENSION TEST DATA TO TRUE STRESS - STRAIN DATA

CONVERSION OF TENSION TEST DATA TO TRUE STRESS-STRAIN DATA

Nomenclature

A = specimen cross-section

A_o = initial value of A

L = specimen gage length

L_o = initial value of L

P = load

σ = engineering stress

σ_t = true stress

ε = engineering strain

ε_t = true strain

Tension Test Results

Test gives load P vs. elongation $L - L_o$. These results furnish σ and ε via the relations,

$$\sigma = P/A$$

$$\varepsilon = (L-L_o)/L_o$$

Plot of σ vs. ε yields conventional stress-strain curve.

Computation of True Stress

Volume change in specimen is very small in tension test. Neglecting the change gives:

$$AL = A_oL_o$$

Therefore, since $L = L_o(1 + \varepsilon)$,

$$A = A_o/(1 + \varepsilon)$$

Then, σ_t may be computed from σ and ε,

$$\sigma_t = P/A = (P/A_o)(1 + \varepsilon) = \sigma(1 + \varepsilon)$$

Computation of True Strain

True strain is obtained by integration of instantaneous elongation dL,

$$\varepsilon_t = \int_{L_o}^{L} (1/L)\, dL = \ln(L/L_o)$$

Since L/L_o equals $1 + \varepsilon$, ε_t can be computed from ε,

$$\varepsilon_t = \ln(1 + \varepsilon)$$

Reference: A. Nadai, Theory of Flow and Fracture of Solids, McGraw-Hill, 1950 (Chapter 8)

TABLE G-1

Example: A-216, Grade WCB steel at 600°F

ε in/in	σ ksi	ε_t in/in	σ_t ksi
0.01	37.0	0.0100	37.4
0.02	42.3	0.0198	43.1
0.03	46.6	0.0296	48.0
0.04	49.7	0.0392	51.7
0.05	52.0	0.0488	54.6
0.06	54.0	0.0583	57.2
0.07	55.4	0.0677	59.3
0.08	56.5	0.0770	61.0
0.09	57.3	0.0862	62.5
0.10	58.0	0.0953	63.8
0.11	58.3	0.1044	64.7
0.12	58.5	0.1133	65.5
0.13	58.6	0.1222	66.2
0.14	58.7	0.1310	66.9
0.15	58.6	0.1398	67.4
0.16	58.5	0.1484	67.9

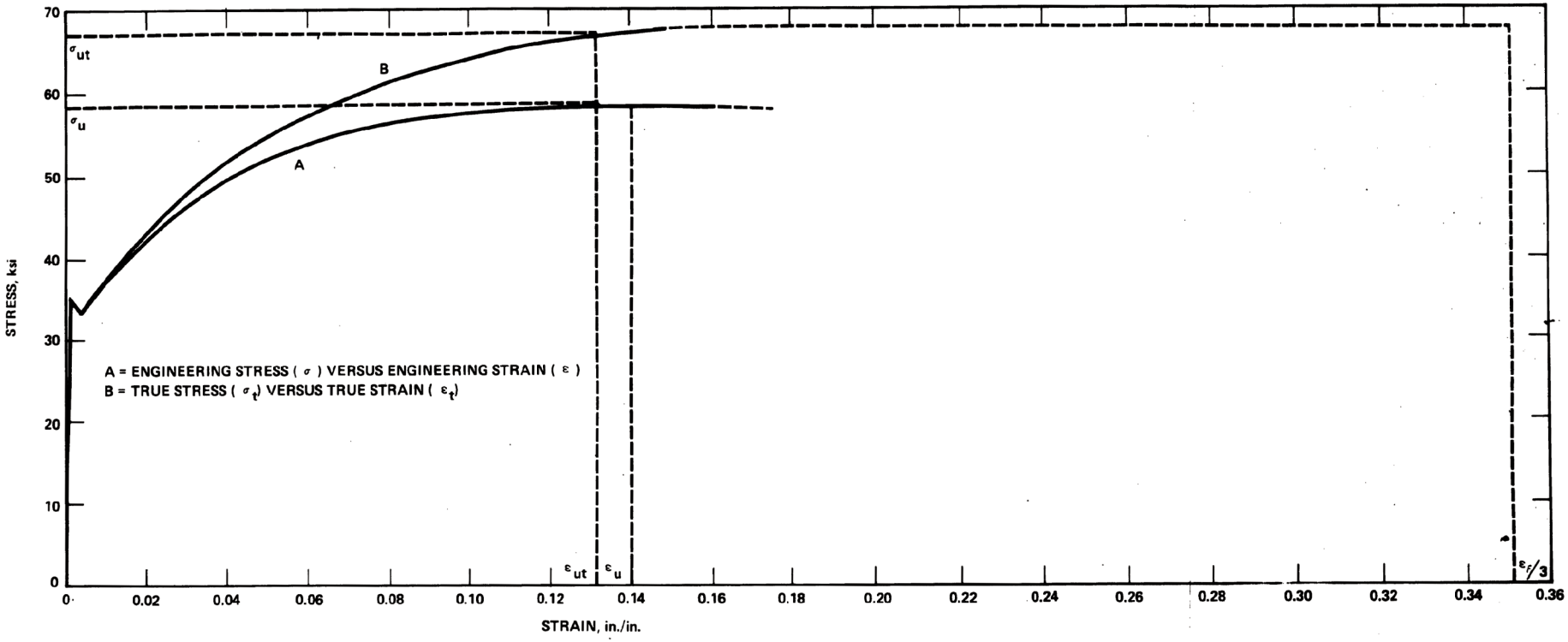

REV 21 5/08

SOUTHERN COMPANY
Energy to Serve Your World©

JOSEPH M. FARLEY
NUCLEAR PLANT
UNIT 1 AND UNIT 2

STRESS-STRAIN CURVES FOR
A-216 GRADE WCB STEEL

FIGURE G-1